EVALUATING NOVEL ANALYTICAL TECHNIQUES TO ASSESS THE INITIAL STEPS OF PROTEIN AGGREGATION USING VARIOUS ANTIBODY SOLUTIONS

By
© 2018
Samantha E. Pace

Submitted to the graduate degree program in Pharmaceutical Chemistry and the Graduate Faculty of the University of Kansas in partial fulfillment of the requirements for the degree of Doctor of Philosophy.

_____

Chair: David B. Volkin, Ph.D.

_____

C. Russell Middaugh, Ph.D.

_____

Michael Hageman, Ph.D.

_____

Teruna Siahaan, Ph.D.

_____

Mark Ritcher, Ph.D.

Date Defended: June 14th 2018

The dissertation committee for Samantha E. Pace certifies that this is the approved version of the following dissertation:

EVALUATING NOVEL ANALYTICAL TECHNIQUES TO ASSESS THE INITIAL STEPS OF PROTEIN AGGREGATION USING VARIOUS ANTIBODY SOLUTIONS

_____

Chair: David B. Volkin, Ph.D.

Date Approved: June 14th 2018

ABSTRACT

Antibody-based therapeutics continue to be a fast growing field in pharmaceutics due to their increased selectivity for a specific target over small molecule drugs. Antibody solutions are often formulated at high protein concentrations in order to achieve low injection volumes, especially for subcutaneous administration, which can cause many challenging problems when it comes to stabilization. The instability of antibodies can often lead to aggregation which can occur during many parts of the manufacturing process including purification, fill-finish, shipping and storage. Aggregation of antibodies can cause many problems such as not injecting the proper dose, due to a decrease in the protein's concentration, or causing immunogenic responses that may affect the safety or efficacy of the drug potentially causing harm to patients. Therefore, the aggregation pathway(s) of antibody drug candidates need to be characterized in great detail and well understood before they reach the market. Currently, several common analytical techniques are being used to distinguish the amount and size of aggregation impurities produced when an antibody undergoes accelerated stresses during formulation development. However, more novel techniques are needed to get a better, more in-depth understanding of the types of aggregates formed along of the aggregation pathway. The development of novel techniques to screen antibody stability and aggregation propensities can not only elucidate degradation mechanisms that proteins undergo throughout the lifetime of the drug, it can also allow us to better understand effective ways to increase the shelf-life and maintain product safety. In this study, various monoclonal antibodies (mAb) and bispecific antibodies (biAb) were examined under varying stress conditions and their physical stability monitored using conventional and novel techniques. New techniques examined include a high throughput GroEL-based BLI (Biolayer interferometry) assay that helps identify less stable antibodies, formulations (excipients, pH values), and storage

conditions (temperatures) by being able to detect pre-aggregate species forming prior to more established techniques show the formation of larger sized aggregates (methods such as size exclusion chromatography and micro-flow digital imaging). Another novel technique examined in these studies is the use of hydrogen-deuterium exchange mass spectrometry, which is used to identify problematic portions of the antibody molecule, by monitoring changes in local flexibility or rigidity, when exposed to different excipients and pH levels. Finally, the use of Langmuir trough to examine interfacial and intermolecular interaction properties of various antibodies and formulation conditions was evaluated. Understanding antibody molecules tendencies to drive to the air-water interface or have intermolecular interactions can predict physical instability problems throughout the purification process and during long term storage conditions. This type of aggregation risk assessment during early formulation development can decrease the resources spent on protein drug candidates that will be problematic. Each of these novel analytical techniques can increase the understanding of antibody instability issues in solution, and therefore, allow for an increased likelihood of successful drug design and development overall.

ACKNOWLEDGEMENTS

The work in this dissertation would not have been possible without the help of numerous people. I would like to thank my research advisor, Professor David Volkin, for his guidance over the past several years and for allowing me to be a part of his laboratory. I have enjoyed working with him on the numerous projects we have had the pleasure of investigating and have learned a great deal from them. I want to thank Dr. Sangeeta Joshi for her assistance and friendship throughout the years. She has been very encouraging and supportive during this journey along with insightful. I also owe a great deal of thanks to Dr. C. Russ Middaugh for his scientific guidance and encouragement along with many life lessons. I admire his passion for teaching and his vast knowledge and understanding of pharmaceutical sciences. I would like to thank all my lab mates have from Macromolecule and Vaccine Stabilization Center (MVSC) have helped me grow as a scientist and the many friendships I have made from working with such a wonderful group of people.

I would like to acknowledge financial support from Siegfried Lindenbaum Fellowship for my tuition throughout the course of my graduate studies and the NIH Biotechnology Training Grant (5T32GM008359-25).

I would like to thank all the professors from Pharmaceutical Chemistry Department for their support and setting up an excellent foundation of the coursework. Every professor has helped me grow into a better scientist and taught me a vast of scientific knowledge. I would like to thank Dr. Michael Hageman for not only providing me with the necessary background but for also his career advice.

I would like to thank Dr. Borchardt for the opportunity to be a part of the GPEN2016 organizing committee and for his career guidance. The experience gained from participating in an international community and organizing a scientific event is invaluable. I would like to thank Nancy Helm for friendship and for helping me answer any question I came to her with along with her tremendous help organizing GPEN2016.

I would like to thank my wonderful group of new friends discovered during my time at The University of Kansas, Dr. Michaela McNiff for being such a wonderful and understanding person, Saad Alotaibi for always challenging me to go outside my comfort zone and discover more, and all my new friends found through the soccer community. I would like to expand a special thank you to Daniel Hesselschwerdt for his friendship, love, and support from the very start of procuring my career. I would like to thank my parents and many other family members that have supported me and cheered me on along the way. I would like to thank my brother, Shawn Pace, for always providing healthy competition, pushing me to be my best, and always being there for me. I would like to thank Philip and Kelly Elrod for their continued support and encouragement throughout the years. They have always believed I could do anything I put my mind to and have helped me to achieve all my goals.

TABLE OF CONTENTS

LIST OF TABLES

LIST OF FIGURES

LIST OF SUPPLEMENTARY FIGURES

Chapter 1 Introduction

1.1 Monoclonal Antibodies Structure and Function

Antibodies are an important part of the human immune system. There are many roles antibodies can play in a protective immune response including neutralization of the infectious agent, phagocytosis, antibody-dependent cellular cytotoxicity (ADCC), and complement-mediated lysis of infected cells or pathogens.[1,2] There are five classes of antibodies which consist of IgG, IgA, IgM, IgD, and IgE[3] with IgG being the most prevalent at 75% of the total. These classes are highly conserved structurally but can differ not only in their variable binding regions, but also in their constant regions and therefore have different effector functions and therefore differ in physicochemical and behavior.[4] IgG's can further be broken down into subclasses of IgG1, IgG2, IgG3, and IgG4, with IgG1 being the most abundant in human serum at ~65% of the total IgG amount.

The structure of an IgG antibody is made up of a homodimer containing two heavy chains and two light chains connected by intra and intermolecular disulfide bonds and has a size of ~150 kDa. The homodimer is folded in a Y-shaped structure to form two fragment antigen-binding (Fab) domains and a fragment crystallizable (Fc) domain. The Fab domains contain a light chain linked to a heavy chain while the Fc domain is made up of two heavy chains (Figure 1). The light chain has two domains, V_L and C_L. The heavy chain has four domains V_H and three C_H regions that consist of C_H1, C_H2, and C_H3 (or $C\gamma1$, $C\gamma2$, and $C\gamma3$). Within the C_H2 domain of all γ chains there is an N-linked glycosylation site (N297) in which is attached oligosaccharides of varying carbohydrate group(s) that helps determine the overall quaternary structure of the antibody. The Fab region contains three complementarity-determining regions (CDRs) each that are about 10 amino acid residues in length and form a three-dimensional cleft that is the antigen-binding region.

Depending on the amino acid sequence, the shape and local ionic strength can change greatly and are highly specific for a specific antibody.

The subclasses of IgGs have 90-95% conservation compared to one another in the constant region. The subclasses of IgG differ in their constant regions, mainly around the hinges and upper portion of the C_H2 domain.[4] These regions are involved in binding to receptors which results in them having various effector functions, such as triggering phagocytosis or antibody-dependent cell mediated cytotoxicity and activating complement. In addition, IgGs, IgAs, and IgDs have segmental flexibility where the Fab portions can move relative to each other bending at the hinge region which is located between C_H1 and C_H2. IgMs and IgAs antibodies form multimeric molecules and have a polypeptide called the joining (J) chain to stabilize the structure.

IgG1 is the most common IgG subclass and are involved in biological activities including opsonization, agglutination, placental transfer, ADCC, and neutralization of toxins.[2] The IgG4 subclass is the least common of the IgGs and is unique in its structure and function properties. IgG4 antibodies are induced by repeat exposure to antigen in a non-infectious setting.[4] The main structural difference is that IgG4 antibodies can also undergo changes between the disulfide bonds in the hinge region. These changes can form either inter-chain or intra-chain which also allows it to undergo 'half-antibody' exchange *in vivo* that result in recombination of antibodies domains that result in two different binding specificities.[5] This is due to the presence of a serine residue at position 228 rather than the lysine found in an IgG1. This also makes it so IgG4 cannot crosslink the target antigen. Overall, the average conformation stability(e.g. T_m values) of an IgG4 is about 10°C less stable than that of an IgG1.[6] This reduction in structural stability can cause an increase in physical instability problems (including aggregation) being seen with IgG4.

1.2 Bispecific Antibodies Structure and Function

Bispecific antibodies (biAb) comprise of two individual binding entities instead of just one seen in the monoclonal antibodies (mAb). This allows biAbs to bind simultaneously to two different epitopes on the same antigen or onto two separate antigens.[7] BiAbs can potentially achieve numerous more clinical applications compared to mAbs. This includes recruitment of T-cells to tumor cells, increasing binding specificity and affinity, and by addressing the binding of two different antigens. Currently, there are two biAb based drugs (catumxomab and blinatumomab) approved for therapy.[8]

There are over 50 different formats for biAb combinations that have been developed.[9] This diversity allows for the design and development of antibodies with more desirable specific attributes such as size, flexibility, half-life, and bio-distribution. BiAbs can be divided into two main structural categories and classified as either whole-IgG that comprises an Fc-portion or Fc-less which has a small fragment. Whole -IgG biAb have two different heavy chains and light chains. In contrast, Fc-less are able to penetrate tissues more readily but have the disadvantage of not having Fc-mediated functions like ADCC. This type of BiAb also has a shorter half-life *in vivo*. They consist of different Fab fragments from different antibodies and are chained together by a linker.

1.3 Protein Folding and Stability

Protein molecules can follow different pathways for folding, unfolding, and aggregating due to competition between various interactions.[10] To reach its properly folded, three dimensional native state, a protein can go through several transition barriers (intermediate states) to reach the free energy thermodynamic minimum[11] (Figure 2). The thermodynamic minimum

can be determined by intrinsic factors, the protein molecule itself, and extrinsic factors like the environment around the molecule.[12] Intrinsic factors include the protein's amino acid sequence while extrinsic factors include the solution conditions (e.g., formulation additives, temperature, pH, ionic strength). Both intrinsic and extrinsic factors can play a role in the proper folding and resulting conformational stability of the protein molecule.

One of the major driving forces for protein folding into its native, three-dimensional structure is the polar and apolar surfaces. Apolar surfaces or regions of a protein, containing more dense concentration of hydrophobic amino acid residues, tend to bury into the center of the folded protein to be excluded from the presence of water. The folding of a protein molecule requires the removal of water from the core.[13] This process has an energy cost as well as entropic cost of organization in order for this to be a favorable reaction. This protein folding process is described by Gibbs free energy in the equation that follows:

(1) $\Delta G=\Delta H-T\Delta S$

Where ΔG is the change Gibbs free energy, ΔH is the change in enthalpy, T is the temperature in Kelvin, and ΔS is the change in entropy in the system. The folding and removal of water will spontaneously occur if the end result is lower in energy (smaller Gibbs free energy). Lower overall energy of the protein in the folded state can be driven by many of the intrinsic properties of the protein such as the hydrophobicity, electrostatic interactions, steric considerations, hydrogen bonding, and more.[11]

Protein folding due to hydrophobicity effects has shown to be a driving force due to the large change in heat capacity.[13] Aromatic residues can contribute to the hydrophobicity and also have pi-pi interactions.[14] Sterics and packing of the core can play a major role in the stabilization

of the protein molecules three-dimensional structure.[15] Steric constraint limits the possible conformations the protein can pack into. Due to the inherent secondary structure based on the protein's amino acid sequence,[16] Ramachandran plots of proteins allow the prediction of protein folding based on the possible secondary structures elements from the dihedral angles.[17] Electrostatic interactions through charged residues like Arg, Asp, Lys, and Glu can not only play a major role in the inner core of the folded protein molecule through the formation of salt bridges, but can also stabilize the protein on the surface due to their favorable interaction with polar solvents like water.[18,19] Secondary structural elements also play a major role in the three dimensional folding of proteins. Alpha helix structures rely on interactions formed from the CO and the NH components of the polypeptide chain from amino acids four residues away[11], while beta sheets can form due to hydrogen bonding between amino acid residues distant in the protein molecule's primary sequence.[20]

1.4 Protein Aggregation

Aggregation of proteins can occur due to numerous factors. These can be categorized into intrinsic properties of the protein, which consist of the primary, secondary, tertiary, and quaternary structure, or extrinsic factors such as the solution conditions, environment stresses or various processing conditions.[21] Many problems during clinical development can be attributed to protein aggregation such as reduced biological activity, increased immunogenicity, or other side effects for the patients. While protein-based drug products can be formulated at the optimal conditions based on the proteins stability profile, several steps, such as purification, can also present the protein to unfavorable environments during manufacturing.

1.4.1 Types of Protein Aggregates

Aggregates can be classified by several categories and defined in several terms. Four common ways to group different types of protein aggregates are by conformation, linkage, reversibility, and size.[11] Conformation can be broken down into native or non-native states depending on if the higher-order secondary and tertiary structure of the protein within the aggregate is significantly altered. Linkage can be defined by covalent or non-covalent. Covalent linkages are a result of chemical bonds such as disulfide bonds.[22] Non-covalent bonds are often dissociable and are formed due to forces like hydrophobic and electrostatic interactions.[23] Reversibility is defined as returning to the native state upon returning to the stable environmental condition such as a change in temperature or concentration. Irreversible aggregates stay in the non-native form even with the removal of the stress and return to ambient conditions. Size of the aggregates are categorized into soluble, subvisible, and visible aggregates. Soluble aggregates are in the form of oligomers such as dimers and trimers that are soluble in solution.[24] Subvisible particles are typically in the size range from 100 nm to 100 μm.[25] Differences in the morphology can be seen with the formation of subvisible aggregates.[26] Visible aggregates can be seen by the naked eye and classified as 100 μm or greater in size.

Overall, when protein aggregation occurs in vivo it can take the form of misfolded aggregates, inclusion bodies, or amyloid fibers.[27] Some aggregates observed are in in the form of amyloid fibers, which that have an increased amount of β-sheet content and reduced amount of alpha helicity compared to the native state, which can be due to the increase of intermolecular contacts.[28] Inclusion bodies are another form where monomeric aggregates self-assemble into growing polymers typically during overexpression within host cells during production of recombinant proteins.[29]

1.4.2 Protein Aggregation Pathway

The aggregation of proteins can happen through numerous different pathways that are kinetically available. It is a complex pathway and can have several intermediate states before reaching one of many possible end states (Figure 3).[30] A protein molecule can go from the native folded state to another stable intermediate state readily due to the small energy barrier and because proteins are in constant flux.[31] The energy from a stable protein to an unfolded protein can be as little as 5-20 kcal/mol which is equivalent to two or four hydrogen bonds which demonstrates that the native, folded state of a protein molecule is only marginally stable.[32]

The aggregation process can start by the local unfolding within a protein molecule that can allow for the aggregation prone "hot spots" to be exposed and available.[33] Native, globular proteins in solution are in equilibrium with this partially unfolded state and the folded.[34] The local unfolding event allows there to be an interaction between monomers by the exposure of amino acid residues that were previously sterically unavailable.[35] These partially unfolded intermediates are also in equilibrium with the unfolded state[25,27] and therefore proteins can unfold in a reversible fashion and obey a two-step kinetic model.[36] This process suggests that the population of partially unfolded intermediates can lead to an increase in larger amounts and sizes of irreversible aggregation.[37] This effect can be due to the exposure of hydrophobic sites that have been shown to have an increase in flexibility of the intermediate state compared to the native state.[38] Exposure of hydrophobic sites and their ability to come in contact with others, could stabilize the aggregation state, just as such contacts can stabilize the native state.[39] If the aggregation kinetics depend on the rate of unfolding, and even if the unfolding is not the rate limiting step, the levels of this intermediate can have a significant impact on the overall aggregation pathway.[40]

It is also possible for protein aggregation to occur without going through these structurally altered intermediate states.[41] This is possible by the direct association of native state proteins to one another by electrostatic or hydrophobic interactions under the right experimental conditions including protein concentration.[42] This association can be reversible and can depend on the second virial coefficient (B_{22}), where a positive value indicates repulsion between the proteins and a negative value indicates attraction.[12] Thus, when the protein aggregation process is controlled by the self-association step of multiple protein molecules coming together then it is primarily linked to the protein molecule's colloidal stability, while when aggregate formation process is controlled by the formation of structurally altered, unfolded intermediates, this process is linked to the protein molecule's conformational stability.[11]

The initially formed protein aggregates start as small and soluble and grow into larger insoluble particles as they grow in size. The insoluble aggregates can form into different types such as amorphous precipitates or fibrils.[43] The type of aggregate formed will depend on the intrinsic and extrinsic conditions that are present as described above. Another possible rate limiting step in the aggregation pathway can be the process of nucleation.[40] That is, one aggregate that causes the formation of others to aggregate and increase in size and number and even polymerization.[44] This nucleation process often follows first-order kinetics due to the rate limiting step by a monomer addition. This can be seen by a lag time before aggregation is seen.

Depending on the environmental conditions, multiple different aggregation pathways can occur for any given protein molecule, since the environment around the protein can affect its conformational and colloidal stability properties, and these different aggregation pathways can lead to the formation of different types of aggregates such as amorphous aggregates or fibrils.

Some proteins, such as IgG4 antibodies can swap domains and has been suggested that this can be an intermediate on the pathway of formation of IgG4 antibody aggregation.[45]

1.4.3 Causes of Protein Aggregates

Proteins may contain aggregation-prone regions (APR), and in antibodies these APRs are usually located in the CDR region.[11] The APR has been shown to be one of the largest driving factors to the physical instability of antibodies.[46] Environmental stresses during the manufacturing process like cell culture, purification, formulation, filling/packaging, and shipping can all potentially cause proteins to aggregate.[47] Such stresses include temperature, pH, high concentrations, shear, air-liquid interfaces, light, and much more. All these stresses and solution conditions can cause a specific protein molecule to go through several different aggregation pathways.[48] Due to protein molecules being dynamic in nature, the slightest of change in environment towards the non-native state can initiate the process that can cause aggregation.[49,50]

1.4.3.1 *Temperature*

Temperature is a major factor that can impact protein stability and aggregation rates. The thermal stability of a protein can be measured by the free energy of unfolding ($\Delta G_{unfolding}$). The higher the $\Delta G_{unfolding}$ the more resistant the protein is to unfold at increased temperatures. The maximum free energy is usually found in a narrow temperature range. Increasing and decreasing the temperature can cause the protein to be less stable.[51] Protein molecule's thermal stability is often measured by their thermal melting temperature (T_m) which is a relative measure that can be compared across other various conditions.[52] Proteins are unfolded at their T_m values and can start to aggregate[53] but higher T_m values does not necessarily mean the protein is less likely to aggregate.[54] Lower the temperature of the solution can cause an increase in protein aggregation

as well. Lower temperatures can decrease the strength and number of hydrophobic interactions[55] within a protein molecule. In addition, excipients can crystalize, which can lead to phase separation and decrease their protection effects on protein stability.[56,57] The diffusion coefficient is also related to the temperature. When the temperature of the solution is increased, protein molecules move more rapidly and are able to collide more frequently with one another.[38,58] The increase in collision frequency can increase unfavorable interactions that allow protein aggregation to occur along with faster diffusion to and from the interface.[59] A change from the optimal temperature range can also play a role in increasing the chemical degradation rate of proteins that in turn can lead to aggregation by the change in molecular motion.

1.4.3.2 *Solution pH*

Solution pH is another important factor that can dictate the aggregation of a protein. Changes in the pH value can change the type and distribution of the charges on the surface of a protein molecule.[60] This change can affect the folding interaction within the protein as well as the interactions between proteins. Protein's have a minimal solubility at their isoelectric point (pI) where the net charge is zero because the charge repulsion of the protein is at its lowest.[61] Changing the charge on the surface of a protein can also change the way it interacts with the excipients in solution, which can also affect the likeliness of a protein to aggregate.[62] Another way solution pH affects protein aggregation is by altering the chemical degradation rates the protein will undergo creating chemically altered proteins with increased propensity to aggregate.[63]

1.4.3.3 *Ionic Strength*

Ionic strength is dependent on the concentration of ions in the solution and can have many effects in the protein aggregation pathway.[64] When the ionic strength is increased, it allows for better neutralization of the charges seen on the surface of the protein.[61] This can decrease the amount of charge interaction by electrostatic screening. The salt type can also play an important role in how it stabilizes or destabilizes the protein including effects on protein solubility as well as protein structural integrity.[65]

1.4.3.4 *Excipients*

Excipients added to the solution can change the stability of a protein in many different ways. There are many different categories of excipients used in pharmaceutical drug products such as sugars, amino acids, polymers, and surfactants, and many different types of excipients within each category.

Sugars are small, often neutral compounds that can have a stabilizing effect on the protein's stability.[66] Sugars commonly used in formulations are sucrose, lactose, and trehalose. Sugars help stabilize proteins by maintaining their correct conformation and this effect usually increases with increasing concentrations of additive.[67] Although sugars usually have a stabilizing effect on proteins, there are some cases that shows an increase in aggregation as a result of their addition.[68] This could be due to a chemical reaction with the protein's lysine residues and the reducing end of a sugar molecule.[69] Sugar alcohols such as sorbitol and mannitol can have similar stabilizing effects without the potential for chemical degradation byproducts.

Amino acids can have several effects on the stabilization or destabilization of protein.[70] Charged amino acids, such as lysine and aspartate, have been shown to decrease protein

aggregation by decreasing protein interactions.[71,72] Arginine is also another common charged amino acid used for it beneficial effects with protein refolding assistance.[71]

Polymers have many different way of decrease protein aggregation such as surface activity and viscosity effects which decrease diffusion of the proteins in solutions.[73] There are many types of polymers used in protein formulation such as neutral, amphoteric, polycationic, and polyanionic. A couple of ways polymers can increase the stability of proteins is increase the distance between them or cover the hydrophobic regions of both the unfolded and folded state.[74]

Surfactants used in protein formulation work come in two general classes, ionic and nonionic. The ionic surfactants have been shown to have a large effect on protein aggregation due to their ability to form a stronger bond with the protein.[75] Nonionic surfactants have hydrophobic tails that can interact with the hydrophobic areas on the protein.[76] Surfactants have been shown to be very effective against agitation stresses like shaking and stirring by outcompeting the protein molecules for the air-water interface.

1.4.3.5 *Protein Concentration*

Increasing the concentration of protein can have several results on protein aggregation. One of the limitations of high concentrations of proteins is an increase in aggregation rates due to the increase in colloidal interactions.[41,42] Another common problem with high concentrations of proteins is the limited solubility of a protein. If the concentration of the protein is higher than the limit, precipitation can occur. A high protein concentration, however, can also stabilize proteins in solution due to the crowding effects.

1.4.3.6 *Agitation*

Agitation is a common stress that is seen throughout the manufacturing and shipping process and can cause protein aggregation through a number of different mechanisms. Shaking and stirring are common types of agitation that increase the colloidal interaction propensities of protein.[77] These agitations can also increase interaction at the air-water interface which can lower the energy barrier of unfolding and thus allowing the hydrophobic surfaces of a protein molecule to be exposed and increasing aggregation.[78,79] Stirring can then increase the transfer of these unfolded proteins at the surface into the bulk solution and nucleate further protein aggregation.[80] Agitation stresses can also enable certain chemical degradation reactions that in turn increase protein aggregation.[81]

1.4.3.7 *Tangential Flow Filtration*

Tangential flow filtration (TFF) is a commonly used unit operation used for diafiltration and ultrafiltration during protein purification and formulation, but TFF processing can lead to many different stresses on protein molecules such as shear, cavitation, exposure to air-liquid interfaces, and protein-membrane surface interactions.[82] These stresses can cause many problems with the protein during processing including structural alterations and aggregation.

1.4.3.8 *Light*

Light exposure can cause proteins to have a wide variety of chemical degradation reactions.[83] UV light can cause cross-linking between cysteine and tryptophan residues as well as the cleavage and formation of disulfide bonds.[84] Changes within the protein primary structure due to chemical degradation reactions can also shift the protein away from its native structure to an aggregated state. This can be seen by mutations in the amino acid sequence or chemical modifications such as Asn deamidation.[85] Oxidation can also lead to aggregation by forming

crosslinking and has been seen to be involved in amyloid plaques that has been associated with protein misfolding diseases.[11]

1.4.4 Predicting Protein Aggregation

Prediction of rate and extent of aggregation of proteins would be an extremely useful tool. Although there is no model that is able to predict all proteins likeliness to aggregate, there are several approaches used to give an initial evaluation. One common approach is the use of computer models, such as TANGO, to simulate the dynamics based on the hydrophobicity, aggregation prone sequences, and other indicators.[86] The amino acid sequence and structural features are another indication of the likeliness of aggregation to occur.[87]

1.4.5 Controlling Protein Aggregation

Controlling protein aggregation is challenging and a large amount of information and experimental data need to be gathered to best formulate a candidate protein drug product. Common strategies to decrease protein aggregation are to control solvent and temperature conditions or to identify and remove the "hot spots" by altering the sequence.[33] Engineering and altering the aggregation prone areas can cause problems of its own, however, such as disrupting the proper folding of the protein or affecting biological activity.[88] Other ways to control protein aggregation include identification of proper formulation and storage conditions.

1.5 Analytical Tools to Monitor Protein Aggregation

There are many commonly used analytical tools used to monitor protein aggregation across size ranges 1 nm to 1 mm (Figure 4). These techniques are robust and can provide large amounts of information to characterize the protein aggregate's physical and chemical properties. These tools includes such techniques as size exclusion chromatography, dynamic light scattering, static

light scattering, microflow digital imaging for aggregate size analysis, and Fourier transform infrared spectroscopy for structural information about the protein molecules within an aggregate.[40]

1.5.1 Size exclusion chromatography

Size exclusion chromatography (SEC) is perhaps the most common technique used to quantify the amount and size of soluble aggregates and can be routinely adopted for characterization of biopharmceutics.[89] It has relatively high resolution and accuracy. This technique works by separation of macromolecule by a silica-based microparticles of the size range from 5-10 μm.[90] The sample flows through the column and the smaller molecule weight species diffuse inside the pores of the microparticles resulting in a later elution time. The larger molecular weight species cannot enter the micropores and therefore elute at an earlier time. The concentration of each species can be seen by spectrophotometric detector. Standard molecule weight species are injected and can be compared to the elution times of the protein sample under the same experimental conditions. The column size and microparticles and their pore sizes can be optimized to detect aggregates from 5-10^3 kDa in size. SEC has some limitations such as a dilution effect when the sample is injected. This dilution effect can cause aggregates to dissociate.[91] Another downfall is the possibility of the protein and the aggregates to interact with the column material causing a misrepresentation of the elution peaks.[92] The mobile phase can be altered to decrease this effect, but this can cause the modification of aggregates.

1.5.2 Dynamic light scattering

Dynamic light scattering (DLS) is the measure of the fluctuation of light scattering intensity due to the random motion of the molecules over a period of time.[93] This provides information about the diffusion coefficient (*D*) of the particles. When assuming a spherical shape

and no interactions, *D* can be correlated to the hydrodynamic radius (R_H) by the Stokes-Einstein equation. This technique is used to measure the size of aggregates from the size range of 1 nm to 1 μm.[94] In a heterogeneous mixture of protein aggregates, various size distributions can be detected. The light scattering information obtained is intensity weighted and can be converted to number based, volume based, or weight based, but these numbers are based on assumptions of the particle shape.[94] The light scattering from the DLS measurements are typically collected at a 90° angle, but newer instruments can now collect back-scattering data as well which allows for higher sample concentration to measure without secondary scattering effects.[95] Some drawbacks to the DLS method is that since the data is intensity weighted, larger aggregation can have a large effect of the size distribution obtained. Another limitation is that the method assumes the protein molecules being measured are spherical in shape.

1.5.3 Static light scattering

Static light scattering (SLS) is the measure of time and average intensity of scattered monochromatic light from particles at various angles. This depends on the molecular weight, concentration, shape, virial coefficient (*B*), wavelength, and angle of detection and is analyzed by the Zimm plot.[96] The light scattering from multiple angles (MALS) can be collected and provides accurate information about higher molecular weight aggregates. SLS can measure aggregates with the molecular weight greater than 5 kDa. SLS is commonly combined with SEC along with UV and refractive index detection.[97] This separates the aggregates and allows the SLS detectors to be more accurate in determination the molecular weights. Due to high background scatter, the readouts of low concentration of smaller molecular weight aggregates are not as accurate or reproducible.

1.5.4 Microflow digital imagining

Microflow digital imaging (MFI) is used to detect subvisible particles that are important to characterize in a protein solution. These particles fall into the size range of ~1-100 µm. The lower end is hard to detect by SEC and the higher end can be seen by the naked eye. MFI is based on digital images being taken from the flow of the sample solution through a flow cell and images are collected by microscopy.[98] The particle count, size, transparency, and morphology of the particles can be analyzed. Some limitations with MFI occurs with the resolution of particles at high concentrations and how many particle images are captured per frame, which can lead to over or under estimations.

1.5.5 Fourier Transform Infrared Spectroscopy and Circular Dichroism

Fourier transformation infrared spectroscopy (FTIR) and circular dichroism (CD) as essential to obtaining information about the overall secondary structure of proteins. This information is important for understanding the mechanism that aggregates form through the detection of conformational changes.[99] FTIR is used to obtain information about the overall secondary structure content of the protein. CD can be used in the far-UV (180-260 nm) providing information on the secondary structure and it can also be used in the near-UV (240-340 nm) which provides information on the tertiary structure. A limitation of these techniques is that low concentration of aggregated species can be masked by the native protein, therefore, aggregates may need to be separated to be analyzed properly.

1.5.6 Transmission electron microscopy

Transmission electron microscopy (TEM) is used to provide images of protein aggregates to gain information about their morphology, size and shape.[90] An electron beam is used and focused on the sample. The contrast from the surrounding and the sample produces a high magnification image. TEM works from the size range of a few nm to several microns. One

limitation of TEM is that it cannot be used for quantifying the number of aggregates. Sample preparation, such as staining, can also affect the state the aggregation is in. Finally, small subsets of the sample are viewed and may not represent the entire sample distribution.

1.6 Novel Tools used to Detect Protein Aggregation

There are many other approaches that can give a deeper understanding of the aggregation of proteins. In order to dive deeper into this, more novel applications can be used. The novel techniques come with many limitations such as low throughput and increased optimization steps. But overall, a larger amount of information can be gained to understand exactly what is happening when a protein is aggregating and/or forming particulates.

1.6.1 GroEL-Biolayer interferometry

GroEL-Biolayer interferometry (GroEL-BLI) has been used to study the pre-aggregate species of several proteins. Pre-aggregate species are defined as partial unfolded proteins and cannot be detected by other pharmaceutical methods such as SEC or DLS. Biotinylated-GroEL, a chaperonin, is coupled to a streptavidin biosensor and is able to capture the pre-aggregate species. Association of the protein to the GroEL is detected using BLI. This method was developed using several proteins including monoclonal antibodies, polyclonal antibodies, and FGF.[100] Further optimization allowed for a high-throughput screening on several antibodies under various stress and buffer conditions resulting in the detection of pre-aggregates prior to soluble aggregates detected by SEC or subvisible detected by MFI as described in this thesis work. [101] This method can help screen different excipients and can potentially be correlated to longer term storage stability.

1.6.2 Hydrogen-deuterium Exchange Mass Spectrometry

Hydrogen-deuterium exchange mass spectrometry (HX-MS) is a technique to observe flexibility and rigidness of a protein by the rate of hydrogen exchange. A detailed map of the proteins local structural flexibility can be analyzed.[102] Certain segments of the protein can be identified as being stabilized or destabilized depending on the extrinsic conditions such as excipients. Areas of the proteins seen to increase in flexibility under certain conditions can point to areas of the protein that are problematic and can lead to aggregation.

1.6.3 Langmuir trough

The Langmuir trough is a valuable technique that can provide a large amount of information about interfacial properties of a protein molecule.[103] The air-water interface can cause proteins to increase the exposure of otherwise buried hydrophobic patches. The likeliness of a protein to go to the interface can help predict its ability to aggregate under agitation stresses. The more a protein tends to go and stay at the air-water interface can be correlated to the initial unfolding event (as well as nucleating further aggregation when it returns to the bulk). Langmuir trough measures the surface pressure of the solution. When a higher surface pressure is observed, an increased amount of protein is presented at the air-water interface.

1.6.4 Small-angle X-ray scattering

Small-angle X-ray scattering (SAXS) is a novel method that is used to study structural properties at a nanoscale.[104] This method can be used to build 3D models of macromolecular complexes and study equilibria and kinetic along with flexible components. SAXS work provides information about the elastic scattering of photons. SAXS has been used to correlate the structure information to the protein stability information obtained by SEC and protein thermal shifts.[105] It was able to show important differences between an IgG1 and an IgG4 such as the IgG1 having smaller molecular volumes than the IgG4 and could be fitted to the 3D molecular

envelopes. SAXS can also provide more accurate atomic-level information of molecules in solution, which is an advantage over crystallization techniques which allows the detection of conformational flexibility.[106] The use of this technique allows for important information such as flexibility, dynamic conformational changes, and is not affected by rotation of the molecules, that provide a more in-depth understanding of the interaction and aggregation properties of macromolecules.

1.7 Chapter Reviews

1.7.1 The Use of a GroEL-BLI Biosensor to Rapidly Assess Preaggregate Populations for Antibody Solutions Exhibiting Different Stability Profiles. (Chapter 2)

An automated method using biotinylated GroEL-streptavidin biosensors with Bio-Layer Interferometry (GroEL-BLI) was evaluated to detect the formation of transiently formed, pre-aggregate species in various pharmaceutically relevant monoclonal antibody (mAb) samples. The relative aggregation propensity of various IgG1 and IgG4 mAbs was rank-ordered using the GroEL-BLI biosensor method, and the least stable IgG4 mAb was subjected to different stresses including elevated temperatures, acidic pH, and addition of guanidine-HCl. The GroEL-BLI biosensor detects mAb pre-aggregate formation mostly prior to, or sometimes concomitantly with, observing soluble aggregates and subvisible particles using size exclusion chromatography (SEC) and microflow imaging (MFI), respectively. A relatively unstable bispecific antibody (Bis-3) was shown to bind the GroEL-biosensor even at low temperatures (25^{o}C). During thermal stress (50°C, one hour), increased Bis-3 binding to GroEL-biosensors was observed prior to aggregation by SEC or MFI. Transmission electron microscopy (TEM) analysis of Bis-3 pre-aggregate-GroEL complexes revealed, in some cases, potential hydrophobic interaction sites between the Fc domain of the bispecific antibody and GroEL protein. The automated BLI method not only enables

detection of transiently formed pre-aggregate species that initiate protein aggregation pathways, but also permits rapid mAb formulation stability assessments at low volumes and low protein concentrations.

1.7.2 Evaluation of Hydrogen Exchange Mass Spectrometry as a Stability-Indicating Method for Formulation Excipient Screening for an IgG4 Monoclonal Antibody. (Chapter 3)

Antibodies are molecules that exhibit diverse conformational changes on different timescales, and there is ongoing interest to better understand the relationship between antibody conformational dynamics and storage stability. Physical stability data for an IgG4 monoclonal antibody (mAb-D) were gathered through traditional forced degradation (temperature and stirring stresses) and accelerated stability studies, in the presence of different additives and solution conditions, as measured by differential scanning calorimetry, size exclusion chromatography, and microflow imaging. The results were correlated with hydrogen exchange mass spectrometry (HX-MS) data gathered for mAb-D in the same formulations. Certain parameters of the HX-MS data, including hydrogen exchange in specific peptide segments in the CH2 domain, were found to correlate with stabilization and destabilization of additives on mAb-D during thermal stress. No such correlations between mAb physical stability and HX-MS readouts were observed under agitation stress. These results demonstrate that HX-MS can be set up as a streamlined methodology (using minimal material and focusing on key peptide segments at key time points) to screen excipients for their ability to physically stabilize mAbs. However, useful correlations between HX-MS and either accelerated or real-time stability studies will be dependent on a particular mAb's degradation pathway(s) and the type of stresses used.

1.7.3 A Formulation Development Approach to Identify and Select Stable Ultra-High-Concentration Monoclonal Antibody Formulations With Reduced Viscosities. (Chapter 4)

High protein concentration formulations are required for low-volume administration of therapeutic antibodies targeted for subcutaneous, self-administration by patients. Ultra-high concentrations (150 mg/mL) can lead to dramatically increased solution viscosities, which in turn can lead to stability, manufacturing, and delivery challenges. In this study, various categories and individual types of pharmaceutical excipients and other additives (56 in total) were screened for their viscosity reducing effects on 2 different mAbs. The physicochemical stability profile, as well as viscosity ranges, of several candidate antibody formulations, identified and designed based on the results of the excipient screening, were evaluated over a 6-month time period under accelerated and real-time storage conditions. In addition to reducing the solution viscosities to acceptable levels for parenteral administration (using currently available and acceptable delivery devices), the candidate formulations did not result in notable losses of physicochemical stability of the 2 antibodies on storage for 6 months at 25°C. The experiments described here demonstrate the feasibility of a formulation development and selection approach to identify candidate high-concentration antibody formulations with viscosities within pharmaceutically acceptable ranges that do not adversely affect their physicochemical storage stability.

1.7.4 Development of Scale-Down Assays for Assessment of Mechanism(s) of Tangential Flow Filtration Instability of Proteins. (Chapter 5)

During the formulation process of drug product development, many proteins have to go through diafiltration and concentration. Tangential Flow Filtration (TFF) is one of the most

common ways to do this. Due to the high shear rate, contact with the membrane, pump strain, and pressure, this process is can cause major stress of the protein and induce aggregation. This instability has a great effect on some molecules compared to others. This is the case with molecules 8 and 9 compared to the more stable molecules 1 and 2. The four antibodies were studied by their biophysical components, colloidal stability, and interfacial properties. The information was used to look at trends between these studies and their aggregation propensities when using TFF.

1.7.5 Conclusions and Future Work. (Chapter 6)

Protein aggregation can cause many pharmaceutical issues when developing a protein drug product. When proteins aggregate, they can have a reduced or even no biological activity.[107] Another problem is the immunogenicity effects aggregation can cause when administered.[44,108] Therefore, aggregation needs to be monitored and controlled throughout the manufacturing process and during long terms storage as well as during patient administration. Newer techniques are needed in order to better predict and understand how and why protein therapeutic candidates aggregate. With the development of these techniques, more can be done to create more stable and better quality protein drug products for treating patients in need.

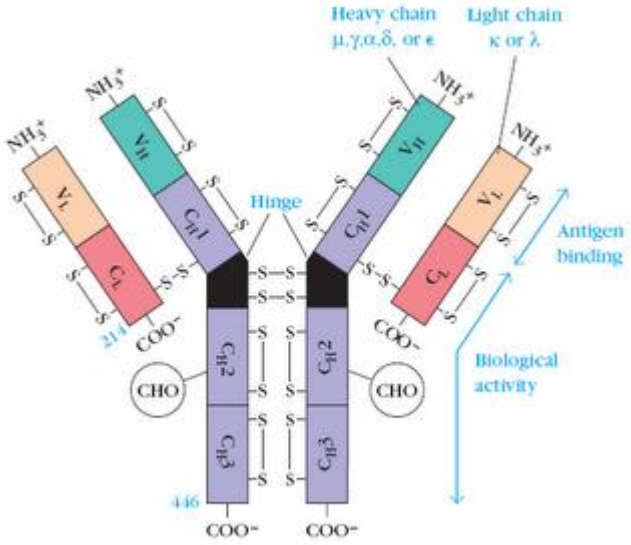

Figure 1.1: Schematic of the primary structure of an IgG1 antibody.[109]

A representation of an IgG1 antibody consisting of two heavy chains and two light chains that are connected by disulfide bonds. Each heavy chain has 3 constant domains (purple) and 1 variable domain (teal). Each light chain has one constant domain (pink) and one variable domain (yellow). The constant domain controls the Fc effector function biological activity and the variable domains control the antigen binding biological activity.

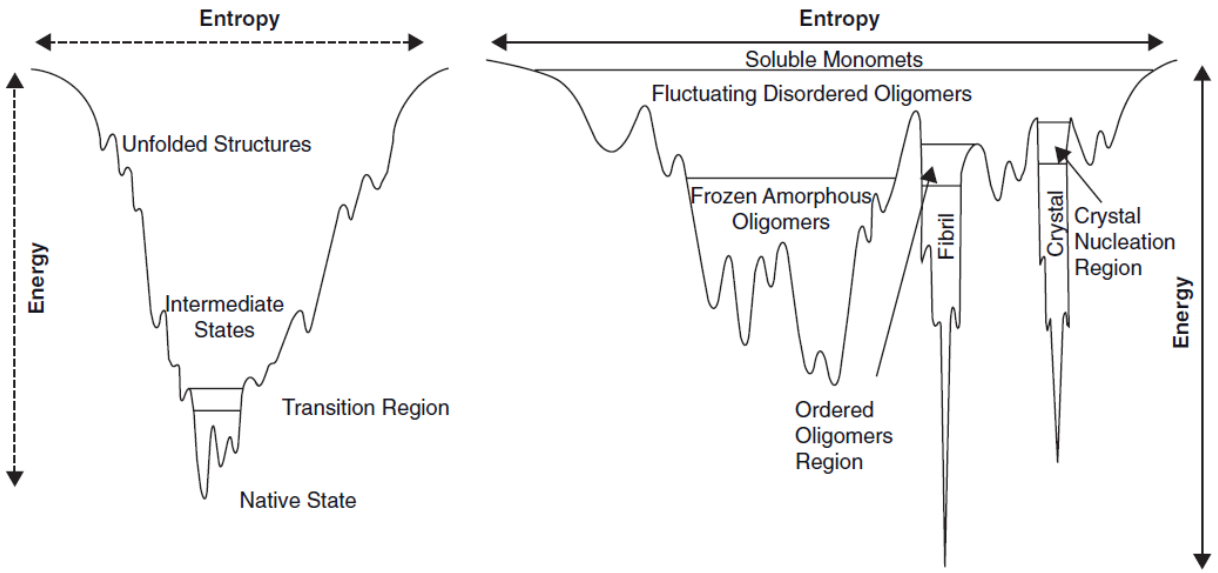

Figure 1.2: Energy states of protein molecules during folding (left panel) and aggregation (right panel).[44]

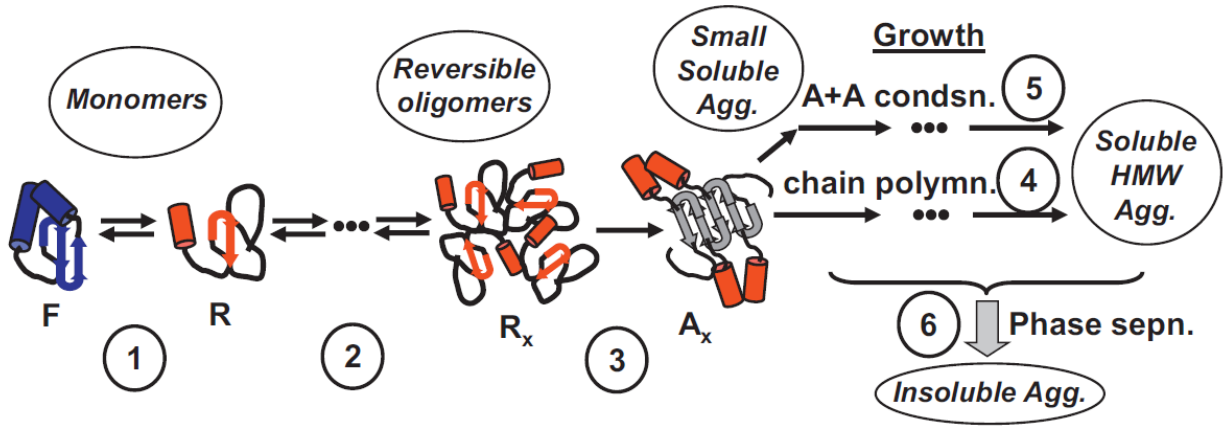

Figure 1.3: Overview of protein aggregation pathway.[110,111]

The native state (F) can take multiple pathways when aggregating that initiates with a common intermediate. R and R_x represent reversible intermediates followed by irreversible formation of small soluble aggregates (A) that may grow through several mechanisms to reach the size of soluble higher molecule weight (HMW) aggregates and eventually the formation of insoluble aggregates (particles of varying size).

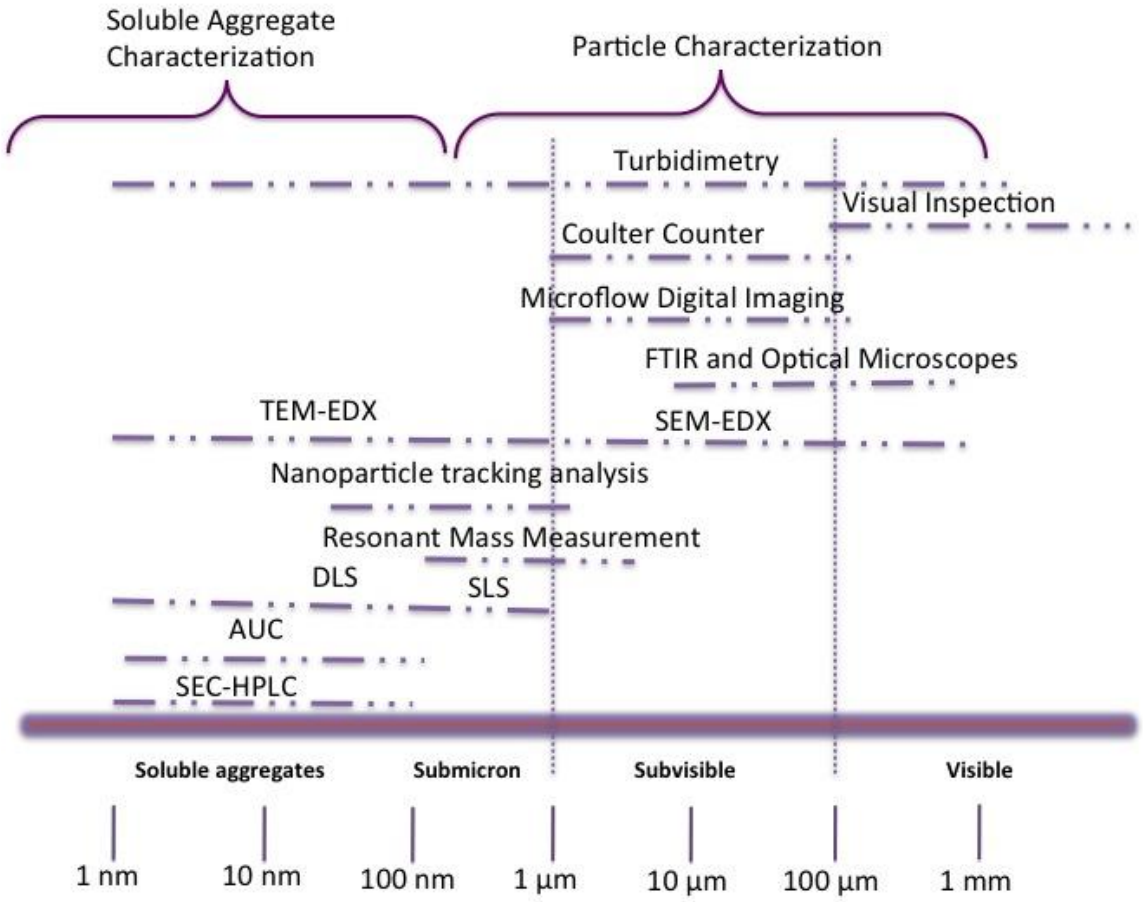

Figure 1.4: Analytical methods for characterizing protein aggregation and particle formation.[112]

1.8 References

1. Forthal DN 2014. Functions of Antibodies. Microbiology Spectrum 2(4):1-17.

2. Harry W. Schroeder J, Cavacini L 2010. Structure and function of immunoglobulins. Journal of Allergy and Clinical Immunology 125(2):S41-S52.

3. Boundless. Antibody Structure and Function. ed.

4. Vidarsson G, Dekkers G, Rispens T 2014. IgG subclasses and allotypes: from structure to effector functions. Frontiers in Immunology 5(520).

5. Nirula A, Glaser SM, Kalled SL, Taylora FR 2011. What is IgG4? A review of the biology of a unique immunoglobulin subtype. Current Opinion in Rheumatology 23:119-124.

6. Heads JT, Adams R, D'Hooghe LE, Page MJT, Humphreys DP, Popplewell AG, Lawson AD, Henry AJ 2012. Relative stabilities of IgG1 and IgG4 Fab domains: Influence of the light–heavy interchain disulfide bond architecture. Protein Science 21:1315-1322.

7. Kraha S, Sellmann C, Laura Rhielb, Christian Schrötera, Dickgiesser S, Beck J, Zielonka S, Toleikis L, Hock B, Kolmar H, Becker S 2017. Engineering bispecific antibodies with defined chain pairing. New Biotechnology 39:167-173.

8. Spiess C, Zhai Q, Carter PJ 2015. Alternative molecular formats and therapeutic applications for bispecific antibodies. molecular Immunology 67:95-106.

9. Kontermann RE, Brinkmann U 2015. Bispecific antibodies. Drug Discovery Today 20(7):838-847.

10. Dinner AR, Karplus M 1999. Is Protein Unfolding the Reverse of Protein Folding? A Lattice Simulation Analysis. Journal of Molecular Biology 292:403-419.

11. Want W, Roberts CJ. 2010. Aggregation of Therapeutic Proteins. ed.

12. Chi EY, Krishnan S, Randolph TW, Carpenter JF 2003. Physical Stability of Proteins in Aquesous Solution: Mechanism and Driving Forces in Nannative Protein Aggregation. Pharmaceutical Research 20(9):1325-1336.

13. Dill KA 1990. Dominant forces in protein folding. Biochemistry 29(31):7133-7155.

14. McGaughey GB, Gagne M, Rappe AK 1998. pi-Stacking Interactions. The Journal of Biological Chemistry 25:15458-15462.

15. Zhou Y, Linhananta A 2002. Thermodynamics of an all - atom off - lattice model of the fragment B of staphylococcal protein. Journal of Physical Chemistry B 106:1481-1485.

16. Street AG, Mayo SL 1999. Intrinsic β-sheet propensities result from van der Waals interactions between side chains and the local backbone. Proceedings of the National Academy of Sciences of the United States of America 96(16):9074-9076.

17. Ramakrishnan C, Ramachandran GN 1965. Stereochemical Criteria for Polypeptide and Protein Chain Conformations. Biophysical Journal 5(6):909-933.

18. Dong F, Zhou H-X 2002. Electrostatic Contributions to T4 Lysozyme Stability: Solvent-Exposed Charges versus Semi-Buried Salt Bridges. Biophysical Journal 83(3):1341-13447.

19. Kumar S, Nussinov R 2002. Relationship between ion pair geometries and electrostatic strengths in proteins Biophysical Journal 83:1595-1612.

20. Wang W, Hecht MH 2002. Rationally designed mutations convert de novo amyloid-like fibrils into monomeric B-sheet proteins. Proceedings of the National Academy of Sciences of the United States of America 99(5):2760-2765.

21. Wang W, Nema S, Teagarden D 2010. Protein aggregation—Pathways and influencing factors. International Journal of Pharmaceutics 390:89-99.

22. Trivedi M, Davis RA, Shabaik Y, Roy A, Verkhivker G, Laurence J, Middaugh CR, Siahaan TJ 2009. The role of covalent dimerization on the physical and chemical stability of the EC1 domain of human E - cadherin. Journal of Pharmaceutical Sciences 98(10):3562-3574.

23. Bam NB, Cleland JL, Yang J, Manning MC, Carpenter JF, Kelley RF, Randolph TW 1998. Tween protects recombinant human growth hormone against agitation induced damage via hydrophobic interactions. Journal of Pharmaceutical Sciences 87(12):1554-1559.

24. Li Y, IV WFW, J.Roberts C 2009. Characterization of High-Molecular-Weight Nonnative Aggregates and Aggregation Kinetics by Size Exclusion Chromatography With Inline Multi-Angle Laser Light Scattering. Journal of Pharmaceutical Sciences 98(11):3997-4016.

25. Carpentera JF, Randolph TW, Jiskoot W, Crommelind DJA, Middaugh CR, Winter G, Fan Y-X, Kirshner S, Verthelyi D, Kozlowski S, Clouse KA, Swann PG, Rosenberg A, Cherney B 2009. Overlooking Subvisible Particles in Therapeutic Protein Products: Gaps that may compromise product quality. Journal of Pharmaceutical Sciences 98(4):1201-1205.

26. IV WFW, Hodgdon TK, Kaler EW, Lenhoff AM, Roberts CJ 2007. Nonnative Protein Polymers: Structure, Morphology, and Relation to Nucleation and Growth. Biophysical Journal 93:4392-4403.

27. Fink AL 1998. Protein aggregation: folding aggregates, inclusion bodies and amyloid. Folding and Design 3(1):R9-R23.

28. Curtis-Fisk J, Spencer RM, Weliky DP 2008. Native conformation at specific residues in recombinant inclusion body protein in whole cells determined with sold - state NMR spectroscopy Journal of American Chemical Society 130(38):12568-12569.

29. Kopito RR 2000. Aggresomes, inclusion bodies, and protein aggregation. Trends in Cell biology 10(12):524-530.

30. Meredith SC 2006. Protein denaturation and aggregation: Cellular responses to denatured and aggregated proteins. Annals of The New York Academy of Sciences 1066(1):181-221.

31. Plakoutsi G, Bemporad F, Calamai M, Taddei N, Dobson CM, Chiti F 2005. Evidence for a mechanism of amyloid formation involving molecular reorganisation within native-like precursor aggregates. Journal of Molecular Biology 351(910-922):910.

32. Laurence JS, Middaugh CR. 2010. Fundamental Structures and Behaviors of Proteins. ed.

33. Wu H, Kroe-Barrett R, Singh S, Robinson AS, Roberts CJ 2014. Competing aggregation pathways for monoclonal antibodies. Federation of European Biochemical Societies 588:936-941.

34. Clark AC 2008. Protein folding: Are we there yet? Archives Biochemistry Biophysics 469(1):1-3.

35. Vendruscolo M, Paci E, Karplus M, Dobson CM 2003. Structures and relative free energies of partially folded states of proteins. Proceedings of the National Academy of Sciences of the United States of America 100(25):14817-14821.

36. Grantcharova V, Alm EJ, Baker D, Horwich AL 2001. Mechanisms of Protein Folding. Current Opinion in Sturctural Biology 11(1):70-82.

37. Fields GB, Alonso DOV, Stigter D, Dill KA 1992. Theory for the aggregation of proteins and copolymers. Journal of Physical Chemistry 96(10):3974-3981.

38. Damodaran S, Song K 1988. Kinetics of adsorption of proteins at interfaces: Role of protein conformation in diffusional adsorption. Biochimica et Biophysica Acta 954(3):253-264.

39. Uversky VN, Fink AL. 2006. Part A: Protein Aggregation and Conformational Diseases. ed.

40. IV WFW, Young TM, Roberts CJ 2009. Principles, approaches, and challenges for predicting protein aggregation rates and shelf life Journal of Pharmaceutical Sciences 98(4):1246-1277.

41. Liu J, Nguyen MDH, Andya JD, Shire SJ 2005. Reversible self-association increases the viscosity of a concentrated monoclonal antibody in aqueous solution. Journal of Pharmaceutical Sciences 94(9):1928-1940.

42. Kanai S, Liu J, Patapoff TW, Shire SJ 2008. Reversible self-association of a concentrated monoclonal antibody solution mediated by Fab-Fab interaction that impacts solution viscosity. Journal of Pharmaceutical Sciences 97(10):4219-4227.

43. Ecroyd H, Carver JA 2008. The effect of small molecules in modulating the chaperone activity of alpha B-crystallin against ordered and disordered protein aggregation. The FEBS Journal 275(5):935-947.

44. Gsponer J, Vendruscolo M 2006. Theoretical approaches to protein aggregation. Protein and Peptide Letters 13:287-293.

45. Guo Z, Eisenberg D 2006. Runaway domain swapping in amyloid-like fibrils of T7 endomuclease I. Proceedings of the National Academy of Sciences of the United States of America 103(21):8041-8047.

46. Wang X, Das TK, Singh SK, Kumar S 2009. Potential aggregation prone regions in biotherapeutics: A survey of commercial monoclonal antibodies mAbs 1(3):254-267.

47. Cromwell MEM, Hilario E, Jacobson F 2006. Protein aggregation and bioprocessing The AAPS Journal 8(3):E572-E579.

48. Manning MC, Chou DK, Murphy BM, Payne RW, Katayama DS 2010. Stability of protein pharmaceuticals. Pharmaceutical Research 27(4):544-575.

49. S K, B M, CJ T, N S, R. N 2000. Folding and binding cascades: Dynamic landscapes and population shifts. Protein Science 9(1):10-19.

50. CJ T, Kumar S MB, R N 1999. Folding funnels, binding funnels, and protein function. Protein Science 8(6):1181-1190.

51. Jaenicke R 1991. Protein stability and molecular adaptation to extreme conditions. European Journal of Biochemistry banner 202:715-728.

52. Eisenthal R, Peterson ME, Daniel RM, Danson MJ 2006. The thermal behaviour of enzyme activity: Implications for biotechnology. Trends in biotechnology 24(7):289-292.

53. Broersen K, Weijers M, Groot Jd, Hamer RJ, Jongh HHJd 2007. Effect of protein charge on the generation of aggregation-prone conformers. Biomacromolecules 8:1648-1656.

54. Fitzsimons SM, Mulvihill DM, Morris ER 2006. Denaturation and aggregation processes in thermal gelation of whey proteins resolved by differential scanning calorimetry. Food Hydrocolloids 21(4):638-644.

55. Sukumar M, Doyle BL, Combs JL, Pekar AH 2004. Opalescent appearance of an IgG1 antibody at high concentrations and its relationship to noncovalent association. Pharmaceutical Research 21(7):1087-1093.

56. Piedmonte DM, Summers C, McAuley A, Karamujic L, Ratnaswamy G 2007. Sorbitol crystallization can lead to protein aggregation in frozen protein formulations. Pharmaceutical Research 24(1):136-146.

57. Heller MC, Carpenter JF, Randolph TW 1997. Manipulation of lyophilization induced phase separation: Implications for pharmaceutical proteins. Biotechnology Progress 13(5):590-596.

58. Speed MA, King J, Wang DIC 2000. Polymerization mechanism of polypeptide chain aggregation. Biotechnology and Bioengineering 54(4):333-343.

59. Macchioni A, Ciancaleoni G, Zuccaccia C, Zuccaccia D 2007. Determining accurate molecular sizes in solution through NMR diffusion spectroscopy. Chemical Society Reviews 37(3):479-489.

60. Schein CH 1990. Solubility as a function of protein structure and solvent components. Nature Bio 8:308-317.

61. Giger K, Vanam RP, Seyrek E, Dubin PL 2008. Suppression of insulin aggregation by heparin. Biomacromolecules 9:2338-2344.

62. Chung K, Kim J, Cho B-K, Ko B-J, Hwang B-Y, Kim B-G 2007. How does dextran sulfate prevent heat induced aggregation of protein? The mechanism and its limitation as aggregation inhibitor. Biochimica et Biophysica Acta-Proteins and Proteomics 1774(2):249-257.

63. Buren NV, Rehder D, Gadgil H, Matsumura M, Jacob J 2009. Elucidation of two major aggregation pathways in an IgG2 antibody. Journal of Pharmaceutical Sciences 98(9):3013-3030.

64. Alford JR, Kendrick BS, Carpenter JF, Randolph TW 2008. High concentration formulations of recombinant human interleukin-1 receptor antagonist: II. Aggregation Kinetics. Journal of Pharmaceutical Sciences 97(8):3005-3021.

65. Kita Y, Arakawa T 2002. Salts and glycine increase reversibility and decrease aggregation during thermal unfolding of ribonuclease-A. Bioscience, Biotechnology, and Biochemistry 66(4):880-882.

66. Xia Y, Park Y-D, Mu H, Zhou H-M, Wang X-Y, Meng F-G 2007. The protective effects of osmolytes on arginine kinase unfolding and aggregation. International Journal of Biological Macromolecules 40:437-443.

67. Goyal K, Walton LJ, Tunnacliffe A 2005. LEA proteins prevent protein aggregation due to water stress. Biochemal Journal 388:151-157.

68. Schülea S, Schulz-Fademrecht T, Garidel P, Bechtold-Peters K, W.Frie 2008. Stabilization of IgG1 in spray-dried powders for inhalation. European Journal of Pharmaceutics and Biopharmaceutics 69(3):793-807.

69. Rondeau P, Armenta S, Caillens H, Chesne S, Bourdon E 2007. Assessment of temperature effects on beta-aggregation of native and glycated albumin by FTIR spectroscopy and PAGE: Relations between structural changes and antioxidant properties. Archives Biochemistry and Biophysics 460(1):141-150.

70. Ignatova Z, Gierasch LM 2006. Inhibition of protein aggregation in vitro and in vivo by a natural osmoprotectant. Proceedings of the National Academy of Sciences of the United States of America 103(36):13357-13361.

71. Tsumoto K, Ejima D, Kita Y, Arakawa T 2005. Why is arginine effective in suppressing aggregation? Protein & Peptide Letters 12(7):613-619.

72. Katayama DS, Nayar R, Chou DK, Valente JJ, Cooper J, Henry CS, Velde DGV, Villarete L, Liu CP, Manning MC 2006. Effect of buffer species on the thermally induced aggregation of interferon-tau. Journal of Pharmaceutical Sciences 95(6):1212-1226.

73. Wang W, Li N, Speaker S. 2010. External Factors Affecting Protein Aggregation. ed.

74. Zhang L, Lu D, Liu Z 2008. How native proteins aggregate in solution: A dynamic Monte Carlo simulation. Biophysical Chemistry 133(1-3):71-80.

75. Yazdanparast R, Esmaeili MA, Khodagholi F 2007. Control of aggregation in protein refolding: Cooperative effects of artificial chaperone and cold temperature. International Journal of Biological Macromolecules 40(2):126-133.

76. Randolph TW, Jones LS 2002. Surfactant-protein interactions Pharmaceutical Biotechnology 13:159-175.

77. Kiese S , Papppenberger A , Friess W , Mahler HC 2008. Shaken, not stirred: Mechanical stress testing of an IgG1 antibody . J Pharm Sci. 97(10):4347-4366.

78. Vessely CR, Carpenter JF, Schwartz DK 2005. Calcium-induced changes to the molecular conformation and aggregate structure of beta-casein at the air-water interface. Biomacromolecules 6(6):3334-3344.

79. Volkin DB, Klibanov AM 1989. Minimizing protein inactivation. T E Creighton, Ed, Protein Function: Practical Approach:1-24.

80. Kiese S, Papppenberger A, Friess W, Mahler H-C 2008. Shaken, not stirred: Mechanical stress testing of an IgG1 antibody. Journal of Pharmaceutical Sciences 97(10):4347-4366.

81. Hu D, Qin Z, Xue B, Fink AL, Uversky VN 2008. Effect of methionine oxidation on the structural properties, conformational stability, and aggregation of immunoglobulin light chain LEN. Biochemistry 47:8665-8677.

82. Harris RJ, Shire SJ, Winter C 2004. Commercial Manufacturing Scale Formulation and Analytical Characterization of Therapeutic Recombinant Antibodies. Drug Development Research 61(3):137-154.

83. Kerwin BA, Remmele RL 2007. Protect from light: Photodegradation and protein biologics. Journal of Pharmaceutical Sciences 96(6):1468-1479.

84. Vanhooren A, Devreese B, Vanhee K, Beeumen JV, Hanssens I 2002. Photoexcitation of tryptophan groups induces reduction of two disulfi de bonds in goat alpha-lactalbumin Biochemistry 41(36):11035-11043.

85. Reissner KJ, Aswad DW 2003. Deamidation and Isoaspartate Formation in Proteins: unwanted alterations or surreptitious signals? Cellular and Molecular Life Sciences 60:1281-1295.

86. Chennamsetty N, Helk B, Voynov V, Kayser V, Trout BL 2009. Aggregation prone motifs in human immunoglobulin. Journal of Molecular Biology 391(2):404-413.

87. Pawara AP, DuBaya KF, Zurdoa J, Chitib F, Vendruscoloa M, Dobson CM 2005. Prediction of aggregation-prone and aggregation-susceptible regions in proteins in neurodegenerative diseases. Journal of Molecular Biology 350(2):379-392.

88. Roberts CJ 2014. Therapeutic protein aggregation: mechanisms, design, and control. Trends in Biotechnology 32(7):372-380.

89. Llyod L 2014. Size-Exclusion Chromatography of Protein Aggregation in Biopharmaceutical Development and Production. LCGC 32(4):30-35.

90. Hiemenz PC, Rajagopalan R. Colloid and surface chemistry: Scope and variables ed.

91. Shire SJ 2006. 2005 AAPS Biotechnology Conference Open Forum on Aggregation of Protein Therapeutics-Panel Discussion June 5-8, 2005 San Francisco, CA The AAPS Journal 8(4):E644-E654.

92. Arakawa T, Philo JS, Ejima D, Tsumoto K, Arisaka F 2006. Aggregation analysis of therapeutic proteins, part 1: General aspects and techniques for assessment BioProcess International 4(10):42-43.

93. Lomakin AV, Benedek G, Teplow DB 1999. Monitoring protein assembly using quasielastic light scattering spectroscopy. Methods in enzymology.

94. Arakawa T, Philo JS, Ejima D, Tsumoto K, Arisaka F 2009. Aggregation analysis of therapeutic proteins, part 2: Analytical ultracentrifugation and dynamic light scattering. BioProcess International.

95. Mintova S, Petko N, Karaghiosoff K, Bein T 2002. Crystallization of nanosized MEL - type zeolite from colloidal precursors. Materials Science and Engineering 19(1-2):111-114.

96. Zimm BH 1946. Application of the methods of molecular distribution to solutions of large molecules The Journal of Chemical Physics 14(3).

97. Wen J, Arakawa T, S.Philo J 1996. Size-Exclusion Chromatography with On-Line Light-Scattering, Absorbance, and Refractive Index Detectors for Studying Proteins and Their Interactions. Analytical Biochemistry 240(2):155-166.

98. Akers MK, Larrimore D, Guazzo D. 2002. Parenteral Quality Control: Sterility, Pyrogen, Particulate, and Package Integrity Testing. ed.

99. Sharma VK, Kalonia DS. 2010. Experimental Detection and Characterization of Protein Aggregates. ed.

100. Naik S, Kumru O, Cullom M, Telikepalli S, Lindboe E, Roop T, Joshi S, Amin D, Gao P, Middaugh C, Volkin D, Fisher M 2014. Probing structurally altered and aggregated states of therapeutically relevant proteins using GroEL coupled to Bio-Layer Interferometry. Protein Science 23(10):1461-1478.

101. Pace SE, Joshi SB, Esfandiary R, Stadelman R, Bishop SM, Middaugh CR, Fisher MT, Volkin DB 2017. The Use of a GroEL-BLI Biosensor to Rapidly Assess Preaggregate Populations for Antibody Solutions Exhibiting Different Stability Profiles. Journal of Pharmaceutical Sciences 107(2):559-570.

102. IV RTT, Pace SE, Mills BJ, Joshi SB, Esfandiary R, Middaugh CR, Weis DD, Volkin DB 2018. Evaluation of Hydrogen Exchange Mass Spectrometry as a Stability-Indicating Method for Formulation Excipient Screening for an IgG4 Monoclonal Antibody. Journal of Pharmaceutical Sciences 107(4):1009-1019.

103. Ghazvini S, Kalonia C, Volkin DB, Dhar P 2016. Evaluating the Role of the Air-Solution Interface on the Mechanism of Subvisible Particle Formation Caused by Mechanical Agitation for an IgG1 mAb. Journal of Pharmaceutical Sciences 105(5):1643-1656.

104. Blanchet CE, Svergun DI 2013. Small-Angle X-Ray Scattering on Biological Macromolecules and Nanocomposites in Solution. The Annual Review of Physical Chemistry 64:37-54.

105. Song Y, Yu D, Mayani M, Mussa N, Li ZJ 2018. Monoclonal antibody higher order structure analysis by high throughput protein conformational array. mAbs 10(3):397-405.

106. Hammel M 2012. Validation of macromolecular flexibility in solution by small-angle X-ray scattering (SAXS). European Biophysics Journal 41:789-799.

107. Townsend MW, Byron PR, DeLuca PP 1990. The effects of formulation additives on the degradation of freeze-dried ribonuclease. Pharmaceutical Research 7(10):1086-1091.

108. Ellis RJ, Minton AP 2006. Protein aggregation in crowded environments. Biochemal Chemistry 387(5):485-497.

109. Khan M. 2012. Basic Structure of Antibodies,Immune system,Immunity., ed.

110. Roberts CJ, Das TK, Sahin E 2011. Predicting solution aggregation rates for therapeutic proteins: Approaches and challenges. International Journal of Pharmaceutics 418(2):318-333.

111. YiLi, Ogunnaike BA, J.Roberts C 2010. Multi-Variate Approach to Global Protein Aggregation Behavior and Kinetics: Effects of pH, NaCl, and Temperature for a-Chymotrypsinogen A. Journal of Pharmaceutical Sciences 99(2):645-662.

112. MVCS. Overview of Particles and Aggregates. ed.

Chapter 2 The Use of a GroEL-BLI Biosensor to Rapidly Assess Preaggregate Populations for Antibody Solutions Exhibiting Different Stability Profiles

(Pace SE, Joshi SB, Esfandiary R, Stadelman R, Bishop SM, Middaugh CR, Fisher MT, Volkin DB 2018. The Use of a GroEL-BLI Biosensor to Rapidly Assess Preaggregate Populations for Antibody Solutions Exhibiting Different Stability Profiles. Journal of Pharmaceutical Sciences 107(2):559-570.)

2.1 Introduction

Patients worldwide depend on therapeutic protein drugs to treat a wide number of diseases such as diabetes, cancer, immune disorders and infections.[1] The number of protein-based medical drug products on the market is increasing rapidly, especially with the expanded use of monoclonal antibodies (mAbs).[2] The complexity of biopharmaceutical drug candidates is also increasing to now include bispecific antibodies, antibody-drug conjugates, single chain fragments variable (scFv) and modified natural enzymes.[3] To ensure safety and efficacy of protein therapeutic drugs across their shelf-life, key biological and structural characteristics that lead to product degradation need to be well understood and controlled when formulating a new biopharmaceutical candidate. To this end, critical quality attributes[4], such as potency, solubility and physicochemical stability, are used to define the overall stability profile of the protein drug candidate across the entire shelf-life. Numerous strategies now exist where directed engineering methods are implemented to rationally mutate suspect surface residues that decrease aggregation while not impacting biological activity (e.g., maintaining target affinity of mAbs while improving stability).[5] In other instances, purposeful engineering and improvement of antigen binding or Fc receptor binding sites, can have the undesired effect of increasing aggregation[5] or altering the conformational dynamics and physical stability[6], of the engineered antibodies.

Protein-based drugs can be exposed to many types of environmental stresses (e.g., temperature, agitation, light, etc.) during manufacturing, long-term storage, distribution and administration[7]. These stresses can cause proteins to aggregate to varying extents, depending on the specific protein and formulation conditions, thereby reducing potency and/or increasing immunogenicity risk upon patient administration. Aggregation is a complex multistep pathway in which native protein can form dynamic, folded or partially unfolded transient species that lead to

the formation of reversible and nonreversible intermediates or small aggregate clusters.[8] Elucidation of the exact steps of the aggregation pathway for a particular protein, formulation and stress can be experimentally and theoretically challenging. One important analytical challenge is the ability to monitor and capture any initially formed, structurally altered intermediates (i.e., pre-aggregates), which are transiently present and reversible in nature. Since commonly used analytical methods to characterize protein therapeutics are unable to specifically detect this initial step, it is difficult to prevent or limit its occurrence during formulation development or even during initial production since an effective analytical assay that detects these transient states and reports on early stage stabilization by excipients is lacking.

A recent strategy has been developed where a chaperone GroEL biolayer interferometry (BLI) biosensor is constructed to detect dynamic hydrophobic transients that occur prior to the formation of larger scale aggregation.[9] This detection scheme is based on the observation that chaperone proteins in cells capture and prevent or reverse misfolding of cellular proteins and are important in maintaining protein homeostasis within the cell.[10] The GroEL (hsp60) chaperonin is made up of 14 identical subunits with a molecular mass of 58K each that assemble into two stacked heptameric rings. Within the center of these tail to tail assembled rings, a central hydrophobic, 45 Å wide, protein-binding cavity is present that can easily accommodate aggregation prone hydrophobic regions of dynamically fluctuating, partially folded or misfolded proteins. Upon ATP binding, the GroEL binding cavity switches to a hydrophilic interior allowing the bound partially folded or even fully folded protein to be released into solution. The hydrolysis of ATP resets the system back to its higher affinity protein capture state.[11] The form of the chaperonin that is used to construct the biolayer interferometry biosensors is the nucleotide free form of GroEL since its binding affinity for hydrophobic partially folded proteins is high, sometimes approaching antigen

antibody affinities.[11] Previous work in our laboratories has shown that a biotinylated GroEL-streptavidin-BLI biosensor is able to capture and detect pre-aggregate species during stress with several pharmaceutically relevant protein molecules (polyclonal Ab, IgG1 mAb and a heparin binding growth factor, FGF-1) before irreversible aggregation could be detected by size exclusion chromatography (SEC).[9] In addition to increased binding during various stress conditions, the protein molecules also showed some binding under unstressed temperature conditions (25^{o}C). This detection/binding of pre-aggregates was verified to be specific for the chaperonin binding site because the binding was most often reversed by adding ATP to the GroEL-protein substrate complex that was immobilized on the BLI biosensor. In addition, preliminary TEM data of released GroEL complexes from the biosensor surface exposed to stressed mAb solution distinctly showed the presence of bound densities attributed to captured antibody proteins.[9]

In this work, we further explore and develop the utility of this analytical technology[9] by using GroEL-BLI biosensors linked to an automated BLI technology platform (the Octet® 96 well system). The automated method was used to detect the formation of the pre-aggregate species for larger sets of various mAbs (both IgG1 and IgG4), as well as a bispecific antibody, to assess aggregation propensity of multiple samples simultaneously. This series of pharmaceutically relevant mAbs showed variable rates of aggregation when exposed to a variety of different stresses (e.g., acidic pH, Gdn-HCl, temperature cycling), conditions shown previously to generate pre-aggregate species with other mAbs.[12-14] The GroEL biosensor results were compared with the rate and extent of soluble aggregates and sub-visible particulates formation as measured by SEC and MFI, respectively. TEM analysis was also used as an orthogonal method to structurally detect pre-aggregate mAb species that complexed to the GroEL protein (both in solution and released from

the biosensor surface) with the goal of specifically pinpointing particular hydrophobic regions on the Ab structure that leads to aggregation and product degradation.

2.2 Materials and Methods

2.2.1 Materials

Two IgG1 monoclonal antibodies (mAb-E & mAb-J), an IgG4 monoclonal antibody (mAb-D), and a bispecific antibody (Bis-3) were provided by MedImmune (Gaithersburg, Maryland). The mAb-E was provided as a 100 mg/mL protein solution in 25 mM Histidine, 8% Trehalose pH 6.0, mAb-J as a 150 mg/mL protein solution in 25 mM Histidine, 100 mM Arginine-HCl, 90 mM Sucrose, pH 6.5, mAb-D as a 50 mg/mL protein solution in 50 mM Acetate, 100 mM NaCl, pH 5.5, and Bis-3 as a 4.2 mg/mL protein solution in 20 mM Sodium Phosphate, 235 mM Sucrose, pH 7.2. The concentration of the various Abs and GroEL was measured after dialysis (into 5 mM citrate-phosphate buffer (CP) containing either 150 or 500 mM NaCl at pH 7.4 as described below) with an Agilent 8453 UV-visible spectrophotometer (Palo Alto, California). The absorption values at 280 nm were averaged for triplicate analysis and extinction coefficients of 1.42 (mAb-E), 1.56 (mAb-J), 1.68 (mAb-D), and 1.54 $(mg/mL)^{-1}$ cm^{-1} (Bis-3) were used to calculate the protein concentration. FGF-1, used as an assay control in this work, was provided by Professor Mike Blaber at Florida State University.

Streptavidin (SA) biosensors were purchased from Fortébio (Menlo Park, California). Ninety six well black polypropylene plates were purchased from Greiner (Monroe, North Carolina). An XL25 dual channel pH meter, sodium chloride, guanidine hydrochloride, potassium chloride, EDTA, and LC-MS grade water were obtained from Fisher Scientific (Fair Lawn, New Jersey). Sodium phosphate dibasic (anhydrous), citric acid (anhydrous), and magnesium chloride

were purchased from Acros Organics (Fair Lawn, New Jersey). Glycerol, Trizma base, ATP, and BSA were obtained from Sigma Aldrich (St. Louis, Missouri).

2.2.2 Methods

2.2.2.1 *Biolayer Interferometry*

Samples were analyzed by biolayer interferometry using an Octet RED96 system (Fortebio, Menlo Park, CA) with the sample holder set at 25^{o}C, even for cases where samples were initially subjected to thermal stress (as described below). Biotinylated GroEL-Streptavidin biosensors were used to monitor the presence of pre-aggregates in antibody solutions using 9 steps to produce a sensogram as described below. Before a sensogram is obtained, each streptavidin biosensor is first hydrated for 10 min in GroEL buffer (50 mM Tris, 50 mM KCl, 10 mM $MgCl_2$, and 0.5 mM EDTA, pH 7.5) prior to start of the study. The automated nine step procedure is as follows: (1) an initial reference baseline of 30 sec is performed with GroEL buffer alone, (2) Biotinylated GroEL (b-GroEL-1mg/ml – 1 to 3 biotin adducts per GroEL oligomer [8]) is loaded onto the streptavidin biosensor for 170 sec followed by a (3) baseline determination that is performed in PBS. Once loaded, (4) a 220 sec blocking step was implemented to further diminish non-specific binding using BSA (1 mg/ml) as the blocking agent. This blocking step was followed by a 30 sec baseline wash that is performed with buffer identical to that used for the mAb (5). In the testing phase, (6) the association of stressed or unstressed antibody sample (concentration ranges from 0.2 to 5.0 mg/ml) with the GroEL biosensor is performed for 5 min, (7) followed by monitoring the dissociation phase for 220 sec using a buffer identical to that used for the antibody sample. To reverse the specific binding of the stressed antibody from the GroEL biosensor, (8) three pulses of 20 m*M* ATP in an osmolyte mixture of 4M Urea, 4M glycerol is used to remove bound antibody from GroEL (return to baseline indicates specific binding), and (9) a final baseline

is acquired for 60 sec using a buffer identical to that employed for the antibody and compared with the starting amplitude from step 5 (further described in Figure 1 in the Results section). As was shown previously, biotinylated GroEL remains tetradecameric and is fully functional under these solution conditions.[15]

2.2.2.2 *GroEL-BLI Method Optimization*

GroEL-BLI biosensor tips are pretreated with BSA to decrease possible nonspecific binding of mAb to any bare streptavidin biosensor surfaces. To insure that non-specific binding does not occur, the response of 1 mg/ml BSA binding to the streptavidin tip was examined with increasing concentration of GroEL loading. During step 2, concentrations of 0, 2.5, 5 ,10, 25, 100, 500, 1000 µg/mL GroEL were loaded onto individual biosensors in the automated OCTETRed96 system to evaluate loading capacity. Although BSA binding diminishes as GroEL binding increases (see Figure 2 in Naik et al., 2014)[9], as a precautionary step, during automated step 4, 1 mg/mL BSA was included in the buffer to block any nonspecific binding sites on the biosensor surface (Blocking step Figure 3A). The BSA blocking step may seem redundant when GroEL loading has been optimized (see also Figure 2 in reference 9), but in cases where GroEL loading has not been optimized (lower GroEL binding on the Biosensor), inclusion of the BSA blocking step simply insures that nonspecific binding of the test antibody sample does not occur. In fact, BSA loading onto bare streptavidin tips also leads to diminished non-specific Ab binding (Supplemental Figure S1). As a control, Step 6 was performed using a stable nonstressed antibody to evalute the amount of nonspecific/background binding occuring for each mAb prior to exposure of antibody solutions to stress conditions. A final concentration of 500 µg/mL GroEL was used (step 2) for future experiments.

2.2.2.3 *Size Exclusion Chromatography (SEC)*

The monomer, aggregate and fragment content of stressed antibody samples was assessed using a 7.8 x 30 cm^2 TOSOH TSK-Gel BioAssist G3SW_{XL} column and 6.0 mm ID x 4.0 cm TSK-Gel SW_{XL} guard column (TOSOH Biosciences, King of Prussia, Pennsylvania). Prior to analysis, the column was pre-equilibrated with 7-column volumes of mobile phase composed of 0.2 M sodium phosphate, pH 6.8. Removal of insoluble aggregates from the stressed samples was accomplished by centrifugation at 14,000 x *g* for five min before injection onto the column. Elution of the various species from the column was assessed by monitoring the UV absorbance at 214 and 280 nm (as described previously)[16] using a Shimadzu high-performance liquid chromatography system equipped with a photodiode array detector. Molecular weight standards (Biorad Laboratories, Hercules, California) were used to assess the efficiency of separation. Injection of antibody stored in the formulation buffer was also completed on the day of each time-point to assess day-to-day variability and column lifespan. Peaks corresponding to aggregates, monomer, and fragments were selected and the area under each peak was quantified using the LC Solutions data analysis package.

2.2.2.4 *Microflow Imaging (MFI)*

A DPA-4200 microflow imaging system (Protein Simple, Santa Clara, California) was used to count an image micron-sized subvisible particles in the size range of 2-100 μm. Stressed and control samples were added directly to the MFI without any prior dilution as described in detail elsewhere.[17] Buffer controls containing no protein, were also analyzed and subtracted from the protein-containing samples.

2.2.2.5 *Transmission electron microscopy (TEM)*

A JEOL JEM-1400 TEM operating at 100KV equipped with an AMT digital camera system was used to visualize the GroEL and GroEL-complexes. To form the GroEL-mAb complexes, mAb-D and Bis3 samples were heated at 50°C for 60 min in solution with a selected molar ratio of GroEL. To analyze biosensor released GroEL-Ab complexes, the Biosensor was loaded with the 60 min stress Ab sample and the complex was released onto EM grids by reducing the S-S biotinylated GroEL-Ab complexes with 50 mM dithiothreitol (DTT).[9] To assess complexes that form on the GroEL biosensor, S-S biotinylated GroEL was used since the complex is easily removed from the biosensor surface using 50 m*M* containing DTT solution. Two μL of the sample was placed on carbon coated Cu 300 square mesh copper grids (Electron Microscopy Sciences) that were glow discharged prior to use. The samples were incubated on the grids for 10 min, followed by a 3X wash with deionized water. The grids were then negatively stained with filtered (0.02 micron Whatman filters) 0.75% uranyl formate and imaged.

2.2.2.6 *Sample preparation and temperature stress treatment of mAbs*

To determine potential candidates for further analysis, long term thermal stress experiments were performed. Stock solutions of various mAbs that were initially stored at -80°C were dialyzed into 5 mM citrate-phosphate buffer (CP) containing either 150 mM or 500 mM NaCl at pH 7.4. The mAbs were then diluted using the CP buffer to achieve a protein concentration of 5 mg/mL (mAb-E, D, and J). The samples were filtered using 0.22 μm syringe filters in a laminar flow hood (Millipore, Billerica, Massachusetts). Aliquots of 1.5 mL were placed into 3 mL borosilicate glass type I vials and capped with rubber stoppers (West Pharmaceutical Services, Exton, Pennsylvania). Samples of all three mAbs were stored at 4, 50, 55, and 60 °C for various times in triplicate. Samples were then analyzed by GroEL-BLI after storage for two weeks.

2.2.2.7 *Sample preparation and stress treatment by pH shift with mAb-D*

The mAb-D stock solution was diluted using the CP buffer with 150mM NaCl to achieve a protein concentration of 5 mg/mL. The samples were then stressed by shifting the pH to 4.0 for 1 minute using 0.5 M HCl and then increasing the pH back to 7.4 by titrating with a 1 M Na phosphate stock solution. Using a concentrated stock solution allows one to adjust the pH of the solution with minimal dilution. A second set of samples were generated by shifting the pH to 5.0 and back to 7.4 after 1 min incubation. Once the pH reached 7.4, the samples were analyzed immediately using the GroEL-BLI, SEC and MFI.

2.2.2.8 *Sample preparation and stress treatment by thermal cycling of mAb-D*

The mAb-D stock solution was diluted using the CP buffer with 150 mM NaCl to achieve a protein concentration of 5 mg/mL. mAb-D was stressed by thermal cycling from 25 to 45°C and back to 25°C at 3°C per sec resulting in ~68 complete thermal ramps in 15 min and ~ 540 complete thermal ramps over a two 2 h period. The samples were then analyzed using GroEL-BLI, SEC, and MFI.

2.2.2.9 *Sample preparation and stress treatment by addition of Guanidine HCl of mAb-D*

A stock solution of 5 M guanidine was prepared in 5 mM CP, 150 mM NaCl at pH 7.4. The stock mAb-D was diluted using the corresponding CP buffer and the guanidine hydrochloride stock solution to achieve a protein concentration of 5 mg/mL and 0.5 M guanidine HCl. The mAb-D control samples were also prepared using only CP buffer with 150 mM NaCl. The samples were filtered using 0.22 μm syringe filters (Millipore, Billerica, Massachusetts). Aliquots of 1.5 mL were placed into 3 mL borosilicate glass type I vials and capped with rubber stoppers (West Pharmaceutical Services, Exton, Pennsylvania). Triplicates of the perturbed samples were analyzed over 24 h by GroEL-BLI, SEC and MFI at time points of 8 and 68 min, 2, 5, and 24 h.

2.2.2.10 *Sample preparation and stress treatment by 50°C incubation of Bis-3 and of mAb-D*

The mAb-D stock solution (50 mg/mL) was diluted using the CP buffer with 150 mM NaCl to achieve a protein concentration of 5 mg/mL. The stock solution of Bis-3 (4.2 mg/mL) was diluted to a final concentration of 0.2 mg/mL using 20 mM sodium phosphate, 235 mM sucrose at pH 7.2. mAb-D and Bis-3 solutions were stressed over 1 h at 50°C. At time points of 0, 5, 10, 20, 30, and 60 min (mAb-D) and 0, 10, 20, 30, 45, 60 min (Bis-3), the samples were analyzed using GroEL-BLI, SEC, and MFI.

2.2.2.11 *P-value calculation*

p-values were calculated using the t-Test: paired two sample for means data analysis function from Excel software (Microsoft, Redmond WA). The alpha value was 0.05 with N=3 for all sample sets.

2.3 Results and Discussion

2.3.1 Automated GroEL-BLI assay optimization and initial assessment of aggregation propensity of three mAbs

In this work, the utility and pharmaceutical applicability of a previously reported GroEL-BLI biosensor assay[9] to monitor the formation of pre-aggregate species found in various therapeutic mAb candidates exposed to different environmental stresses were evaluated. A key analytical advancement in this work was the development and implementation of an automated BLI platform (OctetRed96 system). By moving from the single channel BLI system described previously[9] to an automated, multichannel platform (96 well plate), this work demonstrates the use of the GroEL biosensor as a part of formulation development of mAbs and other therapeutic protein candidates. Other improvements in the assay described in this work include the addition of a BSA pretreatment step to further minimize non-specific binding of proteins to the biosensor

surface even with variable GroEL loading, and more routine implementation of various controls (including a relatively unstable control protein, FGF-1, and non-stressed mAbs as positive and negative controls). Moreover, by using an automated platform, many more replicates can be run for each sample to further ensure the reproducibility of each set of experiments. The automated GroEL-BLI system was then examined with 4 different therapeutic mAb candidates (two IgG1 molecules, one IgG4 molecule and one bispecific mAb) exposed to different environmental stresses previously shown to induce formation of aggregates using various mAbs.[12-14]

As an initial step to optimize the assay and minimize any potential nonspecific binding to the biosensor, concentrations of 0-1 mg/mL of b-GroEL (0, 2.5, 5 ,10, 25, 100, 500, 1000 µg/mL) were loaded onto the biosensor. This step was followed by a blocking step with concentrations of 0-1 mg/mL bovine serum albumin (BSA). A non-stressed mAb sample was then exposed to the biosensor. The conditions with the least amount of non-specific binding during the association phase were chosen for future studies and consisted of loading with 0.5 mg/mL GroEL and 1 mg/mL BSA (See Supplemental Figure S2).

Following adaptation to the Octet multichannel system and assay optimization, a screening of three pharmaceutically relevant mAbs (mAb-D, E, and J) was performed. Thermal stresses were used to probe each mAb at temperatures approaching their T_{onset} values, at the T_{onset}, and above the T_{onset} (mAb-D: 58.9°C ± 0.5; mAb-E: 56.3°C ± 0.08; mAb-J: 55.3°C ± 0.2 as obtained by differential scanning calorimetry, data not shown). All three mAbs were stressed at temperatures of 50, 55, and 60°C (along with a 4°C control) for 14 days in solutions containing different salt concentrations (150 mM and 500 mM NaCl). Figure 1 represents the average binding amplitude of the different samples (each mAb at 5.0 mg/ml) from the GroEL-BLI biosensor. In general, it was seen that mAb-D showed the highest binding amplitude at both salt concentrations at each of

the three elevated temperatures. In addition, increasing the NaCl concentration from 150 to 500 mM did not have any major effect on the IgG binding amplitudes. The slight decrease in binding amplitude seen from 50°C to 60°C can be due to the smaller pre-aggregate species forming larger sized aggregates in solution (from the increase heat stress) and these larger aggregates cannot be captured by the GroEL as effectively. This decrease in GroEL biosensor capture efficiency could be due to the diminished exposure of hydrophobic patches upon aggregation or the decreased collisional frequency with the biosensor due to a decrease in diffusion or a combination of both these aggregate properties. These results show that different mAbs can be compared for their aggregation propensity in different solutions using this GroEL-BLI biosensor method in an automated platform.

2.3.2 GroEL-BLI, SEC, and MFI analysis of mAb-D aggregation under various stress conditions

To further evaluate the utility of this approach, mAb-D was further exposed to four other environmental stresses involving acidic pH exposure, thermal cycling, Gdn-HCl perturbation, and 50°C incubation as outlined by the flowchart illustrated in Figure 2 (conditions 1, 2, 3, 4, respectively). These experimental conditions were selected based on previous reports for their ability to initiate formation of early intermediates in the mAb aggregation pathways[12-14]. Figure 3A shows a representative GroEL-BLI biosensor sensogram of mAb-D stressed under one of the four conditions (condition 4, 50°C for 60 min). The association step shows triplicate runs of mAb-D stressed solution with the dissociation step conducted in mAb-D formulation buffer alone. The final baseline determination was performed after using the mAb-D formulation buffer with added ATP to induce release of bound mAb-D from the GroEL. The sensogram trace returns at or near the original baseline (compare initial mAb binding reaction starting amplitude with last step

baseline buffer return in Figure 3A), indicating specific binding to the GroEL biosensor. Figure 3B is an enlargement of the association and dissociation phases of the same sample after a 60 min thermal stress treatment. Similar GroEL-BLI experiments were then performed with mAb-D exposed to each of the four stress conditions (Figure 2) and the results are described below and summarized in Figure 3C. The GroEL-BLI results were compared to analysis of the same mAb-D samples by SEC and MFI as summarized in Figure 4A and 4B, respectively.

For condition 1, a brief decrease in solution pH to acidic conditions has been previously shown to cause the formation of a wide range of metastable aggregate species with various mAbs, produced by the unfolding of the Fab region[12]. The mAb-D solution was subjected to a brief exposure (1 min pH jump) by rapidly dropping to pH 4.0 followed by the pH return to 7.4 by readjusting with concentrated phosphate buffer. This pH pulse and return resulted in a significant increase (p-value of 0.0025) in the binding amplitude using the GroEL-BLI assay compared to the non-stressed mAb-D control (Figure 3C). This change in binding amplitude was also observed during a pH 5.0 pulse, but the BLI binding signal was diminished compared with the pH 4.0 pulse amplitude (p-value of 0.0037), thereby indicating that pH 4.0 pulse created a larger population of aggregates compared to the pH 5.0 pulse. When these samples were examined using size exclusion chromatography (SEC), a substantial increase in percent aggregation (soluble and insoluble) of ~18% for the pH 4.0 pulse samples and ~ 15% for the pH 5.0 samples was observed compared to the control sample that contained ~0.2% aggregate (Figure 4A). An increase in formation of both soluble and insoluble aggregates (loss of total area in the SEC chromatogram) with a concomitant decrease in the monomer peak was observed. The samples were assessed for formation of subvisible particles by Microflow Imaging (MFI), with both pH pulsed samples showing an increase in total particle concentration compared to the non-stressed mAb-D control (Figure 4B).

The particle size distribution of the control and stressed mAb-D samples showed the majority of particles to be in the size range of 2-10 µm (data not shown).

For condition 2, mAb-D was exposed to multiple thermal cycles from 25 to 45°C and back to 25°C. The heating phase during thermal cycling has been shown previously to partially unfold the Fab domain of an antibody while the cooling phase minimizes protein aggregation[14]. To determine if these conditions could lead to the formation of pre-aggregate species with mAb-D, the thermal cycling was performed from 25°C to 45°C and back to 25°C at 3°C per second over the course of 15 min and 2 h and resulted in an increase in the binding amplitude using the GroEL-BLI assay compared to the mAb-D non-stressed control (Figure 3C). When the samples were examined using SEC, a relatively small increase in total aggregation was seen. There was ~0.5% increase in aggregation seen for the 15 min thermal cycled samples and ~1% increase for the 2 h cycled samples compared to the non-stressed mAb with ~ 0.2% total aggregation (Figure 4A). This was also accompanied by a loss in total peak area, indicating the formation of insoluble aggregates that did not pass through the column matrix. The samples were assessed by MFI with both 15 min and 2 h samples showing an increase in subvisible particle concentration compared to the non-stressed mAb-D control (Figure 4B). The particle size distribution of the control and stressed mAb-D samples showed the majority of particles to be in the size range of 2-10 µm (data not shown).

Exposing mAb-D to conditions 1 and 2 (Figure 2) showed concomitant formation of pre-aggregate species (GroEL-BLI biosensor), aggregates (SEC) and subvisible particles (MFI). These results with mAb-D can be compared to previous work done on other mAbs[12 12]. For example, a brief low pH shift[12] resulted in polydisperse mAb aggregates from dimers to aggregates of 10 µm in diameter as assessed by SEC and light obscuration. Similar results were observed with

mAb-D with aggregates of varying size (from dimer to subvisible particles of 2-10 μm). For the thermal cycling method[14], however, the heating pulse was reported to lead to partial unfolding of the Fab region allowing Fab-Fab interactions to occur. The cooling period caused the refolding and minimization of detectable aggregation for the examined mAb. Thermal cycling led to an increase in the amount of fragments with a concomitant decrease in the presence of dimers observed by SEC. In contrast, in this study, mAb-D showed a steady increase in the level of insoluble aggregates and increased amounts of subvisible particles after multiple thermal cycling events. These contrasting results could be due to differences in the inherent stability or dynamics of the two mAbs, or possibly differences in experimental solution conditions.

In summary for conditions 1 and 2, mAb-D formed irreversible aggregates under the conditions of acidic pH exposure and temperature cycling as measured by SEC and MFI. Concomitantly, an increase in binding amplitude was observed using the GroEL biosensor. Thus, the GroEL biosensor was detecting either formation of the pre-aggregate species and/or formation of the irreversible aggregates. It was difficult to distinguish these two possibilities under these two experimental conditions because of the formation of multiple types of aggregates during these stresses. Indeed previous results indicate that the GroEL-BLI biosensor binds to stable IgG dimers[8]. Thus, the biosensor results correlate with SEC and MFI data indicate that the GroEL biosensor method can potentially be used as a rapid general assessment of protein aggregation propensities which bodes well implementation of a routine automated assay setup (8 or 16 channel Octet systems and other higher HDXOctet 96 channel BLI throughput systems).

In contrast to the mAb-D aggregation profile observed with conditions 1 and 2, conditions 3 and 4 (see Figure 2) showed a different profile in which the GroEL-BLI biosensor detects hydrophobic substrates (pre-aggregate species) prior to the detection of irreversible aggregate

formation as measured by SEC and MFI. For example, Condition 3 consisted of perturbing mAb-D with 0.5 M guanidine HCl for various times. Exposure to intermediate concentrations of Gdn-HCl has previously been shown to partially unfold the CH_2 domains of a mAb and lead to aggregate formation[13]. Therefore, perturbation of mAb-D with 0.5 M Gdn-HCl was performed to evaluate the ability of these conditions to generate aggregate and/or pre-aggregate species. A significant increase in the binding amplitude using the GroEL-BLI assay (compared to the mAb-D non-stressed control) was observed (Figure 3C). The association phase during the GroEL-BLI study show a slight increase in binding at the 24 h time point compared to earlier times, which showed no significant differences (p-value=0.059). Based on SEC, the mAb-D samples produced less than 1.5% total aggregation (approx. equivalent to the amount observed in the unstressed mAb-D control where no significant GroEL biosensor binding was observed, Figure 4A). Similarly, when the samples were also analyzed by MFI, no notable increase in total subvisible particle concentration (compared to the non-stressed mAb-D control) at the early time points (8 and 68 min, and 2 h) were observed, although the longer time points under these same conditions (5 h and 24 h) showed a small increase in subvisible particle concentration compared to the control (Figure 4B).

Under the final stress condition examined (Condition 4, see Figure 2), mAb-D was incubated at 50°C for various times up to an hour. For the GroEL-BLI results, Figure 3C shows increasing binding amplitudes for the stressed mAb-D samples at 50°C for up to one hour. The stressed mAb-D samples were also evaluated for the presence of aggregates using SEC as well as for the formation of larger, subvisible particles by MFI. Figure 4A displays the percent total aggregate formation as determined by SEC for mAb-D samples for various times along with an unstressed control. It can be seen that no detectable increase in aggregate is observed. Figure 4B

shows the concentration of subvisible particles in the same samples as measured by MFI. Results indicate that no increase in particle formation is observed between 10 and 60 min of incubation at 50°C. The particle size distribution of the control and stressed mAb-D samples showed the majority of particles in the range of 2-10 µm (data not shown).

TEM analysis was used to visualize the GroEL-mAb-D complexes that were formed after exposing the mAb-D sample to heating at 50°C for 60 min (Condition 4). Figure 5 shows TEM images of the different preparations, including 0.05 µM GroEL in the solution as a control (Figure 5A), solution based interaction of the stressed 0.05 µM mAb-D with 0.05 µM GroEL (Figure 5B), dissociation of –S-S- biotinylated-GroEL (SS-b-GroEL) from the streptavidin biosensor with a DTT control (Figure 5C), and dissociation of the mAb-D-GroEL complex from the streptavidin biosensor surface using DTT (Figure 5D). Complexes between the GroEL and mAb-D (or potentially fragments of mAb-D), after temperature exposure, can be seen using both approaches (Figure 5B and 5D) indicating the binding of structurally altered forms of mAb-D species to GroEL upon exposure of the mAb-D to elevated temperature. This is manifested as extra density bound to the GroEL binding site.

Exposing mAb-D to conditions 3 and 4 (Figure 2) showed formation of pre-aggregate species (GroEL-BLI biosensor) prior to formation of aggregates (SEC) and subvisible particles (MFI). These results with mAb-D can be compared to the previous work reported on other mAbs[13] [18]. Mehta et. al. 2014[13] showed unfolding of the CH_2 domain was the interaction site for aggregation of this particular mAb when exposed to 1.2-1.6 M Gdn-HCl. At lower denaturant concentrations, the mAb remained in its native state. In the case of mAb-D in our study, when exposed to 0.5 M Gdn-HCl, SEC and MFI showed no increased amounts of aggregation compared to the control. Interestingly, the GroEL-BLI biosensor method was able to detect the formation of

pre-aggregates. For thermal stress, Hawe et. al. (2009)[18] showed that thermal incubation of a mAb solution (at a few degrees below its visible aggregation temperature) resulted in formation of small aggregates around 30 nm and subvisible particles below 25 μm. During the thermal stress of mAb-D in this work, performed at ~9 degrees below its T_{onset} value, no increase in aggregates was detected using SEC and nor MFI, yet the GroEL-BLI system does detect early structurally altered forms of mAb-D. These results demonstrate that the different environmental stresses lead to the formation of differing levels of mAb-D pre-aggregate, soluble aggregate and subvisible particle species which can be elucidated using a combination of the GroEL-BLI biosensor, SEC and MFI analyses.

2.3.3 Automated GroEL-BLI, SEC, and MFI analysis of Bis-3 bispecific antibody under thermal stress conditions

To further examine the ability of the automated, optimized GroEL-BLI biosensor to detect formation of pre-aggregate species, solutions of a pharmaceutically relevant bispecific Ab (Bis-3) were examined, before and after thermal stress, by a combination of the GroEL-BLI biosensor assay, SEC and MFI. Bis-3 solutions at a low protein concentration (0.2 mg/ml) were incubated at 50°C (for up to 60 min), a temperature well below the T_{onset} of the bispecific antibody (as determined by differential scanning calorimetry where Bis-3 exhibited a multiphasic DSC thermogram with a Tm_1 value of ~64°C). Figure 6A shows representative GroEL-BLI biosensor sensograms of the association and dissociation phase of Bis-3 samples before and after an exposure to elevated temperature (50°C, 10 min) followed by a return to 25°C prior to measurement. Figure 6B shows the association and dissociation phase of Bis-3 samples after 60 min at 50°C. The dissociation step was performed with the formulation buffer alone. Three pulses of a 20 mM ATP

containing solution (with elevated values due to high refractive index of solution due to the glycerol) released the captured Bis-3 specifically bound to the GroEL as evidenced by the return to the original GroEL loaded baseline. For each of the time points, the average binding amplitude (from three replicates) for the association, dissociation, and final baseline were plotted as a bar graph in Figure 6C. An increase in binding amplitude of the unstressed Bis-3 sample (at room temperature) over the buffer control (no Bis-3) is observed indicating the Bis-3 molecule has an exposed hydrophobic GroEL binding interaction site even at room temperature. In contrast, neither the IgG1 nor the IgG4 mAbs showed any such GroEL-BLI binding signal at room temperature. Interestingly, the Bis3 sample concentration tested (0.2 mg/ml) was significantly lower than the mAb-D sample tested (5 mg/ml), yet showed a larger binding amplitude during the association phase.

When the same temperature stressed Bis-3 samples were examined for irreversible aggregate formation using SEC, no substantial increase in percent aggregation was observed (both for soluble aggregates in the chromatogram and insoluble aggregates as indicated by total area recovered), compared to the control Bis-3 sample (both contained ~0.45% aggregate) (Figure 7A). The Bis-3 thermally stressed samples also showed no increase in the levels of subvisible particles as assessed by MFI measurements over the unstressed Bis-3 control (Figure 7B). For both the unstressed and thermally stressed samples, the particle size distribution within the 2-10 μm size range remained the same (data not shown). These results indicate that these thermally stressed Bis-3 samples contained an easily detectable amount of pre-aggregate species by the GroEL-BLI biosensor prior to any detectable formation of irreversible aggregates as determined by SEC and MFI.

TEM was used to visualize the GroEL-Bis-3 complexes. Figure 8 shows representative TEM fields of Bis-3 GroEL complexes generated from both solution formed and biosensor released complexes. The first two image fields represent the complexes that were formed in solution with the GroEL alone (Figure 8A) and GroEL-Bis-3 complexes (Figure 8B) which were heated at 50°C for 60 min. The field in Figure 8B represents a solution containing equal molar amounts of Bis-3 and GroEL; see methods section). In Figure 8C and D, the images were generated by performing the GroEL-BLI assay on streptavidin biosensors loaded with S-S biotinylated GroEL, and then dissociating GroEL alone (Figure 8C) and GroEL-Bis3 complexes (Figure 8D) by reducing the S-S linkage with DTT from three separate biosensors (to enhance complex concentrations, see methods section). In Figure 8D, the released GroEL-Bis-3 complex was formed by heating the Bis-3 sample at 50ºC for 60 min followed by an immersion of the GroEL biosensor into this solution for 5 min. After this immersion phase, the complex was then released from the biosensor with DTT and visualized using negative staining TEM. For both approaches to form the GroEL-Bis 3 complexes, the TEM images clearly show that the GroEL binding site is occupied by extra protein density with prominent extensions. In Figure 8B, some GroEL complexes show clear interactions between the GroEL binding site and the Fc portion of the bispecific mAb with the Fab domains pointing away from the GroEL binding site (Figure 8B). In Figure 8D, the biosensor released complexes also show clear extensions but the complexes are not as resolved as in the GroEL-Bis-3 solution complexes (Figure 8B).

Bispecific antibodies are designed by recombinant DNA technologies to recognize two different antigens to increase effectiveness of the therapeutic protein for certain targets[19]. Due to their asymmetrical, multi-domain nature, such engineered antibody molecules can have very different pharmaceutical properties than IgG mAbs including *in vivo* half-life and *in vitro*

stability[19]. When examining Bis-3 using the GroEL-BLI assay, it was first noted that there was an increase in binding amplitude of unstressed Bis-3 sample (at room temperature) that was not seen with the three other IgG mAbs. Importantly, this GroEL-BLI detection signal with Bis-3 occurred at a ~25-fold lower protein concentration than with the mAb-D samples. This result indicates the Bis-3 molecule has a structurally altered, enhanced hydrophobic nature at room temperature compared to the mAbs. In addition, the Bis-3 samples were also inherently less stable than the IgG1 and IgG4 mAbs when the Bis-3 samples were exposed to limited thermal stresses (i.e., 10 min at 50°C) and the binding amplitudes remained relatively constant over the 60 min sampling period. This constant signal may indicate that the population of pre-aggregate species reaches an equilibrium state after thermal stress that does not diminish even after the samples are returned to ambient temperatures for the GroEL BLI biosensor measurements. This enhanced signal with the GroEL biosensor for both unstressed and thermally stressed Bis3 samples was obtained without any appreciable increase in the formation of irreversible aggregate species as measured by SEC and MFI. One additional difference between the Bis-3 and mAb-D is that Bis-3 had a significantly higher binding amplitude in the GroEL-BLI assay, probably indicating a higher population of the pre-aggregate species. This is also consistent with the increased population of complexes seen with TEM.

Previous results by Naik et al. (2014) [9] showed that the GroEL-BLI biosensor could detect the existing and thermally stressed formation of hydrophobic patches on polyclonal-IgG and mAb samples, with binding amplitudes seen to increase with the time of thermal stress. Likewise, the mAb-D examined in this work also showed time dependent increases in GroEL binding and hence detection as the thermal stress times increased. In contrast, this trend was not observed for the Bis-3 Ab as extended stress times at 50^{o}C did not show any time dependent increases in GroEL binding

over the 60 min sampling period but rather manifested a steady, consistent binding response. In the samples examined in this work, the GroEL binding hydrophobic species (pre-aggregates) remained in solution even after the temperature is returned to ambient temperatures prior to analysis. This is another unexpected advantage of this method because this enhanced detection scheme could be useful in determining conditions that can inhibit the formation of or alternatively reverse the accumulation of these potentially metastable, kinetically trapped, partially unfolded, hydrophobic states.

2.4 Conclusions

In this work, a previously described GroEL-BLI based method[9] was further optimized and automated (using an Octet system, 96 well plate format) to bind and detect partially structurally altered intermediates (pre-aggregates) formed in stressed solutions of several different therapeutic Ab candidates including IgG1, IgG4 and bispecific antibodies. Transmission electron microscope (TEM) images of stressed Ab samples bound to the GroEL showed the formation of Ab pre-aggregate-GroEL complexes. The utility of this approach for use in protein formulation development was explored with various mAbs (IgG1 and IgG4) exposed to various stress conditions as well as by using a relatively less stable bispecific antibody (Bis-3). For the latter, significant binding amplitudes were observed with the GroEL-BLI biosensor at room temperature at significantly lower protein concentrations (i.e., unstressed conditions), compared to the other mAbs, indicating its relatively enhanced hydrophobic nature, and by correlation, aggregation propensity. When Bis-3 was incubated at 50°C, increases in GroEL-BLI binding amplitude were observed before any increases were seen for irreversible aggregate/particle formation as measured by SEC and MFI. When examining the more stable mAb-D (IgG4), upon exposure to different stresses including elevated temperatures, acidic pH, and addition of guanidine-HCl, the GroEL-

BLI biosensor could detect pre-aggregate formation before, or in some cases concomitantly with, irreversible aggregate formation as measured by SEC and MFI. Thus in this case, the GroEL-BLI biosensor can supplement information gained from more traditional aggregation detection methods to better detect pre-aggregate species that may be involved in the formation of longer term deleterious protein aggregates.

The GroEL biosensor technology provides protein specific information about the presence of potentially aggregation prone species. In some instances, this technology reports the formation of pre-aggregate transient species (GroEL binders) before larger scale aggregation is even detected. The specificity of this GroEL-Ab interaction can be confirmed by ATP induced reversal of Ab binding and the GroEL-Ab complexes can be easily visualized by TEM analysis. This method can rapidly assess solution stability and pre-aggregate formation within the relatively short time window of minutes. This rapid detection of pre-aggregate species using an automated platform can be particularly useful for protein formulation development. This early BLI detection method can be used to identify stabilizing conditions and excipients that diminish pre-aggregate formation which may correlate with aggregation profiles during long term stability studies.

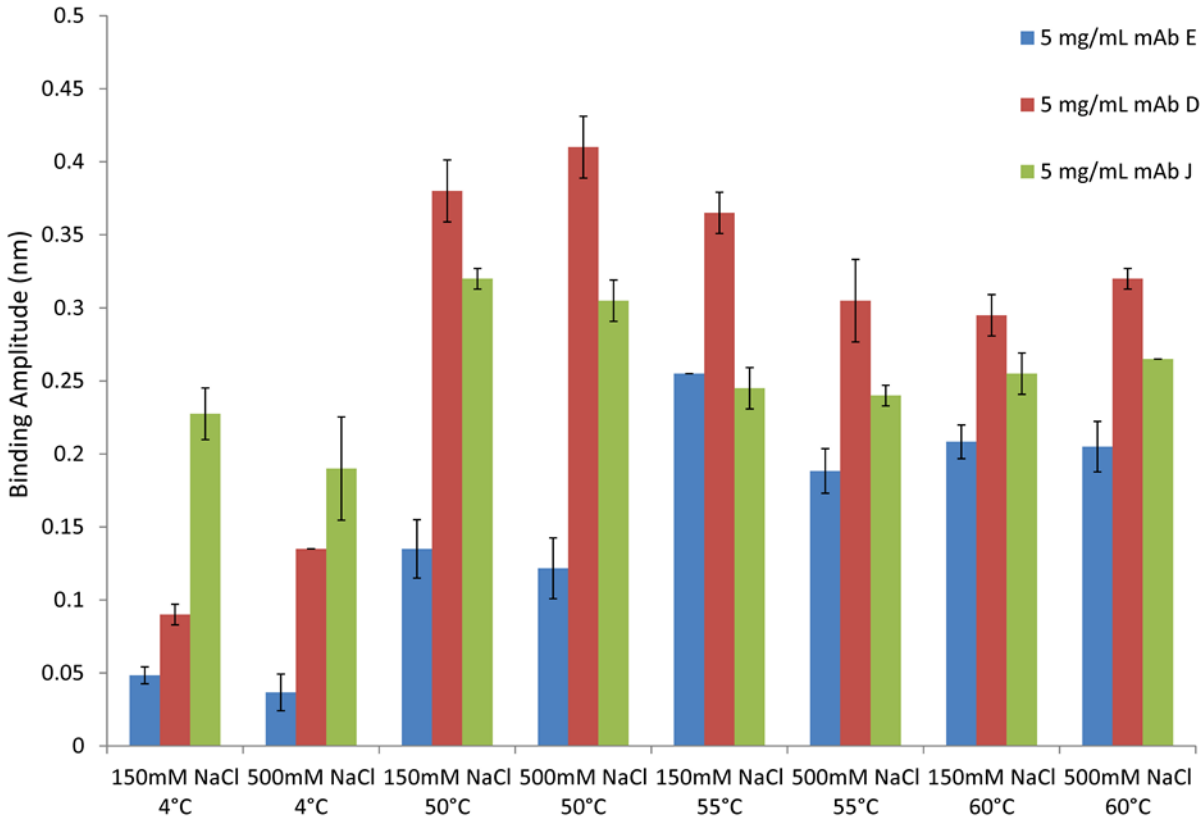

Figure 2.1: Screening of the aggregation propensity of mAb-D (red), mAb-E (blue), and mAb-J (green) performed using the optimized, automated GroEL-BLI biosensor assay.

The mAb solutions were incubated at temperatures of 4, 50, 55, and 60°C for 2 wk. The average binding amplitude of the different samples are shown with mAb-D showing the highest amplitude at both salt concentrations and at each of the three elevated temperatures. Error bars represent one standard deviation (N=3). The mAbs were formulated at 5 mg/mL in 5 mM citrate-phosphate buffer (CP) containing either 150 mM or 500 mM NaCl at pH 7.4.

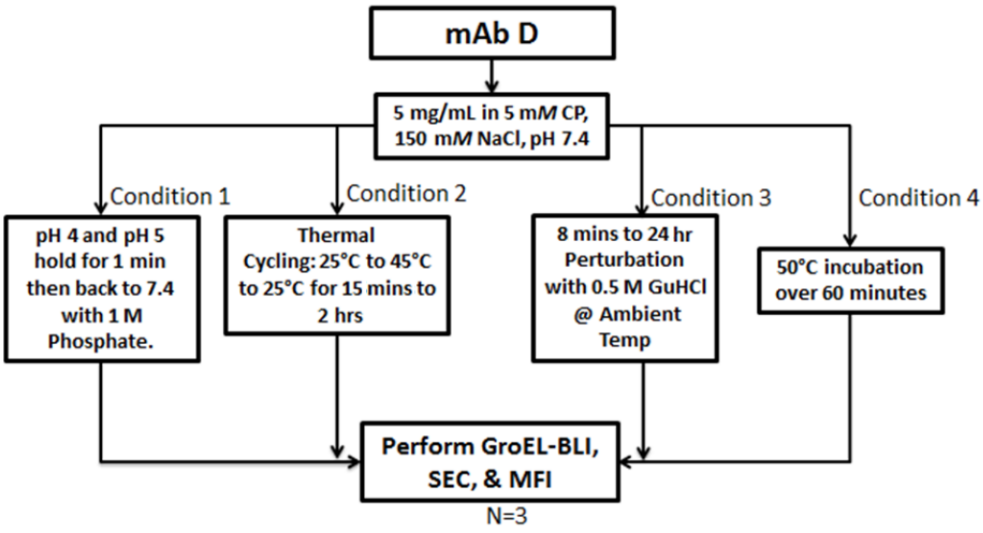

Figure 2.2: Flow chart of the various stresses performed on mAb-D to assess aggregation propensity by a variety of analytical methods (GroEL-BLI, SEC and MFI).

Condition 1 was performed by rapidly dropping the pH of the solution from 7.4 to pH 4.0 or 5.0, holding for 1 min and then returning to pH 7.4 with the addition of 1 M phosphate buffer. For condition 2, thermal cycling was performed from 25°C to 45°C back to 25°C for times between 15 min to 2 h at 25°C. Condition 3 consisted of addition of 0.5 M GdnHCl and incubation from 8 min to 24 h. Condition 4 was a 50°C incubation at various time points over 60 min. The aggregation of mAb-D solutions after exposure to each of the four conditions was examined using the GroEL-BLI biosensor, SEC, and MFI. The mAbs were formulated at 5 mg/mL in 5 mM citrate-phosphate buffer (CP) containing either 150 mM NaCl at pH 7.4.

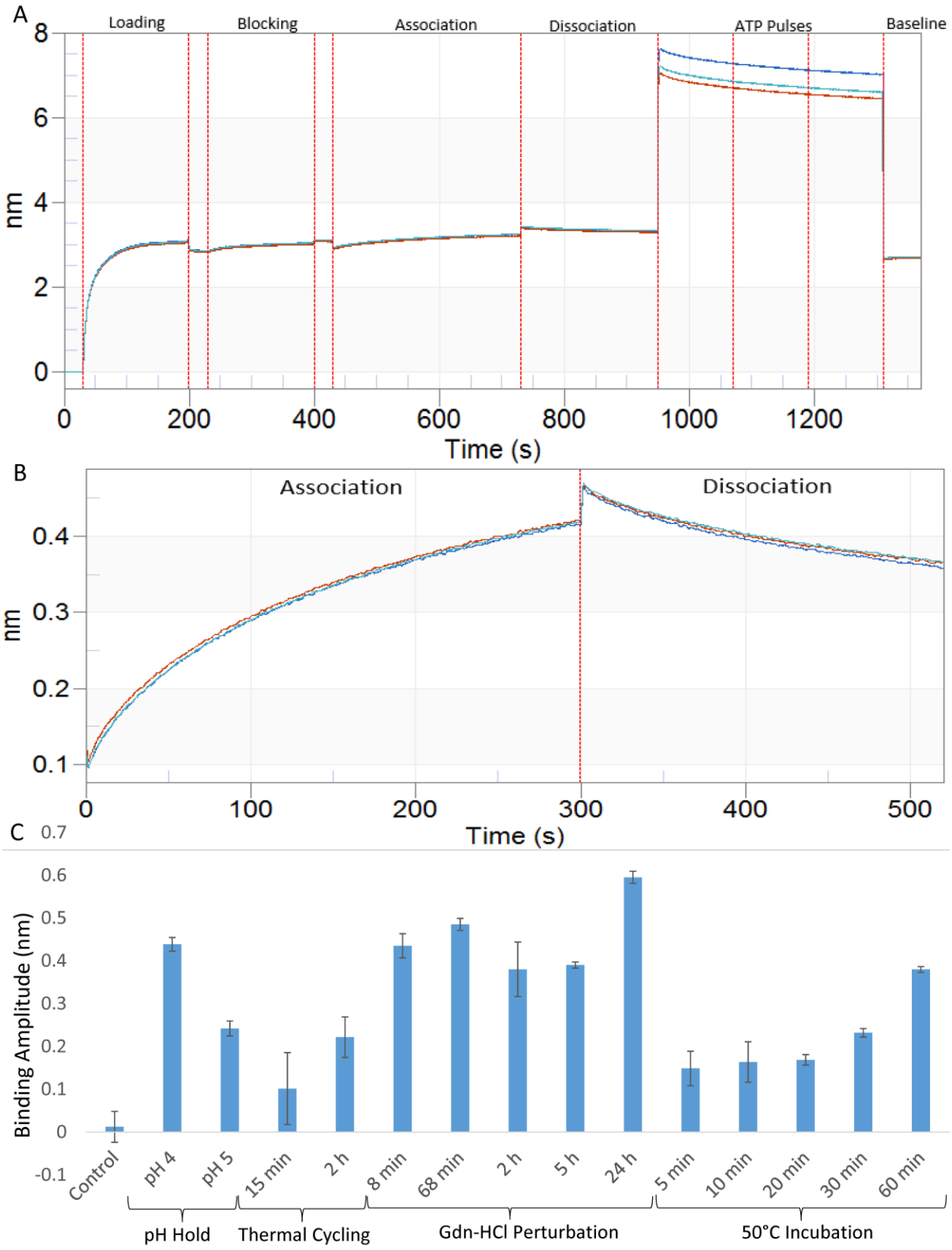
A
Loading
Blocking
Association
Dissociation
ATP Pulses
Baseline
nm
Time (s)
B
Association
Dissociation
nm
Time (s)
C
Binding Amplitude (nm)
Control
pH 4
pH 5
15 min
2 h
8 min
68 min
2 h
5 h
24 h
5 min
10 min
20 min
30 min
60 min
pH Hold
Thermal Cycling
Gdn-HCl Perturbation
50°C Incubation

Figure 2.3: GroEL-BLI biosensor analysis of mAb-D after exposure to different stresses a 50°C for 60 min.

(A) Representative sensogram of mAb-D stressed at 50°C for 60 min in the GroEL-BLI assay showing association and dissociation phases, followed the addition of ATP and subsequent return to baseline (indicating specific GroEL binding; see text). B) Expanded view of the association and dissociation phases of the sensograms, and (C) Comparison of the binding amplitudes at the association phase of each of the mAb-D samples. Error bars represent one standard deviation (N=3). The mAbs were formulated at 5 mg/mL in 5 mM citrate-phosphate buffer (CP) containing 150 mM NaCl at pH 7.4.

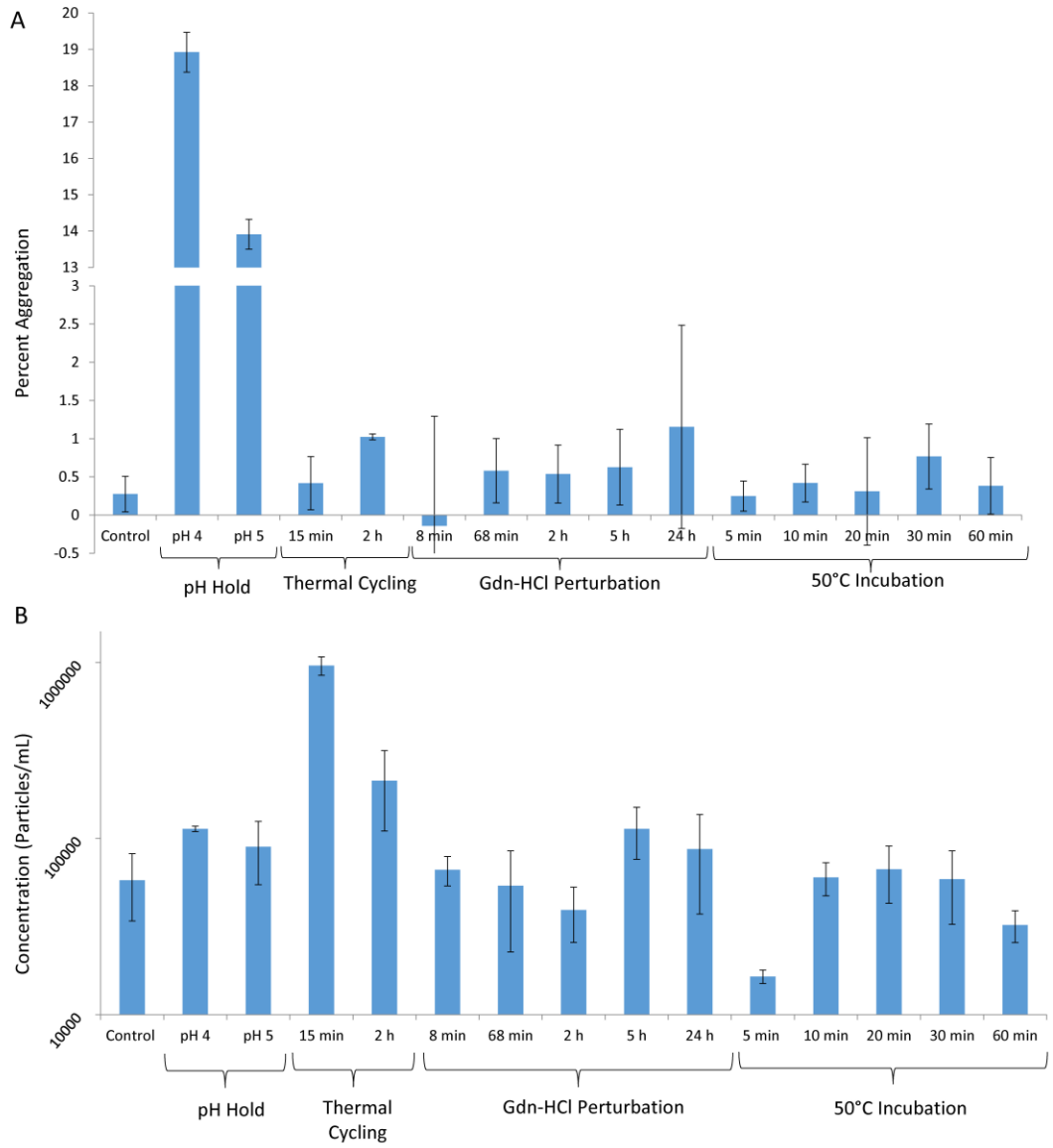

Figure 2.4: Effect of various stress conditions on mAb-D aggregation and particle formation as measured by SEC and MFI, respectively.

(A) Percent total aggregation (soluble and insoluble) of mAb-D before and after various stresses as measured by SEC, and (B) concentration of subvisible particles of mAb-D samples before and after various stresses as measured by MFI. Error bars represent one standard deviations (N=3). The mAbs were formulated at 5 mg/mL in 5 mM citrate-phosphate buffer (CP) containing 150 mM NaCl at pH 7.4.

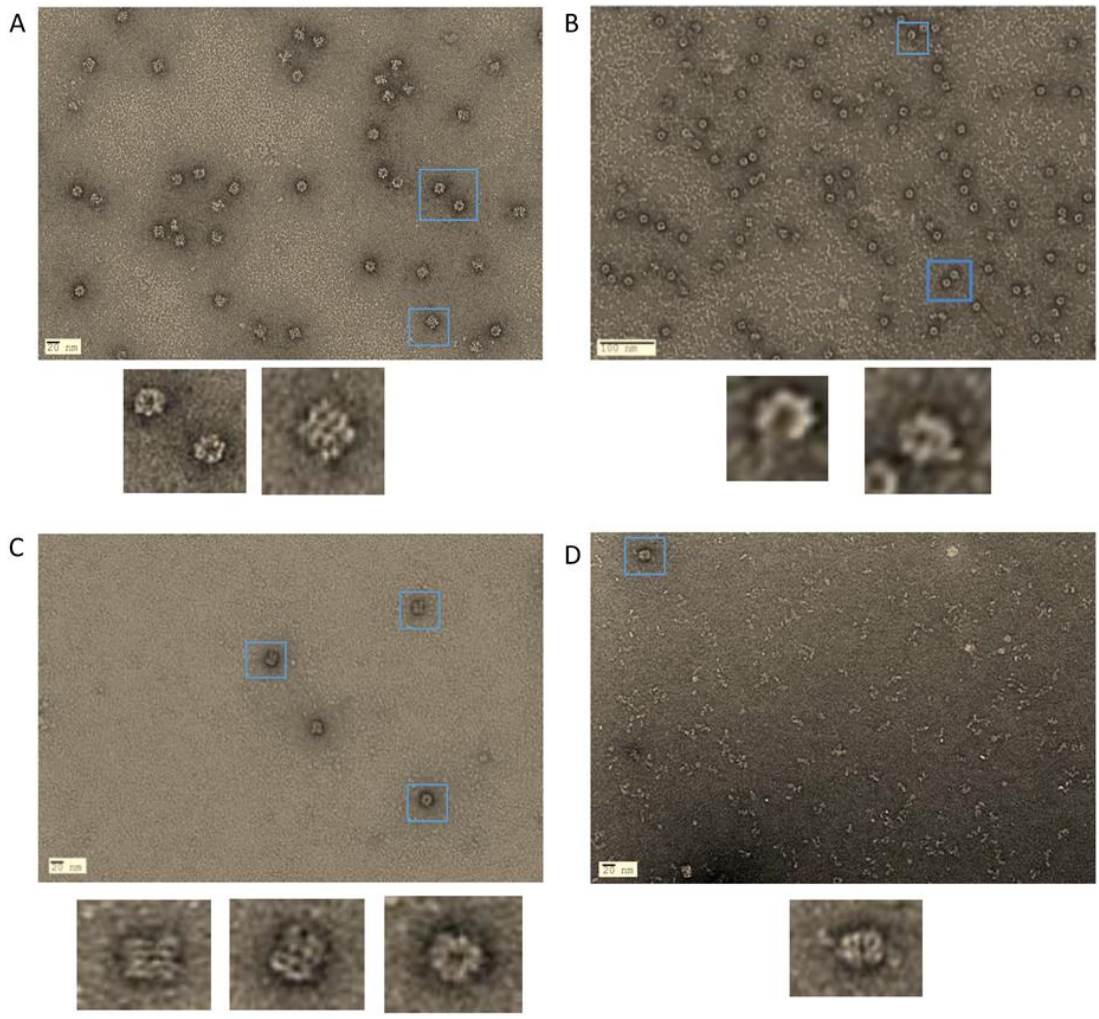

Figure 2.5: Representative TEM images of GroEL alone and GroEL complexed with mAb-D stressed at 50°C for 60 min.

Enlarged images of GroEL molecule (blue boxs) are shown to the right. (A) GroEL alone in solution, (B) GroEL-mAb-D complexes formed in solution, (C) GroEL released from the BLI biosensor surface with 50 mM DTT, and (D) GroEL-stressed mAb-D complexes released from the biosensor with 50 mM DTT. See methods section for further detail.

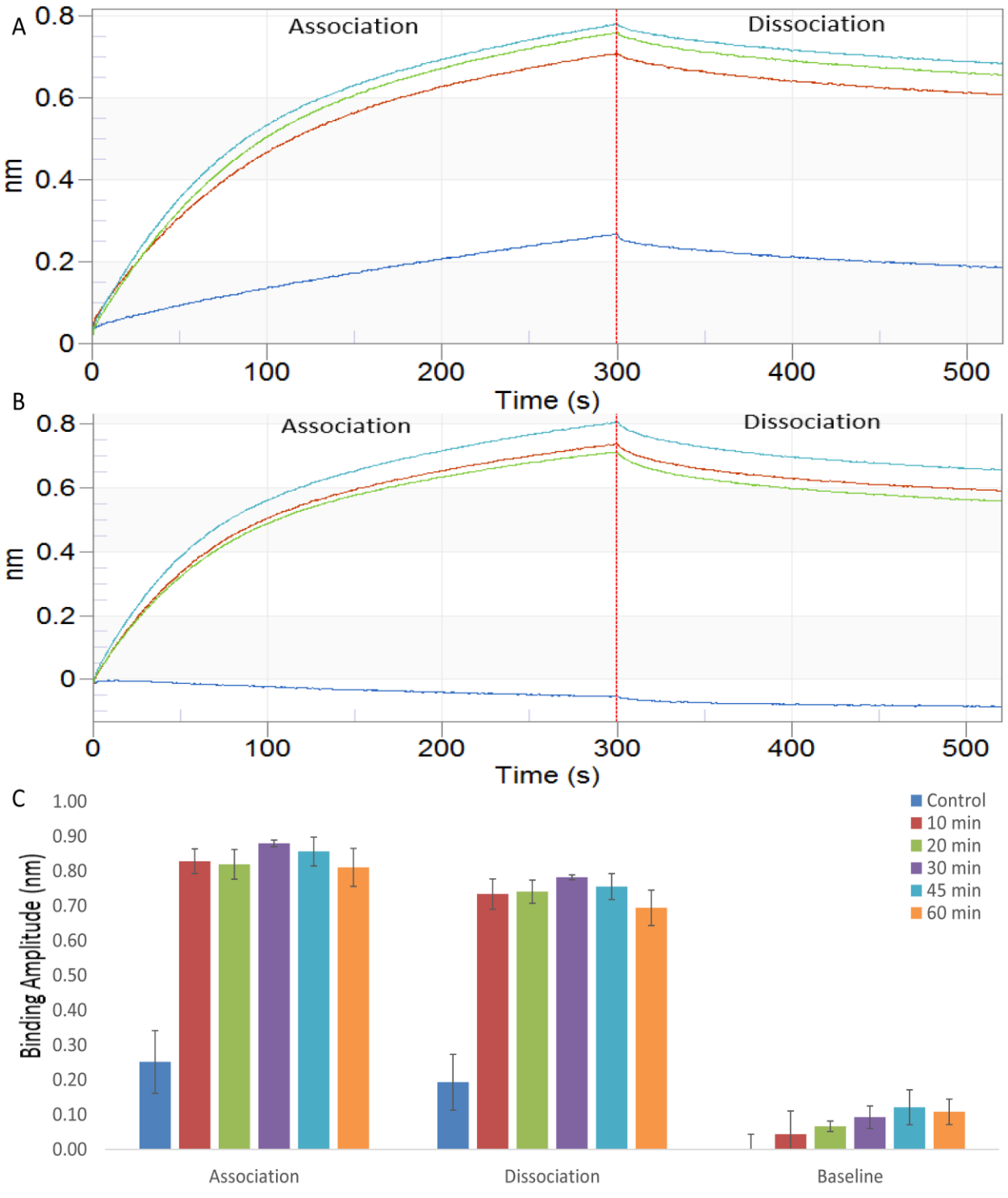
A
Association
Dissociation
nm
Time (s)
B
Association
Dissociation
nm
Time (s)
C
Binding Amplitude (nm)
Control
10 min
20 min
30 min
45 min
60 min
Association
Dissociation
Baseline

Figure 2.6: GroEL-BLI biosensor analysis of a bispecific Ab (Bis-3) during exposure to 50°C over 60 min.

(A) An expanded association and dissociation phase of the sensograms of 50°C stressed Bis-3 sample for 10 min in triplicates (green, red, and teal) and the unstressed sample (Blue) (B) An expanded association and dissociation phase of the sensograms of 50°C stressed Bis-3 sample for 60 min in triplicate (green, red, and teal) and buffer (Blue), and (C) comparison of binding amplitudes in the GroEL-BLI assay of each of the Bis-3 samples at the association, dissociation, and final baseline return after ATP. The baseline binding amplitude returning to near zero values after ATP exposure indicates specific binding to GroEL. Error bars represent one standard deviation (N=3). The Bis-3 was formulated at 0.2 mg/mL in a 20 mM sodium phosphate buffer containing 235 mM Sucrose at pH 7.2.

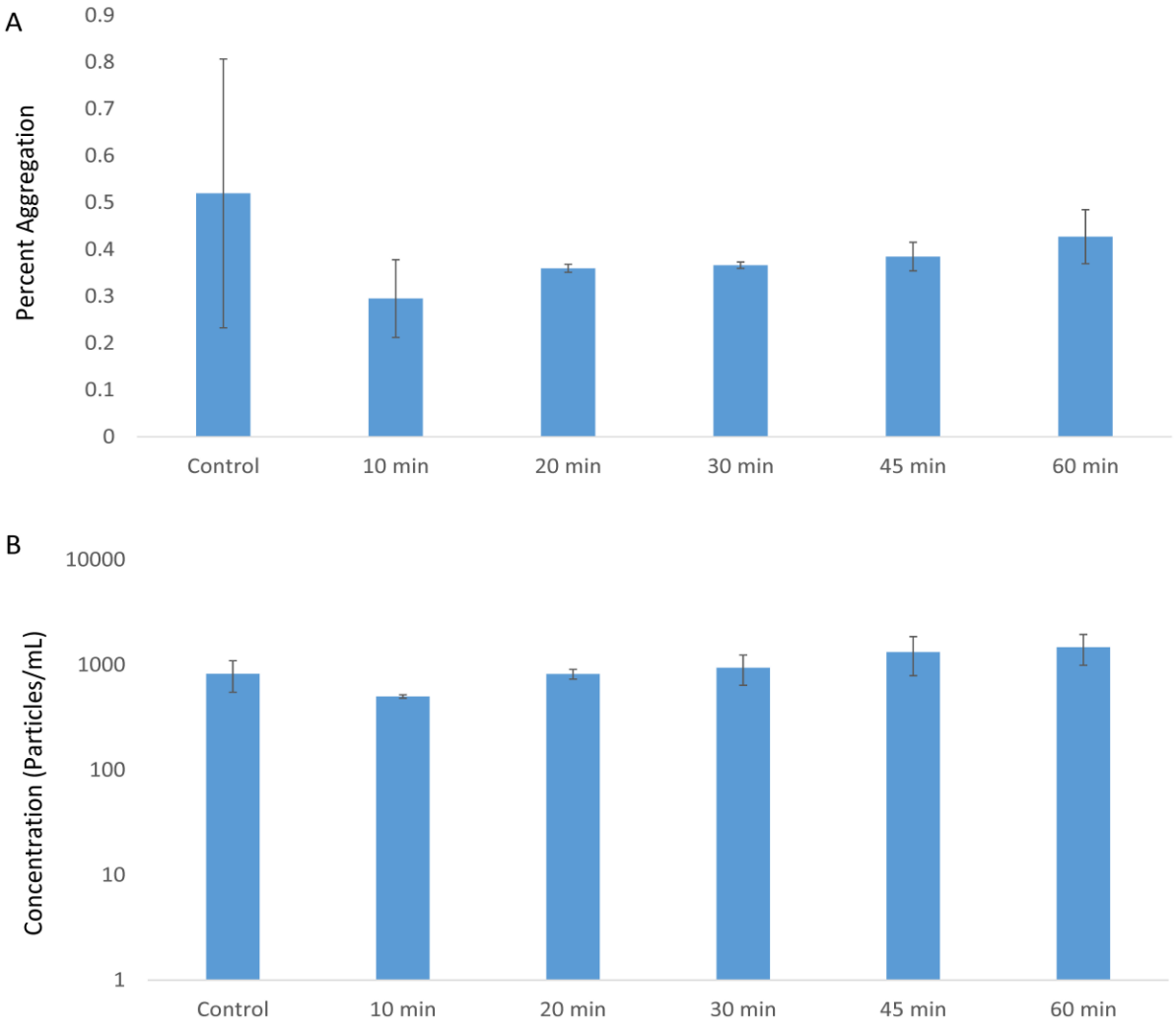

Figure 2.7: Effect of elevated temperature (50°C) on aggregation and subvisible particle formation of the bispecific antibody Bis3 as measured by SEC and MFI, respectively.

(A) Percent total aggregation (soluble and insoluble) of Bis-3 before and after temperature stress as measured by SEC, and (B) concentration of subvisible particles of Bis3 samples before and after thermal stress as measured by MFI from ≥2 <100 . Error bars represent one standard deviation (N=3). The Bis-3 was formulated at 0.2 mg/mL in a 20 mM sodium phosphate buffer containing 235 mM Sucrose at pH 7.2.

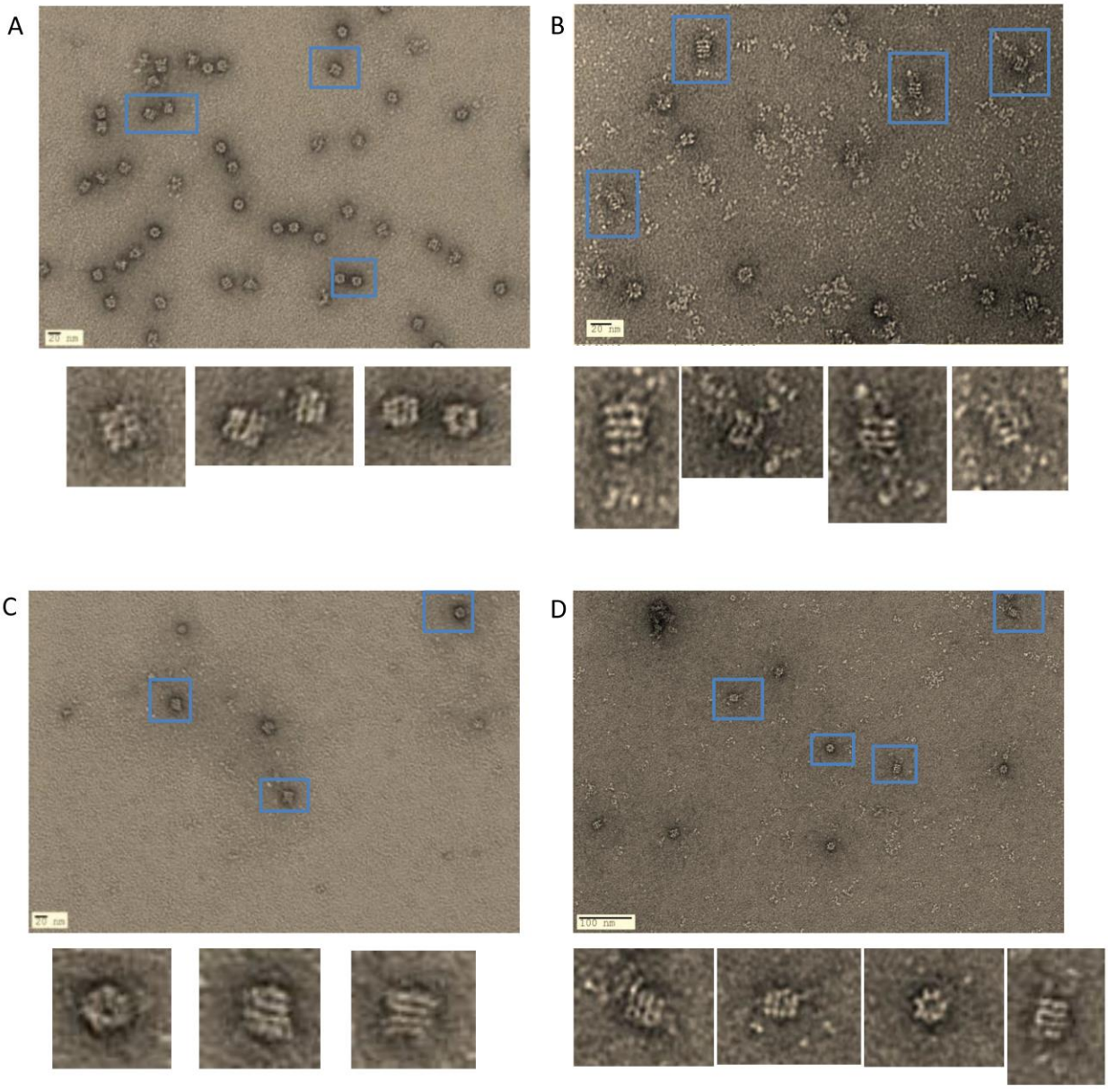
A
B
C
D
100 nm

Figure 2.8: Representative TEM images of GroEL alone and GroEL complexed to the bispecific antibody Bis-3 stressed at 50°C for 60 min.

Representative enlarged images of GroEL from each TEM images (blue boxs) are shown to the right. (A) GroEL alone in solution, (B) GroEL-stressed Bis-3 complexes formed in solution, (C) GroEL released from the BLI biosensor surface with 50 mM DTT, and (D) GroEL-stressed Bis-3 complexes released from the biosensor with 50 mM DTT. See methods section for further detail.

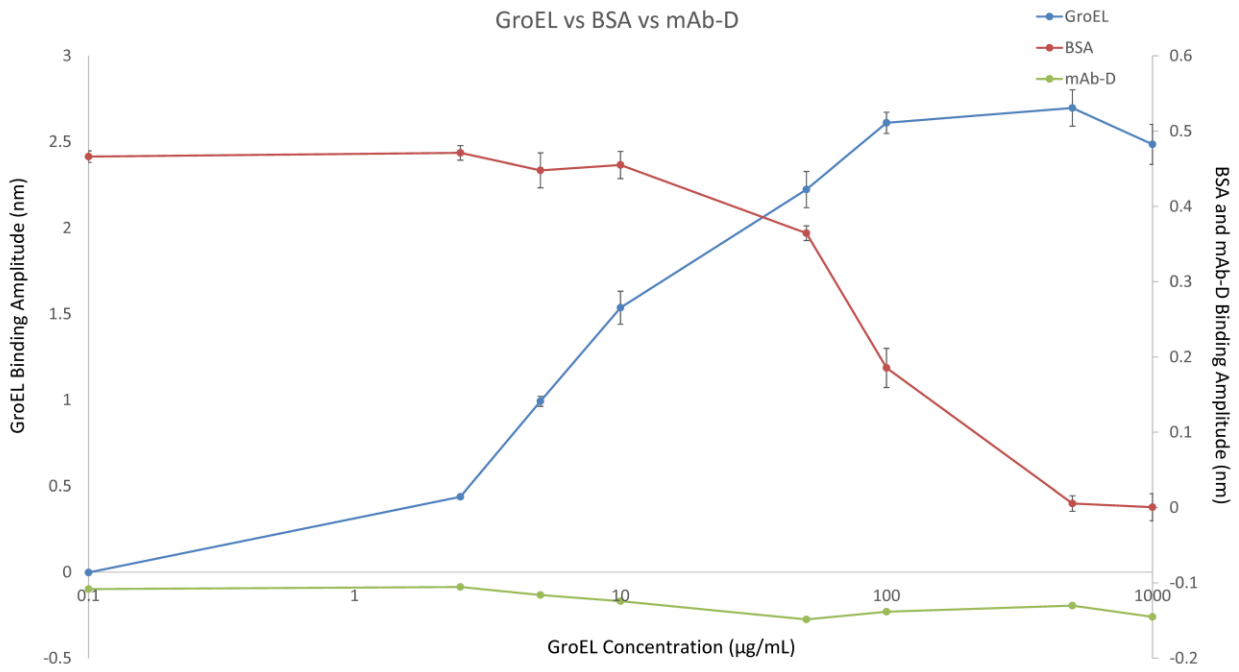

Supplementary Figure 2.1: Optimization of the GroEL-BLI biosensor method.

The binding amplitudes of the different concentrations of b-GroEL was plotted vs BSA (1 mg/mL). Unstressed mAb-D was exposed to the GroEL loaded tip with 150 mM NaCl and the binding amplitude was measured. (n=2-4, mean ± SD) at room temperature (25^{o}C).

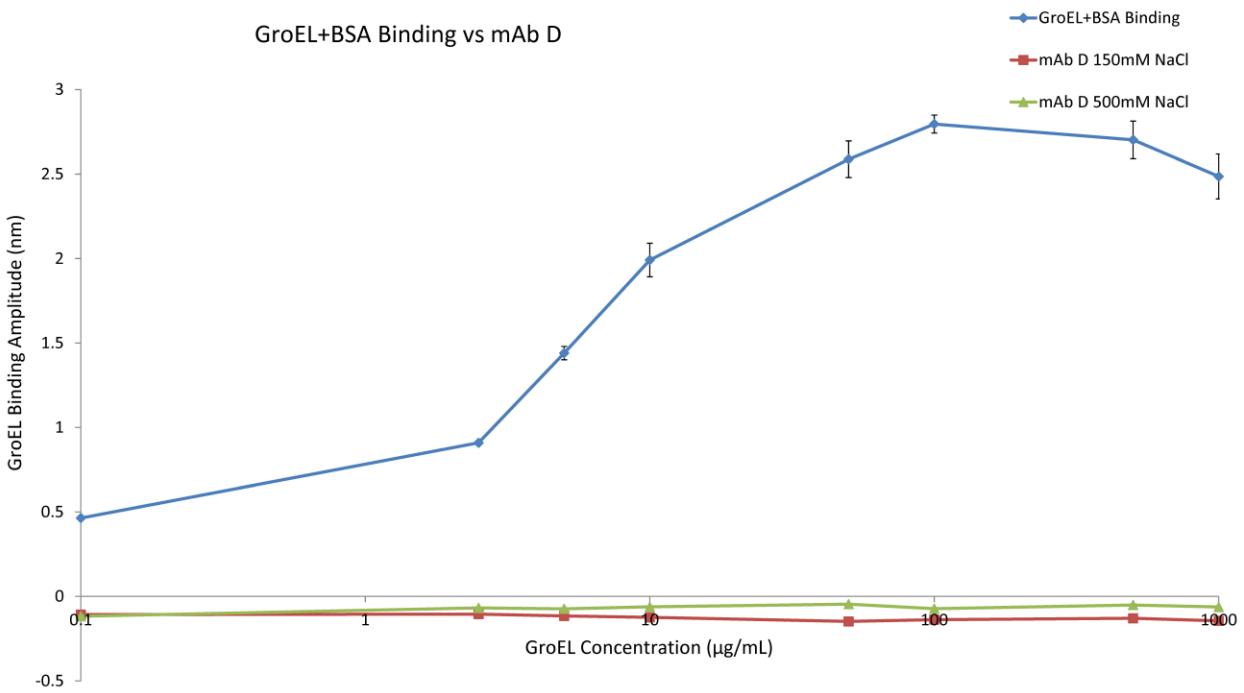

Supplementary Figure 2.2: Optimization of the GroEL-biosensor method.

The binding amplitudes of the different concentrations of b-GroEL and BSA (1 mg/mL) were summed together for total binding onto streptavidin tips. Unstressed mAb-D was exposed to the GroEL loaded tip with 150 and 500 mM NaCl and the binding amplitude was measured. (n=2-4, mean ± SD) at room temperature (25^{o}C).

2.5 References

1. Volkin DB, Hershenson S, Ho RJY, Uchiyama S, Winter G, Carpenter JF 2015. Two Decades of Publishing Excellence in Pharmaceutical Biotechnology. Journal of Pharmaceutical Sciences 104(2):290-300.

2. Ecker DM, Jones SD, Levine HL 2015. The Therapeutic Monoclonal Antibody Market. mAbs 7(1):9-14.

3. Leader B, Baca QJ, Golan DE 2008. Protein Therapeutics: A Summary and Pharmacological Classification. Nature Reviews Drug Discovery 7:21-39.

4. Alt N, Zhang TY, Motchnik P, Taticek R, Quarmby V, Schlothauer T, Beck H, Emrich T, Harris RJ 2016. Determination Of Critical Quality Attributes For Monoclonal Antibodies Using Quality By Design Principles. Biologicals 44:291-305.

5. Dobson CL, Devine PWA, Phillips JJ, Higazi DR, Lloyd C, Popovic B, Arnold J, Buchanan A, Lewis A, Goodman J, Walle CFvd, Thornton P, Vinall L, Lowne D, Aagaard A, Olsson L-L, Wollberg AR, Welsh F, Karamanos TK, Pashley CL, Iadanza MG, Ranson NA, Ashcroft AE, Kippen AD, Vaughan TJ, Radford SE, Lowe DC 2016. Engineering The Surface Properties Of A Human Monoclonal Antibody Prevents Self-Association And Rapid Clearance In Vivo. Nature Scientific Reports 6.

6. Majumdar R, Esfandiary R, Bishop SM, Samra HS, Middaugh CR, Volkin DB, Weis DD 2015. Correlations between changes in conformational dynamics and physical stability in a mutant IgG1 mAb engineered for extended serum half-life. mAbs 7(1):84-95.

7. Chaudhuri R, Cheng Y, Middaugh CR, Volkin DB 2014. High-Throughput Biophysical Analysis of Protein Therapeutics to Examine Interrelationships Between Aggregate Formation and Conformational Stability. The AAPS Journal 16(1):48-64.

8. Roberts CJ, Das TK, Sahin E 2011. Predicting solution aggregation rates for therapeutic proteins: Approaches and challenges. International Journal of Pharmaceutics 418(2):318-333.

9. Naik S, Kumru O, Cullom M, Telikepalli S, Lindboe E, Roop T, Joshi S, Amin D, Gao P, Middaugh C, Volkin D, Fisher M 2014. Probing structurally altered and aggregated states of therapeutically relevant proteins using GroEL coupled to Bio-Layer Interferometry. Protein Science 23(10):1461-1478.

10. Ellis RJ 2013. Assembly chperones: a perspective. Philosophical Transactions of the Royal Society B 368.

11. Sot B, Banuelos S, Valpuesta JM, Muga A 2003. GroEL Stability and Function: Contribution of the Ionic Interations at the Inter-ring Contact Sites. The Journal of Biological Chemistry 278:32083-32090.

12. Filipe V, Kukrer B, Hawe A, Jiskoot W 2012. Transient Molten Globules and Metastable Aggregates Induced by Brief Esposure of a Monoclonal IgG to Low pH. Journal of Pharmaceutical Sciences 101(7):2327-2339.

13. Mehta SB, Bee JS, Randolph TW, Carpenter JF 2014. Partial Unfolding of a Monoclonal Antibody: Role of a Single Domain in Driving Protein Aggregation. Biochemistry 53(3367-3377):3367-3377.

14. Sadavarte RH, Ghosh R 2014. A Thermal-Cycling Method for Disaggregating Monoclonal Antibody Oligomers. Journal of Pharmaceutical Sciences 103:870-878.

15. Fisher MT, Katayama H. 2011. Osmolyte Mixture for Protein Stabilization. In Services ICP, editor, ed.

16. Bond MD, Panek ME, Zhang Z, Wang D, Mehndiratta P, Zhao H, Gunton K, Ni A, Nedved ML, Burman S, Volkin DB 2009. Evaluation of a Dual-Wavelength Size Exclusion HPLC Method With Improved Sensitivity to Detect Protein Aggregates and ItsUse to Better Characterize Degradation Pathways of an IgG1Monoclonal Antibody. Journal of Pharmaceutical Sciences 99(6):2582–2597.

17. Kumru OS, Liu J, Ji JA, Cheng W, Wang YJ, Wang T, Joshi SB, Middaugh CR, Volkin DB 2012. Compatibility, Physical Stability, and Characterization of an IgG4 Monoclonal Antibody After Dilution into Different Intravenous Administration Bags. Journal of Pharmaceutical Sciences 101(10):3636-3650.

18. Hawe A, Kasper JC, Friess W, Jiskoot W 2009. Structural Properties of Monoclonal Antibody Aggregates Induced by Freeze–Thawing and Thermal Stress. European Journal of Pharmaceutical Sciences 38(2):79-87.

19. Chames P, Regenmortel MV, Weiss E, Baty D 2009. Therapeutic Antibodies: Successes, Limitations, and Hopes For The Future. British Journal of Pharmacology 157:220-233.

Chapter 3 Evaluation of Hydrogen Exchange Mass Spectrometry as a Stability-Indicating Method for Formulation Excipient Screening for an IgG4 Monoclonal Antibody

(Toth IV TR, Pace SE, Mills BJ, Joshi SB, Esfandiary R, Middaugh CR, Weis DD, Volkin DB 2018. Evalutation of Hydrogen Exchange Mass Spectrometry as a Stability-Indicating Method for Formation Excipient Screening for an IgG4 Monoclonal Antibody. Journal of Pharmaceutical Sciences 107(4):1009-1019.)

3.1 Introduction

Monoclonal antibodies (mAbs) are an important class of therapeutic biomolecules and represent the majority of protein-based drug candidates currently in development.[1,2] They are molecules that exhibit diverse conformational changes on a variety of timescales, and it is important from a pharmaceutical perspective to better understand the relationship between mAb conformational stability, conformational dynamics, and storage stability.[3,4] A monoclonal antibody consists of 4 polypeptide chains connected by disulfide bonds, 2 heavy chains, and 2 light chains. The heavy chains form the tertiary structural domains CH1, CH2, CH3, and VH, whereas the light chains form the tertiary structural domains CL and VL.[5] The higher order structure of a mAb consists of 2 antigen-binding domains (Fab) and 1 crystalizable domain (Fc). These structural elements are arranged in a "Y-shaped" structure, with the linkages between domains being highly flexible.[6-8] Owing to the flexible linker, mAbs are highly dynamic molecules in solution, capable of movements ranging from small-scale fluctuations to large-scale rearrangements of the domains.[7-9]

The physicochemical stability of mAbs is a critical factor to consider in the effort to develop high-quality efficacious drug candidates. A common strategy to improve long-term storage stability and to help protect protein pharmaceuticals from environmental stresses is to add one or more excipients to the formulation. Some commonly used excipients are salts, amino acids, carboxylic acids, carbohydrates, detergents, sugars, and polyols.[10] Stabilizing excipients are generally identified through excipient screening, an empirical approach where physicochemical stability of the protein of interest is assessed in a large number of test formulations containing excipients of interest. Owing to the large numbers of test formulations, such physical stability

profiles are often measured rapidly by taking advantage of high-throughput screening methods employing multiple monitoring techniques.[11-13]

Previous studies in our laboratory have explored the interrelationships between mAb conformational dynamics as measured by hydrogen exchange mass spectrometry (HX-MS), mAb aggregation propensity and conformational stability, and the influence of various pharmaceutical excipients and other additives on each of these parameters. Similarly, the potential and utility for HXMS to probe for mAb conformational dynamics in pharmaceutical formulations was recently reviewed.[4] It has been shown that backbone dynamics can be significantly altered in specific regions of different mAbs due to varying solution conditions, site-directed mutations, and chemical modifications. In addition, other studies have successfully used HX-MS to characterize aggregation pathways[14] and propensity,[15] and to characterize higher order structural differences resulting from point mutations[16] or between biophysically similar molecules.[17] It has been shown that increased conformational stability and reduced aggregation propensity correlate with small decreases globally in relative local flexibility. In addition, large increases in relative local flexibility in the CH2 domain, HC 241-251, correlated with decreased conformational stability and increased aggregation across several different IgG1mAbs. The ability of HX-MS to monitor backbone dynamics in differing formulations has thus been proposed to be a potential analytical tool for formulation scientists. As opposed to conducting accelerated and real-time stability studies where results take months to years to generate, HXMS could potentially be used to rapidly assess (using minimal material) rigidifications or perturbations in protein structure in the presence of excipients that correlate with stabilization/destabilization effects observed over time in storage stability studies.

To further expand this idea using a case study, HX-MS was used in this work to monitor conformational dynamics of an IgG4 mAb (mAb-D) in the presence of various additives, including pharmaceutical excipients as well as known protein destabilizers (used as controls), and the results were correlated with traditional biophysical techniques. To the best of our knowledge, this report is the first-time HX-MS with an IgG4 mAb that has been performed in the context of formulation development. In addition, although HX-MS has the potential to be an important tool for excipient screening, one barrier to implementing this approach is that differing excipient solutions can alter chemical exchange rates in hydrogen exchange (HX) experiments, rendering HX results from differing formulations difficult to interpret due to combined effects of additives on the protein's conformational flexibility as well as the inherent chemical exchange rate. Recently, we have validated a procedure to correct HX-MS data for these differences with minimal additional experimentation.[18] To more extensively evaluate the potential applicability of HX-MS for excipient screening as part of the formulation development of therapeutic mAb candidates, the effect of various additives on an IgG4 mAb (mAb-D) was evaluated using traditional approaches with standard biophysical techniques: forced degradation study using DSC (conformational stability), and accelerated stability studies using size exclusion chromatography (SEC) and microflow imaging (MFI; to monitor aggregation and particle formation, respectively). The results from the biophysical measurements are compared with those obtained from HX-MS (using a streamlined version of the methodology) to determine if correlations can be drawn between the effects of the additives on mAb-D stability as detected by the different approaches/methods.

3.2 Materials and Methods

3.2.1 Materials

The IgG4 (mAb-D, ~145,000 Da, calculated pI 7.07) was provided by MedImmune (Gaithersburg, MD) at a concentration of 50 mg/mL in 50-mM acetate, 100-mM NaCl, pH 5.5. After dialysis, the mAb concentration was quantified with an Agilent 8453 UV-visible spectrophotometer (Palo Alto, CA). Triplicate samples were prepared by diluting the stock mAb solution 1:50 into buffer. The intensity at 280 nm was averaged for over triplicate analyses. An extinction coefficient of1.68 (mg/mL)1 cm1 was used to calculate the protein concentration. Trehalose dihydrate was purchased from Pfanstiehl (Waukegan, IL). Arginine monohydrochloride, deuterium oxide (99 + %D), D-methionine, D-mannitol, porcine pepsin, sodium sulfate, TWEEN® 20, and liquid chromatography grade acetic acid and phosphoric acid were purchased from Sigma-Aldrich (St. Louis, MO). Premiumgrade tris (2-carboxyethyl) phosphine hydrochloride and liquid chromatography-mass spectrometry (LC-MS) grade formic acid (+99%) were purchased from Thermo Scientific (Rockford, IL). Sodium phosphate dibasic (anhydrous), citric acid (anhydrous), and sodium thiocyanate were purchased from Acros Organics (Fair Lawn, NJ). Sodium chloride, guanidine hydrochloride (Gdn-HCl), LC-MS grade water, acetonitrile, and isopropanol were purchased from Fisher Scientific (Fair Lawn, NJ). For stability studies, glass vials used were from West Pharmaceuticals, (3-mLVial, Fiolax Clear, Item#6800-0316), and the rubber stoppers were from West Pharmaceuticals (V-35 4432/gray, Item#10122128).

3.2.2 Methods

3.2.2.1 *Sample Preparation*

Stock solutions of mAb-D were dialyzed into 5-mM citratephosphate (CP) buffer at pH 6.5 or 7.4, with or without 150-mM NaCl. Dialysis was performed using Slide-A-Lyzer cassettes (30,000 MWCO; Thermo Fisher Scientific, Waltham, MA) with a ratio of sample to dialysate at least 1:500, 3 times with at least 4 h between buffer changes. A stock solution of each additive was also prepared in 5-mM CP at pH 6.5 or 7.4, with or without NaCl, at a higher concentration than desired in the final sample. The mAb-D stock solution was diluted using the corresponding CP buffer and the appropriate additive stock solution to achieve a protein concentration of 5 mg/mL and the desired additive concentration (e.g., 0.3-M arginine, 0.3-M guanidine, 0.3-M sodium thiocyanate, 0.3-M sodium sulfate, 0.2-M methionine, 0.4-M trehalose, 0.8-M mannitol, or 0.05% polysorbate 20 [PS20]). Control samples of mAb-D were prepared using only CP buffer at the appropriate pH, with or without NaCl. After addition ofmAb-D and the additive, the pH value of the samples was adjusted (using acid and base) to be within 0.1 pH unit of the desired pH. Buffer controls were also prepared in the same manner without addition of mAb-D. Both mAb-D and buffer control samples were placed in a laminar flow hood and sterile filtered using 0.22-mm syringe filters (Millipore, Billerica, MA). Aliquots, 1.5 mL, were placed into 3-mL type I borosilicate glass vials and capped with rubber stoppers and an aluminum overseal (West Pharmaceutical Services, Exton, PA). Before use, glass vials were autoclaved in a large beaker and allowed to cool overnight.

For accelerated stability studies, samples of mAb-D were stored at 4°C and 50°C. Triplicate samples from 3 separate vials were analyzed by SEC and MFI at time 0 and after storage for 2 weeks at 4°C and after 1 and 2 weeks at 50°C. Triplicate buffer samples were prepared and

analyzed at time 0 by MFI. For stirring stress studies, mAb-D and buffer control samples were stressed by placing a small pivot-ring-free stir bar (7 x 2mm flea micro; Bel-ArteSP Scienceware, Wayne, NJ) inside each 3-mL vial prepared as described above and stirring on setting 5 at 25°C for 30 min using a ReactiTherm III (Thermo Scientific). No vortex was observed under these conditions.

For the HX-MS studies, additives which contain exchangeable hydrogens were fully deuterated before sample preparation. Each additive was prepared in D2O at a slightly higher than final concentration (to account for dilution effects) and allowed to incubate for 30 min. The additive solution was vacuum dried at 30°C for 48 h. Two additional cycles of dissolution in D2O followed by evaporation were performed. The final powder was dissolved in the appropriate volume of CP buffer prepared using D2O. The pD was adjusted 6.5 or 7.4 with deuterium chloride or deuterium oxide. To account for the offset associated with measuring pD with a pH meter, solutions were adjusted to a pH 0.4 units lower than the desired value.[19]

3.2.2.2 *Size Exclusion Chromatography*

SEC was performed on all samples using a 7.8 mm x 30 cm TOSOH TSK-Gel BioAssist G3SWXL column and 6.0 mm ID x 4.0 cm TSK-Gel SWXL guard column (TOSOH Biosciences, King of Prussia, PA), with UV detection at 214 and 280 nm using a prominence high performance liquid chromatography system (Shimadzu, Tokyo, Japan) equipped with a photodiode array detector. Before analysis, the column was pre-equilibrated with 90 mL of mobile phase, composed of 0.2-M sodium phosphate, pH 6.8. Removal of insoluble aggregates from the stressed samples was accomplished by centrifugation at 14,000 x g for 5 min before injection onto the column. Molecular weight standards (Biorad Laboratories, Hercules, CA) were used to assess the efficiency

of separation. Peaks corresponding to aggregates, monomer, and fragments were selected and quantified using the LC Solutions data analysis package (Shimadzu).

3.2.2.3 *Microflow Imaging*

A DPA-4200 MFI system (Protein Simple, Santa Clara, CA) was used to count and image subvisible particles in the size range of 2-100 mm. The instrument was calibrated using 10-mm polystyrene particle standards (Duke Standards; Thermo Fisher Scientific, Waltham, MA) before measurements. Measurements were made in triplicate at ambient temperature for all samples with no centrifugation before analysis. The cell was flushed with particle free water and illumination was optimized using particle-free water before all measurements. The samples were carefully drawn up in a low protein binding, filter-tip pipette (Neptune Scientific) and analyzed using a flow rate of 0.2 mL/min. The purge volume for each measurement was 0.4 and 0.6 mL of sample was analyzed. Particles with circularity greater than 0.95 were filtered out before analysis to avoid counting air bubbles as protein particles.

3.2.2.4 *Differential Scanning Calorimetry*

Differential scanning calorimetry was performed using a Microcal VP-Capillary DSC equipped withanautosampler (MicroCal, Northampton, MA). Samples were heated from 15°C to 85°C using a scan rate of 1°C/min. Reference thermograms of buffer containing the respective additives were subtracted from the thermograms of mAb-D in the presence of the additive. Each mAb-D sample was analyzed in triplicate, except mAb-D prepared in Mannitol without NaCl at pH 7.4 in which only 1 and 2 thermograms were used for analysis, respectively. The data were fitted to a multistate model with 2 transitions using the MicroCal LLC DSC plug-in for the Origin 7.0 software. The onset temperature (Tonset) was determined using the temperature at which the heat capacity (Cp) reached 500 cal mol^{-1} C^{-1} for the first thermal transition.

3.2.2.5 *Hydrogen Exchange Mass Spectrometry*

HX-MS experiments were performed using a QTOF mass spectrometer (Agilent 6530, Santa Clara, CA) as described previously.[20] Three microliters of mAb-D prepared at 40 mg/mL were labeled with deuterium at 25°C using 21 mL of deuterated buffer. The pD of all labeling buffers was adjusted to 6.5 or 7.4 with deuterium chloride or deuterium oxide, using the offset associated with measuring pD with a pH meter, solutions were adjusted to a pH 0.4 units lower than the desired value.[19] Samples of mAb-D were subjected to the exchange conditions for either 1000 s (pH 6.5) or 125 s (pH 7.4). Incubation at each time point was completed in triplicate. After incubation, the HX reaction was quenched using a 1:1 dilution into quench buffer (4-M Gdn-HCl, 0.2-M phosphate, 0.5-M tris (2-carboxyethyl) phosphine hydrochloride, pH 2.5) at 1°C for 60 s. Twenty-five microliters of quenched mAb-D was injected into the sample loop of a refrigerated compartment (maintained at 0°C) containing a pepsin column (50 X 2.1 mm, pepsin was immobilized and packed as described previously[4]), reversed phase trap (Poroshell 120 EC-C8, 2.1 X 5 mm, 2.7 micron particle diameter; Agilent), and reversed phase column (Zorbax 300SB-C18 2.1 X 50 mm, 1.8 micron particle diameter; Agilent).

MS/MS analysis was used to generate a peptide map of mAb-D consisting of 360 peptides with 97% sequence coverage of the light chain and 98% sequence coverage of the heavy chain. Comprehensive analysis of all of the HX-MS data from all peptides in all formulations would substantially diminish throughput without necessarily adding additional value for this application. As such, from this set of 360 peptides, a subset of 40 peptides was chosen for analysis. To generate this subset of peptides, a similar number of peptides were chosen from each domain of mAb-D, with some peptides exhibiting differences in deuterium accessibility in the presence of additives (based on screening studies) and others showing no differences in deuterium uptake. Peptides

crossing domain boundaries were assigned to the domain belonging to the majority of its residues. The HX data were processed using HDExaminer software (Sierra Analytics, Modesto, CA). Difference plots for each peptide were generated by subtracting the mass of each peptide after labeling in CP control buffer from that of the peptide when labeled in the additive containing buffer. For some figures, the y axis is displayed as "fractional uptake," here defined as the uptake in Da divided by the number of residues in the peptide.

While HX-MS has the potential to be a useful tool for screening of additives for mAb stability effects, a barrier to this type of work is the propensity of differing excipient solutions to alter chemical exchange rates in HX experiments, rendering varying results from differing formulations. Recently, we have outlined a procedure to correct HX-MS data for these potential differences with minimal additional experimentation,[18] briefly, differences in chemical exchange rates in different formulations are determined using a short reporter peptide having the sequence YPI. Then a correction from the YPI data is determined that is used to empirically correct the HX data for differences in the intrinsic HX rate caused by the excipients, ensuring that any differences remaining are a function of protein dynamics.

3.3 Results

3.3.1 Screening of mAb-D for Stabilizing Additives by DSC, SEC, and MFI

Eight different additives were selected for evaluation in this work: trehalose, mannitol, methionine, arginine hydrochloride, sodium sulfate, sodium thiocyanate, and Gdn-HCl. The additives cover different classes of pharmaceutical excipients including salts, amino acids, sugars, polyols, and detergents, or have wellestablished effects including both destabilization and stabilization of proteins.[10] As an initial step in better understanding the effect of these 8 different additives on the stability ofan IgG4 mAb (mAb-D), differential scanning calorimetry was

performed to evaluate their effects on the overall conformational stability of the mAb-D. Figure 1a shows representative DSC thermograms of mAb-D at pH 6.5 with 150-mM NaCl in the control buffer and with the control buffer containing a stabilizing and a destabilizing additive. The DSC thermograms were fitted to 2 thermal transitions (Tm1 and Tm2) as well as a thermal onset value (Tonset) as shown in Figure 1b. The Tm1, corresponds to the CH2 domain, and is likely to be important for the initiation of destabilization and aggregation as its unfolding occurs at the lowest temperature. Figure 2 shows the effect of the 8 additives on the thermal transitions of mAb-D at different solution pH values in the presence and absence of NaCl. It can be seen that thermal transition values of mAb-D trend somewhat higher at pH 7.4 compared with pH 6.5 and that the addition of NaCl had a minimal effect. In contrast, thiocyanate, guanidine, and arginine had a notable destabilizing effect, whereas mannitol and trehalose had a stabilizing effect. Methionine, PS20, and sodium sulfate had no major effects compared with the control mAb-D solution.

The effect of the same formulations on the aggregation propensity of mAb-D during storage at elevated temperatures was then evaluated by a combination of SEC and MFI analysis. SEC was performed on each of the mAb-D samples with and without various additives before and after incubation for 14 days at 50°C. Figure 3 shows the effect of the additives on the total aggregate formation (soluble and insoluble aggregation) of mAb-D following heat stress. As shown in Figure 3a for mAb-D in control buffer alone, on heat stress, the formation of aggregate and fragment species occurs, as well as the loss of total area. The total amount of aggregation is defined as the sum of aggregate peaks (soluble aggregates) and the loss of total area (referred to here as insoluble aggregates; caused either by formation of aggregates too large to enter the column or nonspecific binding to the column which may be related to conformational changes). Also shown in Figure 3a is that additives in the control buffer can either alleviate or promote the

formation of aggregates. Figure 3b shows the additives ranked by their propensity to promote aggregation. It can be seen that aggregation trends higher at pH 7.4 compared with pH 6.5, and that the absence of NaCl led to increased aggregation of mAb-D. The addition of thiocyanate, guanidine, and arginine had a notable destabilizing effect with large increases in aggregate formation. Mannitol had a stabilizing effect. Methionine, PS20, sodium sulfate, and trehalose had no major effects compared with the control mAb-D solution.

The same samples were also analyzed by MFI for formation of subvisible particles before and after incubation for 14 days at 50°C and after stirring stress. For both stresses, the total subvisible particle concentration before stress for each of the additive solutions was below 2500 particles/mL (Supplemental Fig. S1a). For conditions with 150-mM salt, the total particle concentrations of the mAb-D samples before stress were below 16,000 particles/mL for all additives, except sulfate, where total particle concentration before stress was higher, approximately 105 particles/mL (see Supplemental Fig. S1b). For samples without salt, the total particle concentrations before stress were higher but were still below 35,000 particles/mL for all samples (Supplemental Fig. S1b). Particle size distributions in mAb-D samples before stress, in general, have the highest concentration of particles in the smallest size bin and concentrations decrease with particle size (Supplemental Fig. S2). Figure 4a shows the effects of the additives on the total subvisible particle formation by mAb-D following heat stress. Under these conditions, solution pH and NaCl had a complex effect on mAb-D subvisible particle formation with both stabilizing and destabilizing effects caused by the different additives. Thiocyanate, guanidine, arginine, and to a lesser extent sodium sulfate, had destabilizing effects leading to increases in subvisible particle formation. In contrast, methionine, trehalose, mannitol, and PS20 had no major effects compared with the control mAb-D solution with low concentrations of subvisible particles

after stress. For most samples, although total particle concentrations increased on heat stress, the distribution ofparticles among the different size bins did not change (see Supplemental Fig. S3). Exceptions are the additives arginine and Gdn-HCl at pH 6.5 + NaCl, where the concentration of particles in the 5-10 mm size bin increased relative to other bins (when compared to time 0) and guanidine at pH 7.4 without NaCl, where particle concentrations in the 5-10, 10-15, 15-25, and 25-40 μm size bin increased relative to other bins when compared with time 0.

The effect of the same set of the 8 additives on the physical stability of mAb-D after stir stress was then evaluated. The results of MFI analysis of the number and size range of subvisible particles formed because of stirring are shown in Figure 4b. Under stir stress conditions, solution pH and NaCl also had a complex effect on mAbD subvisible particle formation with both stabilizing and destabilizing effects caused by different additives. Gdn-HCl had an effect on the stressed mAb-D samples leading to increases in subvisible particle formation. In contrast, sulfate and methionine had no notable effects compared with mAb-D control buffer. In addition, mAb-D solutions containing thiocyanate, arginine, trehalose, mannitol, and PS20 all displayed low concentrations of subvisible particles. For all samples, the particle size distributions on stir stress were altered compared with time 0, with particle concentrations in the smallest (2-5 μm) size bin increasing relative to other size bins.

3.3.2 Screening of Additives for Effects on mAb-D Local Flexibility by HX-MS

A peptide map was developed for mAb-D consisting of 360 peptides with 97% sequence coverage of the light chain and 98% sequence coverage of the heavy chain. To reduce analysis load, a subset of 40 peptides were chosen for analysis such that a similar number of peptides covered each domain of mAb-D. HX was then measured for mAb-D in 5-mM CP and mAb-D in 5-mM CP with each 1 of the 8 additives, at the salt and pH conditions described previously. After

the reaction was quenched at different exchange times, peptic peptides were generated and analyzed by LC-MS to determine deuterium uptake. A chemical exchange correction factor was established for all solution conditions as described in methods.[18] Figure 5a-5c show plots of the difference (following additive correction) between HX by mAb-D with additives minus mAb-D in control buffers.

Figure 5 demonstrates that additives can have a substantial effect on HX results with mAb-D. For example, the additives arginine, guanidine, sulfate, and thiocyanate caused substantial increases in HX in many peptide segments, relative to mAb-D in the corresponding control buffer, indicating increases in backbone flexibility. Concurrent with these substantial increases in flexibility for specific peptide segments was a trend of small increases in flexibility in the majority of peptide segments for those same additives except thiocyanate. Mannitol, methionine (for pD 7.4 with NaCl), and PS20 (for pD 6.5 + NaCl pD 7.4 + NaCl) caused slight global increases in flexibility without the substantial localized increases that were observed in the presence of arginine, guanidine, sulfate, and thiocyanate. The opposite effect was also noted for some additives, with a global decrease in flexibility for methionine (pD 6.5 + NaCl and pD 7.4) and trehalose. In general, increased pH (comparing left column to middle column) had no notable effect on flexibility with the exception of methionine where increased pH caused a slight global increase in flexibility and thiocyanate where increased pH caused a slight global decrease in flexibility. Addition of salt (comparing right column to middle column) had no notable effect for arginine, guanidine, mannitol, and sulfate, while resulting in a slight increase in flexibility for methionine, PS20, and thiocyanate, and a slight decrease in flexibility for trehalose. For visualization of these HX observations, the most substantial additive effects on local flexibility of mAb-D were mapped onto a homology model of the antibody (based on PDB 5DK3[21]) displayed in Figure 6.

3.4 Discussion

The main goal of this study was to correlate the HX data collected with mAb-D in the presence of various additives with both conformational stability data (DSC) and the propensity of mAb-D to form aggregates and particulates over time (as measured by an accelerated stability study combined with SEC and MFI analysis). We aimed to determine what aspects of mAb-D stability (from a pharmaceutical perspective) can be most directly reported on by local flexibility analysis from HX-MS, and to evaluate whether a streamlined version of HX-MS can serve as a useful screening technique to identify stabilizing excipients. If adequate correlates can be found, HX-MS may serve as a useful technique to predict aspects of mAb storage stability in different solutions and thus has the potential (given additional correlations with more comprehensive stability data sets as part of future work) to be used as an alternative to accelerated stability studies.[22] To this end, as a first step, we focused on various approaches to analyze the HX-MS data generated with mAb-D in the presence of various additives (e.g., commonly used pharmaceutical excipients as well as control additives known to destabilize proteins) to provide an overall description of the trends (in terms of excipient effects) that can be more easily compared with mAb-D stability data collected by more traditional approaches, as outlined below.

3.4.1 Traditional Additive Screening Studies With mAb-D Using DSC, SEC, and MFI

Results from DSC studies (Fig. 2) reveal that mAb-D is conformationally destabilized in the presence of guanidine, thiocyanate, and arginine, listed from greatest to least destabilizer. In addition, trehalose proved to be the most notable conformational stabilizer of mAb-D. In general, increased pH (comparing blue through orange bars) resulted in a trend (although within error) toward an increase in thermal stability for mAb-D in all additive solutions, with the exception of thiocyanate and guanidine, where increased pH slightly decreased thermal stability (also within

error). Addition of salt (comparing black and gray bars) in general caused a slight decrease in thermal stability for mAb-D in all additive solutions (within error) with the exception of arginine, where thermal stability slightly increased (within error) on addition of salt.

Results from SEC studies of aggregation after heat stress (Fig. 3) reveal the same trend, with mAb-D exhibiting the greatest increase in percent aggregation in the presence of guanidine, thiocyanate, and arginine, listed from greatest aggregation to least. In addition, results on subvisible particle formation from MFI studies (Fig. 4) following heat stress further confirm this trend, with mAb-D in the presence of guanidine, thiocyanate, and arginine showing the greatest total particle concentrations, listed in order from greatest total particle concentration to least. Trehalose was not a significant stabilizer in aggregation due to heat stress studies. Results from SEC and MFI studies of aggregation after heat stress reveal that increased solution pH values (comparing blue to gray bars, Figs. 3b and 4a) resulted in a substantial increase in aggregation for destabilizing additives, yet values were within error for stabilizing additives. Addition of salt (comparing black and gray bars) resulted in a substantial decrease in mAb-D aggregation due to heat stress for all additive solutions, both stabilizing and destabilizing. These results indicate that mAb-D is less colloidally stable at pH values above the pI ofmAb-D (~7.07, estimated based on sequence) where mAb-D is net negatively charged, and that addition ofsalt alleviates this colloidal instability, perhaps by screening of electrostatic interactions.

In summary, the results from heat stress of mAb-D in the presence of the 8 additives indicate that conformational destabilization is likely an important step in the pathway to aggregation due to heat stress for mAb-D. In the first step of one of the main aggregation pathways of mAbs proposed by Roberts et al.,[23,24] and confirmed by others,[25] the native monomers become partially unfolded and begin to associate into loose clusters. In the second step, within these clusters the

now exposed aggregation hotspots can align and lead to the formation of irreversible aggregates. It is likely that the DSC results report on this first conformational destabilization step thus its apparent correlation with aggregation due to heat stress.

In general, the results of aggregation due to stir stress (Fig. 4b) do not correlate with DSC results (in contrast to the results described above for heat stress). Most notably, the additives thiocyanate and arginine, while significant destabilizers in DSC (Fig. 2) and aggregation due to heat stress (Figs. 3b and 4a) studies, are significant stabilizers for aggregation due to stir stress. These results indicate that aggregation due to stir stress does not follow the same pathway as aggregation due to heat stress. It is likely that the pathway responsible for aggregation due to stir stress instead involves unfolding and nucleation on the liquid-solid or liquid-air interfaces,[26] thus the ability of surfactants such as PS20 and zwitterions such as arginine to act as stabilizers.

3.4.2 Additive Screening Studies With mAb-D Using HX-MS

To correlate these results with the HX data, we must also treat the HX data to obtain an overall trend. Here we do so by reducing the dimensionality of the HX data in several ways. First, we restrict our view to a CH2 aggregation hotspot region identified previously in our laboratory in IgG1 mAbs[27] (Fig. 7). This region covers residues 241-251 in the heavy chain and contains several hydrophobic residues that pack against glycans in the structure of IgG1 mAbs. This region corresponds to residues 250-260 for mAb-D. In general, the CH2 peptide was significantly more flexible in the presence of thiocyanate, guanidine, arginine, and sulfate than in control buffer, listed in that order from greatest to least increase. In comparison to the control buffer alone, PS20, mannitol, and methionine had no effect within experimental error. Finally, the CH2 peptide was significantly more rigid in the presence of trehalose. This additive trend most closely matches that of the conformational stability of mAb-D as measured by DSC,

suggesting that HX in this case is reporting most directly on conformational stability. This trend also matches that of mAb-D aggregation due to heat stress, and likely this correlation exists for the reason mentioned previously, that conformational destabilization is an important step in the pathway to aggregation due to heat stress for mAb-D, a common aggregation pathway for mAbs.[24,28]

We also averaged the HX data over the 5 peptides from each domain with the greatest magnitude (absolute value) of fractional exchange difference, chosen from among the 40 peptides seen in Figure 5 (Fig. 8). No trends were found in the effects of additives matching those seen in conformational stability and aggregation due to heat stress, with the exception of the CH2 domain. The trend in the CH2 domain explicable by the influence of the CH2 aggregation hotspot peptide discussed previously.

In addition, we restricted our view of the HX data to one peptide (chosen from the subset of 40) spanning each complementarity-determining region (CDR) region (Fig. 9), as well as to the average HX difference over the whole protein (Fig. 10). No correlations were found when examining the HX data from the CDR regions of mAb-D (Fig. 9) or when examining the HX data averaged over the whole protein (Fig. 10). This result may seem at odds with studies where the nature of the CDR loops are found to be important in the aggregation pathway of a mAb[29]; however, it is possible that for mAb-D, the composition of the CDR loops are not prone to induce aggregation, and thus the observed CH2 destabilization (observed by HX within an aggregation "hotspot", residues 250-260 for mAb-D) is the rate-limiting step in the aggregation pathway for this particular mAb. The effects of additives on the whole protein's average flexibility can be seen in Figure 10, showing fractional uptake averaged among all peptides. The overall trends in the HX are that guanidine, sulfate, arginine, mannitol, and PS20 caused an increase in average

global hydrogen exchange across the entire protein. Both thiocyanate and methionine had no effect on the average global exchange, whereas trehalose caused a decrease in average global exchange.

In contrast to heat stress, where a good correlation was observed between HX of the aggregation hotspot (and entire CH2 domain) and mAb-D physical stability, no such correlation was found between HX and aggregation due to stir stress. Likely this is because the aggregation pathway for stir stress is an interfacial phenomenon that does not involve steps that HX-MS can report on directly. It has been established that mAbs often follow differing aggregation pathways depending on the stress applied.[28] Here, an apparent trend is that amphipathic molecules capable of acting as surfactants (e.g., PS20) tend to be stabilizers in aggregation due to stir stress, indicating that the pathway for aggregation due to stir stress likely involves accumulation of protein at the air/water interface, another common pathway.[28]

Results from averaged HX-MS results and biophysical studies, as a function of heat and stir stresses, are summarized in Figure 11, where additives are colored based on HX-MS results for the CH2 aggregation hotspot peptides. In general, additives that promote flexibility in a hotspot peptide (yellow) of mAb-D tend to be destabilizing in terms of conformation (measured by DSC) and aggregation propensity during storage at elevated temperatures (as measured by SEC). The exception to this trend is sulfate, which caused increased flexibility in HX-MS studies in the hotspot region of mAb-D, but was not observed to be a destabilizer in the physical stability studies. In the HX-MS studies, sulfate increased flexibility to a lesser extent than guanidine, thiocyanate, or arginine. It is possible that the smaller increase in flexibility is not sufficient to destabilize mAb-D during storage, or that the destabilization effect would be revealed only with longer incubation times. It is also possible that the destabilization by sulfate is more complex

phenomena given that sulfate is a divalent anion (e.g., charge shielding effects). In contrast, no such consistent trend between additive effects on mAb-D as measured by HX-MS, DSC, and SEC studies were observed when stirring is the stress.

Table 3.1: Percent monomer content by SEC analysis

Mixture	Average Monomer Percent
HM-Fc control	99.7±0.0
Man5-Fc Control	99.7±0.1
GlcNAc-Fc Control	99.8±0.1
N297Q-Fc Control	97.8±0.0
Mixture 1	99.7±0.0
Mixture 2	99.6±0.1
Mixture 3	98.9±0.1
Mixture 4	99.6±0.1
Mixture 5	99.6±0.0
Mixture 6	99.4±0.1
Mixture 7	99.3±0.0

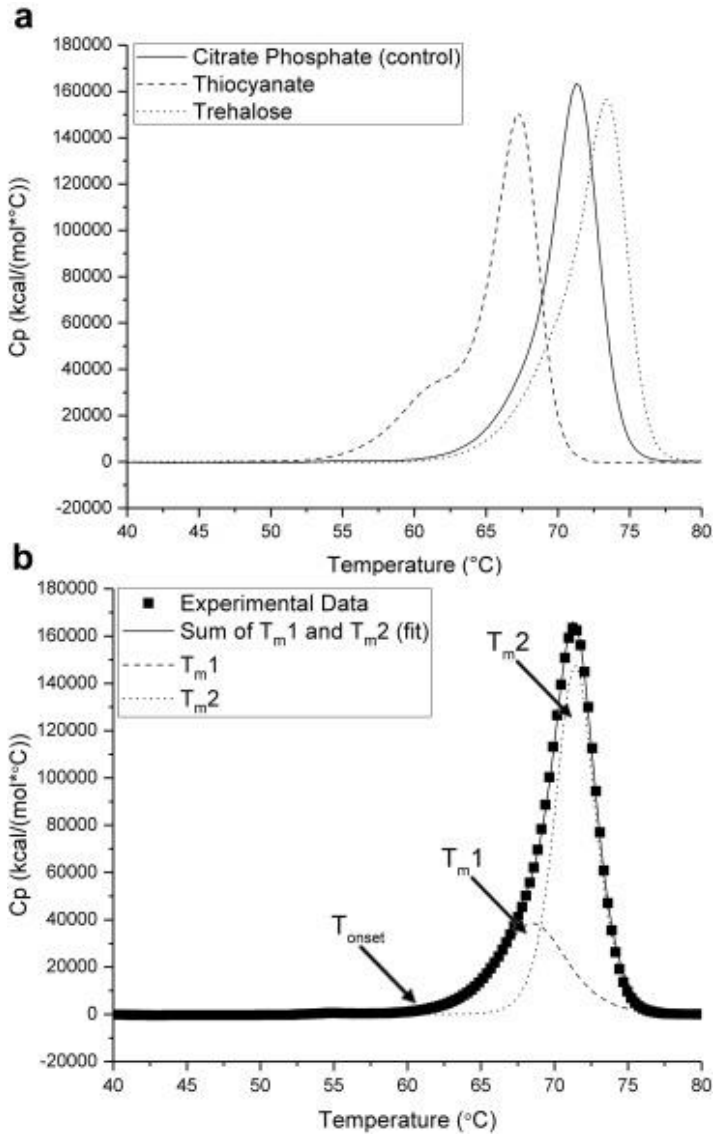

Figure 3.1: Differential scanning calorimetry studies show that additives affect conformational stability of mAb-D.

(a) Representative DSC thermograms of mAb-D in CP buffer, pH 6.0 alone (control) and in the same buffer in the presence of thiocyanate and trehalose. (b) DSC data were fitted to a multistate model with 2 transitions, with the midpoints of each transition, T_m1 and T_m2, identified. Also identified is the temperature at which the first transition begins, T_{onset}.

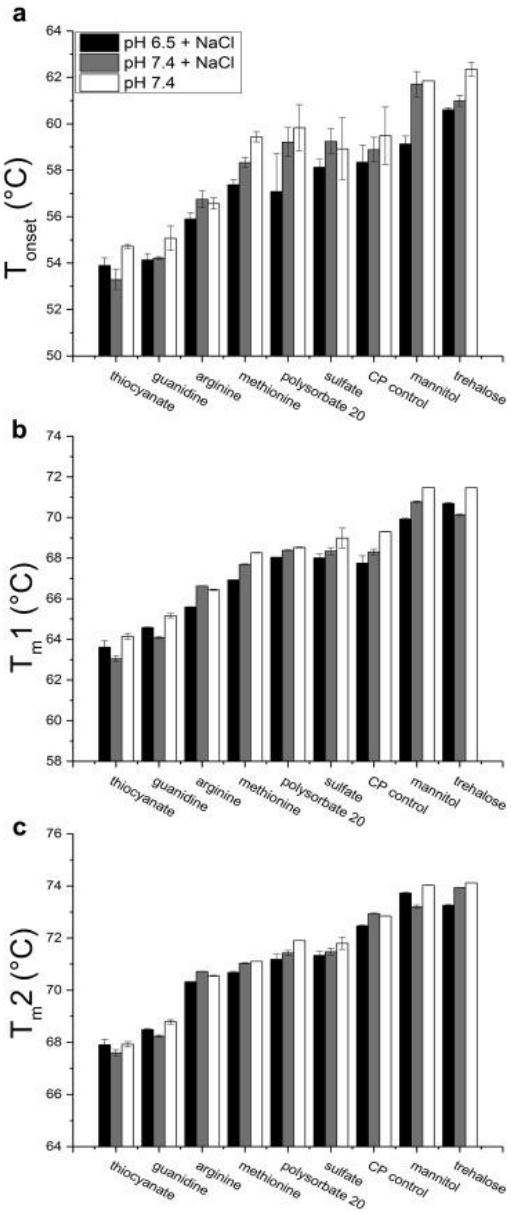

Figure 3.2: Effect of additives on the thermal transition values of mAb-D (T_{onset}, T_m1, and T_m2) as measured by DSC: (a) T_{onset}, (b) T_m1, and (c) T_m2 values are shown.

Additives are ordered from lowest to highest transition temperature of mAb-D, sorted by the average of the 3 different solution conditions. Samples were prepared in CP buffer at indicated pH values in the presence or absence of NaCl (pH 7.4) and different additives (see Materials and Methods section for concentrations). Error bars represent the sample standard deviation for triplicate measurements.

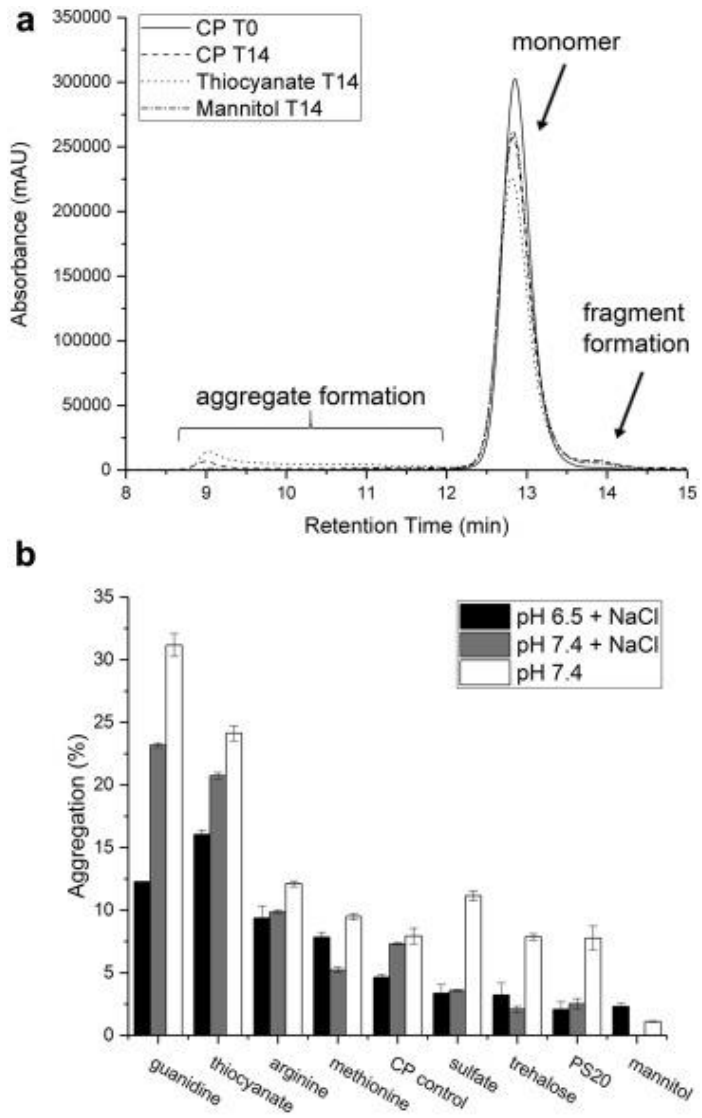

Figure 3.3: Effect of additives on total aggregate formation of mAb-D following incubation at 50°C for 14 days as measured by SEC.

(a) Representative SEC profiles of mAb-D before and after accelerated stability study. (b) Rank ordering of additives from the highest to lowest percent aggregation of mAb-D in 3 different solution conditions. Samples were prepared in CP buffer at indicated pH values in the presence or absence of NaCl (pH 7.4) and different additives (see Materials and Methods section for concentrations). Error bars represent the sample standard deviation for triplicate measurements.

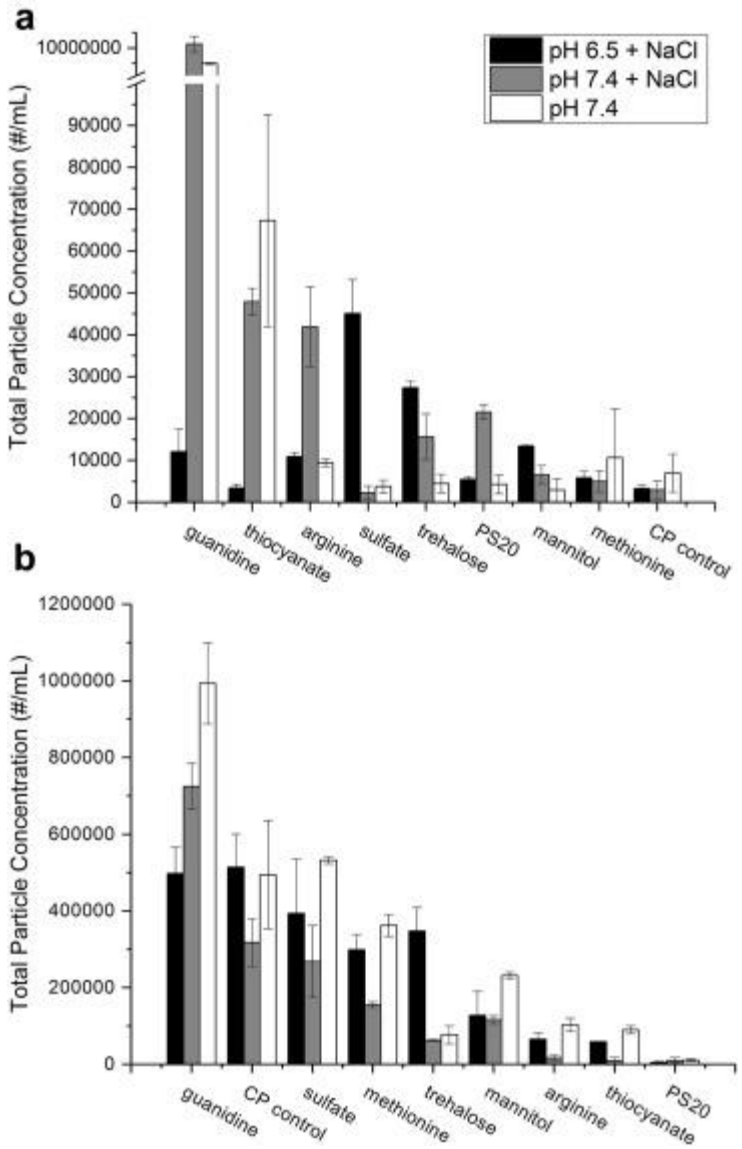

Figure 3.4: Effect of additives on subvisible particle formation by mAb-D as measured by MFI following incubation (a) at 50°C for 14 days, and (b) after stirring stress.

Subvisible particles are defined as particle sized between 1 and 100 μm in diameter. Additives are ordered from the highest to the lowest total particle concentration for mAb-D in 3 different solutions. Samples were prepared in CP buffer at indicated pH values in the presence or absence of NaCl (pH 7.4) and different additives (see Materials and Methods section for concentrations). Error bars represent the sample standard deviation for triplicate measurements.

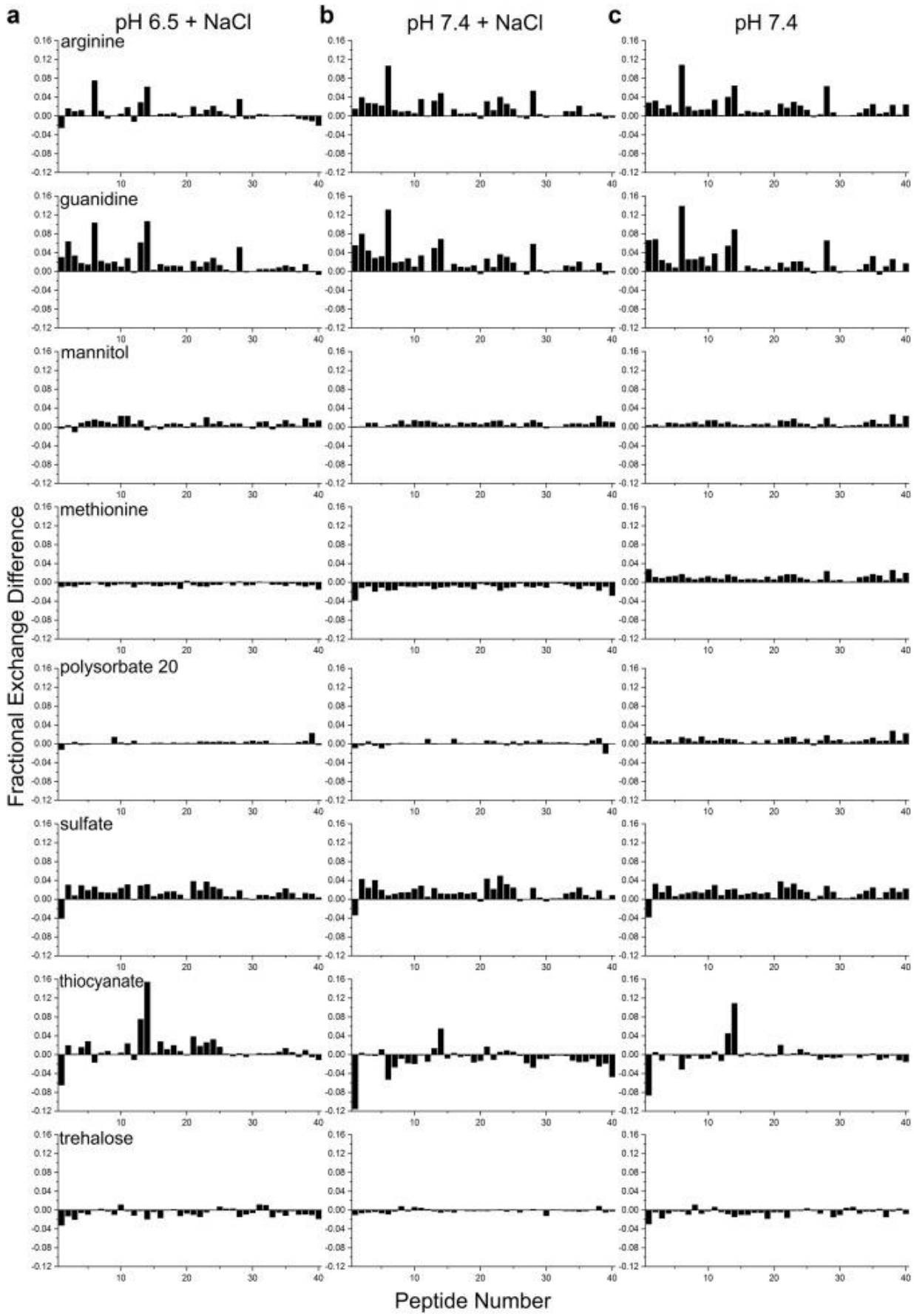
a
pH 6.5 + NaCl
b
pH 7.4 + NaCl
c
pH 7.4
arginine
guanidine
mannitol
methionine
polysorbate 20
sulfate
thiocyanate
trehalose
Fractional Exchange Difference
Peptide Number

Figure 3.5: Difference plots exhibiting the differential fractional exchange by mAb-D in the presence of additives (vs. control buffer)

in (a) CP buffer pH 6.5 with 150-mM NaCl, (b) CP buffer at pH 7.4 with 150-mM NaCl, and (c) CP buffer at pH 7.4 in the absence of salt, following correction for differences in chemical exchange rates (see Materials and Methods section). Fractional uptake is shown for all peptides; positive values indicate additive addition caused in increase in hydrogen exchange by the peptide segments, whereas negative values indicates decreased hydrogen exchange. Difference plots are shown for arginine, guanidine, mannitol, methionine, PS20, sulfate, thiocyanate, and trehalose.

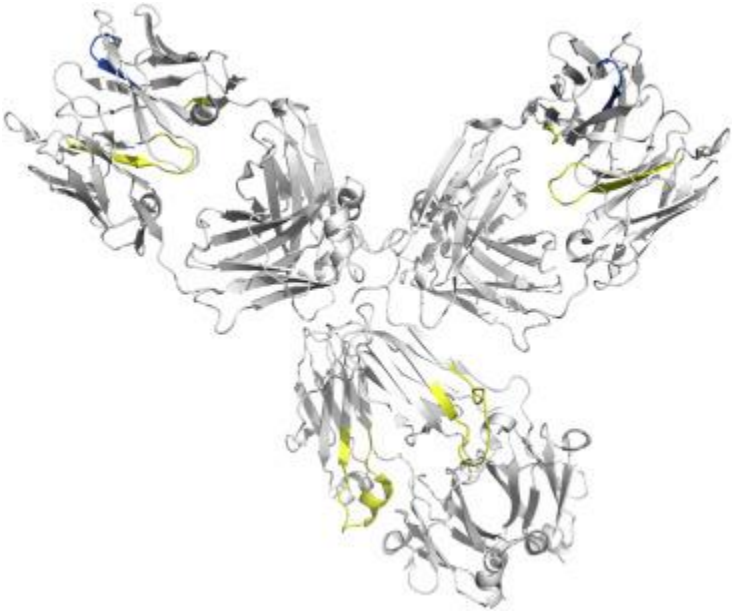

Figure 3.6: Homology model of mAb-D showing effects of selected additives on the local flexibility of mAb-D as measured by HX-MS.

Regions shown in yellow (peptides 6, 13, 14, and 28; residues HC 112-115, HC 243-260, and LC 37-47) exhibited substantial increases in hydrogen exchange in the presence of thiocyanate, arginine, and guanidine. Regions in blue (peptide 1, HC 30-35) exhibited substantial decreases in hydrogen exchange in the presence of thiocyanate and sulfate. The mAb homology model is based on PDB 5DK3.[21]

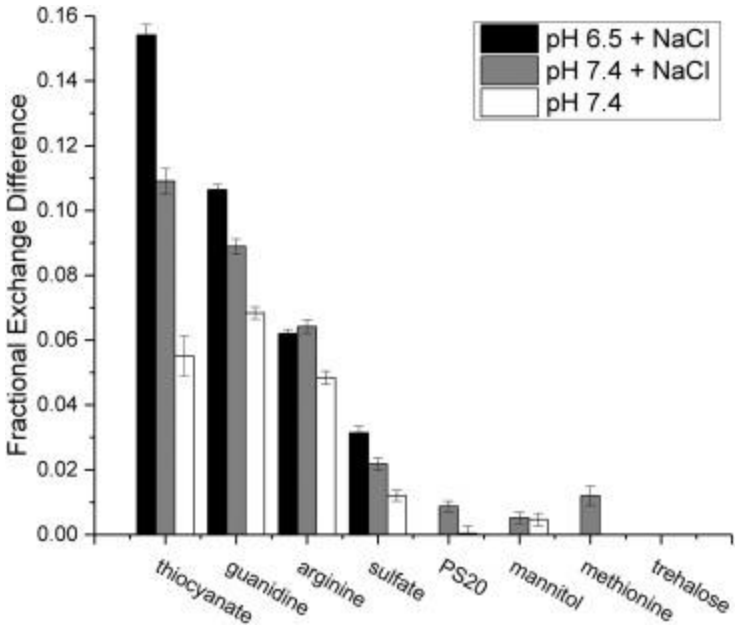

Figure 3.7: Fractional exchange differences in the mAb-D C_H2 aggregation hotspot peptide (heavy chain residues 250-260) in the presence of the indicated additives.

Data are shown for mAb-D at pH 6.5 with 150-mM NaCl and pH 7.4 with and without 150-mM NaCl following correction for differences in chemical exchange rates (see Materials and Methods section). Additives are ordered by the average differential deuterium uptake averaged among the 3 conditions from greatest to least. Error bars represent the sample standard deviation for triplicate measurements propagated over the differences.

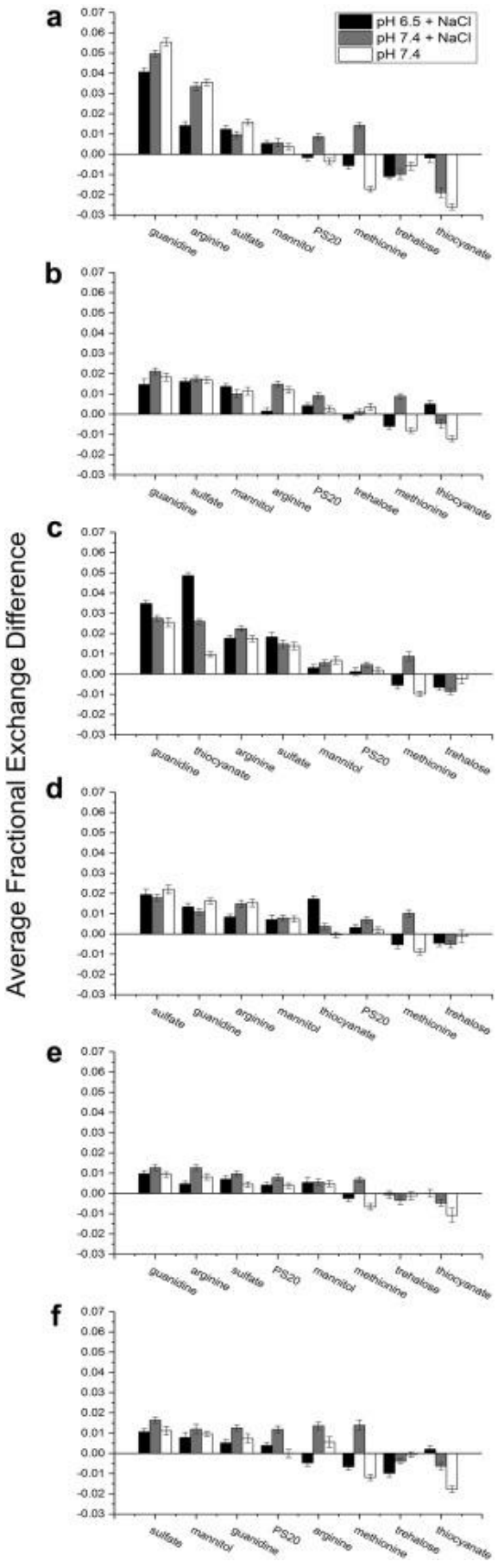
a
b
c
d
e
f
pH 6.5 + NaCl
pH 7.4 + NaCl
pH 7.4
Average Fractional Exchange Difference
0.07
0.06
0.05
0.04
0.03
0.02
0.01
0.00
-0.01
-0.02
-0.03
guanidine
arginine
sulfate
mannitol
PS20
methionine
trehalose
thiocyanate
guanidine
sulfate
mannitol
arginine
PS20
trehalose
methionine
thiocyanate
guanidine
thiocyanate
arginine
sulfate
mannitol
PS20
methionine
trehalose
sulfate
guanidine
arginine
mannitol
thiocyanate
PS20
methionine
trehalose
guanidine
arginine
sulfate
PS20
mannitol
methionine
trehalose
thiocyanate
sulfate
mannitol
guanidine
PS20
arginine
methionine
trehalose
thiocyanate

Figure 3.8: The effect of additives on the domain-averaged fractional exchange differences in mAb-D domains.

Data are shown for the (a) V_H, (b) C_H1, (c) C_H2, (d) C_H3, (e) V_L, and (f) C_L domains of mAb-D in the presence of the indicated additive (vs. control buffer) at pH 6.5 with 150-mM NaCl and pH 7.4 with and without 150-mM NaCl following correction for differences in chemical exchange rates (see Materials and Methods section). Fractional uptake difference was averaged over the 5 peptides (peptides 1-4 and 6 for VH, 8-12 for CH1, 13, 14, and 16-18 for CH2, 21-25 for CH3, 27-31 for VL, and 34, 35, and 38-40 for CL) showing the greatest magnitude of effect in the data set (the same group of 5 for all additives and conditions). Additives are ordered by the average differential deuterium uptake averaged among the 3 conditions from greatest to least. Error bars represent the sample standard deviation for triplicate measurements propagated over the average of the differences.

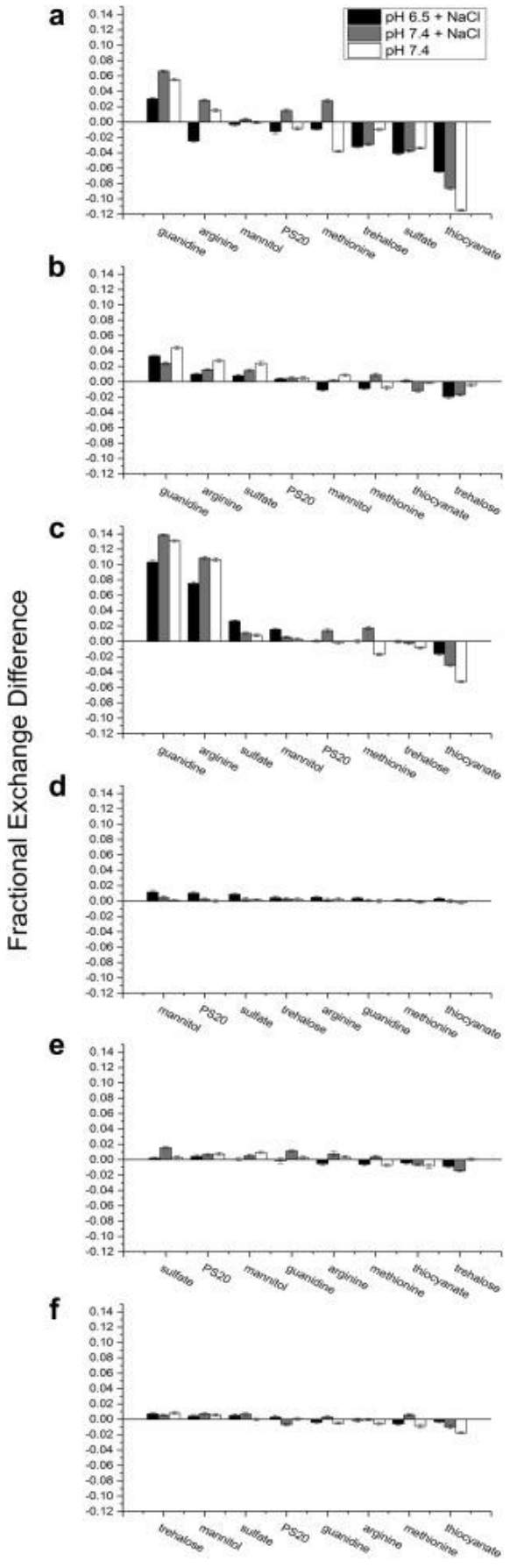
a
b
c
d
e
f
pH 6.5 + NaCl
pH 7.4 + NaCl
pH 7.4
Fractional Exchange Difference
guanidine
arginine
mannitol
PS20
methionine
trehalose
sulfate
thiocyanate

Figure 3.9: Fractional exchange differences in the CDR regions of mAb-D in presence of various additives.

Data are shown for (a, peptide 1) CDR-H1, (b, peptide 3) CDR-H2, (c, peptide 6) CDR-H3, (d, peptide 27) CDR-L1, (e, peptide 29) CDR-L2, and (f, peptide 31) CDR-L3 in the presence of the indicated additive (vs. control buffer) at pH 6.5 with 150-mM NaCl and pH 7.4 with and without 150-mM NaCl following correction for differences in chemical exchange rates (see Materials and Methods section). Additives are ordered by the average differential deuterium uptake averaged among the 3 conditions from greatest to least. Error bars represent the sample standard deviation for triplicate measurements, propagated over the difference.

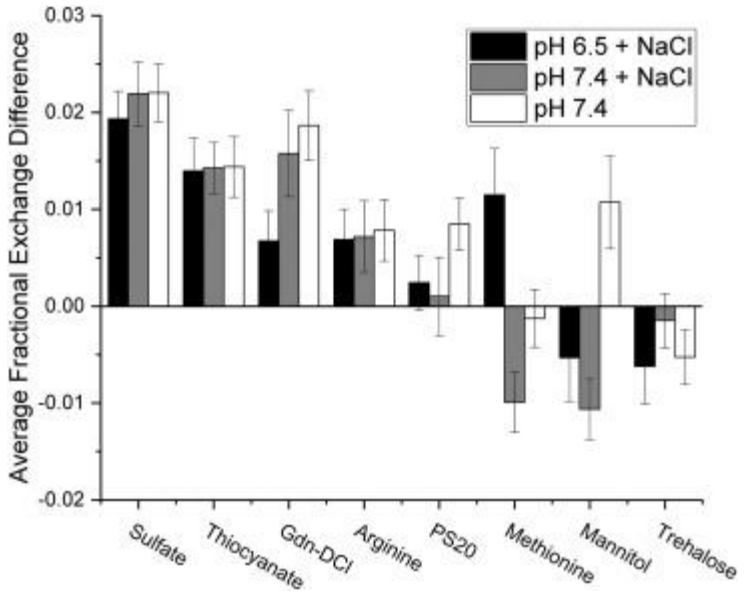

Figure 3.10: The effect of additives on the fractional exchange difference averaged across all peptides in mAb-D.

Data are shown for mAb-D in the presence of the indicated additive (vs. control buffer) at pH 6.5 with 150-mM NaCl and pH 7.4 with and without 150-mM NaCl following correction for differences in chemical exchange rates (see Materials and Methods section). Additives are ordered by the average fractional exchange difference averaged among the 3 conditions from greatest to least. Error bars represent the sample standard deviation for triplicate measurements, propagated over the average of the differences.

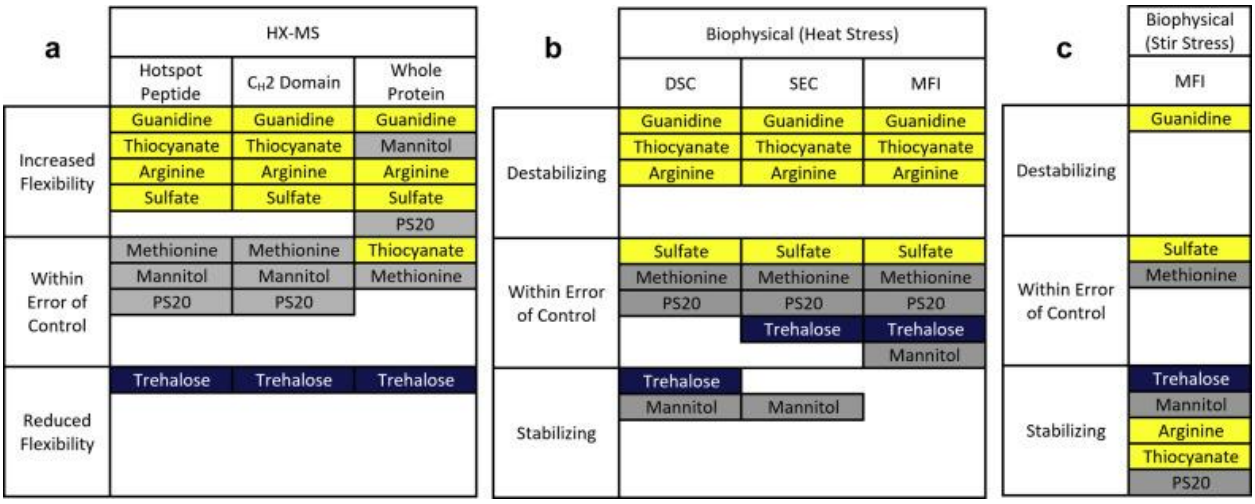

Figure 3.11: Generalized conclusions from biophysical and HX-MS studies of the effect of additives on mAb-D physical stability profile and local flexibility in presence of different additives.

(a) In the first section, additives are placed in 1 of 3 categories based on conclusions from HX-MS data; increased flexibility, within error of control, and reduced flexibility. (b, c) In subsequent sections, additives are placed in 1 of 3 categories based on conclusions from biophysical data; destabilizing, within error or control, and stabilizing. Additives are colored based on HX-MS results for hotspot peptide (first column) and retained in other columns to highlight commonalities (e.g., guanidine ranking highly in all studies).

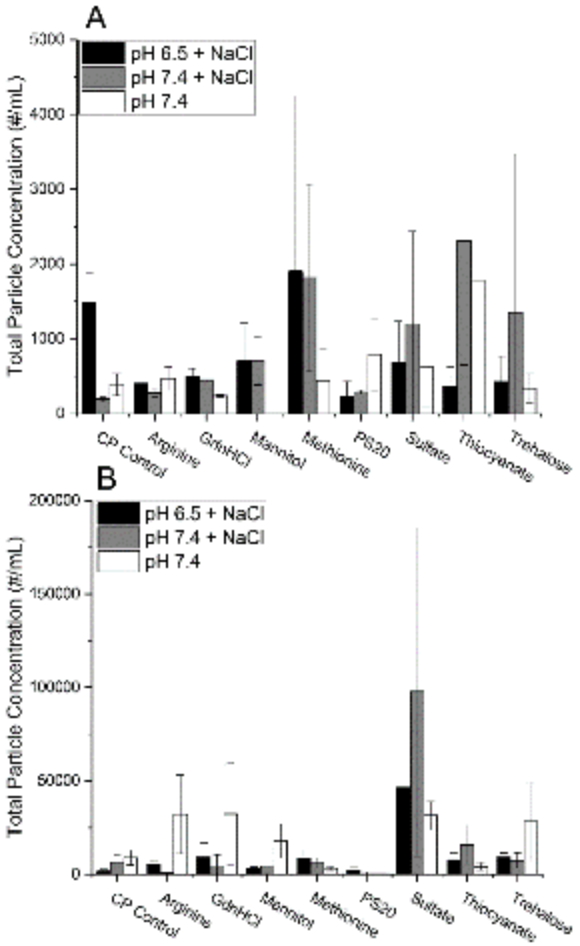

Supplementary Figure 3.1: Total subvisible particle concentrations for additive and control buffers and mAb-D samples in the corresponding buffers at time zero (before stress). Total particle concentrations were measured by MFI (A) before any stress was applied for additive and control buffers alone (with no protein added), and (B) mAb-D protein samples in the same buffers. Error bars represent sample standard deviation of triplicate measurements.

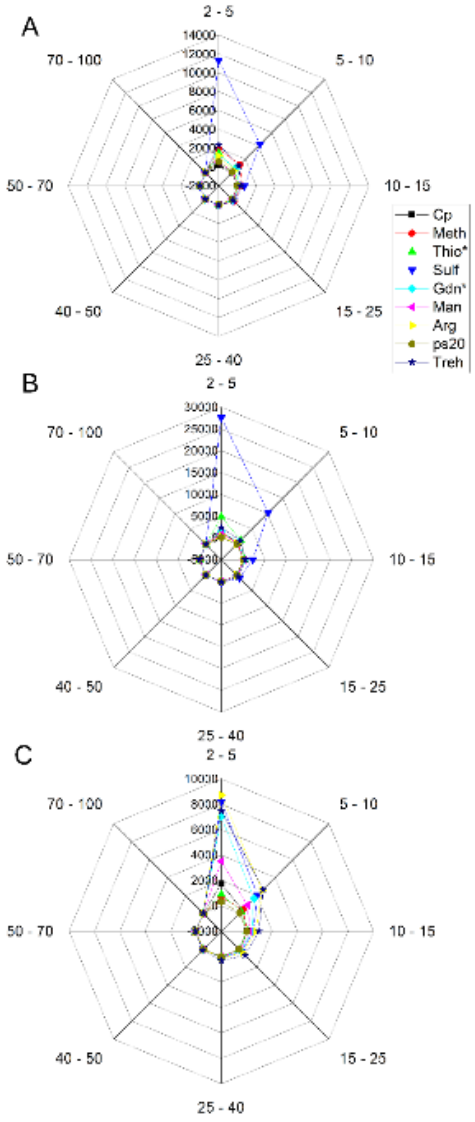

Supplementary Figure 3.2: Particle size distributions for mAb-D + additives prior to heat or stir stress as measured by MFI.

Each vertex of the polygon represents a particle diameter size range (in microns), and the radius of the polygon at each vertex represents the concentration of particles in that size range (in number of particles per mL). Distributions are shown for pH 6.5 + NaCl (A, B), pH 7.4 + NaCl (C, D, E), and pH 7.4 (F, G). Within each row, conditions are the same but samples are separated based to the maximum vertex for sake of visibility. Each vertex has an associated error that is not represented in these charts.

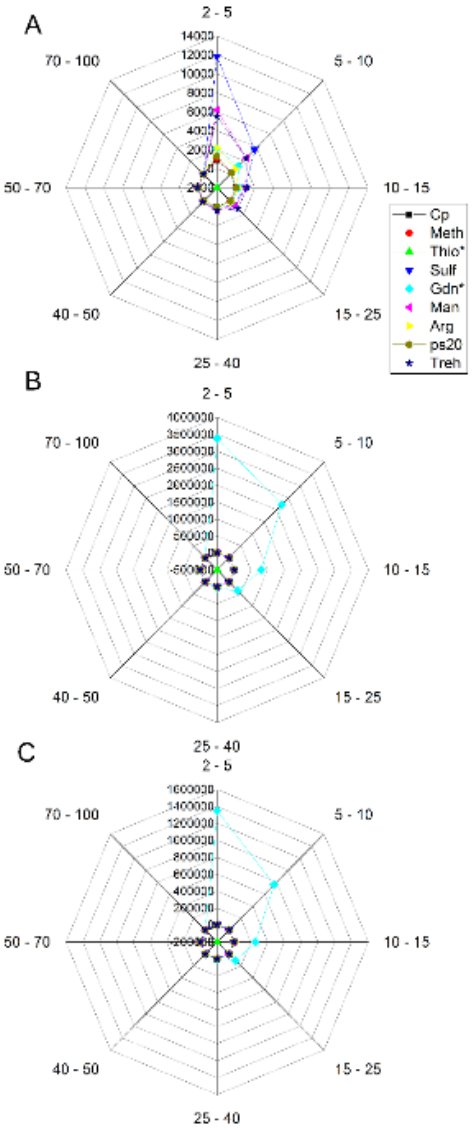

Supplementary Figure 3.3: Particle size distributions for mAb-D + additives after heat stress as measured by MFI.

Each vertex of the polygon represents a particle diameter size range (in microns), and the radius of the polygon at each vertex represents the concentration of particles in that size range (in number per mL). Distributions are shown for pH 6.5 + NaCl (A, B), pH 7.4 + NaCl (C, D, E), and pH 7.4 (F, G, H). Within each row, conditions are the same but samples are separated based to the maximum vertex for sake of visibility. Each vertex has an associated error that is not represented in these charts.

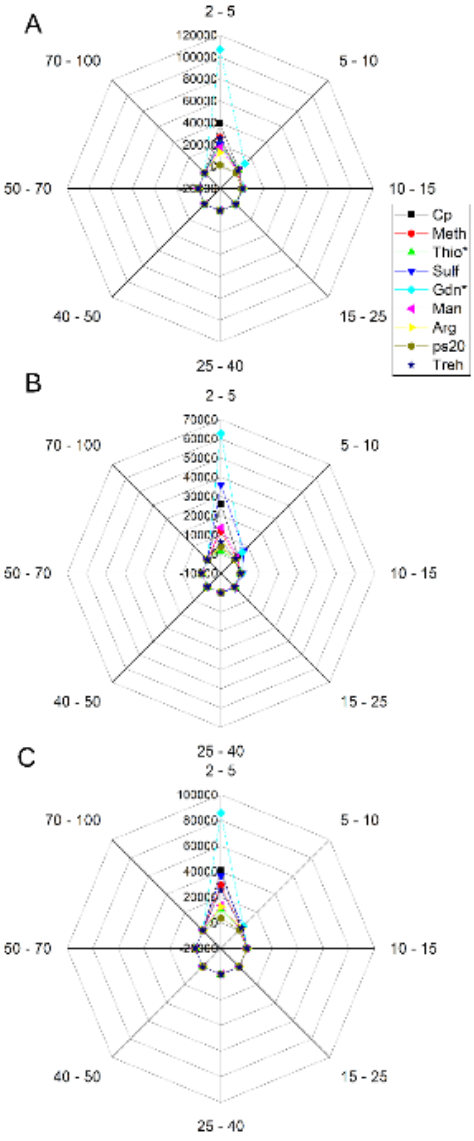

Supplementary Figure 3.4: Particle size distributions for mAb-D + additives after stirring stress as measured by MFI.

Each vertex of the polygon represents a particle diameter size range (in microns), and the radius of the polygon at each vertex represents the concentration of particles in that size range (in number per mL). Distributions are shown for pH 6.5 + NaCl (A, B), pH 7.4 + NaCl (C, D, E), and pH 7.4 (F, G, H). Within each row, conditions are the same but samples are separated based to the maximum vertex for sake of visibility. Each vertex has an associated error that is not represented in these charts.

3.5 References

1. Reichert JM 2011. Antibody-based therapeutics to watch in 2011. MAbs 3(1):76-99.

2. Reichert JM 2014. Antibodies to watch in 2014. MAbs 6(1):5-14.

3. Kamerzell TJ, Middaugh CR 2008. The complex inter-relationships between protein flexibility and stability. Journal of Pharmaceutical Sciences 97(9):3494-3517.

4. Majumdar R, Middaugh CR, Weis DD, Volkin DB 2015. Hydrogen–Deuterium Exchange Mass Spectrometry as an Emerging Analytical Tool for Stabilization and Formulation Development of Therapeutic Monoclonal Antibodies. Journal of Pharmaceutical Sciences 104(2):327–345.

5. Kessler H, Mronga S, Müller G, Moroder L, Huber R 1991. Conformational analysis of a IgG1 hinge peptide derivative in solution determined by NMR spectroscopy and refined by restrained molecular dynamics simulations. Biopolymers 31(10):1189-1204.

6. Nelson AL, Dhimolea E, Reichert JM 2010. Development trends for human monoclonal antibody therapeutics. Nature Reviews Drug Discovery 9(10):767-774.

7. Cohen-Solal JF, Cassard L, Fridman W-H, Sautès-Fridman C 2004. Fc γ receptors. Immunology Letters 92(3):199-205.

8. Raghavan M, Bjorkman PJ 1996. Fc receptors and their interactions with immunoglobulins. Annual Review of Cell and Developmental Biology 12:181-220.

9. Ravetch JV, Bolland S 2001. IgG Fc receptors. Annual Review of Immunology 19:275-290.

10. Kamerzell TJ, Esfandiary R, Joshi SB, Middaugh CR, Volkin DB 2011. Protein-excipient interactions: mechanisms and biophysical characterization applied to protein formulation development. Advanced Drug Delivery Reviews 63(13):1118-1159.

11. Chaudhuri R, Cheng Y, Middaugh CR, Volkin DB 2014. High-Throughput Biophysical Analysis of Protein Therapeutics to Examine Interrelationships Between Aggregate Formation and Conformational Stability. The AAPS Journal 16(1):48-64.

12. Maddux NR, Joshi SB, Volkin DB, Ralston JP, Middaugh CR 2011. Multidimensional methods for the formulation of biopharmaceuticals and vaccines. Journal of Pharmaceutical Sciences 100(10):4171-4197.

13. Alsenaidy MA, Jain NK, Kim JH, Middaugh CR, Volkin* DB 2014. Protein comparability assessments and potential applicability of high throughput biophysical methods and data visualization tools to compare physical stability profiles. Frontiers in Pharmacology 5.

14. Yan Y, Wei H, Jusuf S, Jr. SRK, Chen J, Chen G, Ludwig RT, Tao L, Das TK 2017. Mapping the binding interface in a noncovalent size variant of a monoclonal antibody using native mass spectrometry, hydrogen-deuterium exchange mass spectrometry, and computational analysis. Journal of Pharmaceutical Sciences 106(11):3222-3229.

15. Huang RY-C, Iacob RE, Krystek SR, Jin M, Wei H, Tao L, Das TK, Tymiak AA, Engen JR, Chen G 2017. Characterization of aggregation propensity of a human Fc-fusion protein therapeutic by hydrogen/deuterium exchange mass spectrometry. Journal of The American Society for Mass Spectrometry 28(5):795-802.

16. Li J, Wei H, Jr. SRK, Bond D, Brender TM, Cohen D, Feiner J, Hamacher N, Harshman J, Huang RY-C, Julien SH, Lin Z, Moore K, Mueller L, Noriega C, Sejwal P, Sheppard P, Stevens B, Chen G, Tymiak AA, Gross ML, Schneeweis LA 2017. Mapping the energetic epitope of an antibody/interleukin-23 interaction with hydrogen/deuterium exchange, fast photochemical oxidation of proteins mass spectrometry, and alanine shave mutagenesis. Analytical Chemistry 89(4):2250-2258.

17. Li KS, Chen G, Mo J, Huang RY-C, Deyanova EG, Beno BR, O'Neil SR, Tymiak AA, Gross ML 2017. Orthogonal mass spectrometry-based footprinting for epitope mapping and structural characterization: the IL-6 receptor upon binding of protein therapeutics. Analytical Chemistry 89(14):7742-7749.

18. Ronald T. Toth I, Mills BJ, Joshi SB, Esfandiary R, Bishop SM, Middaugh CR, Volkin DB, Weis DD 2017. Empirical correction for differences in chemical exchange rates in hydrogen exchange-mass spectrometry measurements. Analytical Chemistry 89(17):8931-8941.

19. Paul K. Glasoe, Long FA 1960. Use of glass electrodes to measure acidities in deuterium oxide 1,2. The Journal of Physcial Chemistry 64(1):188-190.

20. Arora J, Joshi SB, Middaugh CR, Weis DD, Volkin DB 2017. Correlating the Effects of Antimicrobial Preservatives on Conformational Stability, Aggregation Propensity, and Backbone Flexibility of an IgG1 mAb. Journal of Pharmaceutical Sciences.

21. Scapin G, Yang X, Prosise WW, McCoy M, Reichert P, Johnston JM, Kashi RS, Strickland C 2015. Structure of full-length human anti-PD1 therapeutic IgG4 antibody pembrolizumab. Nature Structural & Molecular Biology 22(12):953-958.

22. Thiagarajana G, Semplea A, Jamesb JK, Cheunga JK, Shameem M 2016. A comparison of biophysical characterization techniques in predicting monoclonal antibody stability. MAbs 8(6):1088-1097.

23. Roberts CJ 2014. Protein aggregation and its impact on product quality. Current Opinion in Biotechnology 30:211-217.

24. Roberts CJ 2014. Therapeutic protein aggregation: mechanisms, design, and control. Trends in Biotechnology 32(7):372-380.

25. Kalonia C, Toprani V, Toth R, Wahome N, Gabel I, Middaugh CR, Volkin DB 2016. Effects of protein conformation, apparent solubility, and protein-protein interactions on the rates and mechanisms of aggregation for an IgG1 monoclonal antibody. The Journal of Physcial Chemistry B 120(29):7062-7075.

26. Perevozchikova T, Nanda H, Nesta DP, J.Roberts C 2015. Protein Adsorption, Desorption, and Aggregation Mediated by Solid-Liquid Interfaces. Journal of Pharmaceutical Sciences 104(6):1946-1959.

27. Manikwar P, Majumdar R, Hickey JM, Thakkar SV, Samra HS, Sathish HA, Bishop SM, Middaugh CR, Weis DD 2013. Correlating excipient effects on conformational and storage stability of an IgG1 monoclonal antibody with local dynamics as measured by hydrogen/deuterium-exchange mass spectrometry. Journal of Pharmaceutical Sciences 102(7):2136–2151.

28. Amin S, Barnett GV, Pathak JA, Roberts CJ, Sarangapani PS 2014. Protein aggregation, particle formation, characterization and rheology. Current Opinion in Colloid & Interface Science 19(5):438-449.

29. Wang X, Das TK, Singh SK, Kumar S 2009. Potential aggregation prone regions in biotherapeutics: A survey of commercial monoclonal antibodies mAbs 1(3):254-267.

Chapter 4 A Formulation Development Approach to Identify and Select Stable Ultra-High-Concentration Monoclonal Antibody Formulations With Reduced Viscosities

(Whitaker N, Xiong J, Pace SE, Kumar V, Middaugh CR, Joshi SB, Volkin DB 2017. A Formulation Development Approach to Identify and Select Stable Ultra-High-Concentration Monoclonal Antibody Formulations With Reduced Viscosities. Journal of Pharmaceutical Sciences 106(11):3230-3241.)

4.1 Introduction

Due to their high specificity and adaptability, mAbs have become the most rapidly growing class of therapeutic proteins in the pharmaceutical industry.[1,2] Because mAbs are typically relatively low potency drugs, they usually must be administered in relatively high doses.[3] For certain disease treatments, the preferred delivery for many therapeutic mAb candidates is subcutaneous injection administered by the patient, which limits the volume of the drug dose to typically under 1.5 mL,[4] thus necessitating the requirement for highly concentrated mAb formulations. In addition to the physical instability issues commonly associated with concentrated protein formulations, concentrated mAb solutions are at times, depending on the individual mAb candidates, highly viscous that often leads to increased tissue back-pressure and injection pain.[5] Pharmaceutical manufacturing challenges, such as elevated levels of shear stress during pumping, high back-pressure, and clogging of membranes, are also exacerbated by high viscosity solutions.[6] Despite these difficulties, several commercial protein formulations reaching concentrations >150 mg/mL have been developed including, for example, Actemra (180 mg/mL) from Genentech, Cosentyx (150 mg/mL) from Novartis, and Alirocumab (150 mg/mL) from Sanofi-Regeneron.[7]

Protein-protein interactions (PPI) can occur in solutions of monoclonal antibodies. Undesirable PPI can result in concentration-dependent elevated viscosities in highly concentrated mAb solutions arising from a crowded environment of antibodies forming reversible PPI leading to nonideal behavior.[8,9] Additionally, PPI can contribute to issues such as protein aggregation, undesirable levels of solution opalescence, and in some cases, liquid-liquid phase separation.[10] This association of mAb molecules has been attributed to several transient interactions, such as electrostatic, hydrophobic, dipole-dipole, hydrogen bonding, and van der Waals interactions[8,9,11-

[13] via FabeFab,[8] and in some cases Fab-Fc interactions,[14] between immunoglobulin G (IgG) mAbs.

PPI of mAbs in high-concentration mAb solutions can be sequence specific, sometimes depending on single amino acids.[15,16] The variable nature of these interactions has led to reports of a wide variety of excipients with viscosity-reducing effects. Common inorganic salts have been reported by several studies to reduce mAb viscosity,[17-19] suggesting that electrostatic interactions strongly contribute to PPI in many antibodies. However, this is not universally observed.[20] The viscosity-reducing effects of amino acids, especially arginine, have also been reported in multiple studies.[11,21,22] Hydrophobic salts have been evaluated in at least 2 studies that reported significant viscosity-reducing properties of bulky, aliphatic, ionic constituents.[20,23] Polar solvents including dimethyl sulfoxide (DMSO) and dimethylacetamide (DMA) have also been shown to reduce viscosities of concentrated mAbs formulations.[24] Although some studies have examined the relationship between PPI of mAbs and viscosity mechanistically,[8,9] development of relatively low-viscosity, stable high-concentration mAb formulations remains largely an empirical process.

Because PPI are mAb concentration dependent, they are often referred to as reversible self-association. Such reversible self-association behavior can potentially contribute to physical and conformational instability of mAbs, including the formation of aggregates.[17] In this study, 2 monoclonal antibodies (1 IgG1 and 1 IgG4) that were previously formulated to be stable during storage, but are problematically viscous at high concentrations, were evaluated. We sought to add an additional 1-3 excipients to the established formulations of these mAbs that reduced solution viscosity, and at the same time, did not adversely affect their storage stability at ultra-high protein (>150 mg/mL) concentrations. To this end, we screened 56 different pharmaceutical excipients and other additives for their ability to reduce/mitigate solution viscosity and maintain/improve the

2 mAb's physicochemical stability profile. Stability studies of candidate high concentration formulations with each of the 2 mAbs, which were designed and developed based on previous formulation development work and the results from this work, were set up to monitor viscosity and stability changes over time under accelerated and real-time storage conditions.

4.2 Materials and Methods

4.2.1 Materials

Frozen mAb A (an IgG4) and mAb C (an IgG1) stocks were supplied by Janssen Biotech (Malvern, PA); mAb Awas supplied at a concentration of 115 mg/mL in 10 mM histidine, 8.5% sucrose, at pH 5.75. mAb C was supplied at a concentration of50 mg/mL in 10mM histidine, 4% sucrose, at pH 5.75. Sucrose and trehalose were purchased from Pfanstiehl Laboratories (Waukegan, IL). Sodium chloride, polysorbate 80, polysorbate 20, Triton X-100, and urea were purchased from Fisher Scientific (Hampton, NH). Ethanol, sodium camphorsulfonate, and triethylphenylammonium iodide were purchased from Acros Organics (Hampton, NH). Poloxamer 188was purchased from Spectrum Chemical Manufacturing (New Brunswick, NJ). Human serum albumin was purchased from Octapharma (Lachen, Switzerland). Sulfobutyl-b-cyclodextrin was purchased from Ligand (San Diego, CA). All other chemicals were purchased from Sigma Aldrich (St. Louis, MO).

4.2.2 Methods

4.2.2.1 *Sample Preparation, Concentration Determination, and Osmolality Measurements*

Antibody samples were exhaustively dialyzed into 10 mM histidine buffer at the desired pH at 4°C. Samples were then concentrated to >200 mg/mL by spin filtration using Amicon

Ultra 15 mL Centrifugal Filters (30K MW cutoff) (Millipore, Billerica, MS). Concentrated stocks of the excipients were made in 10 mM histidine buffer at the pH values desired in the antibody samples. Excipients were then added from stocks to aliquots of mAb A and mAb C, which were further diluted, if necessary, to the desired concentrations of protein by addition of buffer containing the desired concentration of excipient. Sample pH values were checked to ensure that they did change during the concentration procedure. Protein concentrations were determined by measuring absorbance at 280 nm with either a Thermo Scientific NanoDrop 2000 spectrophotometer (Thermo, Wilmington, DE) or a Solo VPE Cary 50 Bio variable path length spectrophotometer (C Technologies, Bridgewater, NJ) using an extinction coefficient of 1.37 (mg/mL) 1 cm^{-1}. The osmolality of samples were determined using an OSMETTE II osmometer (Precision Systems Inc., Natick, MA). Measurements were made in triplicate.

4.2.2.2 *Accelerated and Long-Term Stability Studies*

Stability studies were performed at 4°C, 25°C, and 40°C in the formulations and concentrations described. Samples were stored in sealed 2-mL glass vials with 13 mm rubber serum stoppers (West Pharmaceutical Services, Exton, PA). At the indicated time points, samples were moved to -80°C for storage until analyzed.

4.2.2.3 *Viscosity Measurements*

Solution viscosities were measured at 25°C with an m-VROC viscometer (Rheosense, San Ramon, CA). Samples of mAb A and mAb C were injected at a rate of100 mL/min at a shear rate of1935.6 1/s for a duration of 100 s using a 1-mL glass syringe (Hamilton Co, Reno, NV). Measurements were made in triplicate. Viscosity values were obtained in units of dynamic viscosity (cP).

4.2.2.4 *Differential Scanning Calorimetry*

DSC measurements were performed using a VP-Capillary DSC System (Microcal, acquired by Malvern Instruments Ltd). Protein concentrations were adjusted to 5 mg/mL before the measurement. The corresponding formulation buffer was used as a reference for each sample. The samples were heated from 10°C to 90°C at a rate of 60°C/h. Resulting thermograms were corrected by subtraction of buffer-only scans and then normalized to the molar concentration of the protein and were analyzed using Origin 7.0 software (OriginLab Corporation, Northampton, MA).

4.2.2.5 *Size-Exclusion Chromatography*

HPLC-size-exclusion chromatography (SEC) was performed in triplicate with a Shimadzu HPLC System (Shimadzu, Columbia, MD) with simultaneous UV absorbance detection at 214 and 280 nm using a Tosoh TSK-Gel BioAssist G3SWXL (PEEK column) (Tosoh Bioscience, King of Prussia, PA) and a corresponding guard column with a Shimadzu HPLC System. Experiments were performed at 25°C with a mobile phase containing 0.2 M sodium phosphate (pH 6.8) at a flow rate of 0.7 mL/min. Samples were diluted to 1 mg/mL and centrifuged at 14,000 x g for 5 min before injection. Resulting data were analyzed as described previously using a dual-wavelength size exclusion high-performance liquid chromatography method.[25]

4.2.2.6 *SDS-PAGE*

Samples were mixed with 4 NuPAGE LDS sample buffer (Thermo Fisher Scientific, Waltham, MA) with and without 5 mM dithiothreitol (Thermo Scientific, Rockford, IL) and incubated at 95°C for 5 min. Samples were then treated with 10 mM iodoacetamide (Thermo Scientific) at 25°C in the dark for 30 min. Each sample (10 mg) was separated on 10-20% Tris-

glycine gels using NuPAGE MES SDS Running Buffer (Thermo Fisher Scientific). SeeBlue Plus2 Pre-stained Protein Standard (Thermo Fisher Scientific) was used as a molecular weight ladder. Protein bands were visualized by staining the gels with Bio-safe Coomassie Blue G250 stain (BioRad Laboratories, Hercules, CA), followed by destaining in destaining buffer (50% methanol, 10% acetic acid).

4.2.2.7 *Capillary Isoelectric Focusing*

Capillary isoelectric focusing (cIEF) experiments were performed on an iCE3 instrument from Protein-Simple (San Jose, CA). Samples were run in triplicate at 4°C using a temperaturecontrolled autosampler. The mAb samples (final concentration of 0.15 mg/mL) were mixed with Pharmalyte® 3.0-10.0 (GE Healthcare, final concentration of 4%), acidic and basic isoelectric point (pI) markers of 6.14 and 9.46 (Protein-Simple), 0.1% tetramethylethylenediamine, and methyl cellulose (final concentration of 0.35%; Protein-Simple). Samples were separated in 2 focusing periods, one at 1500 V for 1 min and a second at 3000 V for 4.3 min.

4.2.2.8 *Microflow Imaging*

Using a microflow imaging (MFI) DPA 4200 instrument (Protein Simple, Santa Clara, CA), subvisible particle formation data were collected by MFI methods described previously.[26] The instrument was primed with purified water before each run to obtain a particle-free baseline. Samples were either diluted to a protein concentration of 1 mg/mL (in the case of samples stored at 40°C) or 50-fold (all other measurements) in the corresponding formulation buffer before being passed through the instrument at a flow rate of 0.1 mL/min. Subvisible particle concentration values were not corrected for dilution factor because counting accuracy vs. dilution factor has been reported (and observed in our laboratories as well) to deviate from linearity in similar

experiments.[27] Rather, data are evaluated in terms of the change in total particle counts compared with previous time points in the stability study. Measurements were made in duplicate.

4.3 Results

4.3.1 Excipient Screening to Reduce Viscosity of mAb A and mAb C Solutions

A total of 56 additives, most of them pharmaceutical excipients used in approved products for parenteral injection (i.e., listed in the FDA inactive ingredient guide[28]), were screened. These additives were grouped into known categories including salts, polyols, alcohols, sugars, detergents, proteins, amino acids, and polymers.[29] The classes and individual types of excipients were screened for their viscosity-reducing effects on mAb A and mAb C solutions prepared at high concentrations between 130 and 165 mg/mL protein (Fig. 1). DMSO, DMA, sodium (þ)-10camphorsulfonate, and trimethylphenyl-ammonium iodide were included in this list based on recent studies reporting reduced viscosities of mAbs formulated at ultra-high (>150 mg/mL) concentrations with polar solvents and hydrophobic salts.[20,23,24] Initial screening was performed at relatively high concentrations of excipients to aid in identification of potential "hits." The measured dynamic viscosities of the mAb formulations were grouped into 3 categories: (1) "preferred" viscosities of 10 cP or lower, (2) "acceptable" viscosities between 10 and 20 cP, and (3) "unacceptable" viscosities of >20 cP. These values were selected based on available internal experience and knowledge of the capabilities of delivery devices, such as pre-filled syringes, auto-injectors, and patch pumps. For example, the SmartDose® system from West Pharmaceutical Services claims to accommodate viscosities as high as 20 cP.[30] Excipients that were observed to reduce viscosities of the mAb formulations <15 cP were identified as "hits" and were down selected for further study (Table 1). The value of 15 cP was used (instead

of 20 cP) to avoid values too close to the viscosity cutoff and to further reduce the number of excipients (and their combinations) to be evaluated in subsequent experiments.

Next, we examined the effects of the lead excipients on the 2 mAbs at different protein concentrations. Due to reversible mAb self-association, ultra-high concentration solutions (150 mg/mL mAb) typically display sharp, exponential increases in solution viscosity.[12] We observed this phenomenon with solutions of both mAb A and mAb C, with dynamic viscosities dramatically increasing at concentrations above about 150 mg/mL (Fig. 2). For example, at 200 mg/mL, differences as high as ~145 and ~85 cP in viscosities were observed in formulations of mAb A and mAb C, respectively.

Because excipient concentrations in these initial excipient screening experiments were comparatively high, the next phase of the study was to work toward developing more isotonic formulations, which are desired for subcutaneous parenteral administration. To this end, titrations of the best-performing classes and types of excipients from Figure 2 were evaluated (see Fig. 3). The promising additives were grouped in the following excipient classes: amino acids, buffer agents, and salts (including divalent, monovalent, and hydrophobic salts). Among the amino acids tested, arginine and lysine had the most pronounced effect on solution viscosity, with arginine outperforming lysine for mAb A and the reverse being observed for mAb C. In both these cases, the viscosity-reducing effects appeared to plateau at an additive concentration of about 50 mM. Among the buffer systems compared, histidine outperformed the other compounds examined in viscosity reduction for mAb A. In the case ofmAb C, each of the buffering agents examined were found to reduce solution viscosity to approximately the same degree. The divalent salts CaCl2 and MgCl2 both reduced the viscosity to a greater extent than NaCl at the same concentrations for both mAbs, possibly due to the ionic strength of the solution

being greater in the case ofthe divalent salts.[31] Further reduction of solution viscosity appeared to diminish at salt concentrations >150 mM (the DebyeeHückel charge shielding limit). The plateauing effect observed with the amino acids in Figure 3 could be attributed to this phenomenon as well but could also potentially be caused by arginine's and lysine's ability to also interact with apolar and aromatic amino acid residues in proteins or a mixture of both effects (also see Discussion).[14]

Formulations comprised combinations of the best-performing excipients (in terms of viscosity reduction) were then designed and evaluated (Table 2). In selecting these formulations, we considered not only viscosity effects but also known protein stabilization effects of certain additives[29] and previously obtained stability data with these 2 mAbs (data not shown). The sugar sucrose was included in these formulations for its known stabilizing effect on monoclonal antibodies, especially during freeze-thaw.[32] Although the same preferential exclusion of sucrose molecules from protein surfaces that leads to this stabilizing effect can potentially also lead to increased intermolecular interactions of proteins at high concentrations and, therefore, can contribute to increased viscosity,[14] no notable effects on dynamic viscosity from 5% sucrose was observed for either mAb A or mAb C when formulated with 75 mM NaCl and 50 mM arginine or lysine, respectively. The storage stability of these 2 mAbs in their original formulations (mAb A in 10 mM histidine, 8.5% sucrose, at pH 5.75, and mAb C in 10 mM histidine, 4% sucrose, at pH 5.75) was previously established before initiation of this work (data not shown). However, because pH can affect the viscosity of protein solutions, we evaluated its effect at pH values at, above, and below the pI range of mAb A and mAb C (Supplementary Fig. S1). None of the alternative pH values (range 5.0 to 8.0) resulted in mAb A or mAb C solution viscosities lower than that observed at pH 5.75.

Based on the results from the excipient screening experiments described earlier, 3 candidate formulations were designed for further evaluation with both mAb A and mAb C (Table 3) at protein concentrations of 50, 150, and 175 mg/mL. For these studies, protein concentrations exceeding 175 mg/mL were not considered due to theoretical limits to the extent viscosity could be reduced due to the impact of the excluded volume effect as described by the Ross-Minton equation.[33] A "base" buffer, formulations F1 and F4 (10 mM histidine, 5% sucrose, 0.02% polysorbate 20, pH 5.3), were used as controls for mAb A and C, respectively. This buffer was selected based on previously determined storage stability data (data not shown). Formulations F2 (base buffer þ 75 mM NaCl and 50 mM arginine) and F5 (base buffer þ 75 mM NaCl and 50 mM lysine) were selected based on their viscosity-reducing properties revealed in the excipient screening studies. Formulation F3 (88 mM histidine, 5% sucrose, 50 mM arginine, 0.02% polysorbate 20, pH 5.3) was included at a single concentration of 175 mg/mL mAb A to compare with formulation F2, which had the same ionic strength. We also included formulation F6 (base buffer þ 75mM sodium camphorsulfonate, 50 mM lysine) at a single concentration of 175 mg/mL mAb C to evaluate the effect of hydrophobic salts (sodium camphorsulfonate) on storage stability of mAb C. Sodium camphorsulfonate was selected over trimethyl-phenylammonium iodide because it has been used more often in pharmaceutical formulations.[34] The experimentally determined osmolality values for each of these formulations are also listed in Table 3.

4.3.2 Evaluation of mAb A and mAb C Stability in Candidate Low-Viscosity, High, and Ultra-High Concentration Formulations

The conformational stability of the antibodies in the candidate formulations was first evaluated by DSC before accelerated and real-time stability studies were performed to assess whether the excipients in the candidate formulations affected the inherent structural stability of

the mAbs (Fig. 4). Both mAb A and mAb C displayed 1 minor and 1 major transition. No notable effect was observed for the mAb C formulations (F4, F5, and F6) when comparing the 3 candidate formulations. In contrast, for mAb A, additional histidine, NaCl, and arginine in formulations F2 and F3 did lower the thermal-onset temperature of the first transition of mAb A (Tonset1) by ~5°C. To determine if the increased ionic strength or the presence of arginine was the cause of this effect, formulations containing the "base buffer" plus 75 mM NaCl or 50 mM Arginine were evaluated (Supplementary Fig. S2). Both excipients seem to have an approximately equal and cumulative effect on lowering the Tonset values ofmAb A at the concentrations used. Although this destabilizing effect was observed, the effect of a relatively small lowering of the Tonset value for mAb A in the candidate formulations F2 and F3 on the actual longer term storage stability of mAb A at much lower temperatures in F2 and F3 was not predicable and was, therefore, subsequently evaluated experimentally as described subsequently.

Both accelerated and real-time storage stability profiles of mAb A and mAb C in newly designed, lower viscosity, high (50 and 150 mg/ mL), and ultra-high (175mg/mL) protein concentration formulations were then evaluated at 3 different temperatures (4°C, 25°C, and 40°C) for 6months. The physicochemical stability of the 2mAbs was monitored by protein concentration using UV spectroscopy, aggregation and fragmentation by SEC and SDS-PAGE, subvisible particle formation by MFI, and charge heterogeneity by cIEF.

Throughout the course of the stability studies, the viscosity of each formulation was also monitored (Fig. 5), and no notable change was observed with the exception of a possible increase in the case of formulation F4 stored at 40°C (Fig. 5b; values for 50 and 150 mg/mL formulations not shown). Similarly, no significant changes in protein concentration were observed by UV spectroscopy (data not shown). Protein aggregation and fragmentation were monitored under

nondenaturing conditions by SEC and under denaturing conditions by SDS-PAGE. For SEC analysis of the 2 proteins at time 0, 0.5%-1.0% soluble aggregates were observed for each of the formulations. No fragmentation was observed for any of the formulations at time 0. When the formulations were then stored at 4°C and 25°C, the total concentration of monomer remained stable in each of the formulations (Figs. 6b-6d). Small losses of monomer (<1%) over this time period indicates that the potential shelf life of both mAbs can be predicted to exceed 2 years when stored at 4°C.[35] However, when mAb A and C formulations were stored under more accelerated stability conditions (40°C), a ~10% reduction in monomer concentration was observed after 3 months. Dimer and fragment formation and loss of protein (presumably from large aggregates being retained on the guard column) all contribute to this loss of monomer content (Fig. 6a, Supplementary Figs S4, S5, and S6). SDS-PAGE analysis (under both reducing and nonreducing conditions) did not reveal any notable changes in any formulation at any temperature evaluated (Supplementary Fig. S3), indicating no notable formation of fragments or covalent aggregates. The fragments observed by SEC (Supplementary Fig. S4, panels C and F) were probably not present in high enough concentrations to be observed by Coomassie Blue G250 staining. This may also be true for the aggregates observed by SEC and not SDS-PAGE (Supplementary Fig. S4, panels A and D), although this more likely could be attributed to formation of noncovalently associated protein in these aggregates.

Subvisible particle formation between 2 and 100 μm was monitored by MFI (Fig. 7). At time 0, formulations contained 10,000 particles/mL or less, with most having <1000 particles/mL after dilution. After storage for 3 months at 40°C, each of the formulations of mAb A contained at least an order of magnitude more particles than t ¼ 0 samples. Formulations of mAb C, however, did not appear to form particles under the same conditions with the exception of

formulation F6. At each of the protein concentrations of mAb A, formulation F1 formed an order of magnitude more particles by 6 months when stored at 25°C. In contrast, at lower temperatures, no notable particle formation in the 2- to 100-μm range was observed for all other formulations stored at either 25°C (Fig. 7, panel B) and 4°C (Fig. 7, panel C) over a 6-month period.

The charge heterogeneity profile of mAb A and mAb C was evaluated by cIEF (Fig. 8). At time 0, both mAb A and mAb C display 3 peaks in the pI range of7.0-7.5 with a major peak at 7.2 and 7.1 for mAb A and mAb C, respectively (Fig. 8a). Electropherograms of samples of each of the mAb formulations stored at 40°C changed notably from T0 to 3M, with significant loss in main peak area and new acidic peaks appearing. No notable changes in the cIEF profile was observed in the same samples stored at either 25°C (Fig. 8, panel C) and 4°C (Fig. 8, panel D) over a 6-month period.

4.4 Discussion

The experiments described here were designed to take 2 existing, storage stable, high-concentration IgG formulations (1 IgG1 and 1 IgG4) and modify them by adding 1-3 pharmaceutical excipients (ideally already used in FDA-approved products) with the goal of reducing their viscosities at high protein concentrations without negatively affecting their stability while still maintaining osmolality values compatible with parenteral (subcutaneous) administration. It should be noted that the goals of this work differ from early formulation development work attempting to simultaneously identify excipients to enhance protein stability at high concentrations and to lower solution viscosity (as some excipient combinations may contribute to stability but increase viscosity or vice versa). Additionally, by screening a wide

variety of excipients, we aimed to obtain a better mechanistic understanding of the nonideal behavior of the 2 antibodies evaluated.

Several factors are well known to contribute to the viscosity of protein solutions. In relatively dilute solutions, the electroviscous effect can contribute significantly to solution viscosity at pH conditions above or below the protein's pI value.[36,37] The viscosity of select formulations (F2 and F5) of mAb A and C were evaluated at pH values below (pH 5.0), above (pH 8.0), and within the range (pH. 7.4) of their measured range of pI values. The solution pH had little effect on the viscosity of these formulations at 175 mg/mL (Supplementary Fig. S1), indicating an insignificant contribution of the electroviscous effect in the formulations used in these stability studies. Although local electrostatic attractions can be modulated by increasing or lowering the solution pH, this effect was apparently masked by ionic screening from the charged excipients present in the formulations in our studies as suggested by the observed saturation effect at 150 mM concentrations (Fig. 3) where the DebyeeHückel effect is optimal. Viscosity is also influenced by excluded volume effects (crowding in solution), particularly at high protein concentrations.[33,38] The excluded volume effect is in part governed by the size of the molecule and limits the degree to which the viscosity of these solutions can be reduced by the addition of excipients. At the concentrations of protein and excipients evaluated in this work, nonspecific PPI are probably the biggest contributor to solution viscosity.[33] These include hydrophobic, electrostatic, van der Waals, and dipole-dipole interactions. For both mAbs, the most pronounced viscosity reduction was observed in formulations containing amino acids or those at high ionic strength (Fig. 3). Hydrophobic interactions likely play a more important role in the PPI of mAb A at high concentrations than mAb C based on the observed effects of methionine, tryptophan, and isoleucine had on solution viscosity (Table 1). Despite this result, ionic screening from

charged excipients (at sufficient concentrations) appears to disrupt PPI in mAb A and mAb C, indicating a significant contribution of electrostatic and dipole-dipole interactions in both molecules as well.

Colloidal stability may be related to the same reversible PPI that lead to increased viscosity.[39,40] We hypothesized that mAb solutions with higher viscosities could also aggregate more and form more particles in accelerated and real-time stability studies. This may, indeed, be the case in samples of formulation F1 stored at 25°C, which did form more subvisible particles than the other, lower viscosity, formulations of mAb A at the 6-month time point as observed by MFI (Fig. 7). However, this was observed at each of the protein concentrations of formulation F1, including the lower viscosity 50 mg/mL and the 150 and 175 mg/mL samples. It should also be noted that no similar increase in aggregation for these samples was observed by SEC. Colloidal instability at elevated temperature (40°C) can most probably be attributed to non-native aggregate formation, where aggregates form from proteins that have partially lost their native or folded structure,[41] and this mechanism may also apply to the observed instability of formulation F1 at 25°C. Clearly, elucidating the actual mechanism of particle formation of mAb A would require further study. Finally, the chemical stability of mAb A and C was similar, with only those samples stored at elevated temperatures showing loss of the main peak in the cIEF electropherograms (Fig. 8). From the formation of additional acidic peaks in the samples stored at 40°C, we can infer that one or more deamination events are also occurring in all the formulations evaluated.

Previous studies have sought to address the problem of elevated solution viscosities in mAb solutions by a variety of different approaches. Similar to the work presented here, some approached this by screening excipients for their viscosity-reducing effects. These studies typically select a class of excipients (i.e., amino acids, hydrophobic salts, polar solvents, etc.) and screen

within a library of select compounds.[19,20,23,24,42] Others have taken a more mechanistic approach and sought to understand how certain compounds reduce solution viscosities by examining their effect on PPI [9,13,14,33] or by seeking to modify the mAb itself to reduce these interactions.[16,43] In this work, by screening a library of diverse pharmaceutical excipients and additives, our approach was able to rapidly screen and select a group of promising compounds for lowering viscosity of ultra-high concentration mAb solutions, while not affecting storage stability, without the time-consuming need of having exact knowledge of the nature of the specific PPI that occur in highly concentrated solutions of the 2 mAbs we evaluated.

Table 4.1: Lead Excipients That Reduce Solution Viscosity to ≤15 cP for Either mAb A or mAb C at 150 mg/mL.

Formulations contain the listed excipients in a base buffer of 10 mm histidine, pH 5.75. Values represent the average and SD from triplicate experiments.

Categories	Excipients	Viscosity, cP	
		mAb A	mAb C
Base buffer	10 mM Histidine, pH 5.75	14.1 ± 1.3	20.1 ± 0.4
Hydrophobic salts	0.5 M Sodium camphorsulfonate	4.3 ± 0.0	5.8 ± 0.0
	0.5 M Trimethylphenylammonium iodide	4.0 ± 0.0	14.2 ± 0.0
Salts	0.1 M NaCl	8.5 ± 0.0	10.5 ± 0.2
	0.5 M NaCl	7.5 ± 0.0	6.4 ± 0.0
	1 M NaCl	5.8 ± 0.0	6.2 ± 0.1
	0.1 M Sodium succinate		8.9 ± 0.0
	10 mM $CaCl_2$	10.5 ± 0.4	13.4 ± 0.1
	10 mM $MgCl_2$	10.6 ± 0.1	
	50 mM Sodium phosphate	7.1 ± 0.1	8.8 ± 0.3
	50 mM Sodium acetate	12.3 ± 0.1	
	50 mM Sodium citrate	7.3 ± 0.2	13.1 ± 0.3
	50 mM Tris(hydroxymethyl)aminomethane	7.7 ± 0.4	13.9 ± 0.3
Detergents	0.05% Brij 35	14.8 ± 0.2	5.0 ± 0.1
Reducing agents	1 mM DTT	14.3 ± 0.3	
Cyclodextrins	5% Sulfobutyl-β-cyclodextrin	12.2 ± 0.0	
	5% γ-Cyclodextrin	14.1 ± 0.0	
Polyols	10% Sorbitol	14.8 ± 0.0	
	10% Glycerol	13.5 ± 0.0	
Carboxylic acids	0.1 M Lactic acid	9.1 ± 0.2	7.2 ± 0.1
	0.1 M Malic acid		7.0 ± 0.3
Amino acids	0.1 M Arginine	6.4 ± 0.3	7.7 ± 0.1
	0.1 M Aspartate	7.7 ± 0.4	12.8 ± 0.2
	0.1 M Glutamate	10.5 ± 0.2	11.1 ± 0.4
	50 mM Histidine	5.1 ± 0.1	10.7 ± 0.2
	0.02 M Isoleucine	9.6 ± 0.3	

Categories	Excipients	Viscosity, cP	
		mAb A	mAb C
	0.1 M Lysine	3.5 ± 0.0	5.0 ± 0.2
	0.02 M Methionine	11.2 ± 0.0	
	50 mM Tryptophan	13.1 ± 0.0	
	0.05 M Arginine + 0.05 M glutamate	8.1 ± 0.0	9.0 ± 0.2
	0.045 M Arginine + 0.045 M glutamate + 0.01 M isoleucine	6.7 ± 0.0	5.9 ± 0.0

Table 4.2: The Effect of Combinations of Lead Excipients on the Solution Viscosity and Osmolality of 175 mg/mL Solutions of mAb A and mAb C Containing 10 mM Histidine (pH 5.75). Values represent the average and SD from triplicate experiments. Arg, arginine; Lys, lysine.

Excipients	Viscosity, cP	Osmolality, mOsm/kg
mAb A		
150 mM NaCl + 50 mM Arg	11.8 ± 0.1	649 ± 11
150 mM NaCl + 10 mM $MgCl_2$	20.1 ± 0.0	396 ± 0
150 mM NaCl + 10 mM $MgCl_2$ + 50 mM Arg	12.3 ± 0.7	489 ± 10
10% sucrose + 50 mM Arg	28.0 ± 0.3	602 ± 9
10% sucrose + 10 mM $MgCl_2$	28.8 ± 0.3	442 ± 1
10% sucrose + 10 mM $MgCl_2$ + 50 mM Arg	15.2 ± 0.2	642 ± 14
5% sucrose + 75 mM NaCl + 50 mM Arg	14.2 ± 0.2	470 ± 3
5% sucrose + 75 mM NaCl + 10 mM $MgCl_2$	21.7 ± 0.2	431 ± 4
5% sucrose + 75 mM NaCl + 50 mM Arg + 10 mM $MgCl_2$	13.5 ± 0.2	500 ± 1
mAb C		
150 mM NaCl + 50 mM Lys	16.1 ± 0.4	500 ± 4
150 mM NaCl + 10 mM $MgCl_2$	19.0 ± 0.1	383 ± 3
150 mM NaCl + 10 mM $MgCl_2$ + 50 mM Lys	12.1 ± 0.1	512 ± 4
10% sucrose + 50 mM Lys	14.1 ± 0.2	375 ± 5
10% sucrose + 10 mM $MgCl_2$	39.9 ± 0.3	561 ± 24
10% sucrose + 10 mM $MgCl_2$ + 50 mM Lys	15.0 ± 0.2	688 ± 3
5% sucrose + 75 mM NaCl + 50 mM Lys	12.3 ± 0.1	530 ± 5
5% sucrose + 75 mM NaCl + 10 mM $MgCl_2$	21.6 ± 0.4	476 ± 20
5% sucrose + 75 mM NaCl + 50 mM Lys + 10 mM $MgCl_2$	12.8 ± 0.1	603 ± 11

Table 4.3: Formulation Compositions, Protein Concentrations and Osmolality Values of mAb A and mAb C Used in Accelerated and Real-Time Stability Studies.

Each of the formulations also contained 5% sucrose, 0.02% polysorbate 20 (pH 5.3). Osmolality values represent the average and SD from triplicate experiments.

	Formulation Composition	Concentration (mg/mL)	mOsm/kg
mAb A			
F1	10 mM Histidine	50	197 ± 0
		150	289 ± 9
		175	332 ± 2
F2	10 mM Histidine + 75 mM NaCl, 50 mM arginine	50	437 ± 12
		150	598 ± 3
		175	640 ± 1
F3	88 mM Histidine, 50 mM arginine	175	501 ± 7
mAb C			
F4	10 mM Histidine	50	194 ± 1
		150	265 ± 0
		175	281 ± 0
F5	10 mM Histidine + 75 mM NaCl, 50 mM lysine	50	401 ± 4
		150	483 ± 9
		175	510 ± 4
F6	10 mM Histidine + 75 mM sodium camphorsulfonate, 50 mM lysine	175	510 ± 3

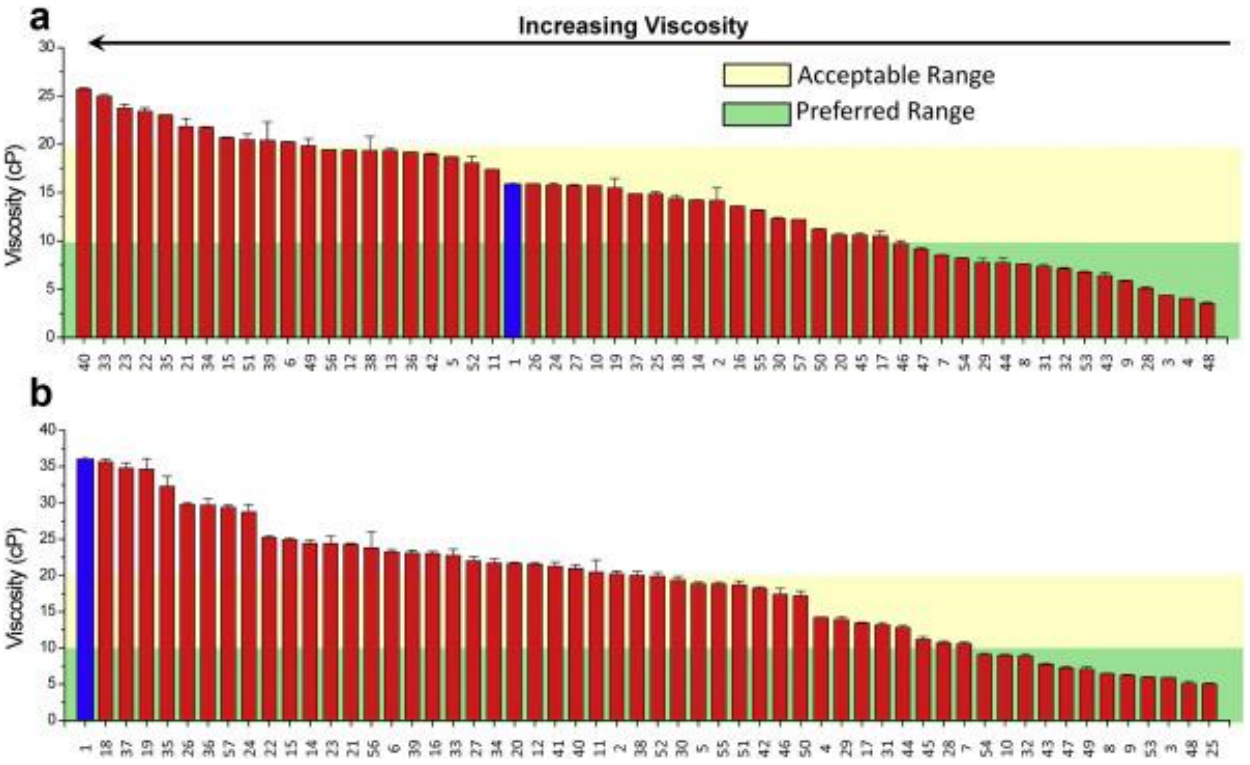

Figure 0.1: Screening of 56 pharmaceutical excipients and additives for their viscosity-reducing effects on high concentration formulations of (a) mAb A and (b) mAb C.

Antibody solutions are between ~135 and ~160 mg/mL with 10 mM histidine (pH 5.75) and the following excipients: (2) no additional excipients, (3) 0.5 M sodium camphorsulfonate, (4) 0.5 M triethylphenylammonium, iodide, (5) 1% DMA, (6) 1% DMSO, (7) 0.1 M NaCl, (8) 0.5 M NaCl, (9) 1 M NaCl, (10) 0.1 M succinate, (11) 4% lactose, (12) 4% trehalose, (13) 4% sucrose, (14) 5% y-cyclodextrin, (15) 5% ethanol, (16) 10% glycerol, (17) 10 mM $CaCl_2$, (18) 1 mM dithiothreitol, (19) 1 mM EDTA, (20) 10 mM $MgCl_2$, (21) 0.05% polysorbate 20, (22) 0.05% polysorbate 80, (23) 0.05% Triton X-100, (24) 0.05% benzalkonium chloride, (25) 0.05% Brij 35, (26), 0.05% sodium docusate, (27) 0.05% Poloxamer 188, (28) 50 mM histidine, (29) 50 mM Tris(hydroxymethyl)aminomethane, (30) 50 mM sodium acetate, (31) 50 mM sodium citrate, (32) 50 mM sodium phosphate, (33) 1% hydrolyzed gelatin, (34) 0.2% protamine sulfate, (35) 1% human albumin, (36) 10% mannitol, (37) 10% sorbitol, (38) 0.5% chitosan, (39) 0.5% dextran 40,

(40) 0.5% PEG 3350, (41) 0.5% hydroxyethyl starch, (42) 0.1 M glycine, (43) 0.1 M arginine, (44) 0.1 M aspartate, (45) 0.1 M glutamate, (46) 0.02 M isoleucine, (47) 0.1 M lactic acid, (48) 0.1 M lysine, (49) 0.1 M malic acid, (50) 0.02 M methionine, (51) 0.02 M proline, (52) 0.1 M urea, (53) 0.045 M arginine + 0.045 M glutamate + 0.01 M isoleucine, (54) 0.05 M arginine + 0.05 M glutamate, (55) 50 mM tryptophan, and (56) 5% propyl-cyclodextrin (57) 5% sulfobutyl-β-cyclodextrin. The original formulations (1) of mAb A (10 mM histidine, 8.5% sucrose, pH 5.75) and mAb C (10 mM histidine, 4% sucrose, pH 5.75) are present as controls (blue bars). Error bars are SDs from triplicate measurements. 0.1 M maleic acid, 0.5% carboxymethyl cellulose, 0.5% dextran sulfate, 0.5% sodium hyaluronate, and 0.1 M sodium sulfate precipitated both mAb A and C. Hydroxyethyl starch precipitated mAb A. “Acceptable” (≤20 cP) and “preferred” (≤10 cP) viscosity ranges are indicated by the yellow and green regions, respectively.

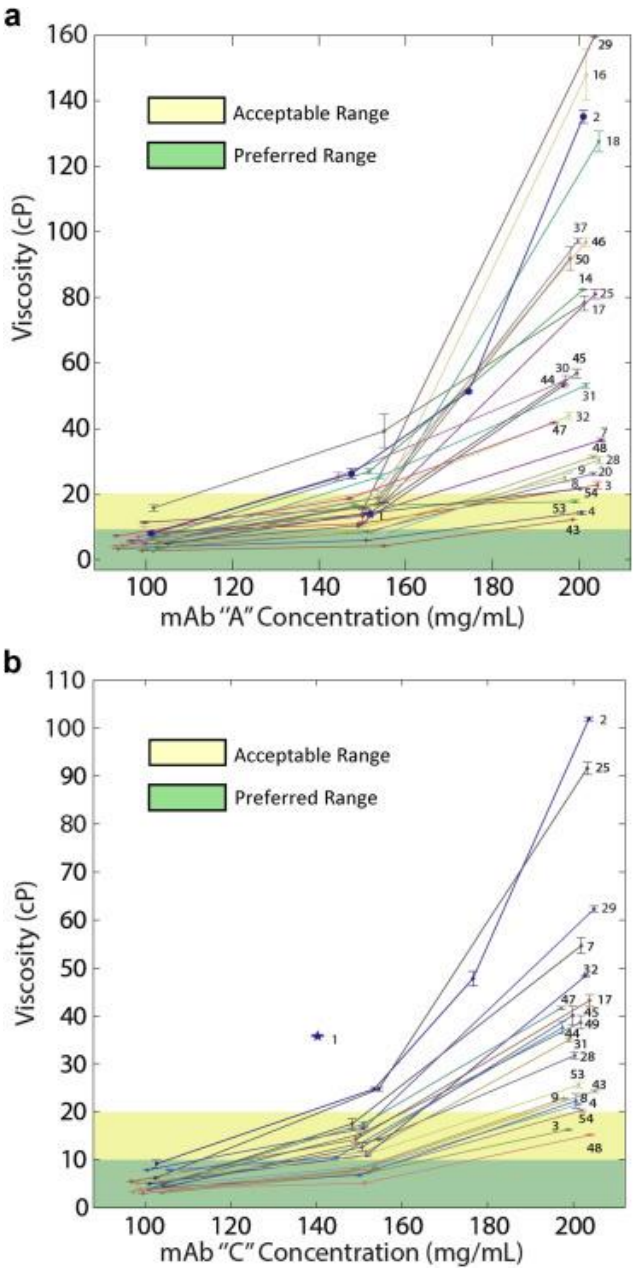

Figure 0.2: Protein concentration dependence on solution viscosity of (a) mAb A and (b) mAb C in the presence of lead excipients.

Excipients were identified and listed here by the same numbers used in Figure 1. The original formulation (1) is listed in Figure 1 and was included as a control at a single protein concentration. Error bars are SDs from triplicate measurements. "Acceptable" (≤20 cP) and "preferred" (≤10 cP) viscosity ranges are indicated by the yellow and green regions, respectively.

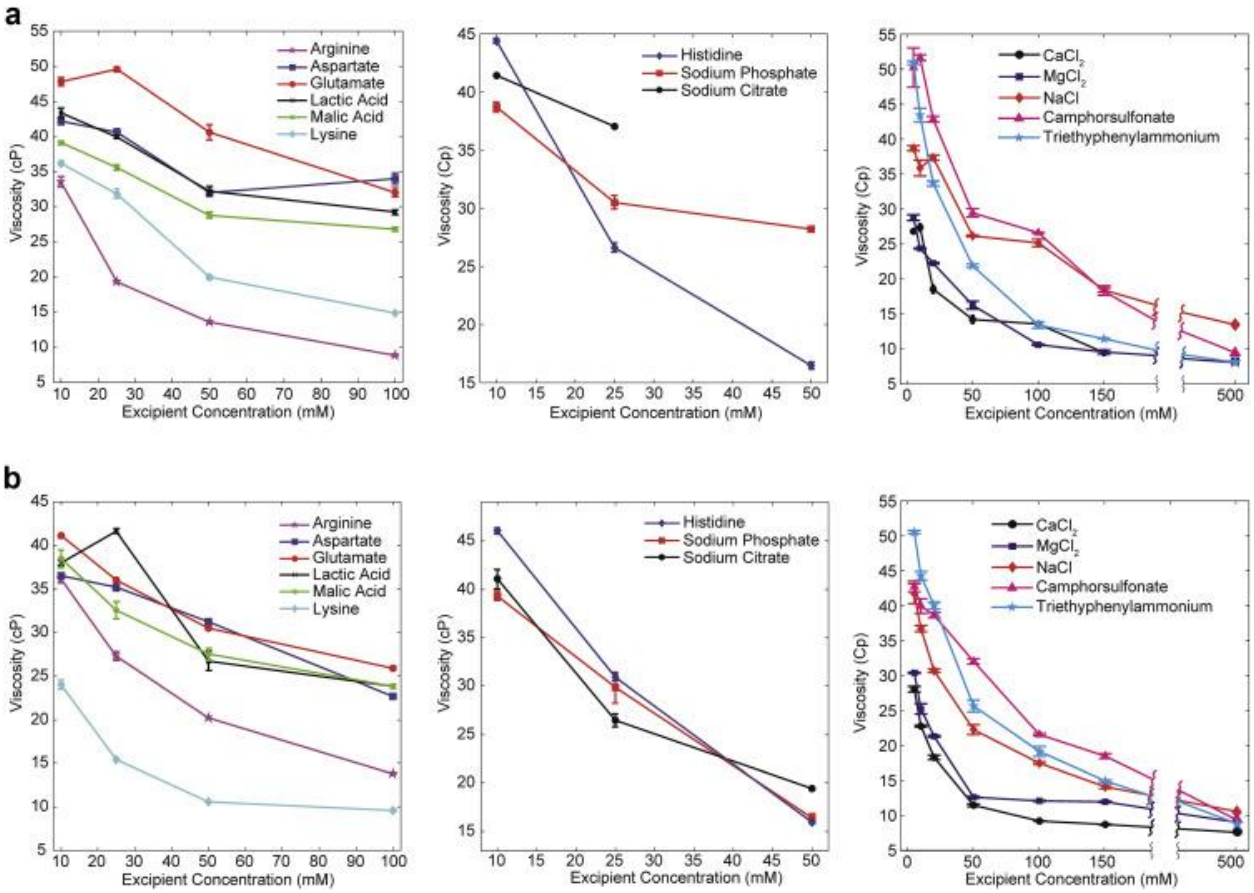

Figure 0.3: The effect of the concentration of selected excipients on the solution viscosity of 175 mg/mL solutions of (a) mAb A and (b) mAb C containing 10 mM histidine at pH 5.75.

MAb A precipitated in formulations containing sodium citrate concentrations of about 25 mM and higher. Values are average and SD from triplicate measurements.

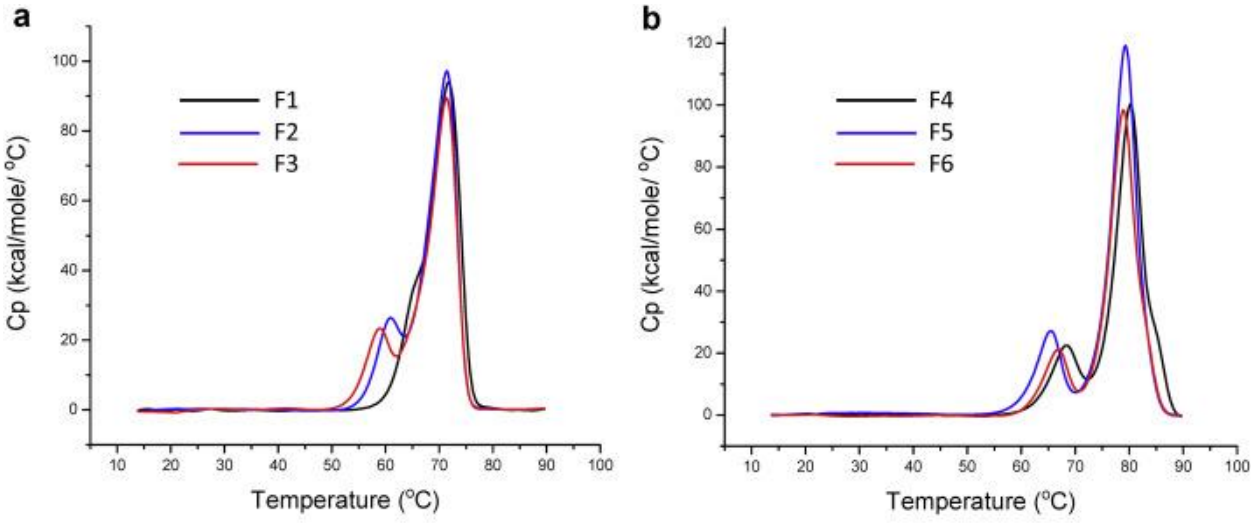

c

Formulation	$T_{onset}1$ (°C)	$T_{onset}2$ (°C)	T_m1 (°C)	T_m2 (°C)	T_m3 (°C)
mAb A					
F1	60.1 ± 0.8		66.2 ± <0.1	70.8 ± <0.1	73.0 ± <0.1
F2	55.6 ± <0.1	63.6 ± <0.1	61.2 ± <0.1	69.1 ± <0.1	72.0 ± <0.1
F3	53.4 ± 0.1	63.8 ± <0.1	59.2 ± 0.1	68.4 ± <0.1	71.9 ± <0.1
mAb C					
F4	62.1 ± <0.1	74.4 ± <0.1	68.1 ± <0.1	80.1 ± <0.1	
F5	60.1 ± 0.4	74.3 ± 0.1	66.2 ± 0.6	79.7 ± 0.2	
F6	59.9 ± 0.6	73.6 ± 0.1	66.1 ± 0.8	79.0 ± 0.3	

Figure 0.4: Conformational stability of mAb A and mAb C in candidate formulations as determined by differential scanning calorimetry.

(a) Representative thermograms of 3 formulations of mAb A. (b) Representative thermograms of 3 formulations of mAb C. (c) Thermal onset temperatures (T_{onset}) and thermal melting temperatures (T_m) were determined from DSC thermograms. Values are average and SD from triplicate measurements. See Table 3 for description of each formulation.

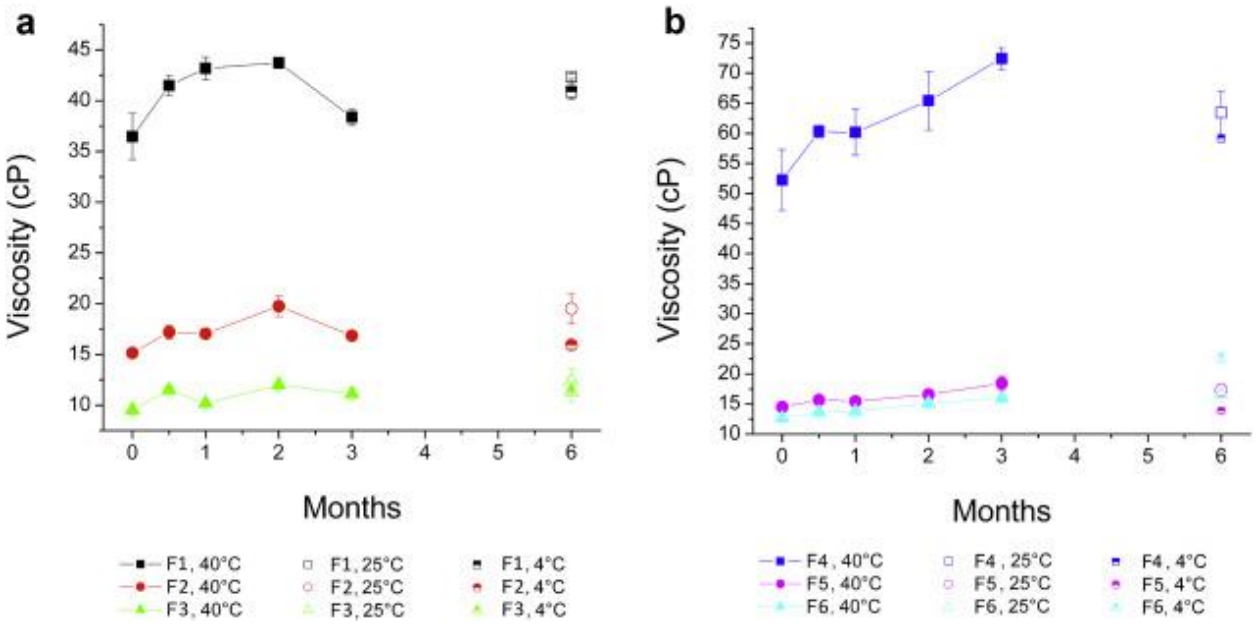

Figure 0.5: Solution viscosity of ultra-high concentrations of mAb A and mAb C in candidate formulations after 3 months storage at 40°C.

(a) Viscosity of mAb A at 175 mg/mL and (b) viscosity of mAb C at 175 mg/mL. For 25°C and 4°C, only data for the 6-month time point are shown. Values are average and SD from triplicate measurements.

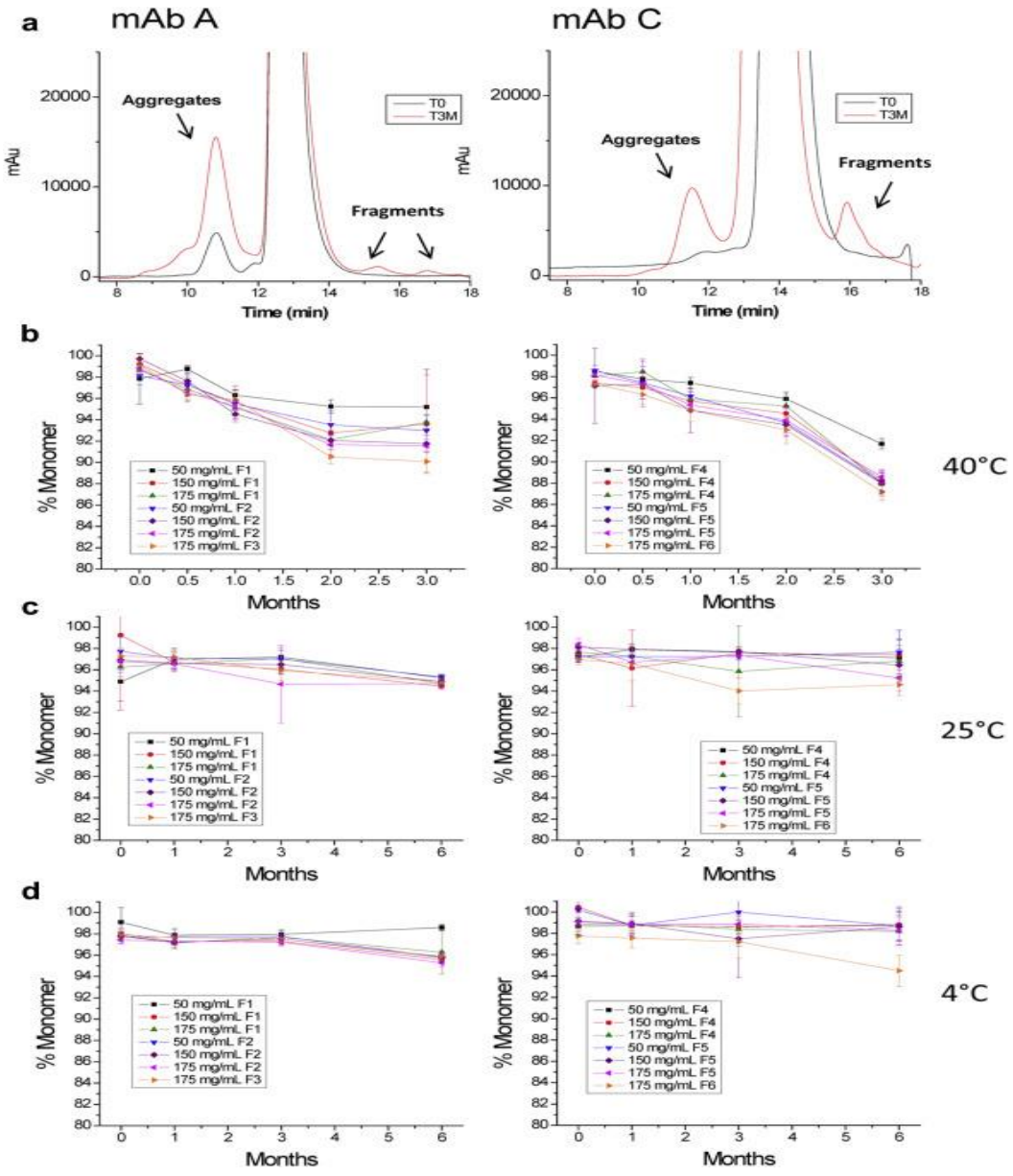

Figure 0.6: Protein aggregation profile of ultra-high concentrations of mAb A and mAb C in candidate formulations during stability as measured by SEC.

(a) Representative overlay of SEC chromatograms of mAbs before and after storage at 40°C for 3 months with aggregate, monomer, and fragment peaks indicated. Loss of monomer over time for mAbs stored at (b) 40°C, (c) 25°C, and (d) 4°C over 6 months. Formulation composition and protein concentrations are listed in Table 3. Values are average and SD from triplicate measurements.

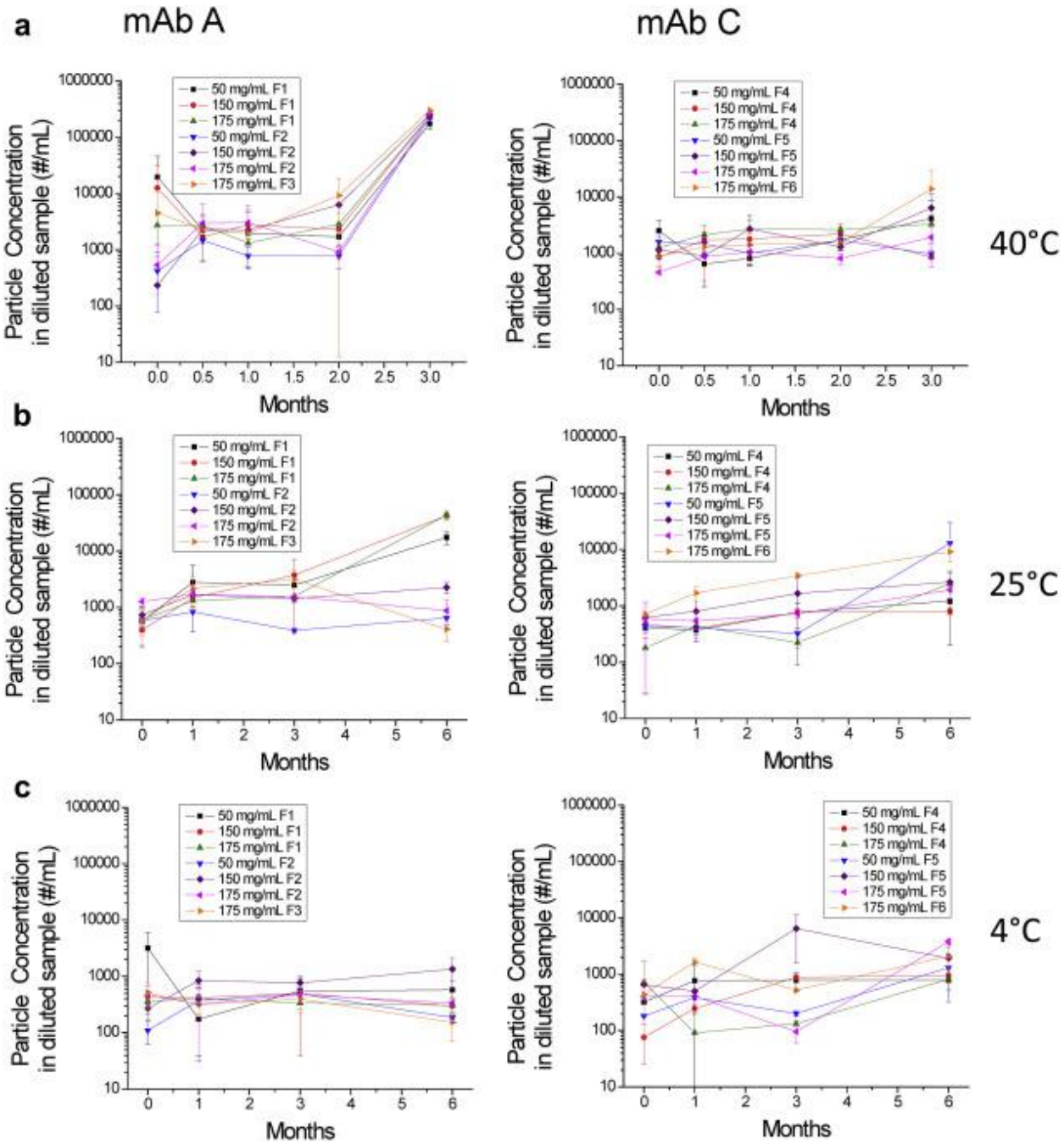

Figure 0.7: Subvisible particle formation in mAb A and mAb C over time observed by MFI. (a) Particle formation in mAb formulations over time at 40°C, (b) 25°C, and (c) 4°C.Formulation composition and protein concentrations are listed in Table 3. Values are average and SD from triplicate measurements.

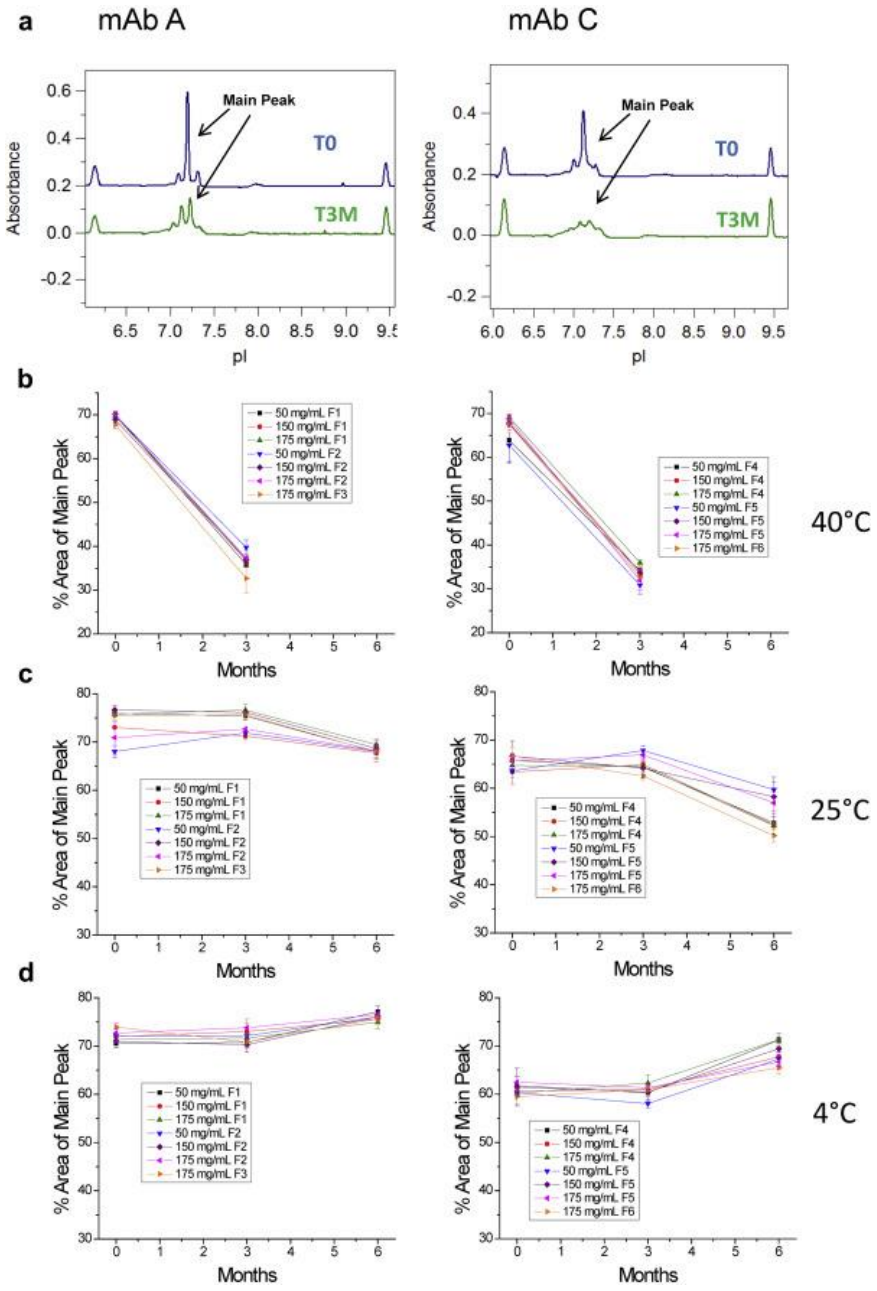

Figure 0.8: Charge heterogeneity profile of mAb A and mAb C as analyzed by cIEF during storage.

(a) Representative overlay of electropherograms of mAbs before and after storage at 40°C for 3 months. Loss of main peak area over time for mAbs stored at (b) 40°C, (c) 25°C, and (d) 4°C. Formulation composition and protein concentrations are listed in Table 3. Values are average and SD from triplicate measurements.

4.5 References

1. Samaranayake H, Schenkwein TWD, Räty JK, Ylä-Herttuala S 2009. Challenges in monoclonal antibody-based therapies. Annals of Medicine 41(5):322-331.

2. An Z 2010. Monoclonal antibodies—a proven and rapidly expanding therapeutic modality for human diseases. Protein Cell 1(4):319-330.

3. ElBakri A, Nelson PN, Odeh ROA 2010. The state of antibody therapy. Human Immunology 71(12):1243-1250.

4. Shire SJ, Shahrokh Z, Liu J 2004. Challenges in the development of high protein concentration formulations. Journal of Pharmaceutical Sciences 93(6):1390-1402.

5. Jezek J, Rides M, Derham B, Moore J, Cerasoli E, Simler R, Perez-Ramirez B 2011. Viscosity of concentrated therapeutic protein compositions. Advanced Drug Delivery Reviews 63(13):1107-1117.

6. Thomas CR, Nienow AW, Dunnill P 1979. Action of shear on enzymes: studies with alcohol dehydrogenase. Biotechnology and Bioengineering 21(12):2263-2278.

7. Baldo BA 2016. Other Approved Therapeutic Monoclonal Antibodies. Safety of Biologics Therapy:141-215.

8. Buck PM, Chaudhri A, Kumar S, Singh SK 2015. Highly viscous antibody solutions are a consequence of network formation caused by domain-domain electrostatic complementarities: insights from coarse-grained simulations. molecular Pharmaceutics 12(1):127-139.

9. Arora J, Hickey JM, Majumdar R, Esfandiary R, Bishop SM, Samra HS, Middaugh CR, Weis DD, Volkin DB 2015. Hydrogen exchange mass spectrometry reveals protein interfaces and distant dynamic coupling effects during the reversible self-association of an IgG1 monoclonal antibody. mAbs 7(3):525-539.

10. Raut AS, Kalonia DS 2015. Opalescence in monoclonal antibody solutions and its correlation with intermolecular interactions in dilute and concentrated solutions. Journal of Pharmaceutical Sciences 104(4):1263-1274.

11. Esfandiary R, Parupudi A, Casas-Finet J, Gadre D, Sathish H 2015. Mechanism of reversible self-association of a monoclonal antibody: role of electrostatic and hydrophobic interactions. Journal of Pharmaceutical Sciences 104(2):577-586.

12. Connolly BD, Petry C, Yadav S, Demeule B, Ciaccio N, Moore JMR, Shire SJ, Gokarn YR 2012. Weak interactions govern the viscosity of concentrated antibody solutions: high-throughput analysis using the diffusion interaction parameter. Biophysical Journal 103(1):69-78.

13. Singh SN, Yadav S, Shire SJ, Kalonia DS 2014. Dipole-dipole interaction in antibody solutions: correlation with viscosity behavior at high concentration. Pharmaceutical Research 31(9):2549-2558.

14. Arora J, Hu Y, Esfandiary R, Sathish HA, Bishop SM, Joshi SB, Middaugh CR, Volkin DB, Weis DD 2016. Charge-mediated Fab-Fc interactions in an IgG1 antibody induce reversible self-association, cluster formation, and elevated viscosity. mAbs 8(8):1561-1574.

15. Bethea D, Wu S-J, Luo J, Hyun L, Lacy ER, Teplyakov A, Jacobs SA, O'Neil KT, Gilliland GL, Feng Y 2012. Mechanisms of self-association of a human monoclonal antibody CNTO607. Protein Engineering, Design & Selection 25(10):531-537.

16. Wu J, Schultz JS, Weldon CL, Sule SV, Chai Q, Geng SB, Dickinson CD, Tessier PM 2015. Discovery of highly soluble antibodies prior to purification using affinity-capture self-interaction nanoparticle spectroscopy. Protein Engineering, Design and Selection 28(10):403-414.

17. Kanai S, Liu J, Patapoff TW, Shire SJ 2008. Reversible self-association of a concentrated monoclonal antibody solution mediated by Fab-Fab interaction that impacts solution viscosity. Journal of Pharmaceutical Sciences 97(10):4219-4227.

18. Liu J, Nguyen MDH, Andya JD, Shire SJ 2005. Reversible self-association increases the viscosity of a concentrated monoclonal antibody in aqueous solution. Journal of Pharmaceutical Sciences 94(9):1928-1940.

19. Wang S, Zhang N, Hu T, Dai W, Feng X, Zhang X, Qian F 2015. Viscosity-lowering effect of amino acids and salts on highly concentrated solutions of two IgG1 monoclonal antibodies. molecular Pharmaceutics 12(12):4478-4487.

20. Du W, Klibanov AM 2011. Hydrophobic salts markedly diminish viscosity of concentrated protein solutions. Biotechnology and Bioengineering 108(3):632-636.

21. Wallace VP, Ferachou D, Ke P, Day K, Uddin S, Casas-Finet J, Walle CFVD, J.Falconer R, Zeitler JA 2015. Modulation of the hydration water around monoclonal antibodies on addition of excipients detected by Terahertz time-domain spectroscopy. Journal of Pharmaceutical Sciences 104(12):4025-4033.

22. Inoue N, Takai E, Arakawa T, Shiraki K 2014. Specific decrease in solution viscosity of antibodies by arginine for therapeutic formulations. Molecular Pharmaceutics 11(6):1889-1896.

23. Guo Z, Chen A, Nassar RA, Helk B, Mueller C, Tang Y, Gupta K, Klibanov AM 2012. Structure-activity relationship for hydrophobic salts as viscosity-lowering excipients for concentrated solutions of monoclonal antibodies. Pharmaceutical Research 29(11):3102-3109.

24. Kamerzell TJ, Pace AL, Li M, Danilenko DM, Mcdowell M, Gokarn YR, Wang YJ 2013. Polar solvents decrease the viscosity of high concentration IgG1 solutions through hydrophobic

solvation and interaction: formulation and biocompatibility considerations. Journal of Pharmaceutical Sciences 102(4):1182-1193.

25. Bond MD, Panek ME, Zhang Z, Wang D, Mehndiratta P, Zhao H, Gunton K, Ni A, Nedved ML, Burman S, Volkin DB 2009. Evaluation of a Dual-Wavelength Size Exclusion HPLC Method With Improved Sensitivity to Detect Protein Aggregates and ItsUse to Better Characterize Degradation Pathways of an IgG1Monoclonal Antibody. Journal of Pharmaceutical Sciences 99(6):2582–2597.

26. Kumru OS, Liu J, Ji JA, Cheng W, Wang YJ, Wang T, Joshi SB, Middaugh CR, Volkin DB 2012. Compatibility, Physical Stability, and Characterization of an IgG4 Monoclonal Antibody After Dilution into Different Intravenous Administration Bags. Journal of Pharmaceutical Sciences 101(10):3636-3650.

27. Quiroz AR, Finkler C, Huwyler J, Mahler H-C, Schmidt R, Koulov AV 2016. Factors Governing the Accuracy of Subvisible Particle Counting Methods. Journal of Pharmaceutical Sciences 105(7):2042-2052.

28. Administration USFaD. Inactive ingredient search for approved drug products. ed.

29. Kamerzell TJ, Esfandiary R, Joshi SB, Middaugh CR, Volkin DB 2011. Protein-excipient interactions: mechanisms and biophysical characterization applied to protein formulation development. Advanced Drug Delivery Reviews 63(13):1118-1159.

30. Reynolds G 2014. Integrated solutions for the delivery of high-volume biologics. ONdrugDelivery 51:26-29.

31. Salinas BA, Sathish HA, Bishop SM, Harn N, Carpenter JF, Randolph TW 2010. Understanding and modulating opalescence and viscosity in a monoclonal antibody formulation. Journal of Pharmaceutical Sciences 99(1):82-93.

32. Thakkar SV, Joshi SB, Jones ME, Sathish HA, Bishop SM, Volkin DB, Middaugh CR 2012. Excipients differentially influence the conformational stability and pretransition dynamics of two IgG1 monoclonal antibodies. Journal of Pharmaceutical Sciences 101(9):3062-3077.

33. Raut AS, Kalonia DS 2016. Viscosity analysis of dual variable domain immunoglobulin protein solutions: role of size, electroviscous effect and protein-protein interactions. Pharmaceutical Research 33(1):155-166.

34. Paulekuhn GS, Dressman JB, Saal C 2007. Trends in active pharmaceutical ingredient salt selection based on analysis of the Orange Book database. Journal of Medicinal Chemistry 50(26):6665-6672.

35. Thiagarajana G, Semplea A, Jamesb JK, Cheunga JK, Shameem M 2016. A comparison of biophysical characterization techniques in predicting monoclonal antibody stability. MAbs 8(6):1088-1097.

36. Tanford C, Buzzell JG 1956. The viscosity of aqueous solutions of bovine serum albumin between pH 4.3 and 10.5. The Journal of Physcial Chemistry 60(2):225-231.

37. Yadav S, Shire SJ, Kalonia DS 2011. Viscosity Analysis of High Concentration Bovine Serum Albumin Aqueous Solutions. Pharmaceutical Research 28(8):1973-1983.

38. Minton AP 2012. Hard quasispherical particle models for the viscosity of solutions of protein mixtures. Journal of Physical Chemistry B 116(31):9310-9315.

39. Kheddo P, Tracka M, Armer J, Dearman RJ, Uddin S, Walle CFvd, Golovanov AP 2014. The effect of arginine glutamate on the stability of monoclonal antibodies in solution. International Journal of Pharmaceutics 473(1-2):126-133.

40. Dear BJ, Hung JJ, Truskett TM, Johnston KP 2017. Contrasting the influence of cationic amino acids on the viscosity and stability of a highly concentrated monoclonal antibody. Pharmaceutical Research 34(1):193-207.

41. Wu H, Kroe-Barrett R, Singh S, Robinson AS, Roberts CJ 2014. Competing aggregation pathways for monoclonal antibodies. Federation of European Biochemical Societies 588:936-941.

42. He F, Woods CE, Trilisky E, Bower KM, Litowski JR, Kerwin BA, Becker GW, Narhi LO, Razinkov VI 2011. Screening of monoclonal antibody formulations based on high-throughput thermostability and viscosity measurements: design of experiment and statistical analysis. Journal of Pharmaceutical Sciences 100(4):1330-1340.

43. Tessier PM, Wu J, Dickinson CD 2014. Emerging methods for identifying monoclonal antibodies with low propensity to self-associate during the early discovery process. Expert Opinion on Drug Delivery 11(4):461-465.

Chapter 5 Development of Scale-Down Assays for Assessment of Mechanism(s) of Tangential Flow Filtration Instability of Proteins

5.1 Introduction

Tangential flow filtration (TFF) is the most widely used unit operation in the final stages of large scale purification of protein drug candidates during the downstream process.[1] TFF is commonly used at this final step of the purification to concentrate protein molecules (ultrafiltration) and to perform buffer exchanges (diafiltration) into the desired final formulation buffer at the target dose.[2,3] Ensuring protein stability and minimizing aggregation can be difficult to manage at this stage of the manufacturing process, since proteins can go through many different environmental stresses during TFF.[4] For example, shear stress, cavitation, air-liquid interface, and protein-membrane surface interactions[5] can all potentially lead to protein structural alterations, aggregation and particle formation. In this study, the impact of various stresses imposed on protein molecules during TFF processing on key physicochemical and structural properties of four different antibodies (Abs) was examined (i.e., two IgG4 molecules, an IgG1 molecule and a bispecific Ab based on IgG4). These four Ab molecules were selected based on different levels of instability observed previously during large-scale TFF processing. Two Ab molecules (termed "molecule 1" and molecule 2") were shown to be stable with good protein recovery and low amounts of aggregation while the other two Ab molecules (termed "molecule 8" and "molecule 9") were shown to be problematic with unacceptable levels of protein loss and aggregation during processing with a large scale TFF system.

To better understand the causes and mechanisms that result in some Ab molecules being more susceptible to TFF related instability compared to others, the first step was to establish a small-scale TFF method in the laboratory to emulate the observations seen during large scale TFF processing. This is a critical practical first step since large scale TFF processing requires impractical amounts and volumes of protein to perform process/formulation development

experiments. Using this benchtop model TFF setup, the effect of the TFF processing on the recovery and aggregation/particle formation was examined with the four Ab molecules during processing (as the solution changes from their respective initial buffer/protein concentration and to their final formulation buffers/protein concentrations). The lab scale TFF setup was shown to mimic reasonably well the previous observations of behavior of the these four Ab molecules during large scale TFF processing.

For the second phase of the work, the ability to better understand and ultimately predict this TFF behavior by examining the inherent properties of these four Ab molecules (using minimal material and without the need to perform any TFF processing) was examined. First, the inherent structural integrity, relative solubility and conformational stability of the four Ab molecules were determined and compared to evaluate if correlations could be established with TFF results. This evaluation was performed in both PBS buffer (so the four Ab molecules are compared under the same conditions) and in their respective TFF processing buffers (so the four Ab molecules are compared under the actual solution conditions of TFF processing). Second, the colloidal properties of the four Ab molecules (i.e., the propensity of the molecules to interact with each other and to aggregate), in both PBS buffer and in their respective TFF processing buffers, was examined in a series of stirring and shaking studies and again comparisons are made with TFF results. Finally, the interfacial properties of the four Ab molecules (i.e., the propensity of the four Abs to go to air-water interfaces), in both PBS buffer and in their respective TFF processing buffers, was examined and similar correlations to TFF behavior was performed.

By examining the impact of various TFF stresses on the recovery and aggregation of the four Ab molecules using a laboratory scale TFF setup, and then comparing those results to the conformational, colloidal, and interfacial properties of each molecule, we were to gain a better

mechanistic understanding of TFF associated instability of molecules. Overall, it was observed that evaluating the interfacial properties of these molecules, both in comparison to each other in PBS buffer and in their respective TFF processing buffers, is a key step to better understanding the propensity of these four Ab molecules to behave "good" or "bad" during TFF processing. To this end, with the ultimate goal of being able to identify key analytical tools to perform early stage prediction and risk assessment of antibody behavior during TFF using small amounts of protein, additional work further exploring the utility of a Langmuir trough method to evaluate the interfacial properties of four Ab molecules in various solution conditions is recommended. This additional work permit for a better understanding of the predictive ability of the Langmuir trough technique in terms of identifying an Ab molecule's TFF behavior (at both laboratory and large-scale processing) using minimal amount of protein.

5.2 Materials and Methods

5.2.1 Materials

One IgG1 monoclonal antibody (molecule 2), two IgG4 monoclonal antibodies (molecules 1 and 8), and a bispecific antibody (molecule 9), were provided by Bristol Myers Squibb (New Jersey). Molecules 1 and 2 were provided as 50 mg/mL protein solutions in 20 mM histidine, 8.5% sucrose pH 6.0, molecule 8 as an 18.3 mg/mL protein solution in 20 mM histidine, 8.5% sucrose, pH 5.5, and molecule 9 as a 50 mg/mL protein solution in 20 mM histidine, 90 mM arginine, 4.0% sucrose pH 5.6. The concentrations of the various Abs were measured with an Agilent 8453 UV-visible spectrophotometer (Palo Alto, California) after dilution. The extinction coefficients of 1.68 (molecule 1 and 8), 1.45 (molecule 2), and 1.78 (mg/mL)-1 cm-1 (molecule 9) were used to calculate the protein concentration.

An XL25 dual channel pH meter, sodium hydroxide, sodium chloride, and potassium chloride were obtained from Fisher Scientific (Fair Lawn, New Jersey). Sodium phosphate dibasic (anhydrous), histidine, sucrose, mannitol, DTPA, arginine, sodium acetate, potassium phosphate, trizma HCl, and trizma base were obtained from Sigma Aldrich (St. Louis, Missouri). Polysorbate 80 was obtained from Thermo Scientific (Rockford, Illinois). For shaking and stirring studies, glass vials used were from West Pharmaceuticals, (3-mLVial, Fiolax Clear, Item#6800-0316), and the rubber stoppers were from West Pharmaceuticals (V-35 4432/gray, Item#10122128).

5.2.2 Methods

5.2.2.1 Sample Preparation

Stock solutions of molecule 1, 2, 8, and 9 were diluted into the corresponding buffers to achieve a final concentration of 0.2 mg/mL for biophysical assays including UV-Visible, CD, intrinsic and extrinsic fluorescence spectroscopy as well as static light scattering. Stock solutions were diluted to 1 mg/mL for biophysical assays including DSC, FTIR, and DLS. One mg/mL protein samples were also prepared for the shaking and stirring stability studies and aliquots of 1.1 mL were placed into 3-mL type 1 borosilicate glass vials and capped with rubber stoppers (West Pharmaceutical Services, Exton, PA). Before use, the glass vials were autoclaved. Stock samples were diluted to 2 mg/mL for TFF and Langmuir trough studies. All samples were sterile filtered with 0.22-µm syringe filters after preparation (Millipore, Billerica, MA). The antibody concentration was quantified with an Aglient 8453 UV-Visible spectrophotometer (Palo Alto, CA) or with a NanoDrop spectrophotometer (NanoDrop Products, Wilmington, DE) in triplicates at A280. The extinction coefficients of 1.68 (molecule 1 and 8), 1.45 (molecule 2), and 1.78 (mg/mL)-1 cm-1 (molecule 9) were used to calculate the protein concentration.

5.2.2.2 Laboratory Scale Tangential Flow Filtration

A laboratory tangential flow filtration (TFF) system (Pall) with Minimate TFF capsule was used to perform diafiltration and concentration of the four molecules. Molecules 1, 2, and 8 used capsules with 50K MWCO and molecule 9 used 30K MWCO capsules. Typically, a starting volume of 100 mL was used, with a target final volume of 20 mL. A peristaltic pump was used at 300 RPM to circulate the sample through the capsule. Valves were manually tightened or loosened to obtain a pressure of 20 psi across the capsule. The formulation buffer was added at the same rate as the filtrate was removed from the system to keep the concentration constant throughout the diafiltration steps. Eight diafiltration steps occurred by exchanging the complete starting volume with formulation buffer each time. The sample was then concentrated using the system via ultrafiltration to achieve a 5X concentration. During the process, samples were removed for testing by UV-Vis spectroscopy and MFI. These samples consisted of the starting and final material along with various sample in buffer ratios (initial:formulation) of 5:1, 3:1, 1:1, 1:3, 1:5, and after the first diafiltration, second diafiltration, forth diafiltration, and eighth diafiltration.

5.2.2.3 Microflow Imaging

The total number and distribution of sub-visible particles in the range of 2 to 100 μm were examined using an MFI 5200 with an autosampler (Protein Simple, Santa Clara, CA) with a 100 μm silane coated flow cell. Measurements were made in duplicate at ambient temperature for all samples. Illumination was optimized using deionized water filtered with a 0.22-μm filter prior to all measurements.

5.2.2.4 Differential Scanning Calorimetry

DSC measurements were performed using a VP-Capillary DSC System (Microcal, acquired by Malvern Instruments Ltd). Protein concentrations were adjusted to 1 mg/mL before

the measurement. The corresponding formulation buffer was used as a reference for each sample. The samples were heated from 10 to 90°C at a rate of 60°C/h. Resulting thermograms were corrected by subtraction of buffer-only scans and then normalized to the molar concentration of the protein and analyzed using Origin 7.0 software (OriginLab Corporation, Northampton, MA).

5.2.2.5 Far-UV Circular Dichroism

Far-UV circular dichroism (CD) spectroscopy of protein samples was performed using a Chirascan-plus Circular Dichroism Spectrometer (Applied Photophysics Ltd, Leatherhead UK) equipped with a peltier temperature controller and a 4-position cuvette holder. Quartz cuvettes (0.1 cm path length) sealed with a teflon stopper (Starna Cells Inc., Atascadero, CA) were used. The spectra were collected from 200-260 nm using 1 nm steps and 0.5 s sampling time. Thermal melts were performed over a temperature range of 10 to 90°C. The spectra were collected at 2.5°C intervals with a 2 min equilibration time at each temperature. The final protein concentration of the sample was 0.2 mg/mL and the measurements were conducted in triplicate.

5.2.2.6 Fourier Transform Infrared Spectroscopy

FTIR spectroscopy of Molecules 1, 2, 8 and 9 (at 1.0 mg/mL) was performed (in triplicate) at 10°C using a Bruker Tensor-27 FTIR spectrometer (Bruker Optics, Billerica, MA) equipped with a KBr beam splitter. The MCT detector was cooled with liquid N_2 for at least 20 min prior to use and the interferometer was constantly purged with N_2 gas. All instrument validation tests were performed and passed prior to daily measurements. Two hundred fiftysix scans were recorded from 4000 to 600 cm-1 with a 4 cm-1 resolution using a Bio-ATR cell. Background measurements were acquired with the appropriate buffer alone and subtracted from the sample spectra. Atmospheric and baseline corrections were applied using OPUS V6.5 (Bruker Optics, Billerica, MA) software. Calculation of the second derivative was also completed using OPUS V6.5 while applying a 9-point Savitzky-Golay smoothing function. For Fourier self-deconvolution, the deconvolution

factor was 2 and the noise reduction filter was 0.5. Following the deconvolution, between 6 and 9 peaks were fitted to the absorbance spectrum in the Amide I region (1700-1600 cm-1) using a 50% Lorentzian and 50% Gaussian function. The areas of the peaks were used to calculate the relative percentage of secondary structure components in each Ab sample.

5.2.2.7 Intrinsic Fluorescence Spectroscopy

Intrinsic tryptophan fluorescence was measured in triplicate using a Photon Technology International (PTI) spectrofluorometer (Lawrenceville, NJ) equipped with a turreted four-position Peltier-controlled cell holder and a xenon lamp. Fluorescence emission spectra of samples at 0.2 mg/mL using 1 cm path length quartz cuvettes were recorded as a function of temperature (10-90°C). An excitation wavelength of 295 nm was used (>95% Trp emission) with the slit width set at 4 nm. Emission spectra were collected from 305-405 nm with a step size of 1 nm and an integration time of 1 s. The spectra were collected at 2.5°C intervals with a 2 min equilibration time at each temperature. The initial signal was kept at ~800,000 counts per second for fluorescence spectra and an emission maximum of ~20,000 counts per second for light scattering data. Analysis was performed using in-house software (Middaugh Suite). The corresponding buffer spectrum was subtracted from each protein spectrum prior to data analysis. The emission peak position was determined using a mean spectral center of mass method (MSM) executed in the Middaugh Suite. Although this calculation method increases the signal to noise ratio for more accurate determination of lambda max values, it shifts the apparent peak position by 5-10 nm from their actual values. The T_{onset} values were determined by identifying the point at which the baseline deviated from linearity using Origin software.

5.2.2.8 Extrinsic Fluorescence Spectroscopy

8-Anilino-1-naphthalene sulfonate (ANS) was used as an extrinsic fluorescence probe in the presence of antibody with the same instrument described above. A dye to protein molar ratio

of 25:1 was used for sample preparation. ANS was excited at 372 nm, and emission spectra of ANS was collected from 400-600 nm every 2 nm as a function of temperature from 10 to 90^{o}C. The corresponding buffer spectra were subtracted from protein spectra prior to data analysis. The emission peak intensity was determined using a mean spectral center of mass method (MSM) executed in the Middaugh Suite. The T_{onset} values were determined by identifying the point at which the baseline deviated from linearity using Origin 8.0 software.

5.2.2.9 Static Light Scattering

The static light scattering intensity values were collected simultaneously during the intrinsic fluorescence experiments using a second photomultiplier located 180° to the fluorescence detector and a 0.25 nm slit width. The scattering intensities at 295 nm were obtained as a function of temperature (10-90°C). Scattering from the buffer alone was subtracted from each protein sample value before data analysis.

5.2.2.10 Dynamic Light Scattering

Size analysis by DLS was performed employing the dynamic light scattering mode on a ZetaPALS zetasizer (Brookhaven Instruments Corporation, Holtsville, NY) using quartz cuvettes that were cleaned of any dust and air-dried. The hydrodynamic diameters of filtered Molecule 1, 2, 8 and 9 samples (at 1 mg/mL) were analyzed by generating an auto-correlation decay function after centrifugation at 14,000 X g for 5 min. Ten measurements were recorded and averaged for 30 s each. Number and intensity distributions were fitted using multimodal size distribution (MSD) or a cumulant analysis algorithm was employed using the instruments software. All measurements were performed in triplicate at 25°C. The viscosity value used for each DLS experiment was determined prior to analysis (see section 2.2.11).

For determination of the interaction parameter (k_D), DLS measurements were instead made on a Wyatt DynaPro Plate Reader (Wyatt Technology Corporation, Santa Barbara, CA). The mutual diffusion co-efficients (D_m) of each molecule were determined in the specified buffers at 1, 3, 5, 8 and 10 mg/mL. Solvent viscosities used were determined prior to analysis (see section on Viscosity), or (in the case of PBS) selected from calculated values in the instrument software. A linear plot of $1/D_m$ as a function of concentration (c) was used to determine the k_D values and the diffusion coefficient (D_s) for each molecule using the following relation (at low protein concentrations, $k_D = k_{D2}$):

$$\frac{1}{D_m} = \frac{1}{D_s} - \left(\frac{k_{D2}}{D_s}\right) c$$

5.2.2.11 Viscosity

Solution viscosities were measured at 25°C with an m-VROC viscometer (Rheosense, San Ramon, CA). Samples were injected at a rate of 100 mL/min at a shear rate of 1935.6 1/s for a duration of 100 s using a 1-mL glass syringe (Hamilton Co, Reno, NV). Measurements were made in triplicate. Viscosity values were obtained in units of dynamic viscosity (cP).

5.2.2.12 PEG Solubility Assay

The experimental protocol was adapted from Gibson et al.[6] and Toprani et al.[7] Stock solutions of PEG-10,000 ranging from 0 to 40% w/v PEG were prepared in each corresponding buffer. A volume of 200 µL of each of the PEG-10,000 solutions (from 0% to 40% w/v PEG) was added to wells of a 96-well polystyrene filter plate (Corning # 3504, Corning Life Sciences, Corning, NY). Fifty microliters of the protein stock solutions (1 mg/mL) were then added to each well to achieve a final protein concentration of 0.2 mg/mL. The plates were incubated at room

temperature overnight and then were centrifuged at 1233 (× *g*) for 15 min. The filtrate was collected in a clear 96-well collection plate (Greiner Bio-One n # 655001, Greiner Bio-One North America Inc., Monroe, NC). The protein concentration was determined by transferring 200 µL of filtrate into a 96-well UV Star microplate (Grenier#655801). The filtrate was measured on a SpectraMax M5 UV-Visible plate reader at 280 nm to determine the protein concentration The concentrations versus %PEG-10,000 data were fit to a standard 4-parameter, modified hill-slope sigmoidal curve equation (Eq. 1) using Python (x,y) version 2.7.6.0, an open-source scientific software based on Python language. The $\%PEG_{midpt}$ values and apparent solubility value parameters were then calculated from the resulting curve fit50 where *t* = top plateau, *b* = bottom plateau, mid = *x*-axis midpoint, and *s* = slope. The $\%PEG_{midpt}$ values were determined by noting the *x*-axis midpoints.

$$(1)\ y = b + \left(\frac{t-b}{1+e^{s(mid-x)}}\right)$$

The apparent solubility (thermodynamic activity) values were determined by first plotting the same data sets on a logarithmic scale from the transition region and then fitting them using Equation 2 to extrapolate the data to zero %PEG concentrations.

$$(2)\ log\ Sp = \log a_0 - A_{12}[\mathrm{PEG}]$$

5.2.2.13 SDS-PAGE

Samples were mixed with 4 NuPAGE LDS sample buffer (Thermo Fisher Scientific, Waltham, MA) with and without 5 mM dithiothreitol (Thermo Scientific, Rockford, IL) and incubated at 95°C for 5 min. Samples were then treated with 10 mM iodoacetamide (Thermo Scientific) at 25°C in the dark for 30 min. Each sample (10 mg) was separated on 10-20% Tris-

glycine gels using NuPAGE MES SDS Running Buffer (Thermo Fisher Scientific). SeeBlue Plus2 Pre-stained Protein Standard (Thermo Fisher Scientific) was used as a molecular weight ladder. Protein bands were visualized by staining the gels with Bio-safe Coomassie Blue G250 stain (BioRad Laboratories, Hercules, CA), followed by destaining in destaining buffer (50% methanol, 10% acetic acid).

5.2.2.14 Shaking and Stirring Studies

Samples were prepared in triplicates at 1 mg/mL. For shaking stress, the antibodies were agitated at 300 rpm using an IKA AS260.1 shaking platform with time points every hour over the course of 8 hours. For stirring stress, the molecules were stressed by placing a small pivot-ring-free stir bar (7 x 2 mm flea micro; Bel-Art-SP Scienceware, Wayne, NJ) inside each 3-mL vial and the stir setting was set to 5 at 25°C with time points every hour over the course of 8 hours using a Reacti-Therm III (Thermo Scientific). No vortex was observed in the liquid under these stirring conditions.

5.2.2.15 Langmuir trough

Molecules 1, 2, 8, and 9 at 2.0 mg/mL were loaded into a Langmuir trough that was controlled at 23 ± 2°C (Biolin Scientific, Inc., Stockholm, Sweden). A paper plate was used to measure surface pressure during compression-expansion experiments. The Ab solutions were initially allowed to reach a saturation concentration at the interface by allowing the solutions to equilibrate for 2 h. After this initial waiting period, the protein samples were exposed to interfacial compression-expansion cycles using movable Delrin barriers that touch the air-water interface. The available interfacial area changed from 87 to 12 cm^2 during each compression-expansion cycle. The compression ratio, defined as the ratio of the maximum possible interfacial area and the minimum interfacial area of the trough ($CR = A_{max}/A_{min}$), was held constant at 7.25 for this study.

A compression-expansion rate was defined as experiments where the protein solution in the trough was subjected to 750 cycles in 6 h.

5.3 Results

5.3.1 Tangential Flow Filtration

Four Ab molecules were provided to KU-MVSC by BMS that had known behaviors throughout the large scale TFF process. Two Ab molecules (molecules 1 and 2) were deemed "good" by showing acceptable protein recovery and low tendency to aggregate. The other two Ab molecules (molecules 8 and 9) were deemed "bad" molecules due to lower protein recovery and particle formation. These previously recorded results observed during large scale TFF processing, along with some of the key properties of the four Ab molecules (as well as their respective buffer conditions), are summarized in Table 1. As an initial evaluation, the four Ab molecules were characterized using SDS-PAGE (Figure 1) under both reduced and nonreduced conditions. Based on examination the gels, all four Abs appeared to be of high purity and there was no notable covalent aggregation and only minor fragmentation detected in each of four protein molecules.

The first step in determining the causes and mechanisms of protein aggregation and particle formation observed by BMS scientists to be induced during large scale TFF of these antibodies was to develop a miniaturized lab scale TFF system and evaluate its performance in predicting protein stability during large scale TFF processing. Figure 2 denotes the workflow used for these small scale TFF experiments and Figure 3 shows a schematic of the small scale TFF process and the sample points throughout the processes. The laboratory scale TFF was performed with all four Ab molecules using the same processing conditions, but in their respective processing buffers (see Table 1), and samples collected throughout the process were analyzed. These samples consisted of the starting material in the initial buffer, final concentrate material in the formulation buffer,

and intermediate samples collected when buffer ratios of initial:formulation were reached during the diafiltration steps (5:1, 3:1, 1:1, 1:3, 1:5, and after the 1st, 2nd, 4th, and 8th diafiltration). The protein concentration of the starting material was 2 mg/mL in the indicated initial buffers with a starting volume of 100 mL. The final step in the TFF protocol was a 5X concentration to achieve 10 mg/mL final material in the formulation buffer (see Table 1). This processes was optimized prior to reaching these conditions. Previously, runs were performed with 50 mL of the starting material. This was not ideal when the material was concentrated 5X due to the resulting volume equaling the dead volume of the filter. It was seen that a larger amount of protein was lost for all four molecules (~25-55%). This could be due to loss during the final sample recovery and/or to increased aggregation from intensified agitation conditions.

Using these optimized lab scale TFF process conditions (as described above), the protein recovery for each of the four Ab molecules is shown in Figure 4A. Molecules 1 and 2 show greater protein recovery than molecules 8 and 9, which is consistent with the "good" and "bad" results seen by BMS scientists using the large-scale TFF process. The same Ab samples were then analyzed by MFI to observe subvisible particle formation throughout the TFF process (Figure 5A). All four Ab molecules showed the presence of subvisible particles in the initial buffer and an increase in the subvisible particle concentration during processing into the final formulation buffer (ultrafiltration) and at higher protein concentrations (diafiltration). Molecule 8 had the highest levels of subvisible particles in both the initial solution at 2 mg/mL and after TFF processing into the final formulation buffer at 10 mg/mL.

Next, molecule 2 was examined under various conditions such as performing the ultrafiltration/diafiltration into a different formulation buffer (Formulation 2). This alternative formulation buffer was suggested by BMS scientists. As shown in Figure 4B, molecule 2 showed

lower protein recovery in formulation buffer 2 than formulation 1 buffer (Figure 4B). The third condition using molecule 2 was performing a higher fold concentration step of 20X instead of the previously examined 5X. In order to reach a 20X concentration, the starting volume of 500 mL was used and the targeted final volume was 25 mL. Increasing the concentration from 5X to 20X, led to only a slight decrease, if any, in percent recovery (from ~92% to ~87%, see Figure 4B). The last condition examined for molecule 2 was adding 0.01% PS80 to the initial buffer and formulation 2 buffer and the TFF process was repeated. Compared to running the TFF process in the absence of PS80, the addition of 0.01% PS80 produced similar protein recovery results for Ab molecule 2 (Figure 4B). MFI was performed to compare the subvisible particles concentration under various conditions described above (Figure 5B). Exchanging molecule 2 into formulation 1 vs formulation 2 showed no difference in particle formation. However, concentrating the Ab molecule 2 by 20X compared to 5X showed a 10-fold increase in subvisible particle formation, Not surprisingly, the addition of 0.01% PS80 to the initial and formulation buffers significantly decreased the subvisible particle formation for molecule 2 (Figure 5B). Due to the large amount of material needed for each TFF run, only molecule 2 in formulation 1 buffer was examined in duplicate and the errors were extrapolated for all other conditions. The protein recovery amount error between the two runs was negligible.

As a final set of experiments, due to molecule 8 showing the lowest percent recovery and a large amount of subvisible particle formation during TFF processing, 0.01% PS80 was added to the initial buffer and the formulation buffer and the laboratory scale TFF protocol was performed again. When comparing the protein recovery with and without PS80, there was a slight decrease observed when PS80 was present (Figure 4C). The addition of 0.01% PS80 to the initial and formulation buffers, however, had a major impact on decreasing the subvisible particle formation

with molecule 8 as seen by a ~10-fold decrease in particle levels as measured by MFI (Figure 5C). This result is not necessarily surprising since it is well known that high levels of subvisible particles can form due to aggregation of very low levels of protein.Thus, subvisible particles can form without affecting the total protein concentration.[8]

In summary, the small scale TFF system at KU showed the same trends seen when performing the larger scale procedure at BMS (i.e. Molecule 1&2 are more stable than 8&9). This was shown by higher protein recovery of the "good" molecules vs. that of the "bad" molecules. The percent recovery was optimized by increasing the starting volume to 100 mL instead of the initially tested 50 mL. Molecule 2 was examined using multiple buffer conditions: (1) formulation 1; (2) formulation 2; (3) 20X concentration; and (4) the addition of 0.01% PS80. The percent recovery was lower for formulation 2 buffer vs. formulation 1. The 20X concentration vs. 5X concentration showed a slightly higher percent recovery. The addition of 0.01% PS80 showed a slightly lower percent recovery than the same formulation buffer without it. Molecule 8 was examined with and without 0.01% PS80 and showed a 1% decrease in percent recovery. When examining the subvisible particle concentration for samples taken throughout the TFF run, there was an increase seen for all four molecules but molecule 8 showed the largest amount. There was a comparable amount of subvisible particles observed when comparing molecule 2 in formulation 1 to formulation 2. The 20X concentration vs. 5X concentration showed higher particle counts, which would be expected. Both molecule 2 and 8 were stabilized by the addition of 0.01% PS80 but significantly less subvisible particles were observed.

5.3.2 Structural Integrity and Conformational Stability Properties of the Four Antibodies in PBS Buffer

After a small scale TFF method had been established, we sought to correlate the stability profile obtained with the four Ab molecules with some inherent properties of these molecules to

identify which aspects of the environmental stresses resulting from TFF processing lead to protein aggregation. The first step was to investigate the correlation between TFF stability and key structural integrity and conformational stability properties of the proteins. The four Ab molecules were examined in their respective TFF processing buffers (initial buffer, 50/50 mixture of initial and formulation buffers, formulation buffer; see Tables 1 and 2) and in PBS buffer (Table 2). Molecule 2 was examined in two different formulation buffers (form 1 and form 2) and therefore in two 50/50 mixtures (50/50(1) and 50/50(2)). The structural attributes examined include overall secondary structure, tertiary structure, conformational stability, size and aggregation behavior, and reversible self-association. These were analyzed by a wide variety of analytical techniques (Table 3).

The four Ab molecules were examined in PBS buffer to better compare each of the molecules inherent properties to one another, prior to analyzing the structural attributes of each molecule in their respective TFF processing buffers. Both CD and FTIR spectroscopy were used to examine the overall secondary structure of the four Ab molecules (Figures 6 and 7, respectively). As expected, both techniques showed each of the four molecules to consist primarily of beta-sheets, in the case of CD with a λmin around 218nm (Table 4.) After the initial CD scan at 10ºC, a ramp to 90ºC was performed and the T_{onset} values were determined (Figure 4B). Molecule 2 showed the highest T_{onset} value at 60ºC, while molecule 9 had the lowest at ~55ºC (Table 4). Both intrinsic and extrinsic fluorescence spectroscopy were used to monitor tertiary structural changes. Intrinsic tryptophan fluorescence showed that molecule 2 had the lowest peak maximum at 328 nm and molecule 1 had the highest at 343 nm (Figure 8A). Molecule 1's higher peak position may be due to a surface exposed tryptophan that was also seen by CD. The samples were then ramped from 10 to 90ºC and the thermal data were analyzed using MSM Peak Intensity to determine the

T_{onset} values. Molecule 2 showed the highest T_{onset} at 63ºC, followed by molecule 1, and molecule 8 had the lowest T_{onset} value at 46ºC (Figure 8B). The data were also analyzed by MSM Peak Position and showed molecules 1 and 2 with comparable T_{onset} values at ~61ºC and molecule 8 with the lowest at 48ºC (Figure 8C). Next, ANS extrinsic fluorescence analysis was performed starting with a scan of each molecule at 10ºC (Figure 9A). A temperature ramp was performed from 10 to 90ºC (Figure 9B) and MSM Peak Intensity was used to determine the T_{onset} values of each molecule. This experiment showed molecule 2 with the highest T_{onset} value at 63ºC followed by molecule 1. Molecule 8 had the lowest T_{onset} value at 53ºC (Table 4).

UV-Visible spectroscopy showed that the protein concentration range of each of the molecules were sufficiently comparable for these experiments (Figure 10A) and the 2nd derivative of the spectrum was used to show comparable overall tertiary structures (Figure 10B). Differential scanning calorimetry (DSC) ca be used to determine the overall conformational stability of molecules and was used to determine T_{onset} values of the four molecules by performing a temperature ramp from 10 to 90 ºC (Figure 11). The T_{onset} values were selected since the DSC thermogram of each molecule displayed distinct profiles and it was thus difficult to compare T_m values. Again, molecule 2 had the highest T_{onset} value at 64ºC and molecule 9 had the lowest at 60ºC (Table 4). SLS was used to determine the aggregation propensities over the course of the temperature ramp during the intrinsic fluorescence scan (Figure 12). Molecule 2 had the highest T_{onset} by over 10ºC (T_{onset} = 71ºC) while molecule 8 had the lowest at 56ºC (Table 4). DLS was used to determine the particle size for each molecule (Figure 13). Molecule 9 had the highest particle size and molecule 1 had the lowest but overall they all were very similar.

In summary, the molecules were compared in PBS. Both CD and FTIR revealed the presence of primarily beta-sheet structure as expected for immunoglobulins. CD also revealed

molecule 2 to have the highest T_{onset} value. Molecule 1 showed a lower than expected T_{onset} value that was comparable to molecule 8. Intrinsic fluorescence showed molecule 2 to have the highest T_{onset} value by peak intensity followed by molecule 1 while molecule 8 had the lowest. For peak position, molecule 1 and 2 had comparable T_{onset} values which were higher than molecule 8 and 9. Extrinsic fluorescence showed molecule 2 manifesting the highest thermal stability with the highest T_{onset}. Molecule 1 had the second highest, followed closely by molecule 8 and 9. DSC and SLS showed the same trend as extrinsic fluorescence. These biophysical techniques showed some correlation with the TFF processes ("good" vs. "bad" molecules). Overall, molecule 2 ("good") had the highest thermal stability according to the higher T_{onset} values. Molecule 1 ("good") had a trend to either be the second highest stability or comparable to molecules 8 and 9 ("bad"). Molecule 8 had a trend to be either the least stable or comparable to molecule 9 and/or molecule 1.

5.3.3 Structural Integrity and Conformational Stability Properties of the Four Antibodies in TFF Processing Buffer

After the biophysical properties of the four Ab molecules were examined in PBS buffer, the same methods were repeated for each molecule in its corresponding TFF processing buffers including the initial buffer (buffer prior to TFF), 50/50 mixture (50% initial buffer and 50% formulation buffer), and formulation buffer (buffer following TFF)(see Table 2). Due to molecule 2 having two formulation buffers (form 1 and form 2), the 50/50 mix buffers were labeled 50/50(1) (50/50 mixture with form 1) and 50/50(2) (50/50 mixture with form 2). In terms of overall secondary structure, FTIR was performed to determine the secondary structure and the percentage of alpha-helix, b-sheet, and disorder structures was calculated (Figure 14). When comparing the FTIR spectrum, there was no notable change in the secondary structure between buffers for each of the four molecules (Supplementary figure S2).

Intrinsic tryptophan fluorescence spectroscopy was used to look at the overall tertiary structure of each molecule, first by an initial scan at 10ºC (Figure 15). Molecule 1 showed the 50/50 mix buffer to have lower λ_{max} than the initial and formulation (Figure 15A). Molecule 2 in the 50/50 mix (1), formulation 1 (form 1), and formulation 2 (form 2) showed similar λ_{max}, while in the initial and 50/50(2) this molecule had slightly higher λ_{max} values (Figure 15B, C). Molecule 8 and 9 in the 50/50 and formulation buffer had a lower λ_{max} but in the initial buffer these molecules had slightly higher λ_{max} values (Figures 15 D, E). These values were compiled and compared in Table 5 and Molecule 1 had the highest range of λ_{max} in all 3 buffers (~340-350 nm) compared to the other Ab molecules (~325-335 nm). A redshift (increase in wavelength) in the λ_{max} indicates an increase in polarity around buried tryptophan residues. Therefore if buried tryptophan residues become more exposed, the λ_{max} is higher. The opposite is true for a blueshift, as tryptophan residues become more buried in the protein, the λ_{max} will decrease. The changes seen between the different buffers can suggest how tightly the protein is folded and can alter the interaction available to produce aggregation. A temperature ramp was done from 10 to 90ºC and peak intensity vs temperature was used to determine the molecules T_{onset} values (Figure 16). Molecule 1 showed similar T_{onset} values in all 3 buffers with the initial buffer value trending to be slightly lower. Molecule 2 showed the initial buffer with the lowest and formulation 1 with the highest T_{onset} values. Molecule 8 showed that the formulation buffer greatly increased the T_{onset} compared to the initial and 50/50 mix buffer. Molecule 9 showed similar T_{onset} in all 3 buffers with the 50/50 mix buffer being slightly lower. These results were compiled in Table 5 and Molecule 2 had the highest and molecule 8 had the lowest T_{onset} values (Table 5). Peak position vs temperature was also examined to determine the T_{onset} values (Figure 17). Molecule 1, 8, and 9 had the highest T_{onset} in the formulation buffer. Molecule 2 showed the 50/50 mix buffer (1) and form 1 buffer to have an

increase in T_{onset} compared to the initial and 50/50(2), and the formulation 2 buffer had the lowest (Table 5).

Next, a scan at 10 ºC of extrinsic ANS fluorescence was examined (Figure 18). Molecule 1 and 8 had similar λ_{max} at ~500 nm. The majority of the buffer conditions for molecule 2 had a similar λ_{max} at ~500 nm with the exception of 50/50 mix buffer (1) having a lower λ_{max} at 494 nm. These results were compiled in Table 5 and Molecule 9 overall showed a slightly lower λ_{max} compared to the other three molecules (Table 5). A thermal scan from 10 to 90ºC was executed and the temperature dependent ANS peak intensity was plotted (Figure 19). Molecule 1 showed a lower T_{onset} in the formulation buffer than the initial and 50/50 mix buffer. Molecule 2 showed the highest T_{onset} in 50/50 mix buffer (1) and formulation 1 buffer. The 50/50(2) buffer showed the lowest T_{onset}. Molecule 8 showed the highest T_{onset} in the 50/50 mix buffer. Molecule 9 in the initial and 50/50 mix buffers were comparable, but in the formulation buffer had the lower T_{onset}. These results were compiled in Table 5 and Molecule 2 had the highest T_{onset} compared to the other three molecules (Table 5).

UV-Visible spectroscopy was used to determine the protein concentrations of all four antibodies and they were comparable in range (Figure 20). Using the UV-Visible spectrum, the 2nd derivative was determined to compare the tertiary structures of the four molecules. The overall tertiary structure of all four antibodies was comparable across all the TFF buffer systems evaluated for each the four Ab molecules (Figure 21). DSC was performed in the three different TFF process buffers for each molecule (Figure 22). In most cases, T_{onset} values remained unchanged across all three buffer systems. The T_{onset} value for Molecule 8 is higher in the final formulation. Molecule 1 had one major transition while all other molecules had at least 2 transitions reflecting the distinct domain structure of Igs (See Figure 22 and Table 5). SLS data was collected concurrently with

the intrinsic fluorescence spectrometry temperature ramp (Figure 23) and the T_{onset} of each molecule was determined. Molecule 1 and 8 showed higher T_{onset} values in the formulation buffer than the initial and 50/50 mix buffers. Molecule 2 in the formulation buffers were shown to have the highest and in the initial buffer to have the lowest T_{onset} values. Molecule 9 showed the 50/50 mix buffer to have the highest T_{onset}. These results were compiled in Table 5 and Molecule 2 had the highest T_{onset} out of all four molecules (Table 5). DLS was used to determine the particle size of each molecule in the different buffers (Figure 24). There was a trend that the 50/50 mix buffer showed larger hydrodynamic diameters and percent polydispersities. Overall, there was no significant change in diameter or polydispersity of the four molecules in different buffers.

In summary, many of the same trends were seen in the TFF processing buffers as PBS. FTIR revealed the majority were in a beta-sheet structure. Intrinsic florescence peak intensity and position showed molecule 2 with the highest T_{onset} value followed by molecule 1. Molecule 8 had the lowest T_{onset} value. Extrinsic florescence again showed molecule 2 with the highest T_{onset} values, molecule 1 and 9 were comparable and molecule 8 had the lowest. DSC showed very little change between the different buffer compositions for each molecule. Molecule 2 showed the highest T_{onset} values, followed by molecule 1 then 9 and molecule 8 had the lowest. SLS showed molecule 2 with a significantly higher T_{onset} values and molecule 1, 8, and 9 were comparable. Again, in the TFF processing buffer, the biophysical techniques showed some correlation with the TFF processes ("good" vs. "bad" molecules). Overall, molecule 2 ("good") had the highest thermal stability according to the higher T_{onset} values. Molecule 1 ("good") had a trend to either be the second highest stability or comparable to molecules 8 and 9 ("bad"). Molecule 8 had a trend to be either the least stable or comparable to molecule 9 and/or molecule 1.

5.3.4 Reversible Self-Association Properties of the Four Antibodies in PBS Buffer and in their Respective TFF Processing Buffer

A PEG solubility assay was used to determine the % PEG midpoint and apparent relative solubility values for each of the four Ab in PBS buffer and in their respective TFF processing buffers. In PBS, molecule 1 had the highest PEG midpoint and apparent solubility and molecule 8 had the lowest overall (Figures 25A and B). When looking at the % PEG midpoint values of the four molecules in the TFF processing buffers, a trend was seen that the formulation buffers resulted in the highest values, with the exception of molecule 8 where the formulation buffer had the lowest value (Figure 26). When looking at the apparent solubility values, a lot of variability was observed in the extrapolated data sets, making comparisons difficult across the different buffers and molecules (see Supplemental Figure S3). A summary of the % PEG midpoint and relative apparent solubility values for each of the four Ab molecules, and % PEG midpoint values in the TFF processing buffers, is shown in Table 6 (PBS) and Table 7 (TFF processing buffers).

k_{D2} values were determined by DLS analysis for each molecule in their respective 3 TFF process buffers along with PBS buffer to determine its potential for reversible self-association (Figure 27). In the initial buffers, the k_{D2} values were very low (<-0.03) indicating low reversible self-association (RSA) and high solubility. The same trend was observed in PBS buffers, with the exception of molecule 8 where the k_{D2} value was somewhat higher (~-0.05). In buffers containing sugars or sugar alcohols (all formulation buffers), the 1/Dm vs. protein concentration plots were not linear, preventing k_{D2} values from being determined by this method (see representative Mol. 2 inverse Dm plot). As a final evaluation of RSA, the viscosity of the four Ab solutions in their stock solutions was evaluated (Supplementary Figure S3). It was shown that low viscosity values (<2 cp) were observed at the protein concentrations of the stock solutions of 50 mg/mL for molecule 1, 2, and 9 and 18.3 mg/mL for molecule 8.

In summary, the midpoint solubility was highest in the formulation buffers with the exception of molecule 8. When comparing all four molecules in PBS, molecule 1 had the highest midpoint solubility. When examining the k_{D2} values, all four molecules had very low potential for self-association and the viscosities of the stock solutions were very low.

5.3.5 Colloidal Stability of the Four Antibody Molecules by Shaking and Stirring in PBS and their Respective TFF Processing Buffers

The colloidal stability of the four Ab molecules were compared through shaking and stirring agitation studies. Molecules were stressed by shaking at 300 rpm or stirring on a setting of 5 over the course of 8 hours with time points examined every hour. The four Ab molecules were compared in PBS buffer along with the molecules in their TFF processing buffers (initial, 50/50 mix, and formulation buffers). Due to molecule 2 having two formulation buffers (form 1 and form 2), the 50/50 mix buffers were labeled 50/50(1) (50/50 mixture with form 1) and 50/50(2) (50/50 mixture with form 2). In addition, the four Ab molecules were compared in all three TFF processing buffers with the addition of 0.01% PS80. The samples were evaluated by visual assessment for turbidity and visible particle formation, and then examined for protein concentration and subvisible particle concentration (see Tables 6 and 7 for experimental outline and analytical testing plan, respectively).

For visual assessment of Ab solutions in vials that underwent shaking and stirring, each of the four Ab molecules in PBS showed some level of visible aggregation over the 7 hrs of stirring, with molecule 2 only showing slight amounts at the last time point (Figure 28). Molecules 8 and 9 showed the most visible aggregation. When the molecules were under shaking stress, molecules 1, 8, and 9 showed visible aggregation over the course of 7 hrs. Molecule 2 did not show any visible aggregation until 3 days of shaking (Data not shown).

When molecule 1 was examined by visual assessment during the stirring agitation in the three process buffers without PS80, small amounts of visible aggregation was seen in all cases at the later time points of 5 hrs and increased to larger amounts by 8 hrs (Figure 29). When 0.01% PS80 was added into the solution, no visible aggregation could be seen up to the last time point of 8 hrs. Molecule 1 also showed visible aggregation in the three process buffers during shaking agitation starting at 3 hrs in the formulation buffer with large amounts seen at 8 hrs (Figure 30). Less amounts were seen in the initial and 50/50 mix buffers. When 0.01% PS80 was added into the solution, no visible aggregation could be seen up to the last time point of 8 hours.

When molecule 2 was examined by visual assessment during the stirring agitation in the three process buffers without PS80, small amounts of visible aggregation were seen in all cases at the time points of 4 hrs which increased to larger amounts by 8 hrs (Figure 31). Formulation 1 buffer contained the least amount of aggregation out of the 5 different compositions. When 0.01% PS80 was added into the solution, no visible aggregation could be seen up to the last time point of 8 hrs. Molecule 2 showed very little visible aggregation in the process buffers. In the initial and formulation 1 buffer, there was no sign of visible aggregation present. In the 50/50(1) buffer, only a small amount was seen at 8 hrs. In the 50/50(2) and formulation 2 buffer, visible aggregation was seen at 6 and 5 hrs, respectively (Figure 32). When 0.01% PS80 was added into the solution, no visible aggregation could be seen up to the last time point of 8 hrs.

When molecule 8 was examined by visual assessment during the stirring agitation in the three TFF process buffers without PS80, small amounts of visible aggregation were seen in all cases at the later time points of 5 hrs which increased to larger amounts by 8 hrs (Figure 33). When 0.01% PS80 was added into the solution, no visible aggregation could be seen up to the last time point of 8 hrs. Molecule 8 also showed visible aggregation in the three TFF process buffers during

shaking agitation and in greater abundance than seen in stirring (Figure 34). The initial buffer showed visible aggregation after the first hour of shaking and the 50/50 mix and formulation buffer showed similar amounts after 2 hrs, with large amounts forming after a few hours. When 0.01% PS80 was added into the solution, no visible aggregation could be seen up to the last time point of 8 hrs.

When molecule 9 was examined by visual assessment during the stirring agitation in the three TFF processes buffers without PS80, a small amount of visible aggregation was seen in all cases (Figure 35). Both the initial and formulation buffer showed visible aggregation after 2 hrs and the 50/50 mix after 4 hrs. Large amounts were seen after just 4 hrs in all process buffers. When 0.01% PS80 was added into the solution, the visible aggregation was significantly decreased greatly but Abs in all three TFF process buffers still showed small amounts of aggregation after 4 hrs. Molecule 9 showed very little visible aggregation in the three process buffers during shaking agitation (Figure 36). Only small amounts were seen in the 50/50 mix (5 hrs) and formulation buffer (8 hrs). When 0.01% PS80 was added into the solution, no visible aggregation was observed up to the last time point at 8 hrs.

The protein concentration of each Ab sample in PBS was tested by UV visible spectroscopy using the Nanodrop instrument due to volume constraints. A representative absorbance spectrum of molecule 2 in PBS shows no change from the starting material (T=0) to 7 hrs of shaking at 300 rpm (Figure 37A). Figure 37B shows molecule 8 in PBS to represent the absorbance decrease when the protein concentration decreases due to aggregation from the stress of shaking from T=0 7 hrs. When looking at the concentration of the molecules in PBS, molecules 1 and 2 remained stable during the stirring stress over the course of 7 hrs (Figure 38A). Molecule 8 showed a decrease in concentration at 7 hrs (~25% loss) while molecule 9 showed a slight downward trend

in concentration compared to the other molecules. When shaking the molecules in PBS buffer, the concentration of molecules 1, 2, and 9 remained relatively stable after 7 hrs of shaking at 300 rpm while molecule 8 showed a significant decrease over time (Figure 38B).

Next, the protein concentration of each of the four Ab molecule was examined in their respective TFF process buffers (both with and without PS80 addition) over the time course of 8 hrs of stirring (Figure 39). Molecule 1 remained stable in all three buffers conditions (Figure 39A) and with PS80 added (Figure 39B). Molecule 2 had a trend showing a slight decrease in the different buffer compositions but the two formulation buffers were the most stable overall (Figure 39C). When PS80 was added to the molecule 2 buffers, there was no loss in concentration observed with any of the buffer compositions with the exception of the initial buffer (Figure 39D). Molecule 8 formulation buffer showed the biggest decrease in concentration over time compared to the initial and 50/50 mix buffer, which showed little decrease in concentration (Figure 39E). When PS80 was added to molecule 8 buffers, the initial buffer showed the largest decrease in concentration, and the 50/50 and formulation buffers showed no decrease in concentration with time (Figure 39 F). Molecule 9 had a large loss of protein concentration over the course of 8 hrs in all three of the TFF process buffers (~10-20%), with the initial buffer showing the most loss and the formulationthe least (Figure 39G). When PS80 was added to the buffers, the 50/50 and formulation buffer showed little to no loss in the protein concentration while the initial buffer showed less loss compared to the solution without PS80 (Figure 39H).

The protein concentration of each of the four Ab molecule was examined in their respective TFF process buffers (both with and without PS80 addition) over the time course of 8 hrs of shaking (Figure 40). Molecule 1 in the TFF processing buffers showed a steady decrease in concentration over the course of 8 hrs in all three buffers (Figure 40A). When PS80 was added to the buffers,

the concentration did not show a decrease over the 8 hrs of shaking (Figure 40B). Molecule 2 was the most stable in the formulation 1 buffer and the least stable in the formulation 2 buffer (Figure40C). The 50/50(1) buffer was relatively stable throughout the stress while the concentration in the 50/50(2) buffer decreased over time. PS80 was able to minimize this effect and the concentration at all timepoints remained stable compared to the starting material (Figure 40D). Molecule 8 was the most unstable molecule, showing the highest amount of protein loss during the shaking agitation (Figure 40E). All three of the TFF processing buffers showed a large decrease over time with the initial buffer having the greatest loss. When PS80 was added into the buffers, the concentration of molecule 8 remained constant over the 8 hr stress (Figure 40F). Molecule 9 showed little loss of protein during the shaking agitation in all of the TFF processing buffers (Figure 40G). When PS80 was added into the solution, no protein loss was observed (Figure 40H)

To better understand the visible aggregation and protein concentration results for each of the four Abs in their respective TFF buffers, the subvisible particle concentration was determined at each timepoint during stirring agitation for each molecule in each TFF process buffer using MFI. Under stirring conditions, Molecule 1 showed the most increase in subvisible particle levels in the initial buffer followed by the 50/50 mix buffer and the least amount in the formulation buffer (Figure 41A). When 0.01% PS80 was added to the solution, very little increase in subvisible particle concentration was observed for the Molecule 1 in the initial and formulation buffer, although an increase was seen in the 50/50 mix buffer (Figure 41B). Molecule 2 showed a large increase in subvisible particle concentration in the initial, 50/50 mix (2) and formulation 2 (Figure 41C). There was a slight increase in subvisible particle levels for Molecule 2 in the 50/50 mix (2) buffer and very little increase in the formulation 1 buffer. When PS80 was added to the solution,

all the samples were stabilized. Formulation 1 and 2 showed the least amount of particles compared to the initial and 50/50 mix buffers. (Figure 41D). Molecule 8 showed an increase in subvisible particle levels in all of the TFF buffers with the formulation buffer having the highest amount (Figure 41E). When 0.01% PS80 was added to the solution, Molecule 8 in the initial buffer showed very little increase in subvisible particles, while in the 50/50 and formulation buffers, Molecule 8 showed a large increase in subvisible particles (Figure 41F). Molecule 9 showed an increase in subvisble particle concentration for all TFF buffers (Figure 41G) and the same trend after adding PS80 (Figure 41H).

Similar experiments were then performed under shaking conditions. Molecule 1 showed an increase in subvisible particle concentration in the initial and 50/50 mix but very little in the formulation buffer (Figure 42A). When 0.01% PS80 was added, the initial buffers particle concentration dropped greatly, and the formulation showed little increase in concentration but the 50/50 mix buffer still showed an increase (Figure 42B). Molecule 2 showed very large increase in 50/50 mix (2) and formulation 2 buffer, and only a slight increase in initial, 50/50(1), and formulation 1 (Figure 42C). When 0.01% PS80 was added, a significant decrease in all the buffers was seen with little to no increase in particle number (Figure 42D). Molecule 8 showed a comparable increase in particle concentrations in all three buffers (Figure 42E). The PS80 decreased the amount and increased the time it took for the stress to have an effect, but eventually the particle concentration started to increase (Figure 42F). Molecule 9 showed an increase in all three buffers with the initial buffer having the least amount and the formulation having the most (Figure 42G). After adding PS80, the particle concentration decreased greatly and no significant increase was observed compared to time 0 hr (Figure 42H).

In summary, when examining the molecules in PBS, molecules 1, 8, and 9 showed some visible aggregation after shaking and stirring with molecule 8 showing the most after shaking and molecule 9 showing the most after stirring. Molecule 2 showed no signs of visible aggregation during shaking up to 3 days and only a slight amount after stirring for 8 hrs. Molecule 8 had the largest loss in protein concentration after preforming the shaking agitation. Molecule 9 showed protein concentration loss after stirring. Molecules 1 and 2 showed no significant protein concentration loss after shaking or stirring. When examining all four molecules in the TFF processing buffers, the same trends were observed as those seen in PBS. Molecule 2 showed the lowest amount of visible aggregation by shaking and stirring. Molecule 8 showed the largest amount of visible aggregation after shaking and molecule 9 showed the most after stirring. The addition of 0.01% PS80 greatly reduced the amount of visible aggregation which was only seen after the stirring of molecule 9 and 8 hrs of stirring molecule 1 in the 50/50 mix buffer. The protein concentration after stirring produced a gradual decrease with molecule 9 and a slight decrease in molecule 8 formulation buffer. When PS80 was added, there was no significant change observed in the protein concentration. Under the shaking conditions, molecule 8 showed a large decrease in protein concentration. A slight decrease in molecule 1 was also observed. When PS80 was added, there was no decrease inprotein concentration observed. MFI showed an increase in subvisible particle formation after shaking and stirring with few exceptions. The addition of 0.01% PS80 was able to greatly reduce this effect.

The shaking and stirring showed some correlation with the TFF processes (“good” vs. “bad” molecules). Overall, molecule 2 (“good”) had the highest colloidal stability according to lower visible aggregation, subvisible particle formation, and less protein concentration loss compared to the other 3 molecules. Molecule 1 (“good”) had a trend toward either the second

highest stability or comparable to molecules 8 and 9 (“bad”). Molecule 8 had a trend toward be either the least stable (shaking) or comparable to molecule 1 (stirring). Molecule 9 was unstable under the stirring conditions but was comparable to molecule 1 under shaking conditions.

5.3.6 Interfacial Properties of the Four Antibody Molecules as Measured by a Langmuir Trough

A Langmuir trough was used to compare interfacial properties of the four Ab molecules. First, the system was allowed to reach an equilibrium between molecules exposed to the interface and those that remained in the bulk fluid. The surface pressure during this absorption phase was recorded over the course of 120 mins. Figure 43 shows representative graphs of molecules 2 and 8 in their formulation buffers during the absorption phase. Higher surface pressures correlate with higher concentrations of molecules at the interface. Molecule 8 appears to have a higher concentration of molecules present at the interface compared to molecule 2 as reflected by the higher surface pressure observed. Depending on the kinetics, saturation of the molecules at the interface can be very different as well. Molecule 2 reaches saturation after ~60 min while molecule 8 is still increasing after 120 min. This may indicate restructuring or rearrangement of the molecules after they reach the interface. The molecules were first compared in PBS. Molecule 8 had a significantly higher absorption curve at ~17 mN/m (Figure 44). Molecule 1 and 9 produced the same surface pressure of ~13 mN/m while molecule 2 had the lowest at ~11 mN/m. Although molecule 1 and 9 had the same surface pressure at 120 min, molecule 9 had faster adsorption kinetics. When comparing the molecules in the different process buffers, molecules 1 and 2 have lower surface pressure in the formulation compared to the initial and 50/50 mix buffers indicating lower amount of protein at the interface (Figure 45A-C). Molecules 8 and 9 show about the same or greater amounts of surface pressure in their formulation buffers (Figure 45D-E). Overall, molecules 8 and 9 have higher surface pressures than 1 and 2. PS80 was added to each of the TFF

processing buffers and the absorption curves were graphed (Figure 46). Overall, the surface pressure of each were increased greatly (>30 mN/m). This is presumably due to the PS80 creating a layer at the interface.

After the absorption phase was complete, the liquid at the interface was compressed and expanded. The area change vs surface pressure was monitored and the area between the two curves was observed. The area between the 2 curves (the hysteresis) is an indication of inter-molecular interactions. Therefore, the larger the hysteresis, the greater possibility that inter-molecular interactions exist. The more inter-molecular interactions occurring, the greater the tendency to aggregate is presumed. Figure 47 shows representative isotherms of molecule 2 and 9. The hysteresis observed for molecule 9 was larger than that of molecule 2, indicating that it is more likely to display inter-molecular interactions. The area was plotted at the 1^{st}, 2^{nd}, and last cycle (cycle 750) and the area lost over time was monitored. The four molecules in PBS showed molecule 8 and 9 with the highest hysteresis indicating these two are more likely to be seen at the interface and manifest inter-molecular interactions (Figure 48). Molecule 2 showed the lowest hysteresis at all cycles. Next, the molecules were examined in the TFF processing buffers (Figure 49). Molecule 2 showed the lowest hysteresis at cycle 1, indicating it's less likely to go to the interface. Molecule 9 showed the highest hysteresis, indicating it is likely to bind to the interface and possess inter-molecular interactions. Molecules 1 and 8 also show large amounts of hysteresis at cycle 1. PS80 was added to each of the processing buffers and examined (Figure 50). All 4 molecules had similar starting surface pressures around 650 mN/m which over the 750 cycles decreased to about 300 mN/m. This suggests that the PS80 bound strongly at the air-water interface thereby decreasing the ability of the Ab to localize to the surface.

The percent of area loss was also examined to compare across the molecules, first in PBS (Figure 51). Molecule 1 showed the least amount of loss followed by molecule 8. This reflects the Ab's ability to remain at the interface. When examining the molecules in the TFF processing buffer, molecule 8 shows the lowest amount of area loss of the 750 cycles, indicating increased stability at the interface and less loss after material to the bulk (Figure 52D). Molecule 2 shows the most area lost after 750 cycles, indicating it's more likely to move into the bulk than stay at the interface (Figure 52E). When PS80 was added to the buffers, each molecule was similar with a decrease of about 60% the starting surface pressure after 750 cycles (Figure 53).

MFI was used to examine the subvisible particle concentration after the Ab samples were stressed by 750 cycles in the Langmuir trough. In PBS buffer, molecules 8 and 9 showed high particle concentration in the starting material that remained constant after the expansion and compression runs were completed (Figure 54). In contrast, Molecule 1 and 2 had much lower subvisible particle levels in the starting material but showed an increase after the expansion and compression cycles. For all four Ab molecules, the interface showed the highest subvisible particle counts and the bulk solution the lowest. The Ab molecules were then compared across their respective TFF process buffers. Molecules 1, 2, and 9 all showed a slight increase in subvisible particle concentration but molecule 8 did not show an increase (Figure 55). The samples were examined for visible aggregates, however, molecule 8 showed a large amount of visible particulates. While molecules 1 and 9 showed a small amount of visible particles in the initial and 50/50 mix buffers, none were present in the formulation buffer. Molecule 2 showed no signs of visible aggregation. After PS80 was added to each of the TFF processing buffers and the compression and expansion cycles were performed on each of the four Ab molecules, the subvisible particle concentration did not increase as drastically as they did without the PS80

(Figure 56). Molecule 1 showed no significant increase in subvisible particle concentration in any of the phases (bulk, interface or remaining) in the three TFF buffer conditions (Figure 56A). Molecule 2 showed a slight increase in subvisible particles in the initial buffer as well as 50/50(2) and formulation 2, while 50/50(1) and formulation 1 buffer showed little increase in the subvisible particle concentration (Figure 56B-C). Molecule 8 did not show any increase in all three buffers (Figure 56D). Molecule 9 showed a slight increase in the 50/50 mix buffer but there was no increase in the initial and formulation buffer (Figure 56E). All samples with PS80 present in the solution did not show any signs of visible aggregation.

In summary, molecule 2 showed the lowest tendency to be at the air-water interface followed by molecule 1 and 9. Molecule 8 showed a significantly larger surface pressure than the other 3 molecules in PBS, indicating it is the most likely to be at the interface. When looking at the changes of area under the curve, molecule 1 shows the highest percentage remaining at the interface after 750 cycles, while molecule 9 shows the least. When the molecules were examined in the TFF processing buffers, molecule 8 showed the highest tendency to be at the air-water interface and the most visible aggregation. Molecule 2 showed the lowest tendency to be at the air-water interface. There was in increase in sub-visible particles with molecules 1, 2, and 9. When 0.01% PS80 was added to the samples, the surface pressure greatly increased during the absorption phase and were relatively similar across the four molecules and their buffers, indicating the PS80 has the tendency to go to the air-water interface and decrease the binding of the Abs through a competitive effect. After running the compression and expansion cycles, all molecules showed similar decreases in the area under the curve. The Langmuir trough showed good correlation with the TFF processes (“good” vs. “bad” molecules). Overall, molecule 2 (“good”) had the lowest tendency to go to at the air-water interface. Molecule 8 (“bad”) had a

tendency to bind to the air-water interface and remain there through compression and expansion. Molecule 9 (“bad”) had a tendency to be at the air-water interface when at equilibrium, but during the compression and expansion was seen to significantly decrease its interaction.

Table 5.1: Summary of molecules examined in this study and their behavior in large scale TFF. Molecules 1 and 2 were designated as "good" molecules (highlighted in green) that behaved well during large scale TFF. Molecules 8 and 9 were designated as "bad" molecules (highlighted in red) because of their tendency to generate aggregates and particles during large scale TFF. The initial buffers are the buffers used before the TFF process and the formulation buffers are those the molecules are exchanged into during the TFF process.

Molecule Number	Protein type (IgG/fusion, etc)	pI	Existing Stability Data/Comments	Key issues	Initial Buffer	Formulation Buffer	Formulation Buffer 2
1	IgG4 ~ 150kDa	7.7			75 mM Sodium Phosphate pH 6.2	20mM His, 8.9% Sucrose, pH 6.0	
2	IgG1 ~ 150kDa	9.1	No known particle formation seen in platform buffer system. Other buffer systems did show some turbidity upon TFF	Change in buffer type did lead to formation of particles	20mM Sodium Phosphate, 50mM NaCl pH 7.2	20mM His, 8.9% Sucrose, pH 6.0	20mM Sodium Phosphate, 50mM NaCl, 3% Mannitol, 20uM DTPA pH 6.0
8	IgG4 ~150kDa	7.1	Did generate particles during TFF Type of surfactant played a role in reducing particles during filling and upon storage	Change in buffer type did show changes in particle formation during processing	225mM Arginine, 40mM Acetate pH 4.9	20mM His, 8.5% Sucrose, pH 5.5	
9	BiAb with IgG4 constant region ~200kDa	ND	Increase in turbidity and particle formation after TFF. Change in pump helped solve the issue		50mM Tris pH 7.2	20mM His, 90mM Arg, 4% Sucrose, pH 5.6	

Table 5.2: Composition of sample buffers used in biophysical characterization of the four Abs. For each molecule, biophysical experiments were carried out in the initial buffer, formulation buffer, and a mixture of 50% initial and 50% formulation (50/50) buffers.

Molecule	Initial Buffer	50/50	Formulation Buffer
Mol 1 (IgG4)	75 mM $NaPO_4$, pH 6.2	37.5 mM $NaPO_4$, 10 mM His, 4.45% Sucrose pH 6.1	20 mM His, 8.9% Sucrose pH 6.0
Mol 2 (IgG1)	20 mM $NaPO_4$, 50 mM NaCl, pH 7.2	**50/50(1):** 10 mM $NaPO_4$, 25 mM NaCl, 10 mM His, 4.45% Sucrose pH 6.6	**Form 1:** 20 mM His, 8.9% Sucrose pH 6.0
	20 mM $NaPO_4$, 50 mM NaCl, pH 7.2	**50/50(2):** 10 mM $NaPO_4$, 50 mM NaCl, 10mM sodium citrate, 1.5% mannitol, 10uM DTPA pH 6.6	**Form 2:** 20mM sodium citrate, 50mM NaCl, 3% mannitol, 20uM DTPA, pH 6.0
Mol 8 (IgG4)	225 mM Arg, 40 mM Acetate, pH 4.9	112.5 mM Arg, 20 mM Acetate, 10 mM His, 4.25% Sucrose pH 5.2	20 mM His, 8.5% Sucrose, pH 5.5
Mol 9 (BiAb, IgG4 constant region)	50 mM Tris, pH 7.5	25 mM Tris, 10 mM His, 45 mM Arg, 2% Sucrose, pH 6.5	20 mM His, 90 mM Arg, 4% Sucrose, pH 5.6

Table 5.3: Biophysical techniques used to characterize the four Abs grouped by the type of structural changes monitored using each analytical technique.

Type of Structural Change	Analytical Technique
Secondary structure	Far UV Circular Dichroism
	Fourier Transform Infrared Spectroscopy
Tertiary structure	Intrinsic Fluorescence Spectroscopy
	Extrinsic Fluorescence Spectroscopy
	Second Derivative UV Spectroscopy
Overall conformational stability	Differential Scanning Calorimetry (DSC)
Size and Aggregation Behavior	UV-Visible Spectroscopy (+/- Light Scattering correction, +/- Centrifugation)
	Static Light Scattering
	Dynamic Light Scattering (DLS)
Reversible self-association	Viscosity
	PEG Solubility Assay

Table 5.4: Summary of biophysical study results with the four Ab molecules in PBS buffer. Data shown include each molecule's λ_{min} at 10°C and T_{onset} values as measured by CD, λ_{max} at 10°C and T_{onset} values for peak intensity and peak position as measured by intrinsic fluorescence, λ_{max} at 10°C and T_{onset} values for peak intensity as measured by extrinsic fluorescence, T_{onset} values from DSC, and T_{onset} values from SLS. . Errors denote standard deviation for n=3 replicates.

PBS	CD		Intrinsic Fluorescence			Extrinsic Fluorescence		DSC	SLS
	λ_{min} (nm)	T_{onset} (°C)	λ_{max} (nm)	T_{onset} (°C)	Tonset (°C)	λ_{max} (nm)	T_{onset} (°C)	T_{onset} (°C)	T_{onset} (°C)
Molecule 1	217.0 ± 0.0	58.3 ± 0.7	343.0 ± 0.6	56.5 ± 0.5	61.1 ± 0.1	515.2 ± 2.9	57.1 ± 0.2	62.5 ± 1.5	60.8 ± 0.2
Molecule 2	218.1 ± 0.0	69.0± 1.6	327.7 ± 0.6	62.7 ± 0.5	60.3 ± 0.6	515.7 ± 2.9	63.3 ± 0.7	64.4 ± 0.4	71.1 ± 0.2
Molecule 8	217.4 ± 0.5	58.8± 0.4	329.3 ± 0.6	45.7 ± 0.5	48.3 ± 0.9	520.0 ± 0.0	55.3 ± 0.3	61.9 ± 0.1	55.8 ± 0.4
Molecule 9	219.2 ± 0.2	54.7 ± 3.5	335.3 ± 0.6	52.8 ± 0.2	55.8 ± 0.2	504.0 ± 1.7	53.5 ± 0.6	60.0 ± 1.0	56.9 ± 0.1

Table 5.5: Summary of biophysical data results with four Ab molecules examined in the different TFF buffer compositions (Initial, 50/50, and formulation buffers; See Table 2).

Data shown include each molecule's λ_{min} at 10°C and T_{onset} values as measured by CD, λ_{max} at 10°C and T_{onset} values for peak intensity and peak position as measured by intrinsic fluorescence, λ_{max} t 10°C and T_{onset} values for peak intensity as measured by extrinsic fluorescence, T_{onset} values as measured by DSC, and T_{onset} values as measured by SLS. Errors denote standard deviation for n=3 replicates.

Molecule 1	**Intrinsic Fluorescence**			**Extrinsic Fluorescence**		**DSC**	**SLS**
	λ_{max} (nm)	**T_{onset} (°C)**	**Tonset (°C)**	**λ_{max} (nm)**	**T_{onset} (°C)**	**T_{onset} (°C)**	**T_{onset} (°C)**
Initial	350.0±1.0	62.2±0.1	61.4±0.1	499.7±0.6	58.7±0.2	61.7±0.2	62.4±0.3
50/50	340.3±0.6	63.9±0.2	61.6±0.7	499.3±1.2	59.0±0.8	62.1±0.0	62.1±0.3
Formulation	349.0±0.0	63.6±0.3	63.3±0.3	498.7±0.6	46.1±0.2	60.7±0.1	63.9±0.7

Molecule 2	**Intrinsic Fluorescence**			**Extrinsic Fluorescence**		**DSC**	**SLS**
	λ_{max} (nm)	**T_{onset} (°C)**	**Tonset (°C)**	**λ_{max} (nm)**	**T_{onset} (°C)**	**T_{onset} (°C)**	**T_{onset} (°C)**
Initial	334.7±0.6	73.7±0.3	64.3±0.5	499.3±0.6	63.8±0.4	63.6±0.2	72.4±0.7
50/50 (1)	327.3±0.6	75.3±0.3	66.4±0.1	494.0±1.4	68.1±0.2	64.0±0.4	74.5±0.7
50/50 (2)	335.3±0.6	74.3±0.6	64.4±0.7	500.0±0.0	56.0±0.6	63.8±0.3	74.8±0.1
Formulation 1	327.7±0.6	78.6±0.4	65.3±0.3	499.3±0.6	68.8±0.6	64.2±0.9	76.7±0.2
Formulation 2	326.7±0.6	75.4±0.1	62.9±0.1	500.0±0.0	67.3±0.6	62.4±0.1	76.2±0.2

Molecule 8	**Intrinsic Fluorescence**			**Extrinsic Fluorescence**		**DSC**	**SLS**
	λ_{max} (nm)	**T_{onset} (°C)**	**Tonset (°C)**	**λ_{max} (nm)**	**T_{onset} (°C)**	**T_{onset} (°C)**	**T_{onset} (°C)**
Initial	338.0±0.0	53.0±0.3	46.2±0.1	498.3±2.1	43.8±0.5	47.7±0.5	60.4±0.4
50/50	331.3±0.6	53.8±0.7	49.4±0.2	499.7±0.6	55.1±0.3	51.6±0.1	62.2±0.3
Formulation	332.0±0.0	59.0±0.9	55.8±0.8	498.5±0.7	52.6±0.3	55.6±0.3	66.6±0.5

Molecule 9	**Intrinsic Fluorescence**			**Extrinsic Fluorescence**		**DSC**	**SLS**
	λ_{max} (nm)	**T_{onset} (°C)**	**Tonset (°C)**	**λ_{max} (nm)**	**T_{onset} (°C)**	**T_{onset} (°C)**	**T_{onset} (°C)**
Initial	335.7±0.6	59.6±0.1	57.3±0.2	495.3±2.1	58.7±0.3	59.6±0.3	60.8±0.1
50/50	327.3±0.6	58.0±0.7	54.2±0.2	493.7±1.2	58.7±0.2	58.6±0.1	63.4±0.3
Formulation	326.7±0.6	59.3±0.3	61.5±0.1	497.7±1.5	55.8±0.4	55.8±0.1	59.0±0.2

Table 5.6: Summary of PEG solubility assay results for all four molecules in PBS.

The midpoint and the extrapolated apparent solubility were calculated. Errors denote standard deviations for n=3 replicates.

PBS	Midpoint	Extrapolated Apparent solubility (mg/mL)
Molecule 1 (IgG4)	13.0 ± 0.1	>1000
Molecule 2 (IgG1)	10.8 ± 0.05	479
Molecule 8 (IgG4)	8.8 ± 0.05	20
Molecule 9 (BiAb)	12.0 ± 0.08	136

Table 5.7: Summary of PEG solubility assay results for all four molecules in TFF processing buffers.

The midpoint and the extrapolated apparent solubility were calculated. Errors denote standard deviations for n=3 replicates.

Molecule	Buffer	Midpoint	Extrapolated Apparent solubility (mg/mL)
Molecule 1	Initial	13.5±0.2	18.6
	50/50	12.5± 0.1	111.4
	Formulation	14.1 ± 0.05	21.7
Molecule 2	Initial	12.5 ± 0.1	222.2
	50/50 (1)	13.2 ± 0.1	13.1
	50/50 (2)	14.2±0.1	3.8
	Formulation 1	35.6 ± 0.1	15.4
	Formulation 2	15.4 ± 0.0	0.7
Molecule 8	Initial	12.4 ± 0.2	36.4
	50/50	12.5 ± 0.3	473.6
	Formulation	11.8 ± 0.05	>1000
Molecule 9	Initial	10.1 ± 0.1	768.0
	50/50	12.4 ± 0.2	1.1
	Formulation	14.8 ± 0.1	4.8

Table 5.8: Agitation stress experimental outline.

There were two agitation types, i.e., shaking and stirring, used to stress Ab molecules 1, 2, 8, and 9 at a concentration of 1 mg/mL. The agitation was done in four different TFF processing buffers (see Table 2) with and without 0.01% PS80. The shaking stress was performed at a speed of 300 rpm and the stirring stress was performed at setting 5.

Agitation type	Proteins included in study	Processing Buffers	Protein concentration	Time-points	Agitation parameter
Shaking	Molecules 1, 2, 8, and 9	Initial ± PS80 50/50 ± PS80 Formulation ± PS80 and PBS	1 mg/ml	0-8 hrs	300 RPM
Stirring					Setting 5

Table 5.9: Analytical techniques used to examine Ab samples generated before and after shaking and stirring agitation.

The protein concentration was monitored by UV-Visible spectroscopy. The size and characterization of aggregates were monitored by visual assessment and MFI.

Structural attribute	**Analytical techniques for shaking and stirring samples**
Protein Concentration, covalent oligomers/aggregates	UV-Visible Spectroscopy (+/- light scattering, +/- centrifugation)
Characterization of Size and Presence of Aggregates	Visual Assessment
	MFI

Table 5.10: Langmuir trough study outline. Molecules 1, 2, 8, and 9 were examined at 2 mg/mL in the TFF processing buffers (see Table 2) with and without PS80 as well as in PBS buffer. The compression and expansion was done at a rate of 150 mm/min for 6 hrs. Samples were taken from the bulk fluid, the interface, and from the remaining mixture.

Proteins included in study	Buffer	Protein concentration	Time	Compression/ Expansion Rate	Sample to be tested
Molecules 1, 2, 8, & 9	Initial ± PS80 50/50 ± PS80 Formulation± PS80 PBS	2 mg/ml	6 hrs	150 mm/min	Bulk Fluid "Interface" Mixture

Table 5.11: Analytical techniques used to examine Ab samples generated by Langmuir trough studies. Protein concentration was examined using UV-Visible spectroscopy. Characterization of particle size and the presence of visible aggregates were examined using visual assessment and MFI. The interfacial properties were examined by the Langmuir trough generated data.

Structural attribute	**Analytical techniques**
Protein Concentration, covalent oligomers/aggregates	UV-Visible Spectroscopy (+/- light scattering, +/- centrifugation)
Characterization of Size and Presence of Aggregates	Visual Assessment
	MFI
Interfacial Properties	Langmuir Trough

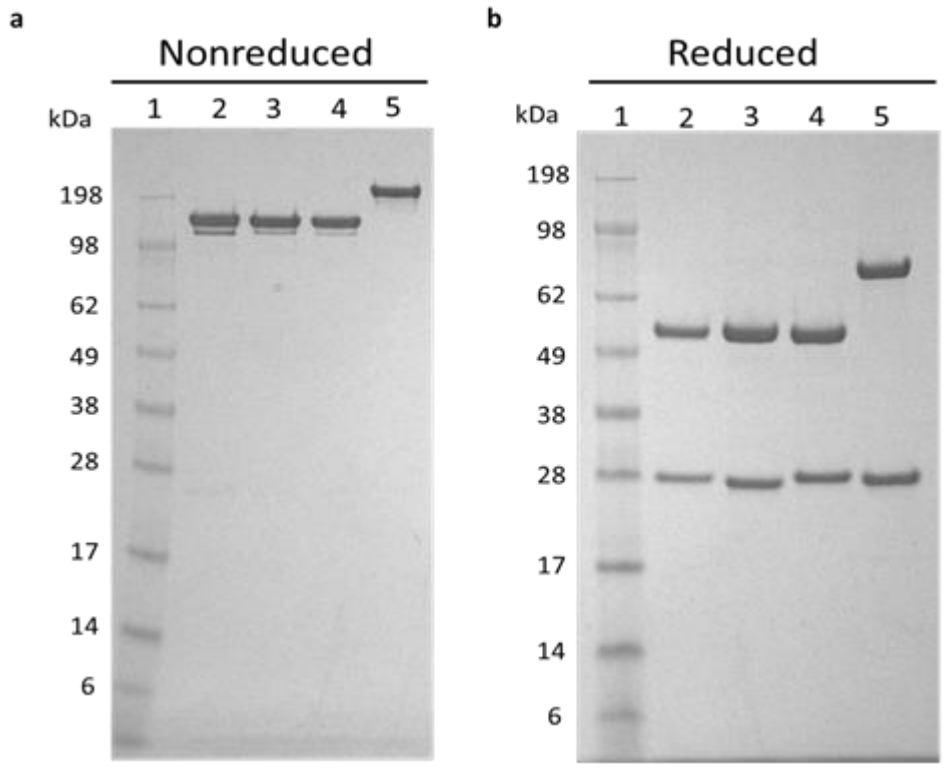

Figure 5.1: Representative SDS-PAGE of molecules 1, 2, 8, and 9.

Ten μg of each sample was separated on a 10-20% Tris-glycine gel using NuPAGE MES SDS Running Buffer. The gel was stained using Bio-safe Coomassie Blue G250 stain. Lane 1: SeeBlue Plus2 Pre-stained molecular weight standard; Lane 2: molecule 1; Lane 3: molecule 2; Lane 4: molecule 8; and Lane 5: molecule 9. Panel a represents nonreduced conditions. Panel b represents reduced conditions.

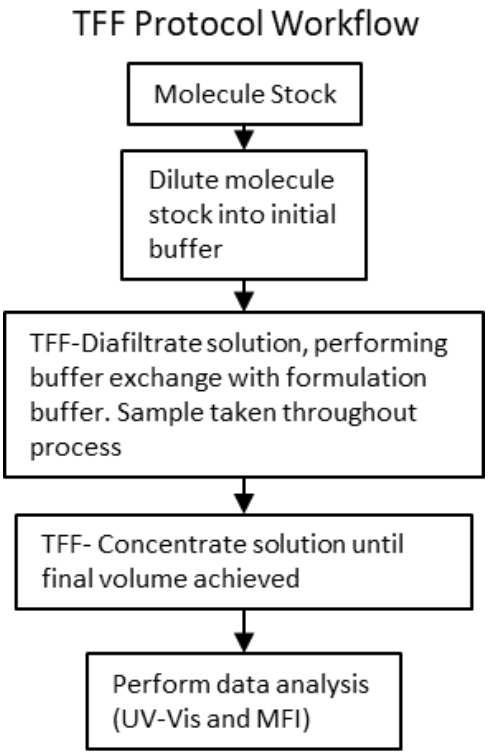

Figure 5.2: Laboratory scale TFF protocol workflow.

The stock solution of the Ab molecules is diluted to 2 mg/mL in the initial buffer. The TFF is performed and the buffer is exchanged into the formulation buffer followed by removal of buffer to reach the desired concentration. Samples are taken throughout the process and analyzed by UV-Visible spectroscopy and MFI.

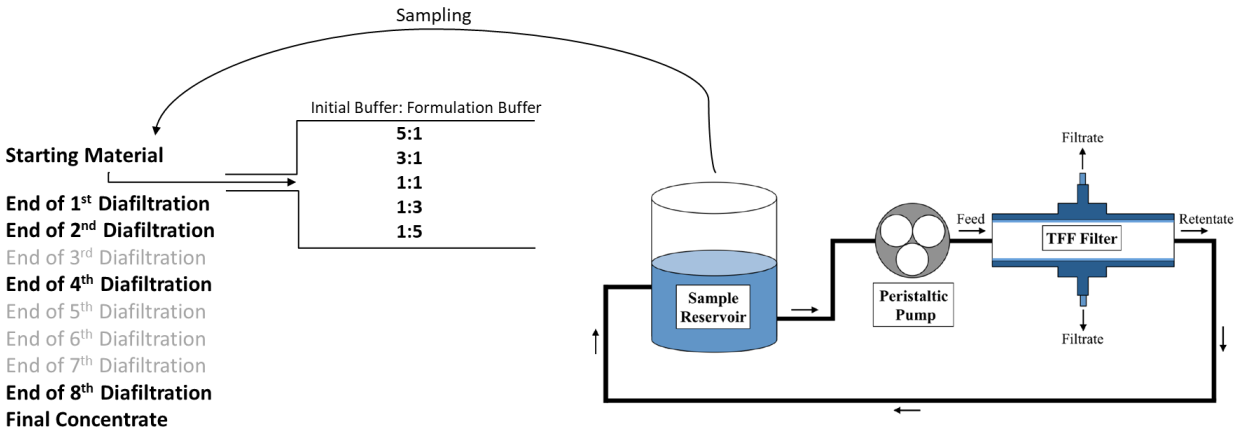

Figure 5.3: Laboratory scale TFF scheme.

One hundred mL of molecules at 2 mg/mL is placed into the sample reservoir. The sample is fed into the TFF filter by a peristaltic pump. The sample with the protein is retained and travels back to the reservoir while smaller molecular weight materials are removed in the filtrate based on the MWCO of the filter. Samples taken throughout the processes are bolded. These include the starting material, final concentrate, samples with buffer ratios (initial:formulation) of 5:1, 3:1, 1:1, 1:3, and 1:5, and samples after completing the 1st, 2nd, 4th, and 8th diafiltration step.

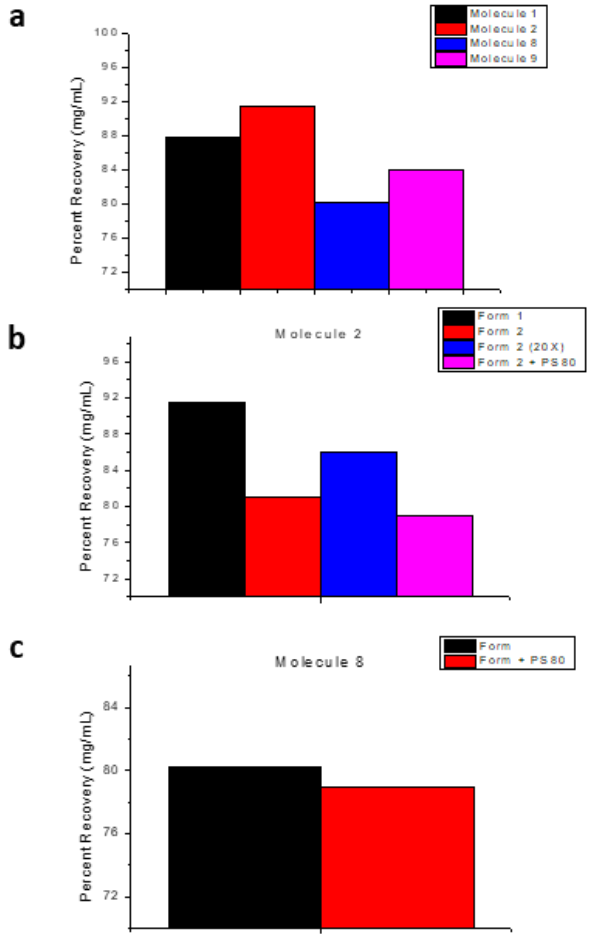

Figure 5.4: TFF protein recovery.

Panel a is the protein recovered of all four Ab molecules ran under standard conditions described in the methods section. Panel b shows the protein recovery for molecule 2 with four different conditions, formulation 1 (black); formulation 2 (red); 20-fold concentration step (blue); and formulation 2 with 0.01% PS80 (pink). Panel c shows the protein recovery of molecule 8 with and without PS80 (black) and with PS80 (red) in formulation buffer. N=1. A duplicate was preformed of molecule 2 in formulation 1 buffer showing insignificant differences in the protein recovery amount.

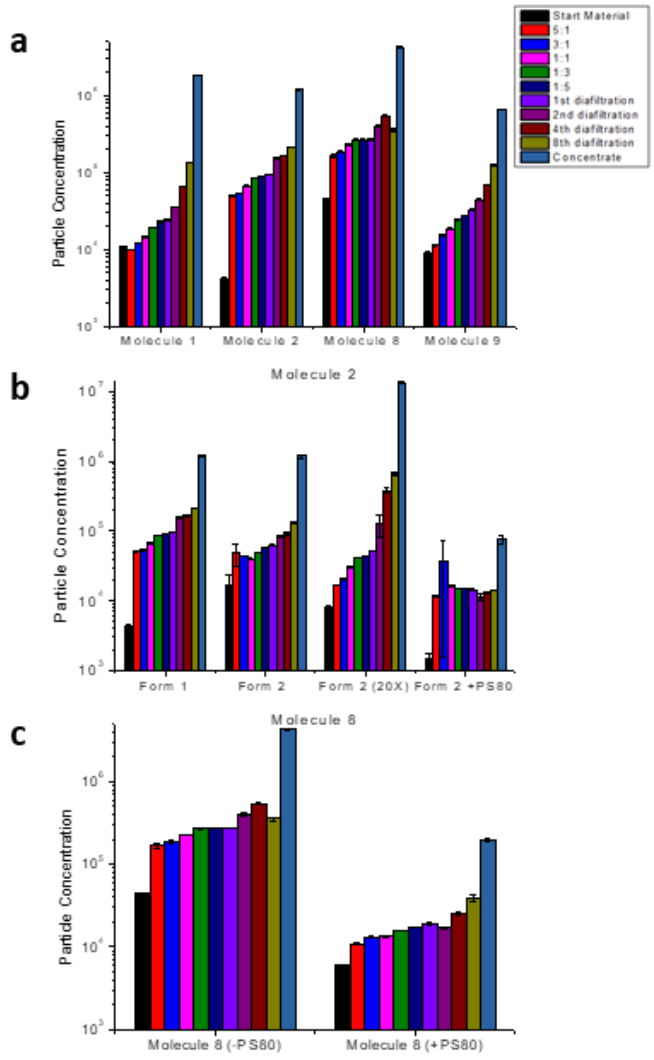

Figure 5.5: Sub-visible particle concentration of TFF samples as measured by MFI.

Panel a shows molecules 1, 2, 8, and 9 under standard laboratory scale TFF running conditions. Panel b shows molecule 2 in various running conditions; formulation 1, formulation 2, formulation 2 with a 20X concentration step, and formulation 2 with 0.01% PS80. Panel c show molecule 8 with and without 0.01% PS80. Data shown is an average of n=2 measurements with error bars representing the data range.

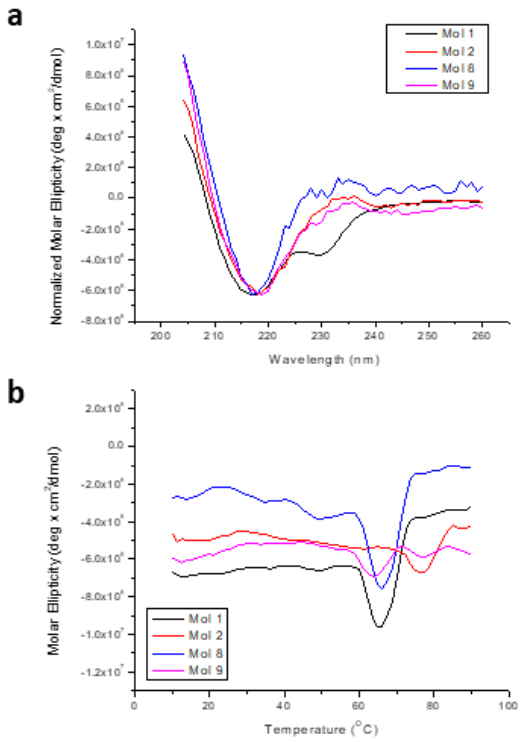

Figure 5.6: Circular dichroism analysis of Ab molecules 1 (black), 2 (red), 8 (blue), and 9 (pink) in PBS buffer.

Panel a shows spectra at 10°C. Panel b represents temperature ramp from 10 to 90°C monitored at 217 nm.

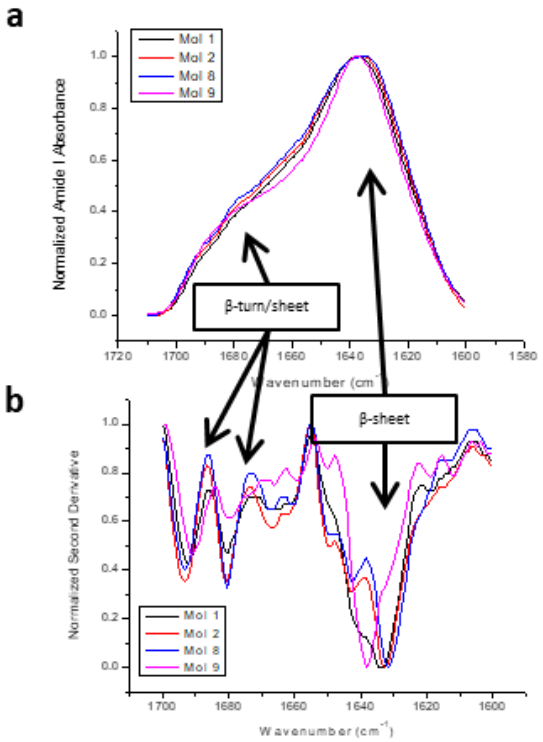

Figure 5.7: FTIR spectroscopy analysis of Ab molecules 1 (black), 2 (red), 8 (blue), and 9 (pink) in PBS buffer.

Panel a represents amide I absorbance. Panel b represents the second derivative spectrum of panel a showing characteristic signals of protein secondary structure elements as indicated by arrows.

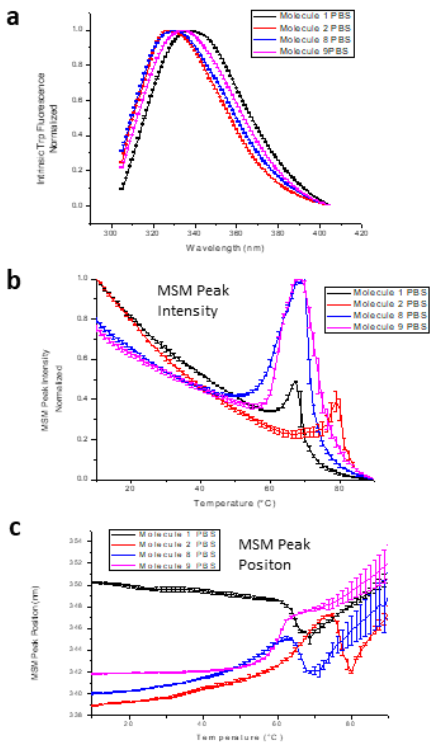

Figure 5.8: Intrinsic fluorescence spectroscopy analysis of Ab molecules 1 (black), 2 (red), 8 (blue), and 9 (pink) in PBS buffer.

Panel a represents 10°C spectrum of the four molecules. Panel b represents MSM peak intensity vs. temperature from 10-90°C. Panel c represents MSM peak position vs. temperature from 10-90°C. Error bars represent standard deviation for n=3 replicates.

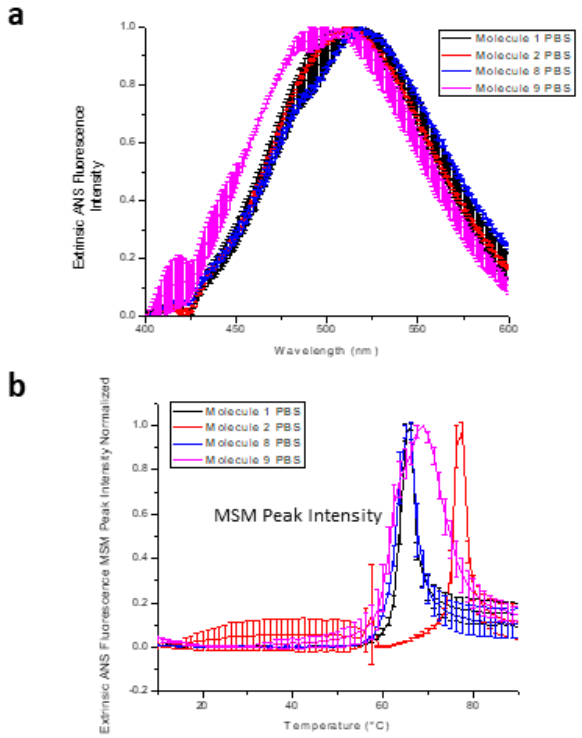

Figure 5.9: ANS Extrinsic fluorescence spectroscopy analysis of Ab molecules 1 (black), 2 (red), 8 (blue), and 9 (pink) in PBS.

Panel a represents 10°C spectrum of the four molecules. Panel b represents MSM peak intensity vs. temperature (thermal melts) of the four molecules from 10-90°C. Error bars represent standard deviation for n=3 replicates.

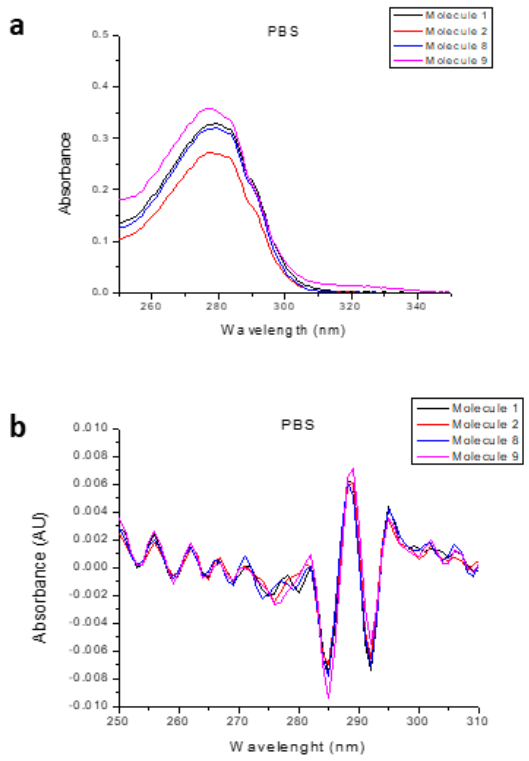

Figure 5.10: UV-Visible spectroscopy and corresponding 2nd Derivative spectra of Ab molecules 1 (black), 2 (red), 8 (blue), and 9 (pink) in PBS at 0.2 mg/mL.

Panel a represents absorbance spectra from 250-350 nm. Panel b represents the 2nd derivative of the absorbance spectrum from 250-310 nm. N=3

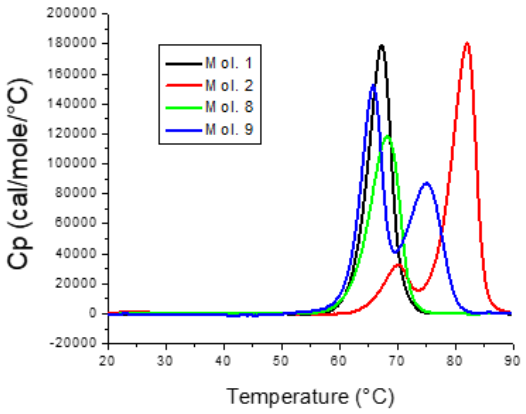

Figure 5.11: DSC analysis of Ab molecules 1 (black), 2 (red), 8 (green), and 9 (blue) in PBS buffer scanning from 10-90°C. n=3 replicates. Representative traces shown.

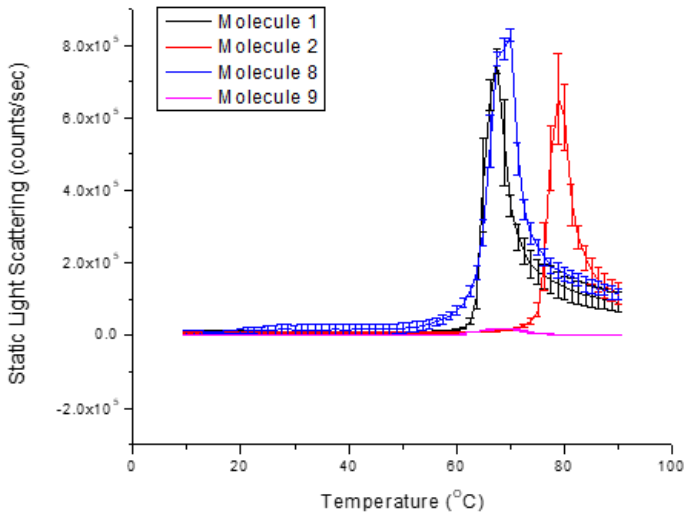

Figure 5.12: Static light scattering analysis of Ab molecules 1 (black), 2 (red), 8 (blue), and 9 (pink) in PBS buffer as a function of temperature.

Error bars represent standard deviation for n=3 replicates.

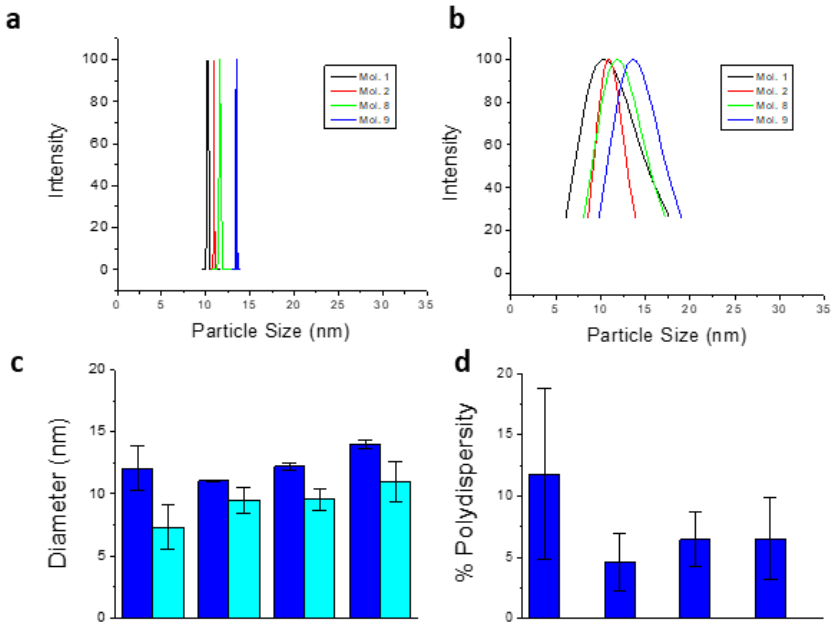

Figure 5.13: Dynamic light scattering analysis of Ab molecules 1 (black), 2 (red), 8 (green) and 9 (blue) in PBS buffer.

Panel a represents intensity fitting with multimodal size distribution. Panel b represents intensity by lognormal distribution. Panel c represents diameter of the molecules by intensity (blue) and number (teal). Panel d represents measured polydispersity values of each of the molecules by intensity. Error bars represent standard deviation for n=3 replicates.

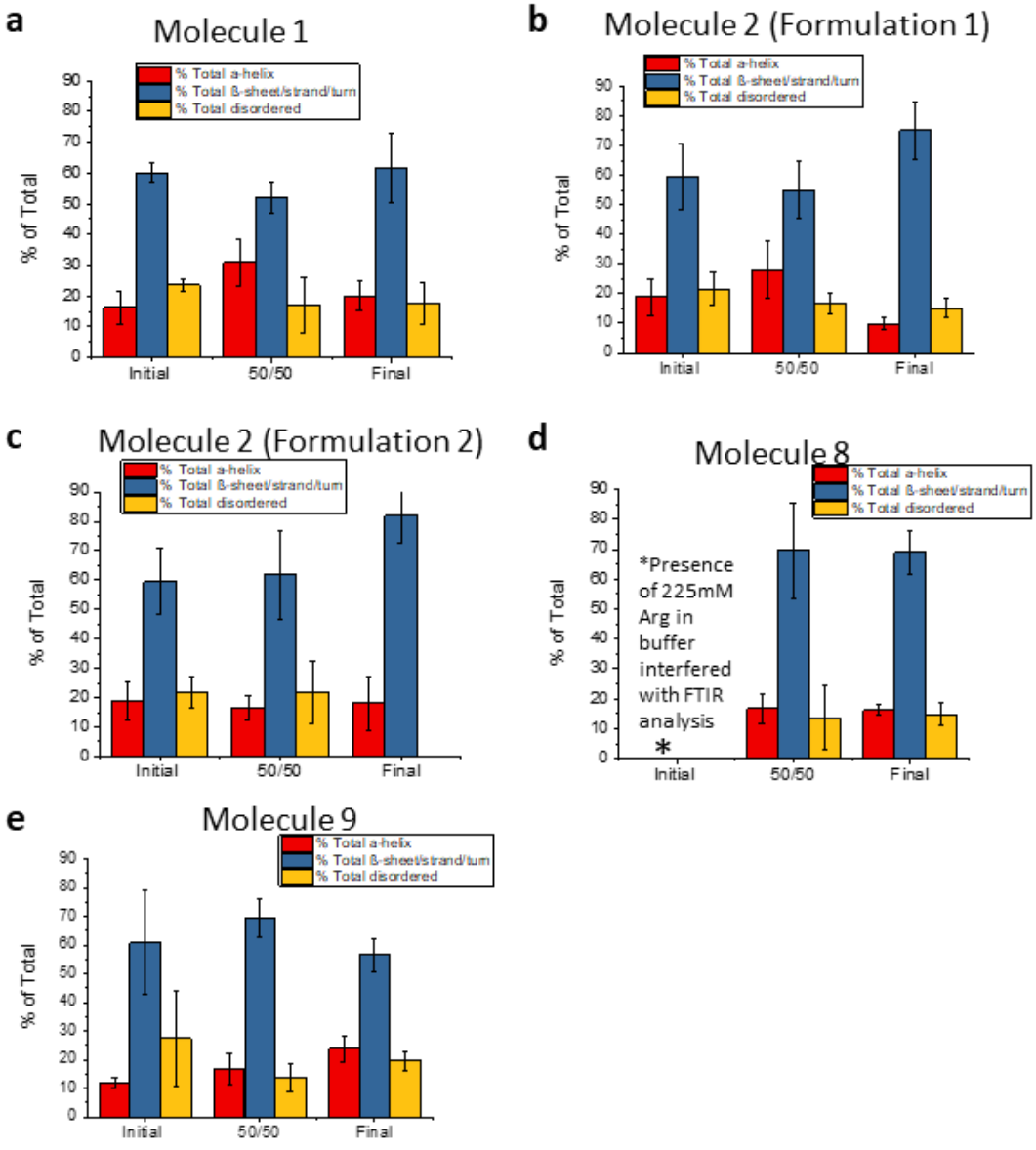

Figure 5.14: FTIR analysis of Ab molecules 1, 2, 8 and 9 in the TFF process buffers.

Panel a represents molecule 1. Panel b represents molecule 2 in formulation 1. Panel c represents molecule 2 in formulation 2. Panel d represents molecule 8. Panel e represents molecule 9. Percent total α-helix (red), percent total β-sheet/strand/turn (blue), and percent total disordered (yellow) are plotted for molecules in their initial, 50/50, and formulation buffers. Error bars represent standard deviation for n=3 replicates.

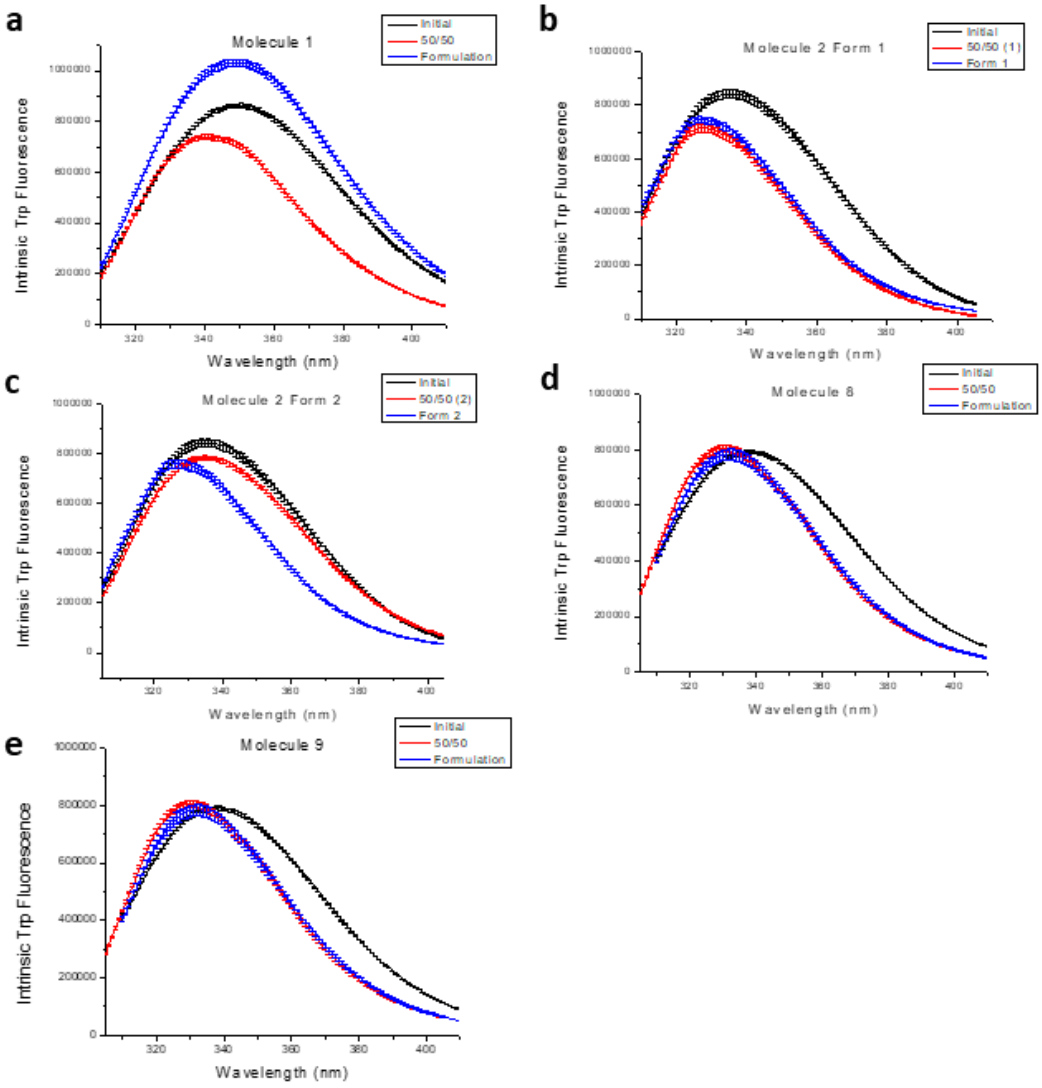

Figure 5.15: Intrinsic fluorescence spectra at 10°C of Ab molecules 1, 2, 8 and 9 in TFF process buffers.

Panel a represents molecule 1. Panel b represents molecule 2 formulation 1. Panel c represents molecule 2 formulation 2. Panel d represents molecule 8. Panel e represents molecule 9. Molecules in their Initial buffer (black), 50/50 mix buffer (red), and formulation buffer (blue) are shown. Error bars represent standard deviation for n=3 replicates.

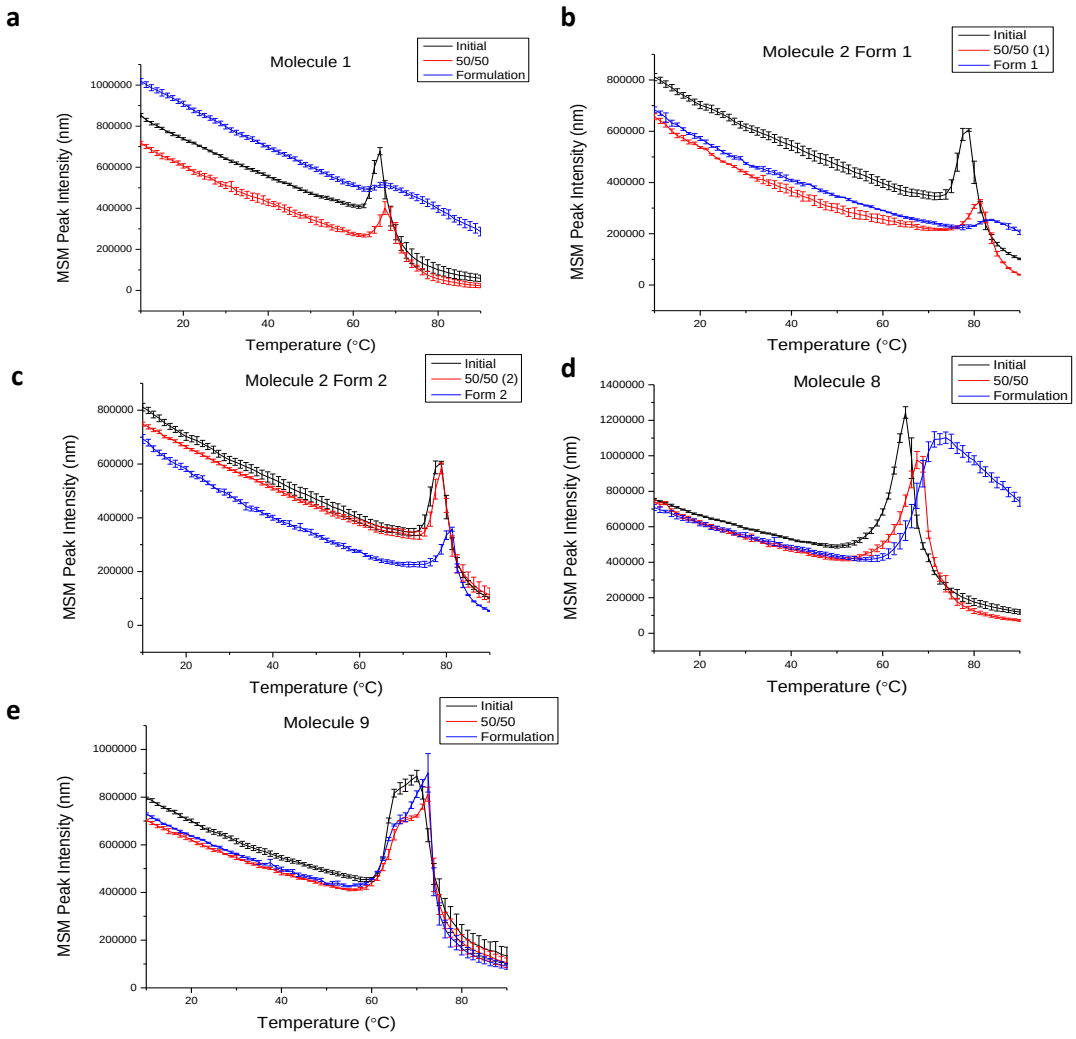

Figure 5.16: Intrinsic fluorescence spectroscopy (peak intensity) vs temperature analysis of Ab molecules 1, 2, 8 and 9 in TFF process buffers.

Panel a represents molecule 1. Panel b represents molecule 2 formulation 1. Panel c represents molecule 2 formulation 2. Panel d represents molecule 8. Panel e represents molecule 9. Molecules in their Initial buffer (black), 50/50 mix buffer (red), and formulation buffer (blue) are shown. Error bars represent standard deviation for n=3 replicates.

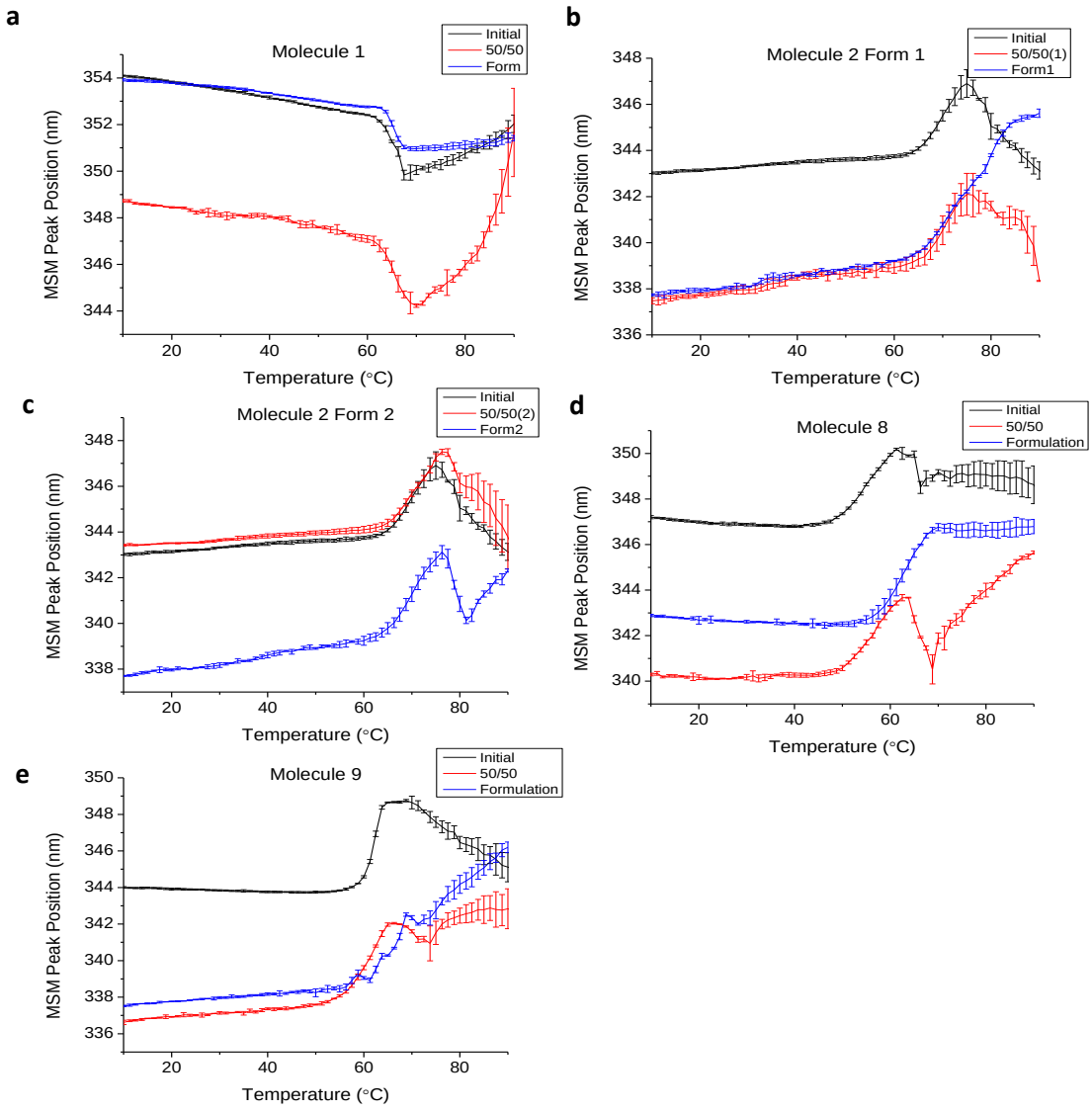

Figure 5.17: Intrinsic fluorescence spectroscopy (peak position) vs temperature analysis of Ab molecules 1, 2, 8 and 9 in TFF process buffers.

Panel a represents molecule 1. Panel b represents molecule 2 formulation 1. Panel c represents molecule 2 formulation 2. Panel d represents molecule 8. Panel e represents molecule 9. Molecules in their Initial buffer (black), 50/50 mix buffer (red), and formulation buffer (blue) are shown. Error bars represent standard deviation for n=3 replicates.

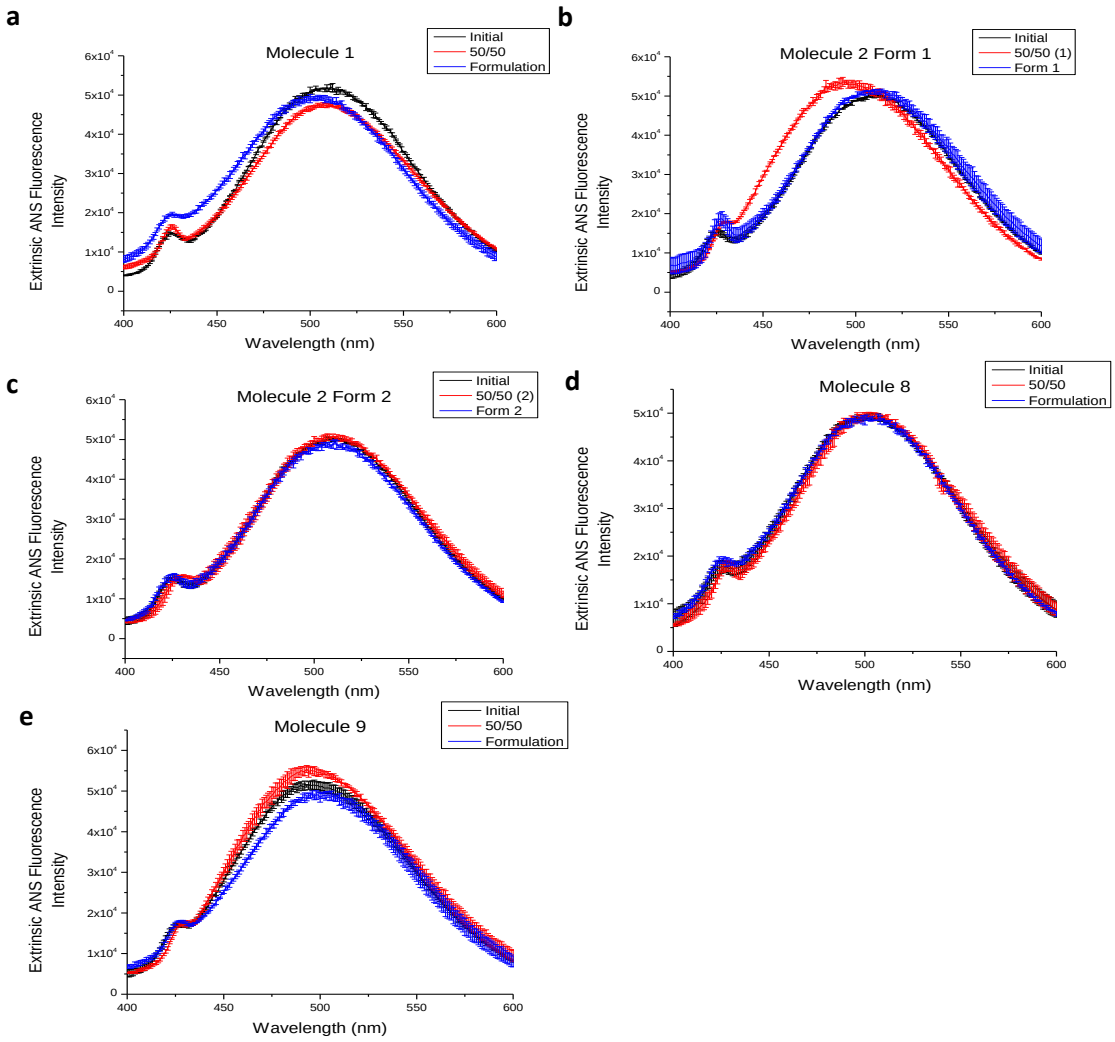

Figure 5.18: Extrinsic ANS fluorescence spectra at 10°C in the presence of Ab molecules 1, 2, 8 and 9 in TFF process buffers.

Panel a represents molecule 1. Panel b represents molecule 2 formulation 1. Panel c represents molecule 2 formulation 2. Panel d represents molecule 8. Panel e represents molecule 9. Results from Initial buffer (black), 50/50 mix buffer (red), and formulation buffer (blue) are shown. Error bars represent standard deviation for n=3 replicates.

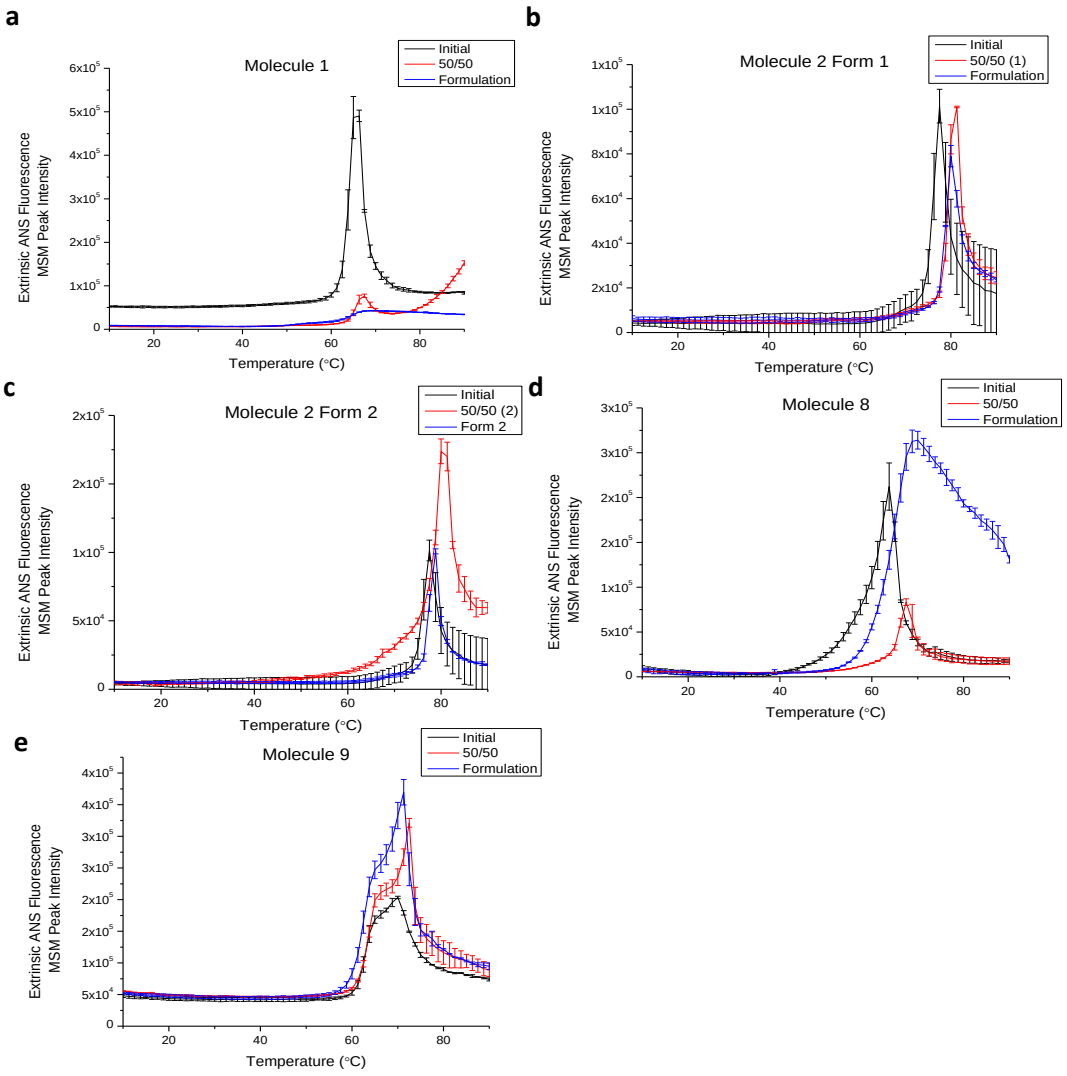

Figure 5.19: Extrinsic ANS fluorescence spectroscopy (peak intensity) vs. temperature in the presence of Ab molecules 1, 2, 8 and 9 in TFF process buffers.

Panel a represents molecule 1. Panel b represents molecule 2 formulation 1. Panel c represents molecule 2 formulation 2. Panel d represents molecule 8. Panel e represents molecule 9. Results in Initial buffer (black), 50/50 mix buffer (red), and formulation buffer (blue) are shown. Error bars represent standard deviation for n=3 replicates.

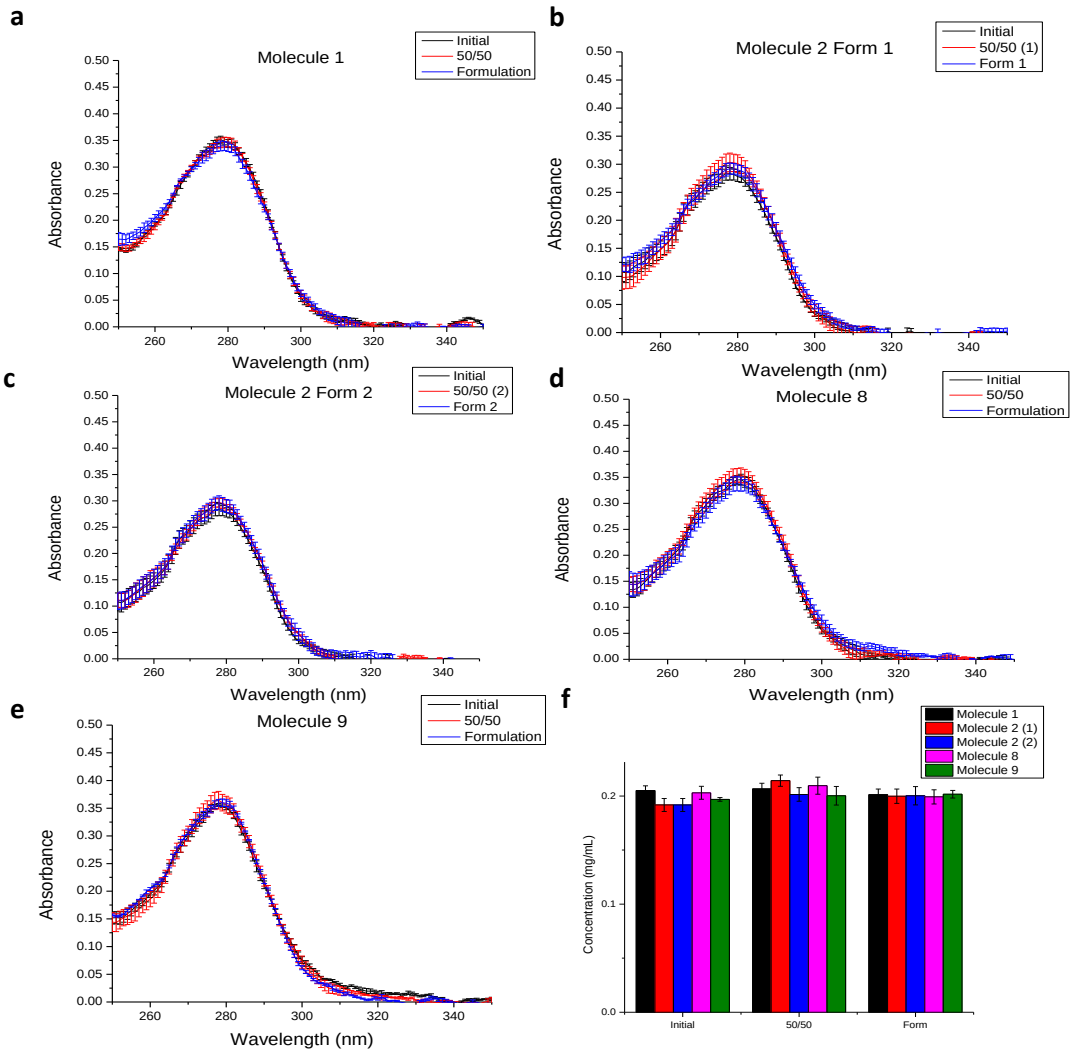

Figure 5.20: UV-Visible spectroscopy analysis of Ab molecules 1, 2, 8, and 9 in TFF process buffers.

Panel a represents molecule 1. Panel b represents molecule 2 formulation 1. Panel c represents molecule 2 formulation 2. Panel d represents molecule 8. Panel e represents molecule 9. Molecules in their Initial buffer (black), 50/50 mix buffer (red), and formulation buffer (blue) are shown. Panel f represents the Ab concentration in the initial, 50/50, and formulation of molecule 1 (black), molecule 2 formulation 1 (red), molecule 2 formulation 2 (blue), molecule 8 (pink), and molecule 9 (green). Error bars represent standard deviation for n=3 replicates.

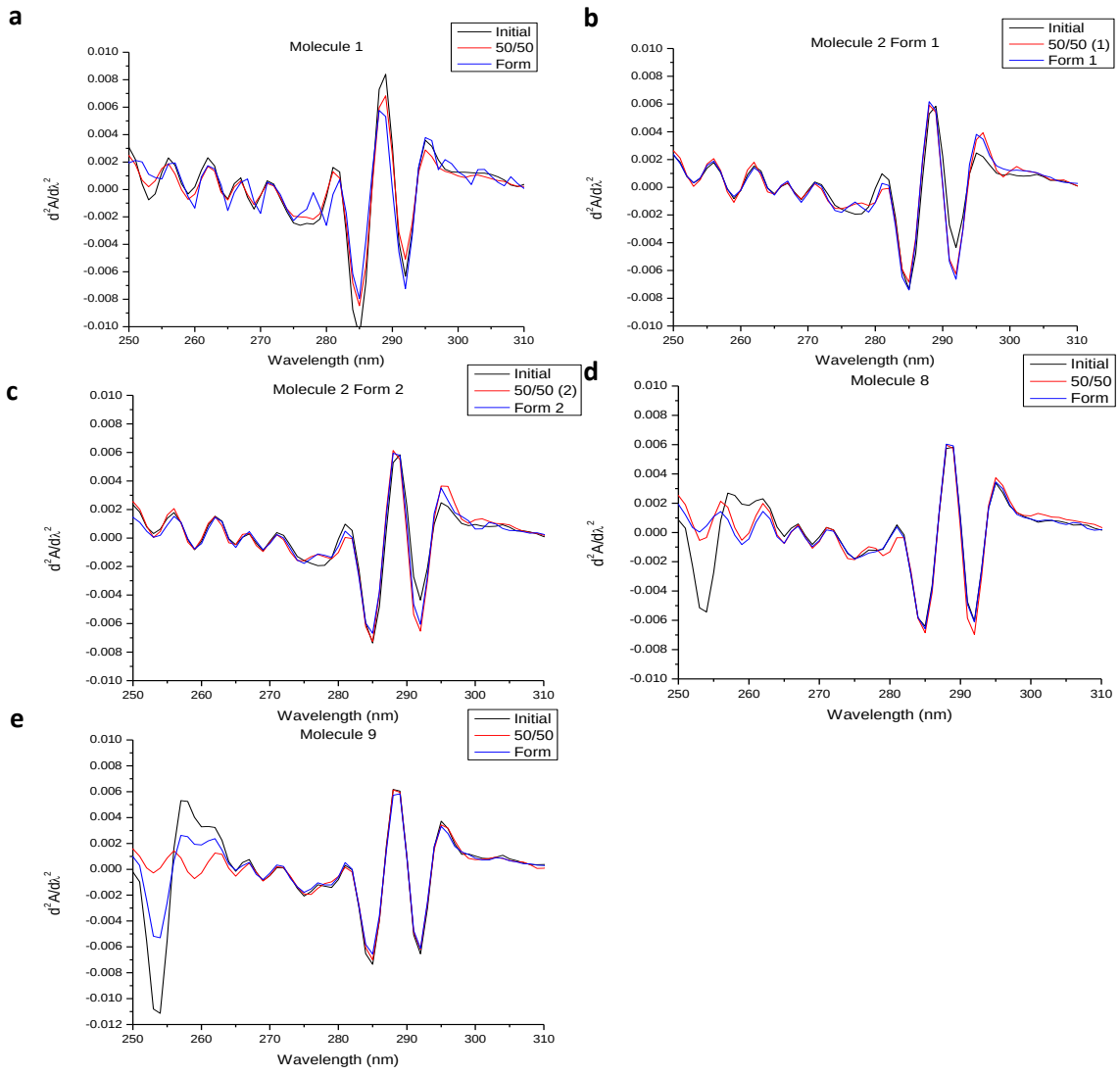

Figure 5.21: 2nd derivative of UV-Visible spectroscopy analysis of Ab molecules 1, 2, 8, and 9 in TFF process buffers.

Panel a represents molecule 1. Panel b represents molecule 2 formulation 1. Panel c represents molecule 2 formulation 2. Panel d represents molecule 8. Panel e represents molecule 9. Molecules in their Initial buffer (black), 50/50 mix buffer (red), and formulation buffer (blue) are shown.

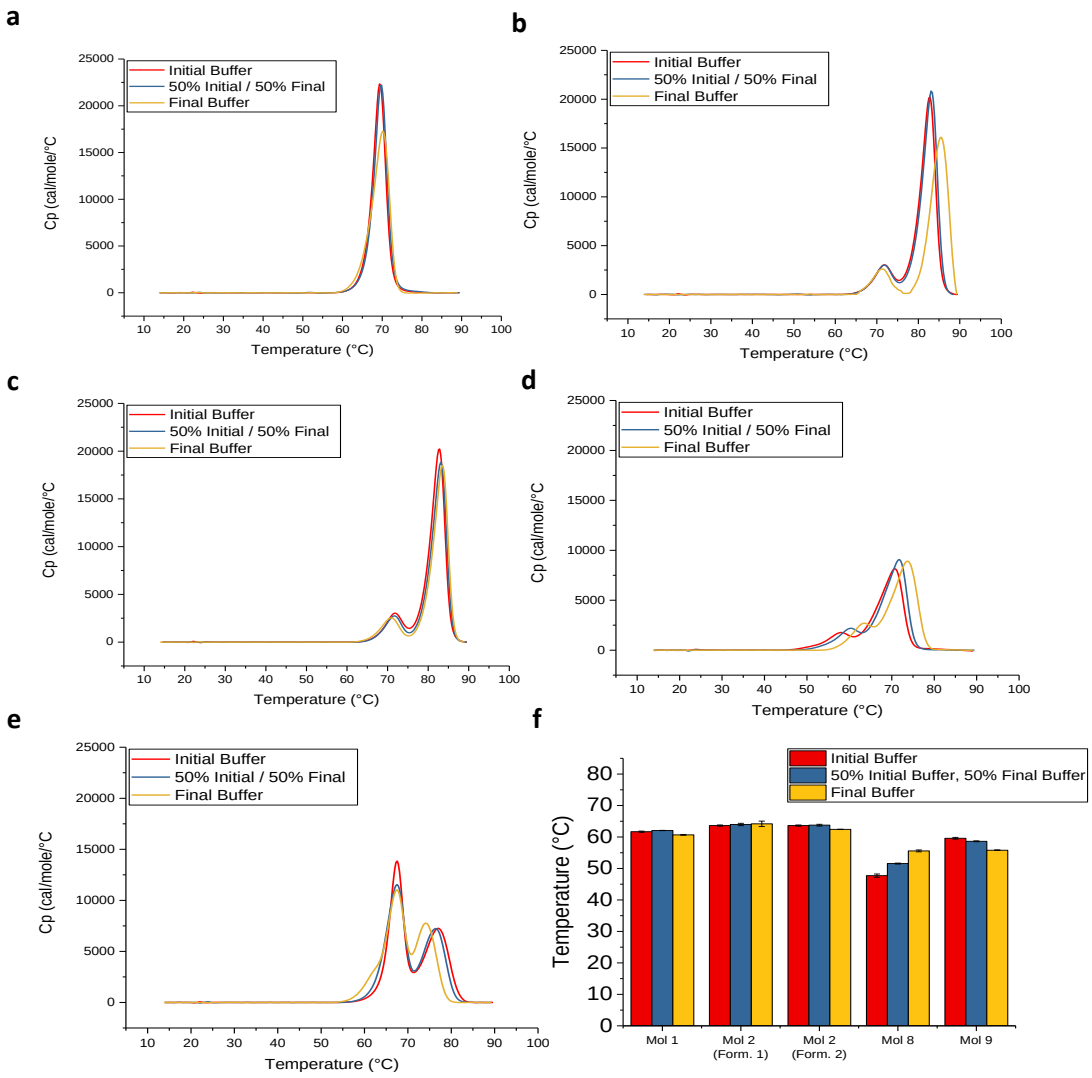

Figure 5.22: DSC analysis of Ab molecules 1, 2, 8, and 9 in TFF process buffers.

Panel a represents molecule 1. Panel b represents molecule 2 formulation 1. Panel c represents molecule 2 formulation 2. Panel d represents molecule 8. Panel e represents molecule 9. Panel f represents the T_{onset} values for each molecule. Molecules in their Initial buffer (red), 50/50 mix buffer (blue), and formulation buffer (yellow) are shown. Error bars represent standard deviation for n=3 replicates.

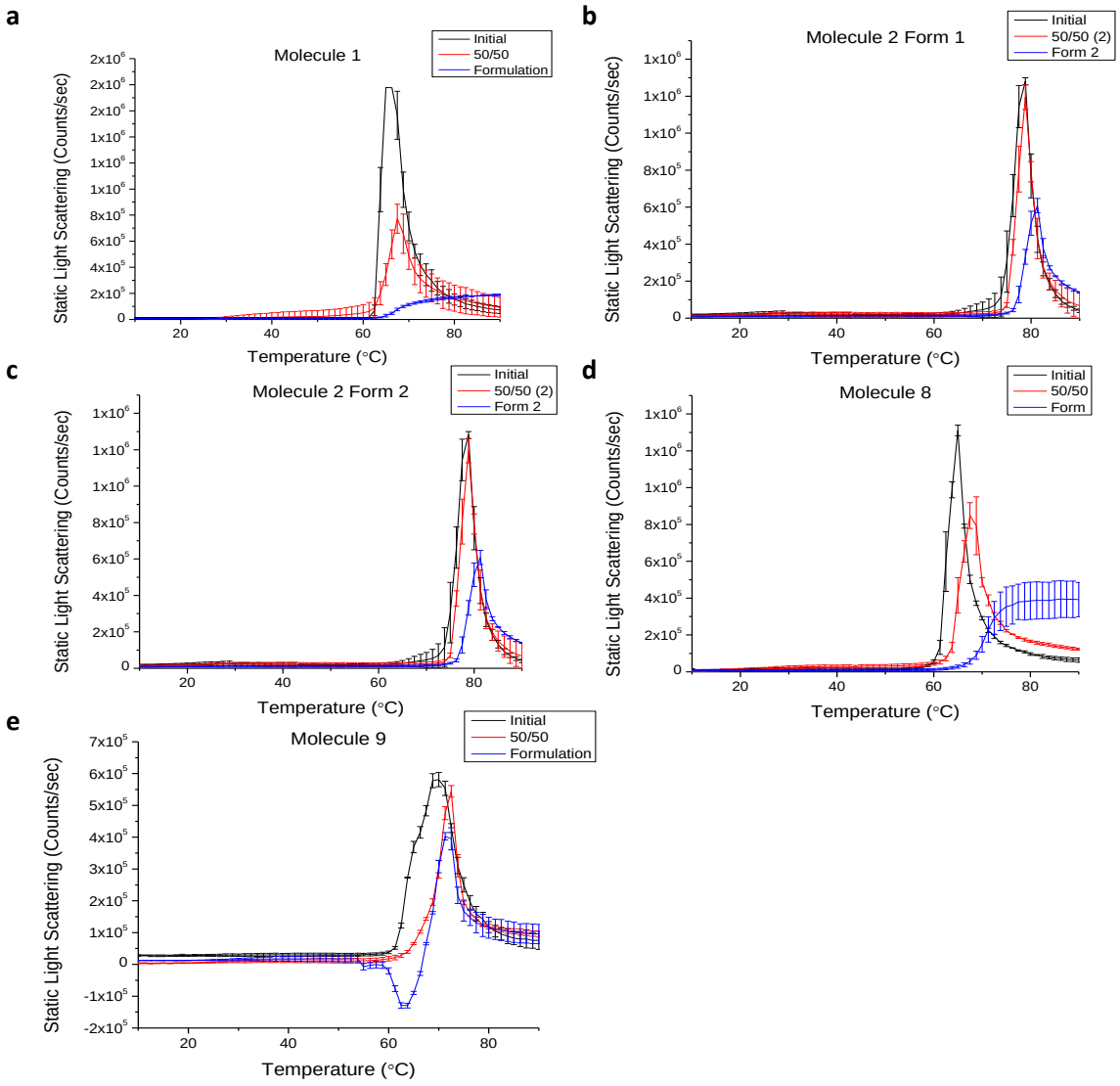

Figure 5.23: SLS analysis vs temperature of Ab molecules 1, 2, 8, and 9 in TFF process buffers. Panel a represents molecule 1. Panel b represents molecule 2 formulation 1. Panel c represents molecule 2 formulation 2. Panel d represents molecule 8. Panel e represents molecule 9. Molecules in their Initial buffer (black), 50/50 mix buffer (red), and formulation buffer (blue) are shown. Error bars represent standard deviation for n=3 replicates.

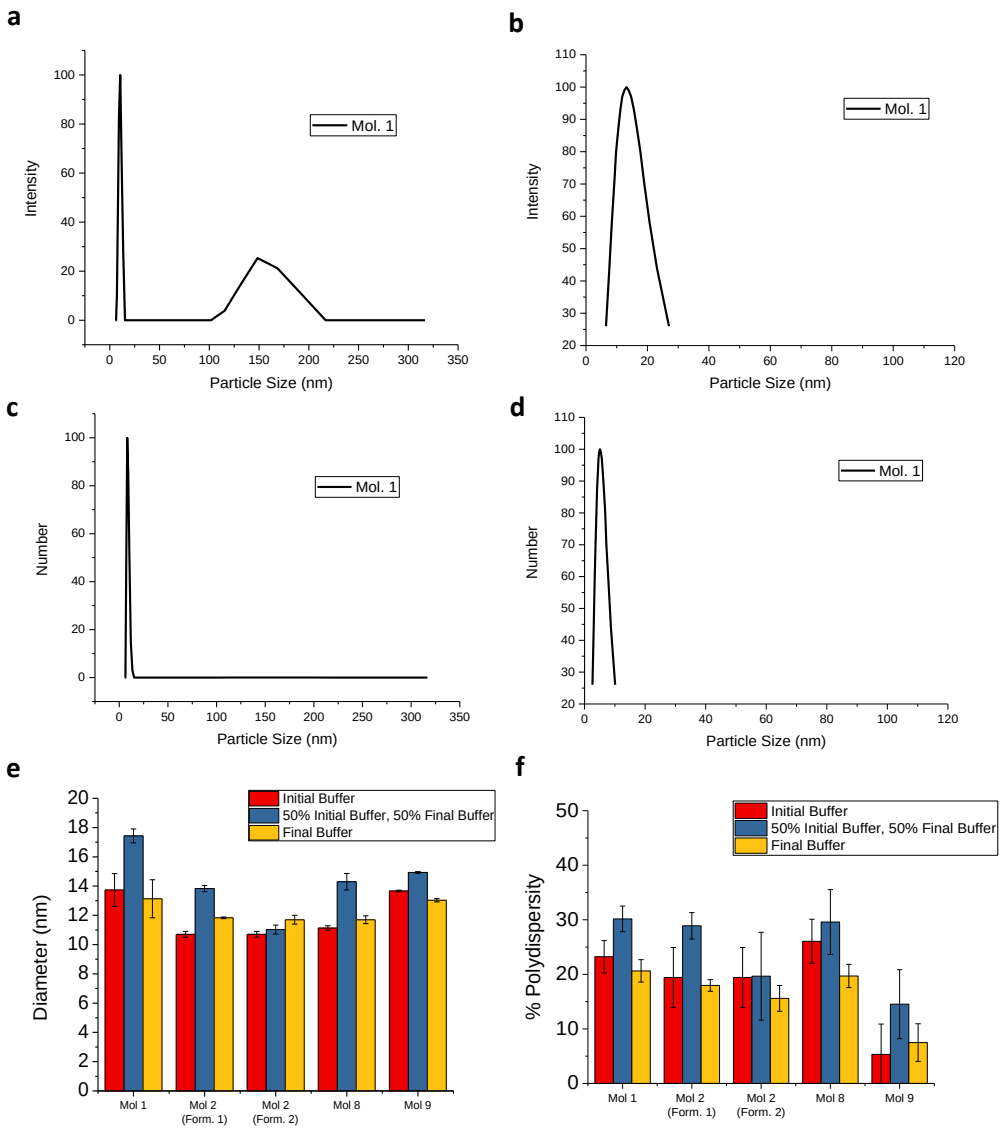

Figure 5.24: Dynamic light scattering analysis of Ab molecules 1, 2, 8, and 9 in TFF process buffers.

Panel a represents intensity with multimodal size distribution fitting. Panel b represents intensity by lognormal fitting. Panel c represents number with multimodal size distribution fitting. Panel d represents number by lognormal fitting. Panel e represents the diameter of each molecule in initial (red), 50/50 (blue), and formulation (yellow) buffers. Panel f represents percent polydispersity values of the molecules in each buffer. Error bars represent standard deviation for n=3 replicates.

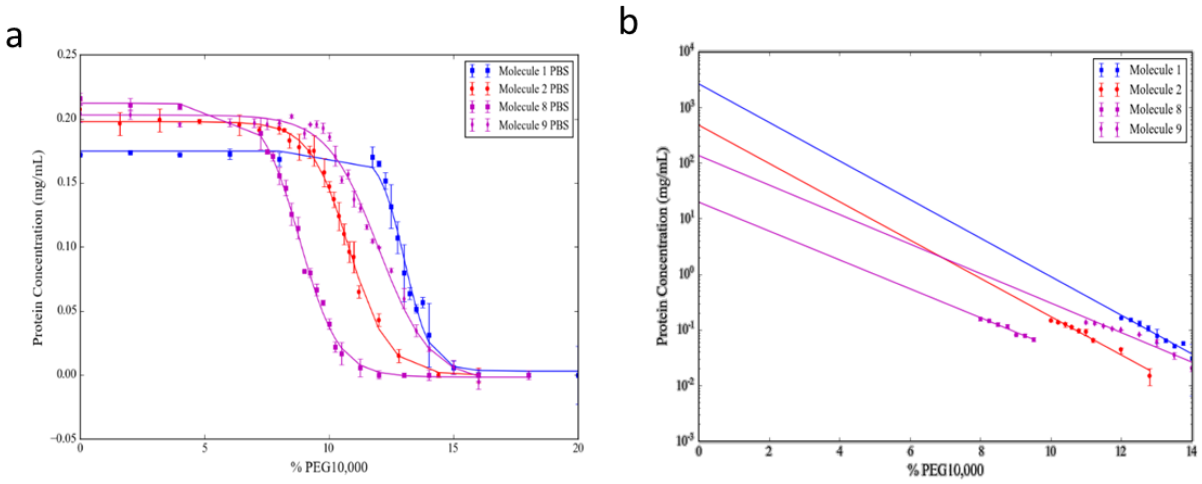

Figure 5.25: PEG solubility assay of the four Ab molecules in PBS.

Panel a represents the relative apparent solubility of molecules 1 (blue), 2 (red), 8 (pink squares), and 9 (pink circles). Panel b represents the PEG solubility assay on a logarithmic scale for extrapolation of linear fit to determine the relative apparent solubility with 0% PEG.

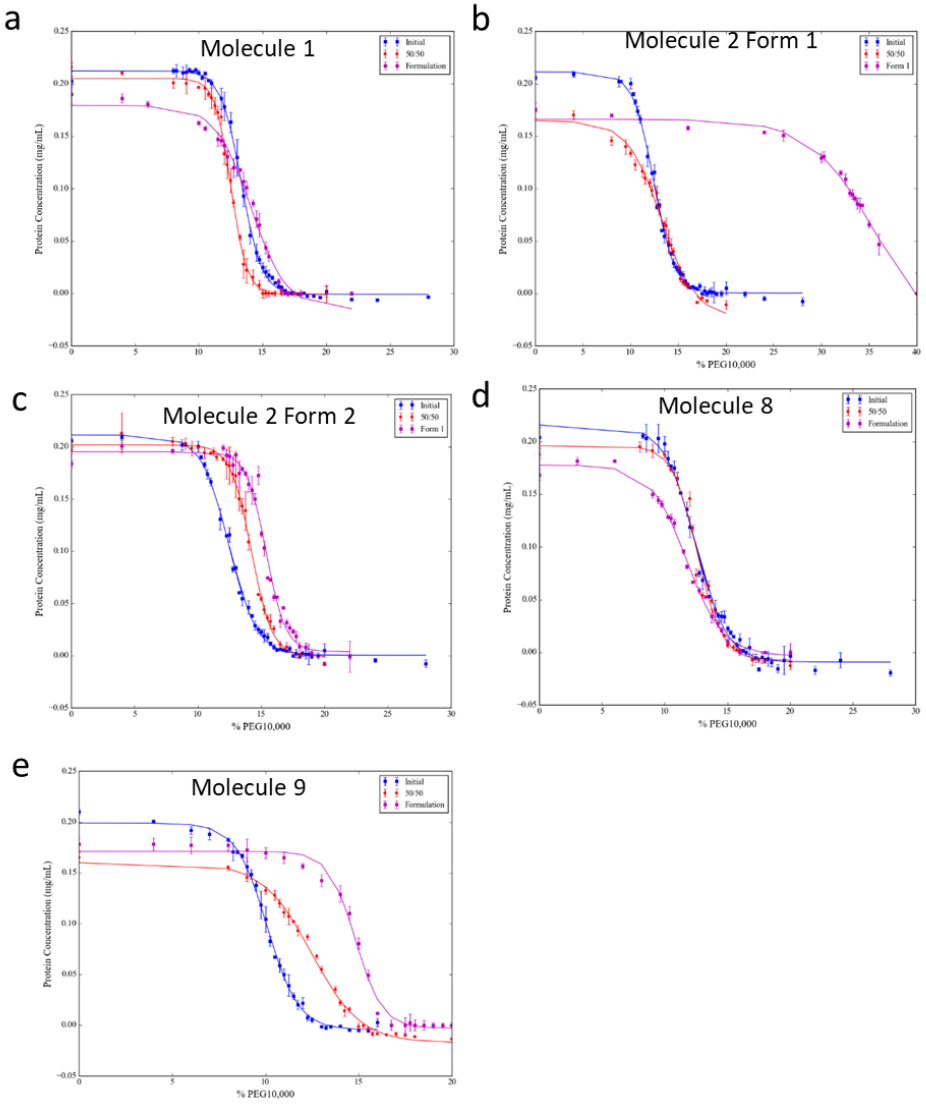

Figure 5.26: PEG relative apparent solubility assay of the four Ab molecules in the TFF processing buffers.

Panel a represents molecule 1 in the TFF processing buffers. Panel b represents molecule 2 (Form 1) in the TFF processing buffers. Panel c represents molecule 2 (Form 2) in the TFF processing buffers. Panel d represents molecule 8 in the TFF processing buffers. Panel e represents molecule 9 in the TFF processing buffers. Molecules in their TFF processing buffers are shown as initial (blue), 50/50 mix buffer (red), and formulation (pink). Error bars represent standard deviation for n=3 replicates.

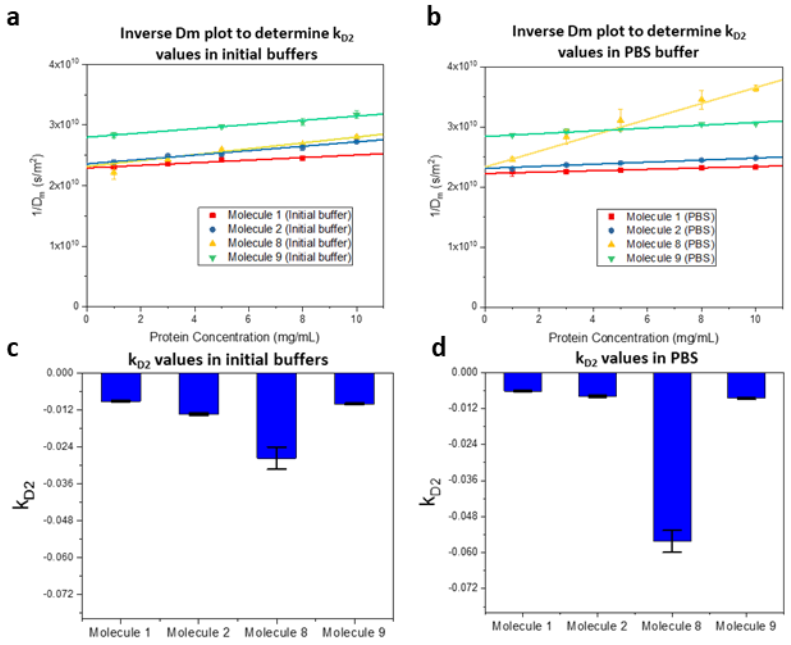

Figure 5.27: Kd2 values determined for Ab molecules 1, 2, 8, and 9 as measured by DLS. Panel a molecule 1 (red), molecule 2 (blue), molecule 8 (yellow), and molecule 9 (green) in TFF process buffers. Panel c molecule 1 (red), molecule 2 (blue), molecule 8 (yellow), and molecule 9 (green) in PBS. Panel d are the k_{D2} values of each Ab molecule in the TFF process buffers. Panel e are the k_{D2} values of each Ab molecule in PBS buffer. Error bars represent standard deviation for n=3 replicates.

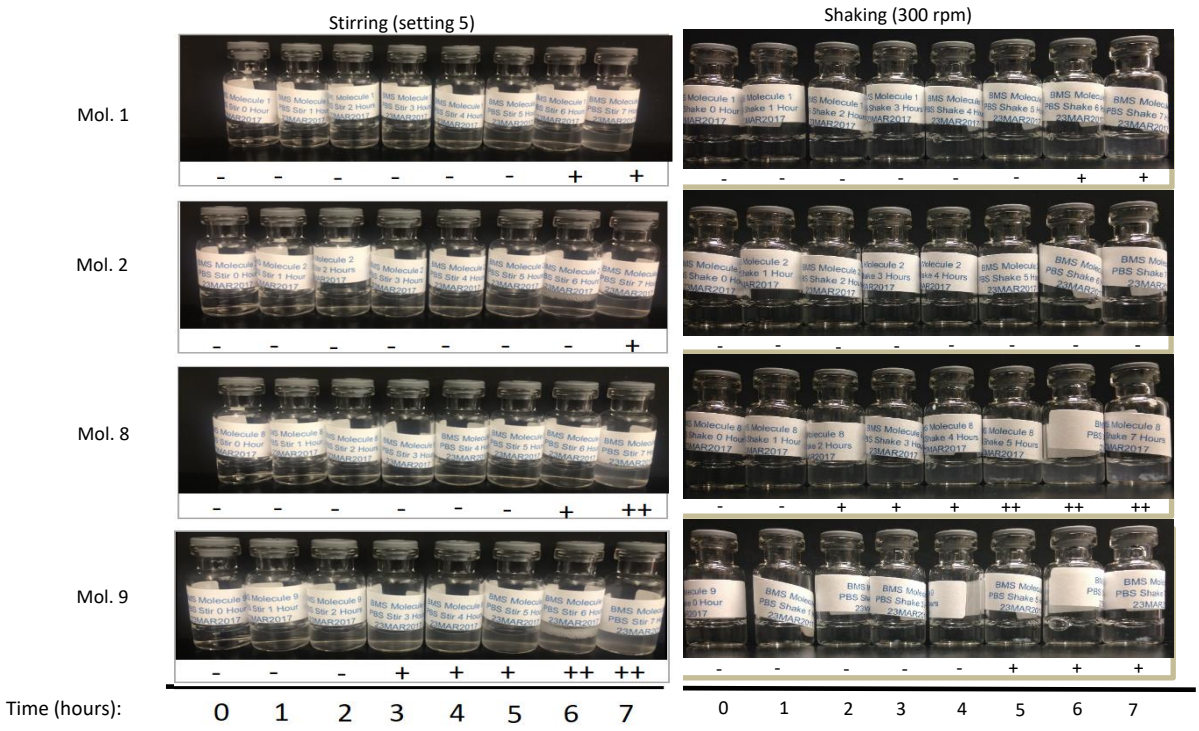

Figure 5.28: Visual assessment of solutions of Ab molecules 1, 2, 8, and 9 in PBS buffer before and after stirring and shaking stress over the course of 7 hrs.

Stirring agitation is shown on the left side panels and shaking agitation is shown on right side panels. "-" represents no visible aggregation seen; "+" represents some visible aggregation seen; "++" represents large amounts of visible aggregation seen.

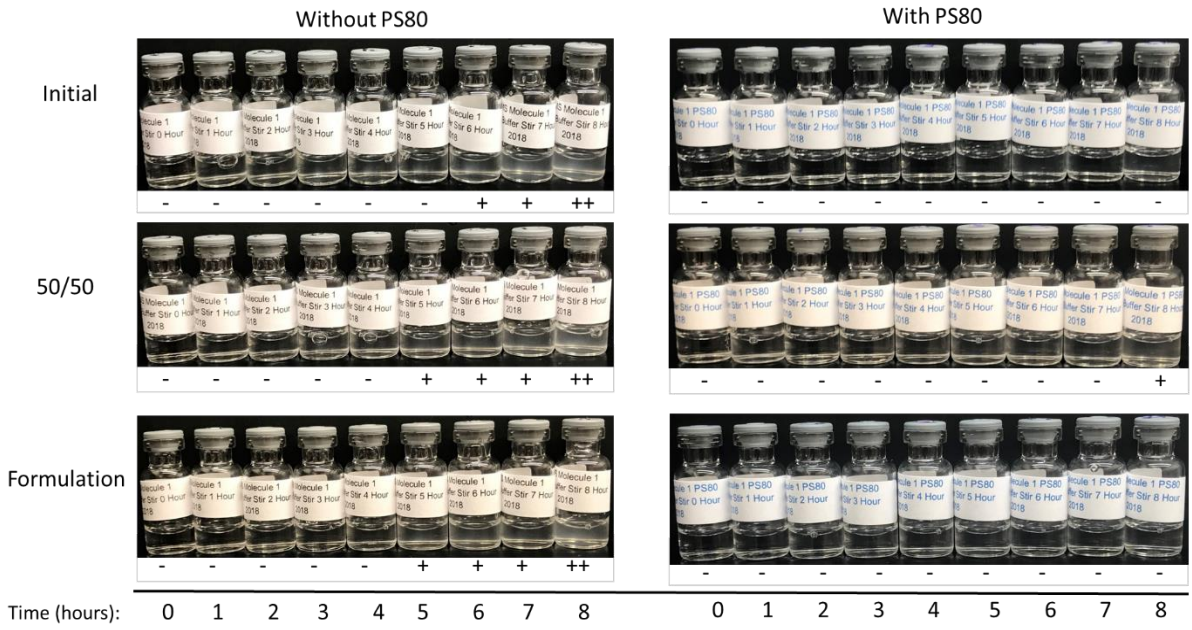

Figure 5.29: Visual assessment of solutions of Ab molecule 1 under stirring agitation over the course of 8 hrs in the TFF processing buffers.

Samples without 0.01% PS80 is shown on the left side panels and samples with 0.01% PS80 is shown on right side panels. "-" represents no visible aggregation seen; "+" represents some visible aggregation seen; "++" represents large amounts of visible aggregation seen.

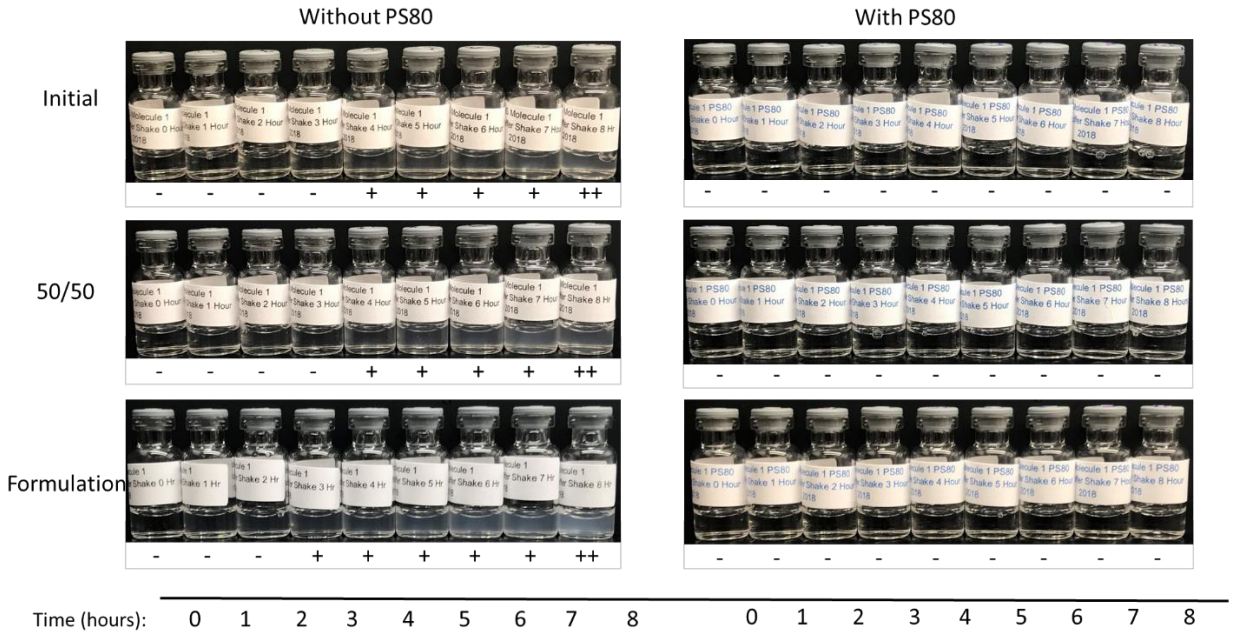

Figure 5.30: Visual assessment of solutions of Ab molecule 1 under shaking agitation over the course of 8 hrs in the TFF processing buffers.

Samples without 0.01% PS80 is shown on the left side panels and samples with 0.01% PS80 is shown on right side panels. "-" represents no visible aggregation seen; "+" represents some visible aggregation seen; "++" represents large amounts of visible aggregation seen.

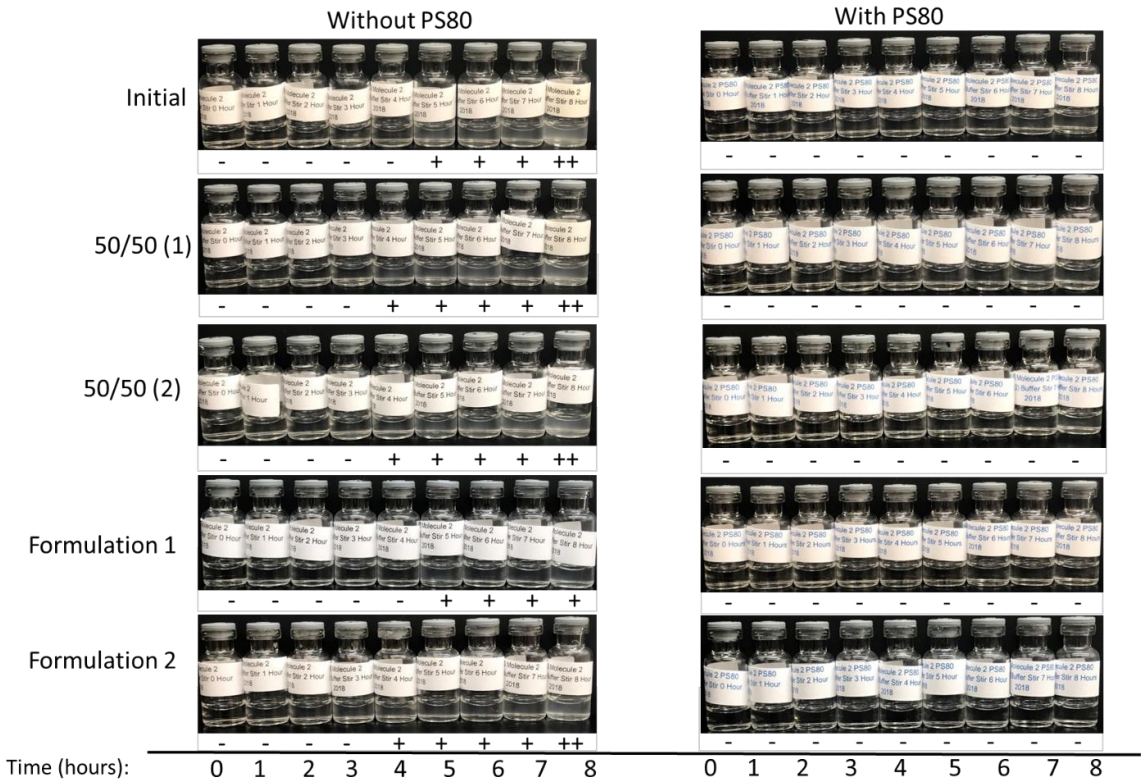

Figure 5.31: Visual assessment of solutions of Ab molecule 2 under stirring agitation over the course of 8 hrs in the TFF processing buffers.

Samples without 0.01% PS80 is shown on the left side panels and samples with 0.01% PS80 is shown on right side panels. "-" represents no visible aggregation seen; "+" represents some visible aggregation seen; "++" represents large amounts of visible aggregation seen.

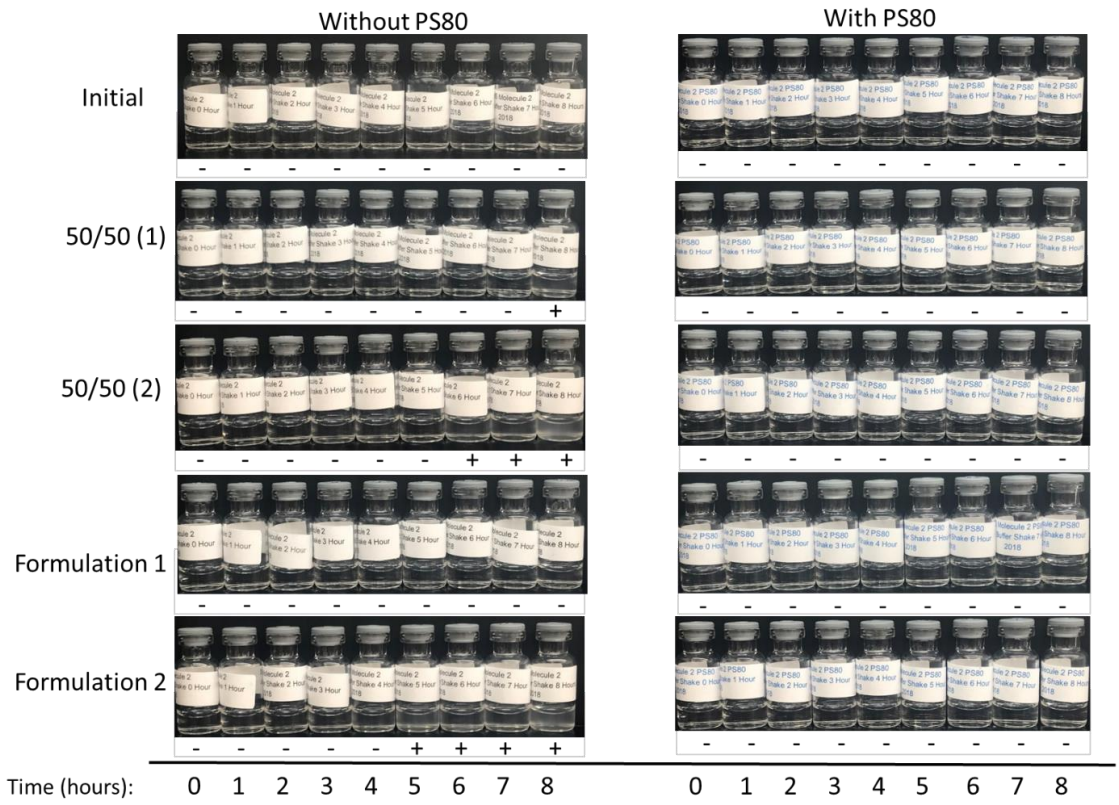

Figure 5.32: Visual assessment of solutions of Ab molecule 2 under shaking agitation over the course of 8 hrs in the TFF processing buffers.

Samples without 0.01% PS80 is shown on the left side panels and samples with 0.01% PS80 is shown on right side panels. "-" represents no visible aggregation seen; "+" represents some visible aggregation seen; "++" represents large amounts of visible aggregation seen.

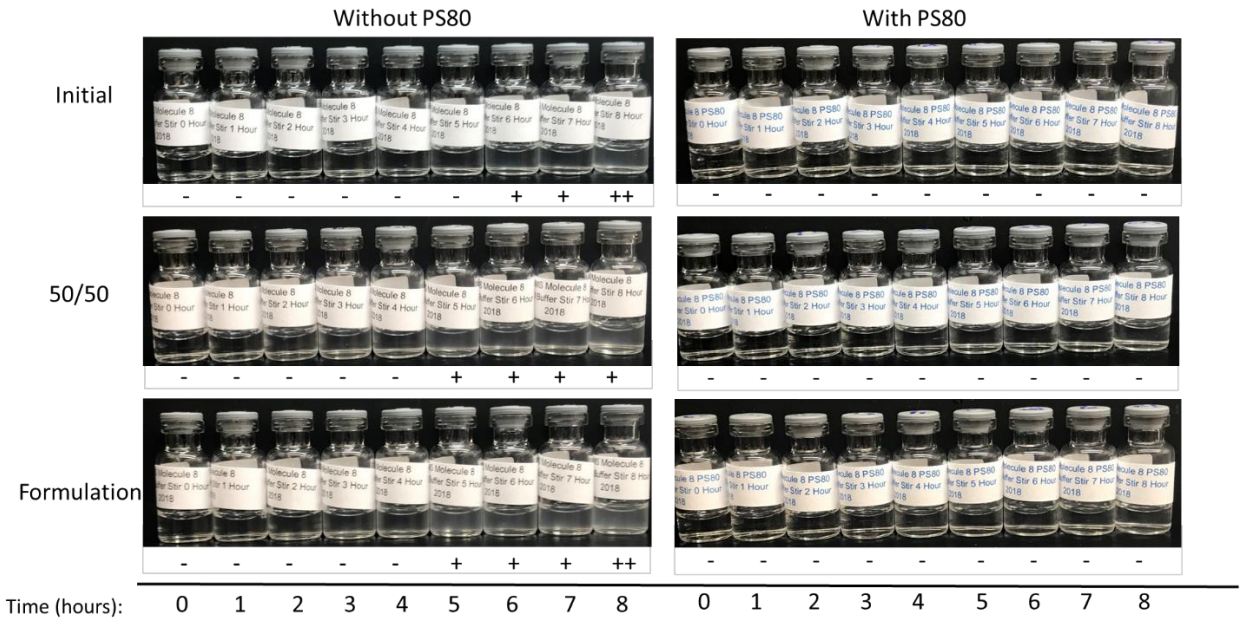

Figure 5.33: Visual assessment of solutions of Ab molecule 8 under stirring agitation over the course of 8 hrs in the TFF processing buffers.

Samples without 0.01% PS80 is shown on the left side panels and samples with 0.01% PS80 is shown on right side panels. "-" represents no visible aggregation seen; "+" represents some visible aggregation seen; "++" represents large amounts of visible aggregation seen.

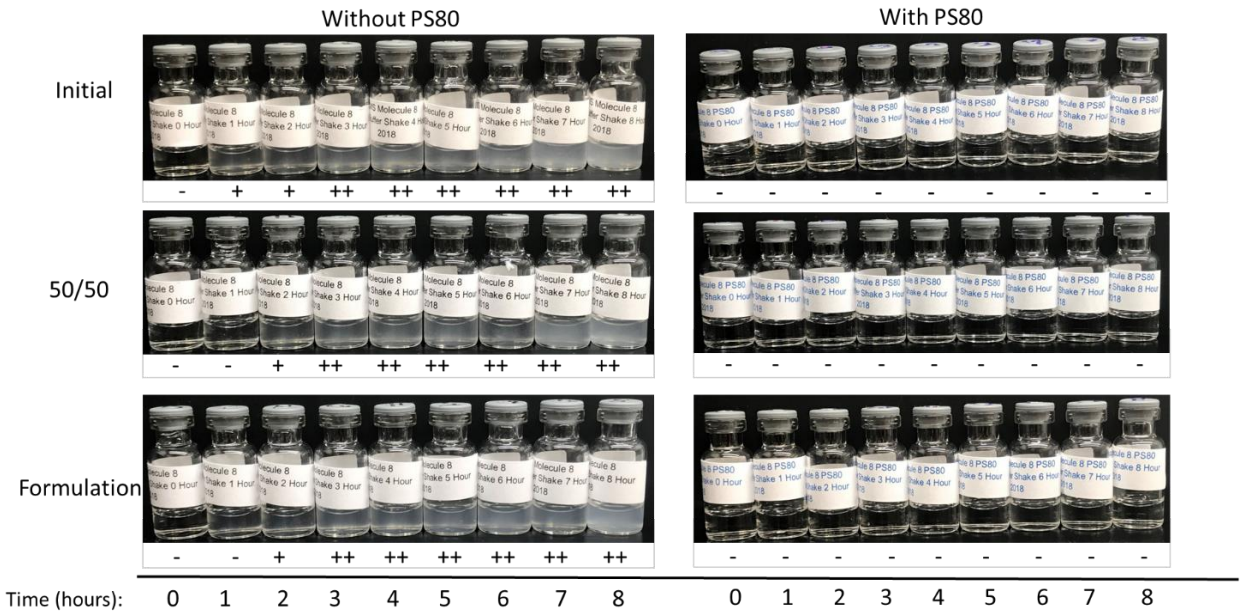

Figure 5.34: Visual assessment of solutions of Ab molecule 8 under shaking agitation over the course of 8 hrs in the TFF processing buffers.

Samples without 0.01% PS80 is shown on the left side panels and samples with 0.01% PS80 is shown on right side panels. "-" represents no visible aggregation seen; "+" represents some visible aggregation seen; "++" represents large amounts of visible aggregation seen.

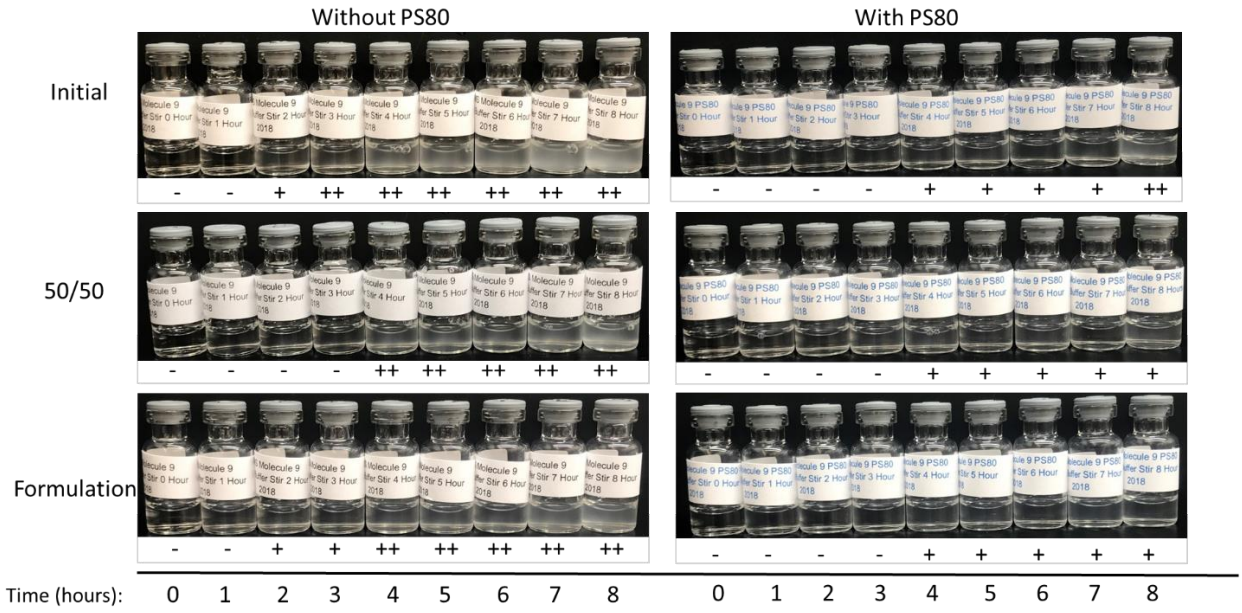

Figure 5.35: Visual assessment of solutions of Ab molecule 9 under stirring agitation over the course of 8 hrs in the TFF processing buffers.

Samples without 0.01% PS80 is shown on the left side panels and samples with 0.01% PS80 is shown on right side panels. "-" represents no visible aggregation seen; "+" represents some visible aggregation seen; "++" represents large amounts of visible aggregation seen.

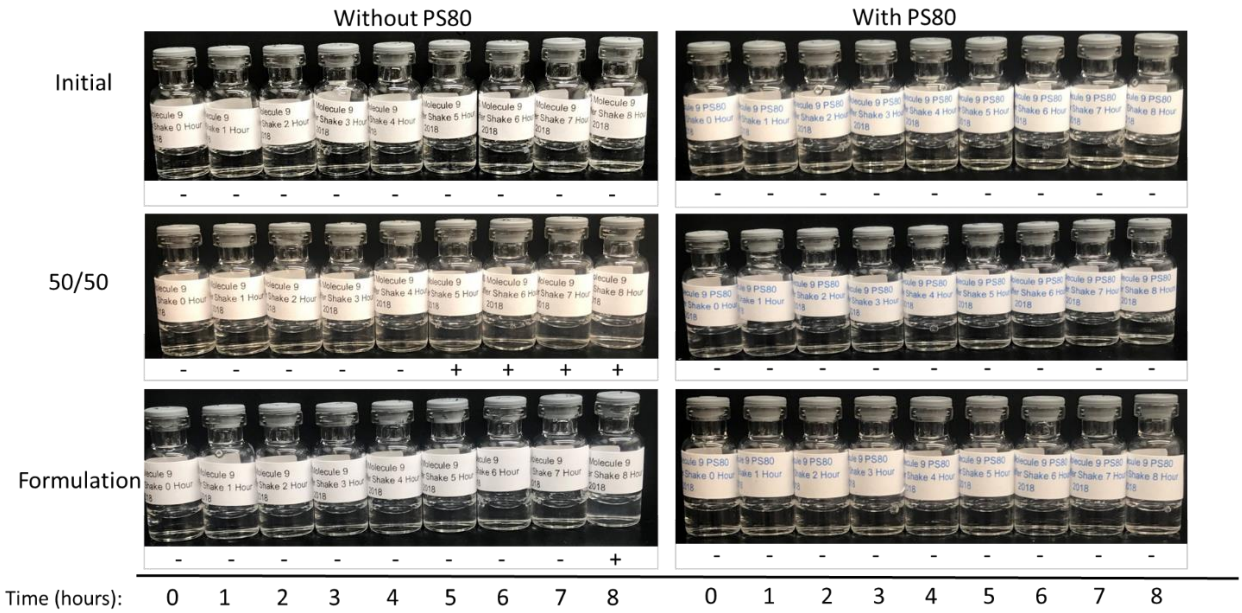

Figure 5.36: Visual assessment of solutions of Ab molecule 9 under shaking agitation over the course of 8 hrs in the TFF processing buffers.

Samples without 0.01% PS80 is shown on the left side panels and samples with 0.01% PS80 is shown on right side panels. "-" represents no visible aggregation seen; "+" represents some visible aggregation seen; "++" represents large amounts of visible aggregation seen.

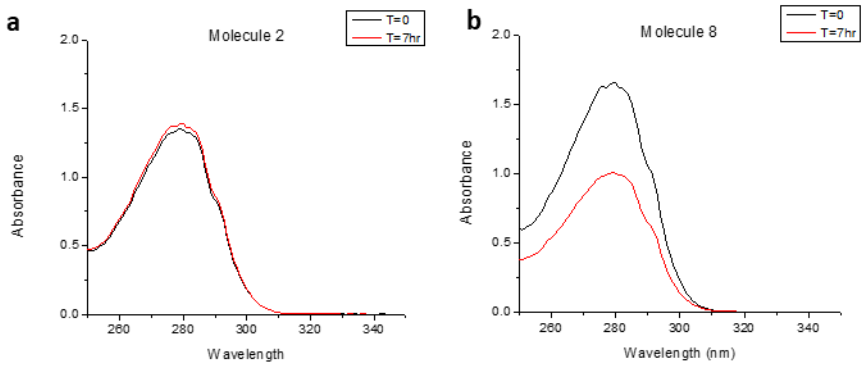

Figure 5.37: Representative UV-visible absorption spectrum of molecule 2 and 8 in PBS buffer before and after agitation stress.

Panel a represents molecule 2 at T=0 (black) and T=7 hrs (red). Panel b represents molecule 8 at T=0 (black) and T=7 hrs (red).

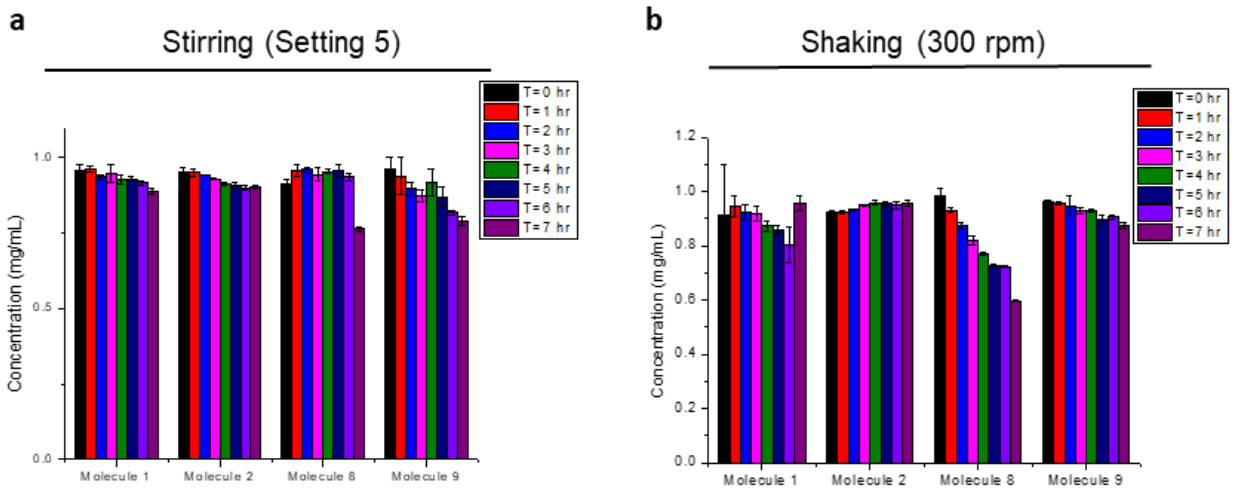

Figure 5.38: Molecules 1, 2, 8, and 9 Ab concentration after stirring and shaking stress in PBS buffer.

Panel a represents stirring over the course of 7 hrs. Panel b represents shaking over the course of 7 hrs. Error bars represent standard deviation for n=3 replicates.

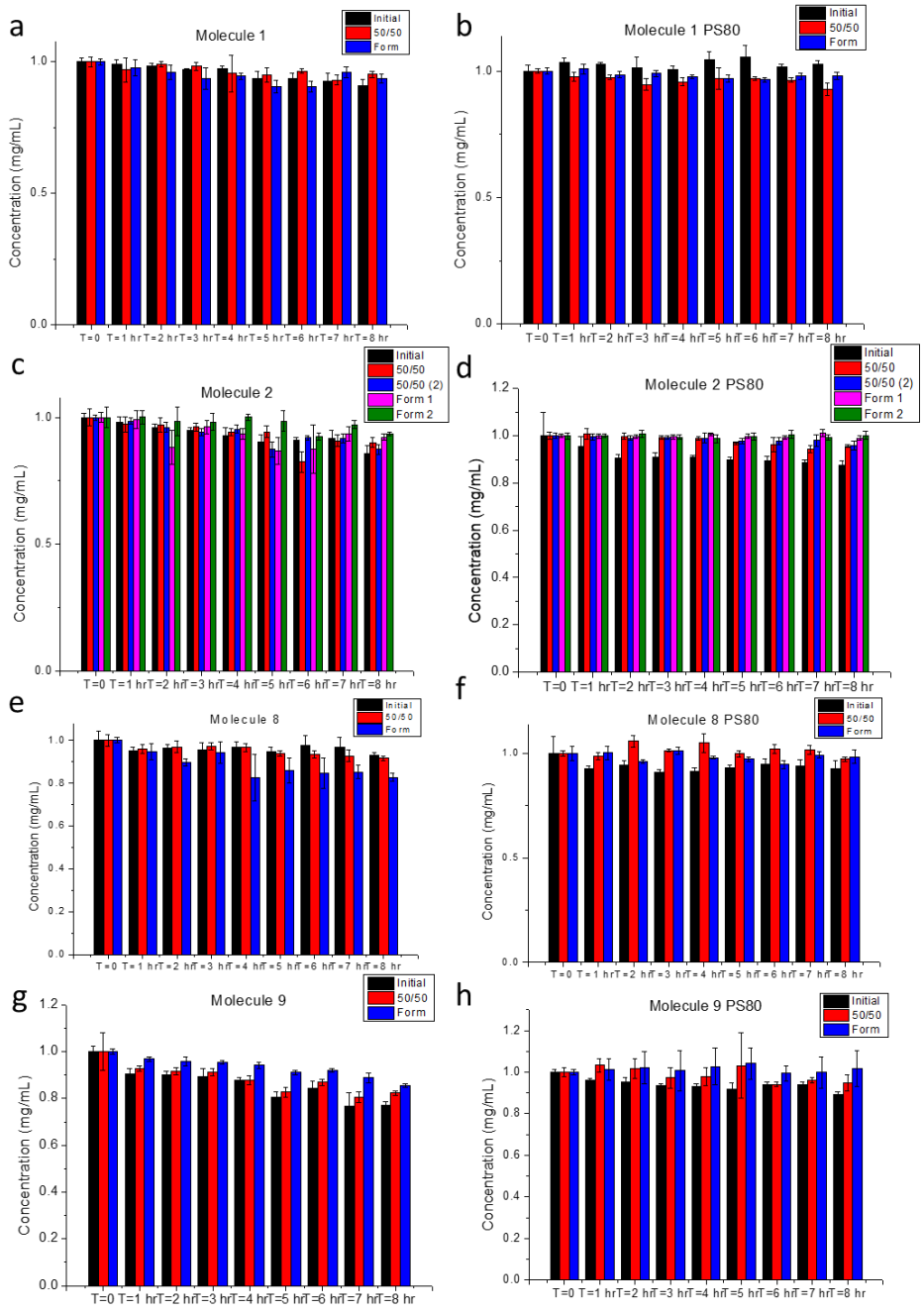

Figure 5.39: Molecules 1, 2, 8, and 9 Ab concentration after stirring in TFF processing buffers. Panel a represents molecule 1. Panel b represents molecule 1 with PS80. Panel c represents molecule 2. Panel d represents molecule 2 with PS80. Panel e represents molecule 8. Panel f represents molecule 8 with PS80. Panel g represents molecule 9. Panel h represents molecule 9 with PS80. Error bars represent standard deviation for n=3 replicates.

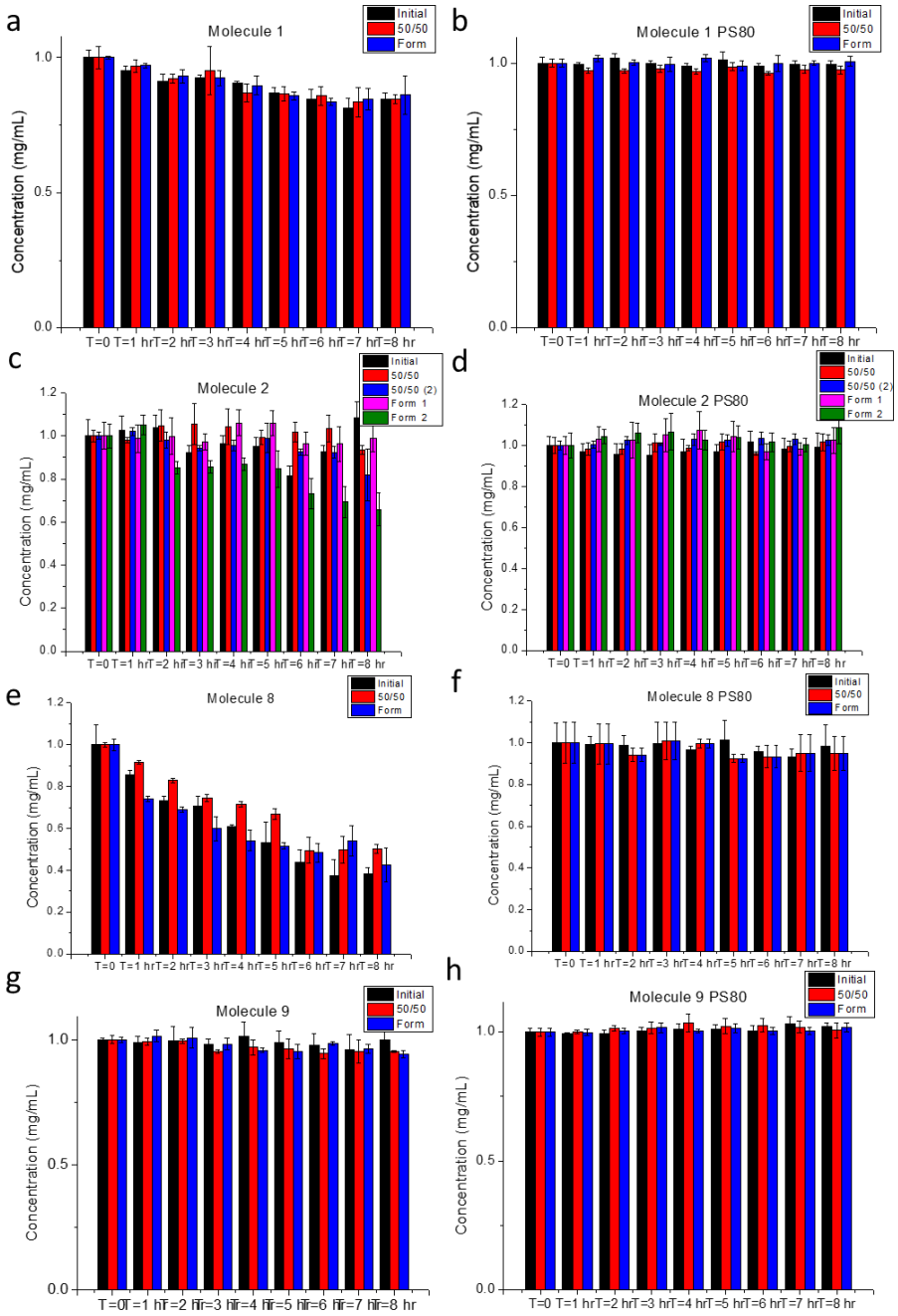

Figure 5.40: Molecules 1, 2, 8, and 9 Ab concentration after shaking in TFF processing buffers. Panel a represents molecule 1. Panel b represents molecule 1 with PS80. Panel c represents molecule 2. Panel d represents molecule 2 with PS80. Panel e represents molecule 8. Panel f represents molecule 8 with PS80. Panel g represents molecule 9. Panel h represents molecule 9 with PS80. Error bars represent standard deviation for n=3 replicates.

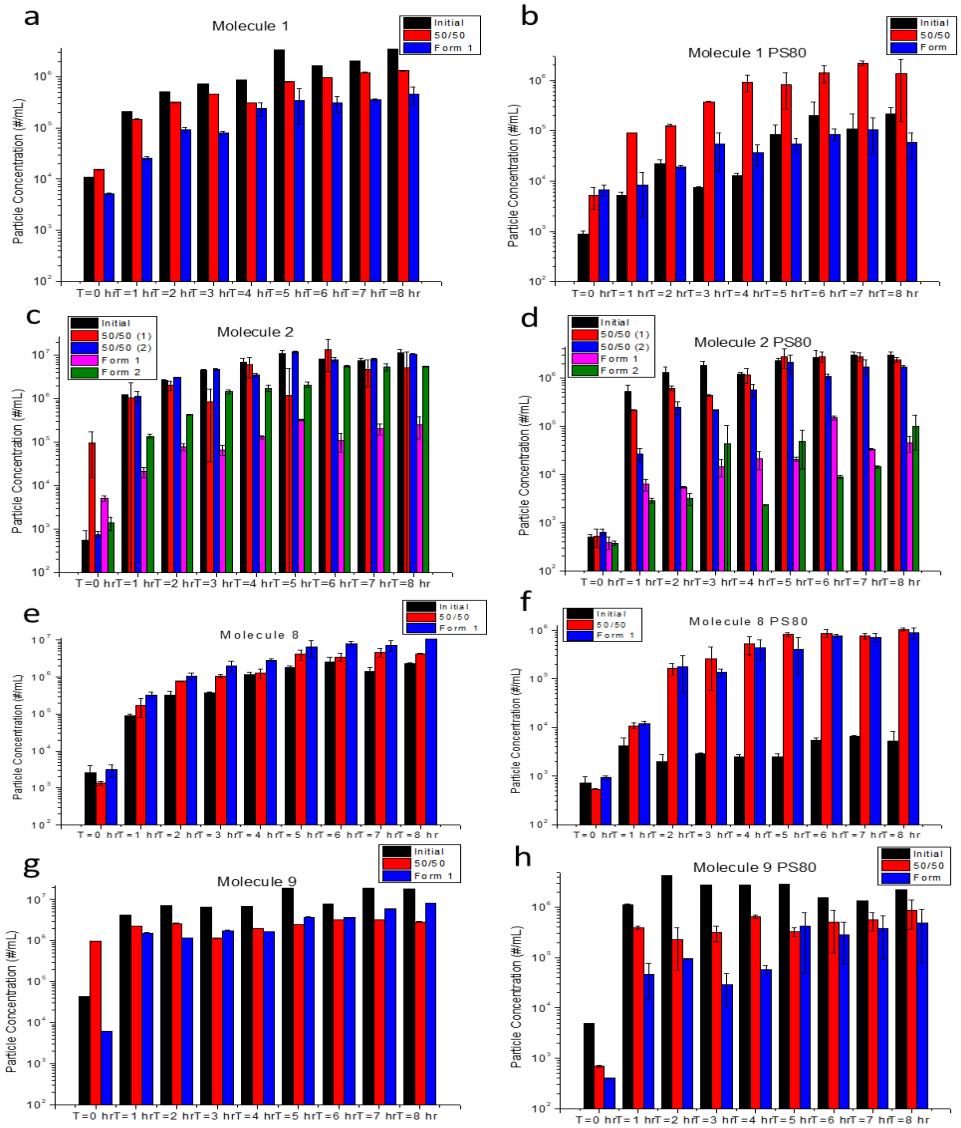

Figure 5.41: Subvisible particle concentration of solutions of Ab molecules 1, 2, 8, and 9 before and after stirring over 8 hrs in TFF process buffers (with and without PS80) as measured by MFI. Panel a represents molecule 1. Panel b represents molecule 1 with PS80. Panel c represents molecule 2. Panel d represents molecule 2 with PS80. Panel e represents molecule 8. Panel f represents molecule 8 with PS80. Panel g represents molecule 9. Panel h represents molecule 9 with PS80. Data shown is an average of n=2 measurements with error bars representing the data range.

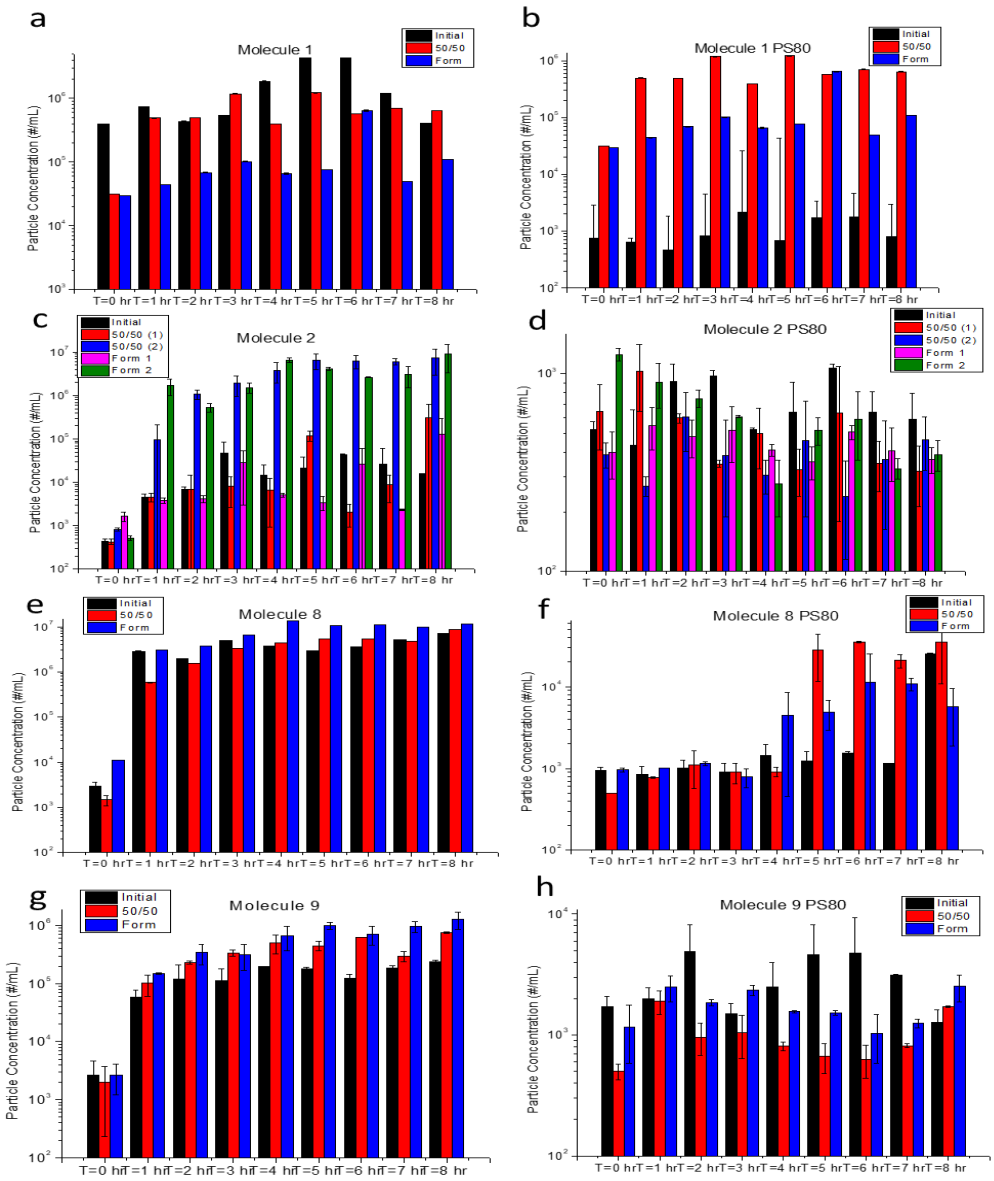

Figure 5.42: Subvisible particle concentration of solutions of Ab molecules 1, 2, 8, and 9 before and after shaking over 8 hrs in TFF process buffers (with and without PS80) as measured by MFI. Panel a represents molecule 1. Panel b represents molecule 1 with PS80. Panel c represents molecule 2. Panel d represents molecule 2 with PS80. Panel e represents molecule 8. Panel f represents molecule 8 with PS80. Panel g represents molecule 9. Panel h represents molecule 9 with PS80. Data shown is an average of n=2 measurements with error bars representing the data range.

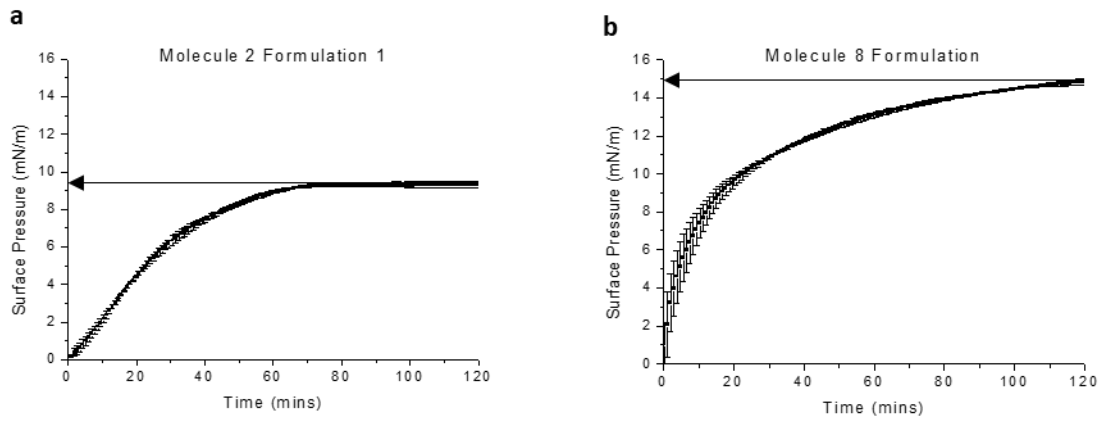

Figure 5.43: Representative absorption curves from the Langmuir trough study.

Panel a represents molecule 1 in the formulation 1 buffer. Panel b represents molecule 8 in the formulation buffer. Arrows indicate the surface pressure at equilibrium. Data shown is an average of n=2 measurements with error bars representing the data range.

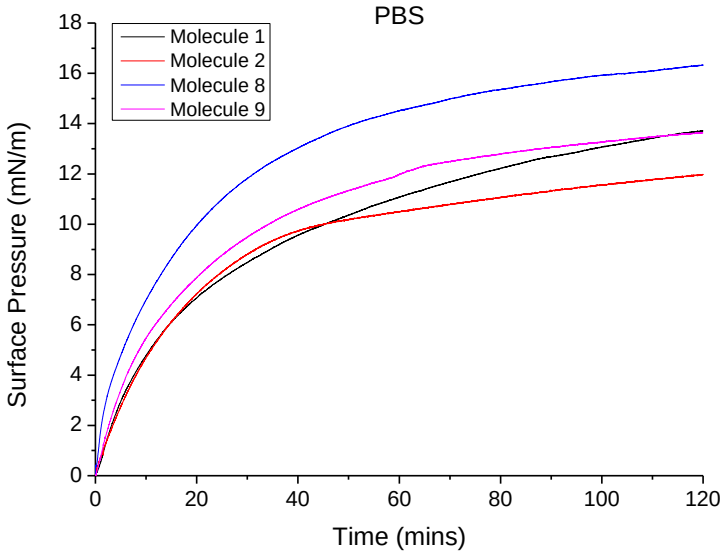

Figure 5.44: Absorption curves of Ab molecule 1 (black), molecule 2 (red), molecule 8 (blue), and molecule 9 (pink) in PBS buffer from Langmuir trough study.

n=2 duplicates. Representative traces shown.

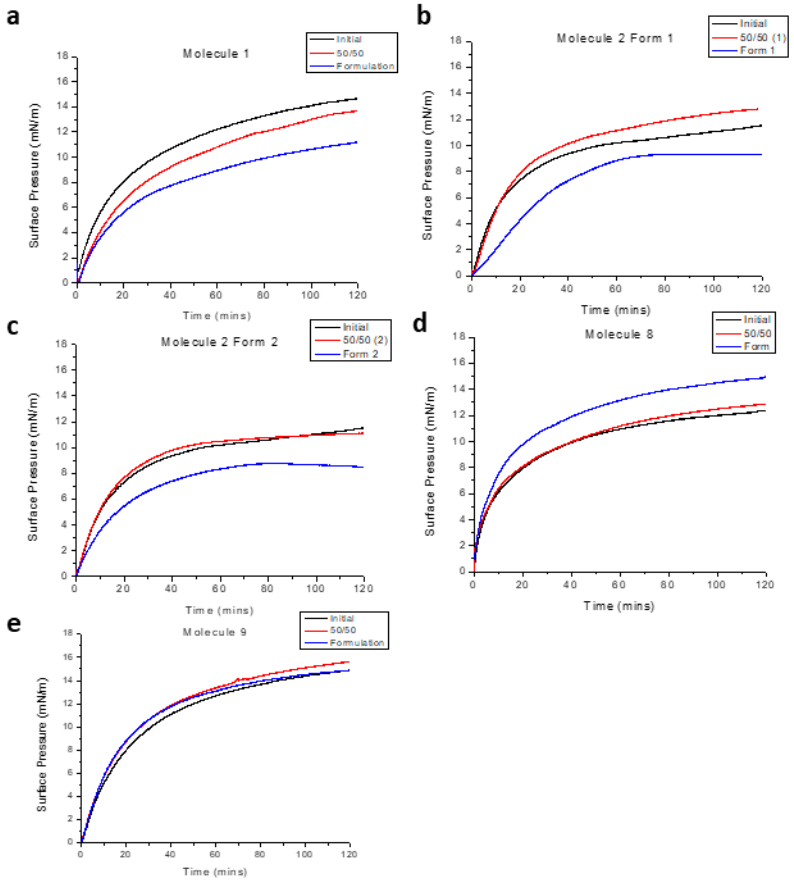

Figure 5.45: Absorption phase of Ab molecule 1, 2, 8, and 9 in the TFF processing buffers from the Langmuir trough study.

Panel a represent molecule 1. Panel b represent molecule 2 (Form 1). Panel c represent molecule 2 (Form 2). Panel d represent molecule 8. Panel e represent molecule 9. The TFF processing buffers used are initial (black), 50/50 (red), and formulation (blue). n=2 duplicates. Representative traces shown.

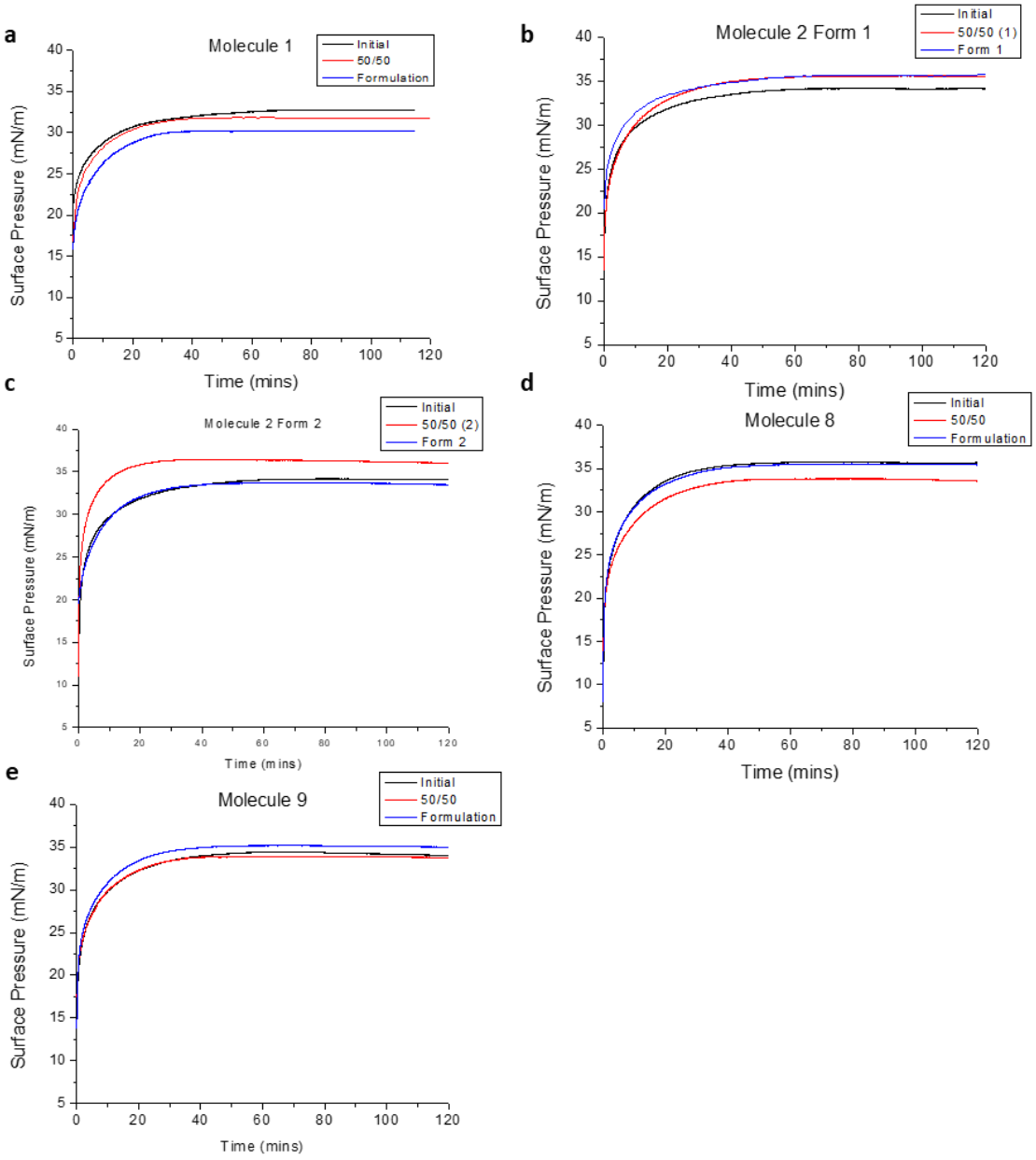

Figure 5.46: Absorption phase of Ab molecule 1, 2, 8, and 9 in the TFF processing buffers with 0.01% PS80 from Langmuir trough study.

Panel a represent molecule 1. Panel b represent molecule 2 (Form 1). Panel c represent molecule 2 (Form 2). Panel d represent molecule 8. Panel e represent molecule 9. The TFF processing buffer used are initial (black), 50/50 (red), and formulation (blue). n=2 duplicates. Representative traces shown.

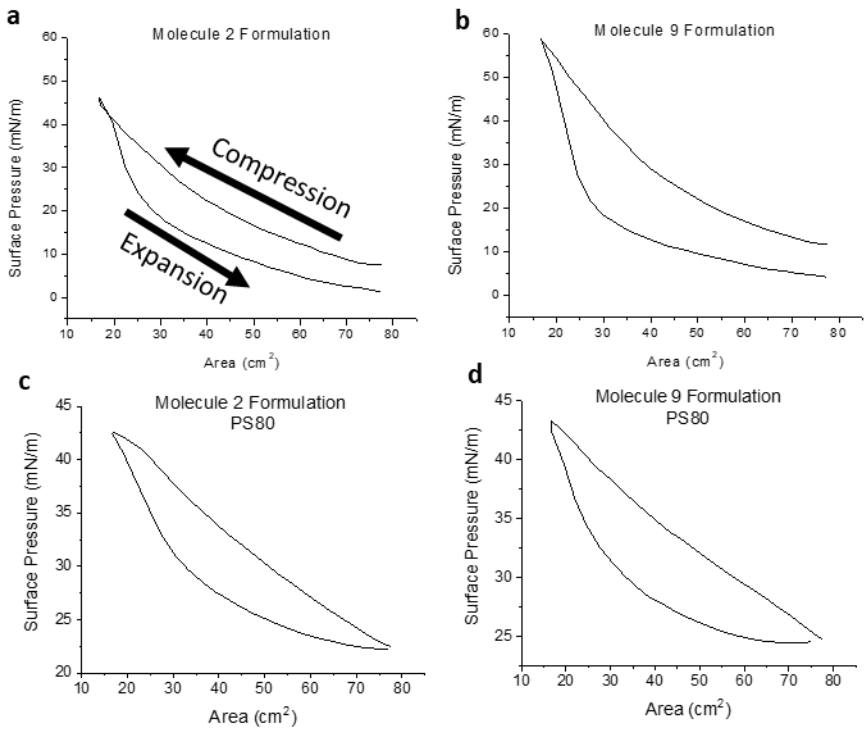

Figure 5.47: Representative Langmuir trough Isotherm from the compression and expansion phases with and without PS80.

Panel a represents molecule 2 in formulation buffer. Panel b represents molecule 9 in formulation buffer. Panel c represents molecule 2 in formulation buffer with PS80. Panel d represents molecule 9 in formulation buffer with PS80. Area between the compression and expansion phase is termed the hysteresis.

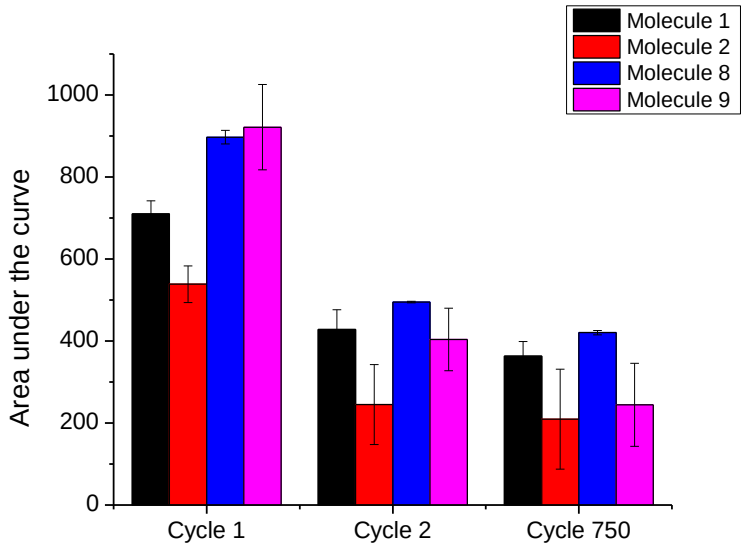

Figure 5.48: The hysteresis in total area of molecule 1 (blue), molecule 2 (red), molecule 8 (blue), and molecule 9 (pink) of the Langmuir trough in PBS at cycle 1, cycle 2 and cycle 750. Data shown is an average of n=2 measurements with error bars representing the data range.

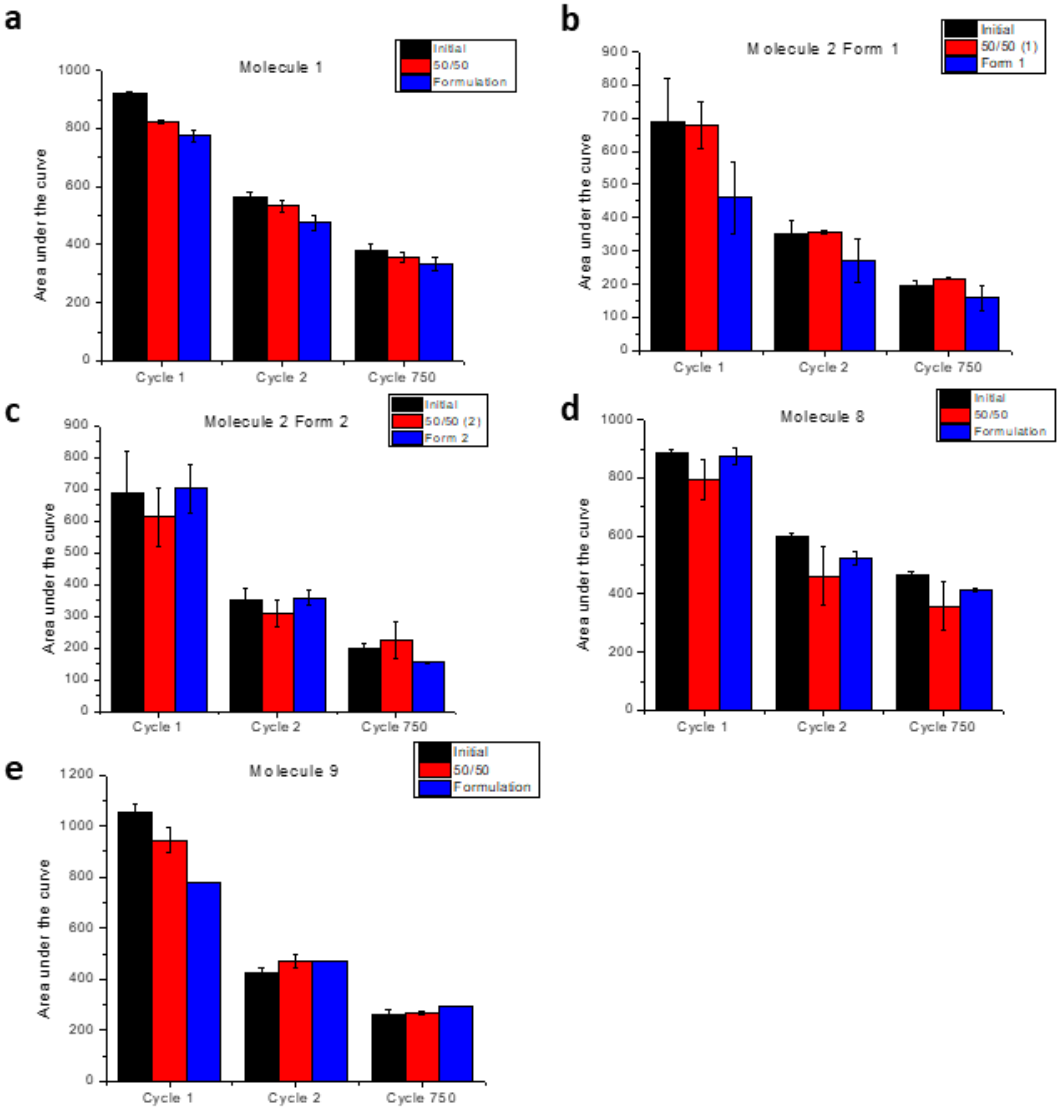

Figure 5.49: The hysteresis in total area of molecule 1, 2, 8, and 9 in the TFF processing buffers. Panel a represents molecule 1. Panel b represents molecule 2 (Form 1). Panel c represents molecule 2 (Form 2). Panel d represents molecule 8. Panel e represents molecule 9. TFF processing buffers used are initial (black), 50/50 (red), and formulation (blue) at cycle 1, cycle 2 and cycle 750. Data shown is an average of n=2 measurements with error bars representing the data range.

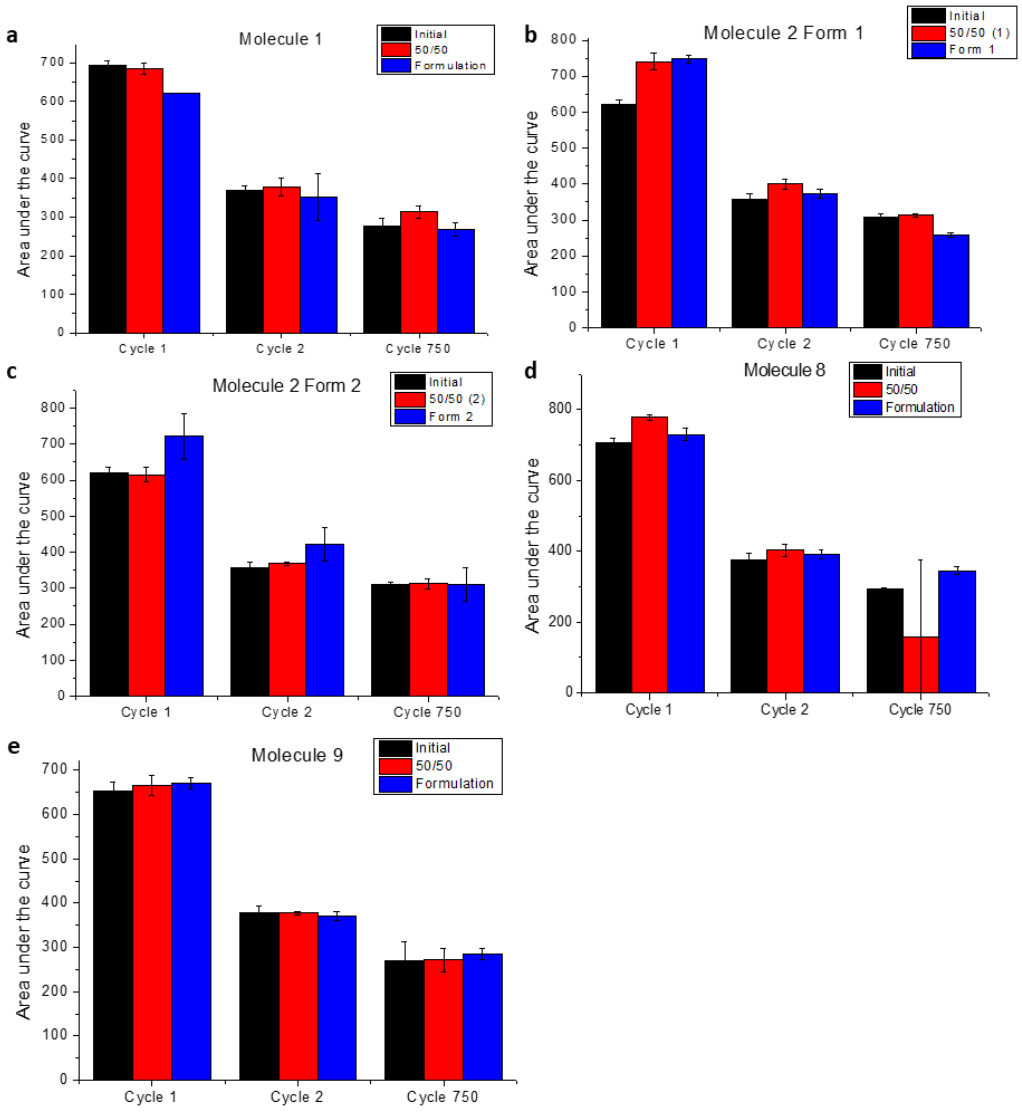

Figure 5.50: The hysteresis in total area of molecule 1, 2, 8, and 9 in the TFF processing buffers with 0.01% PS80.

Panel a represents molecule 1. Panel b represents molecule 2 (Form 1). Panel c represents molecule 2 (Form 2). Panel d represents molecule 8. Panel e represents molecule 9. TFF processing buffers used are initial (black), 50/50 (red), and formulation (blue) at cycle 1, cycle 2 and cycle 750. Data shown is an average of n=2 measurements with error bars representing the data range.

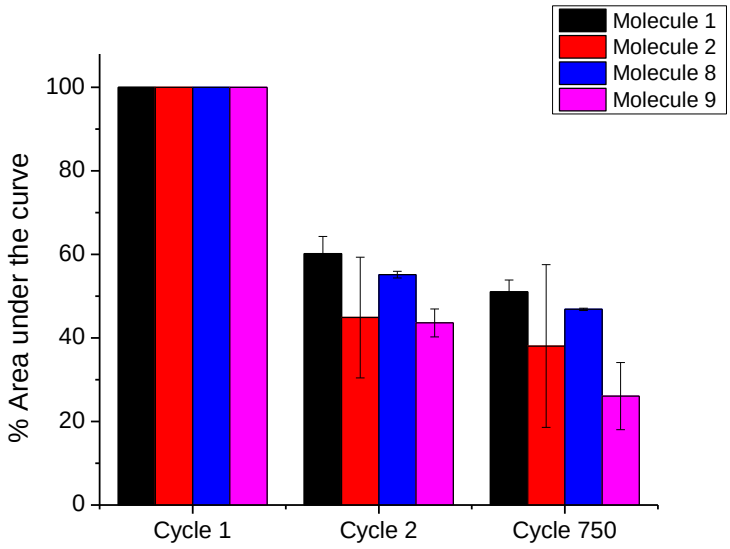

Figure 5.51: The hysteresis in percent area of molecule 1 (blue), molecule 2 (red), molecule 8 (blue), and molecule 9 (pink) in PBS buffer using the Langmuir trough at cycle 1, cycle 2 and cycle 750.

Data shown is an average of n=2 measurements with error bars representing the data range.

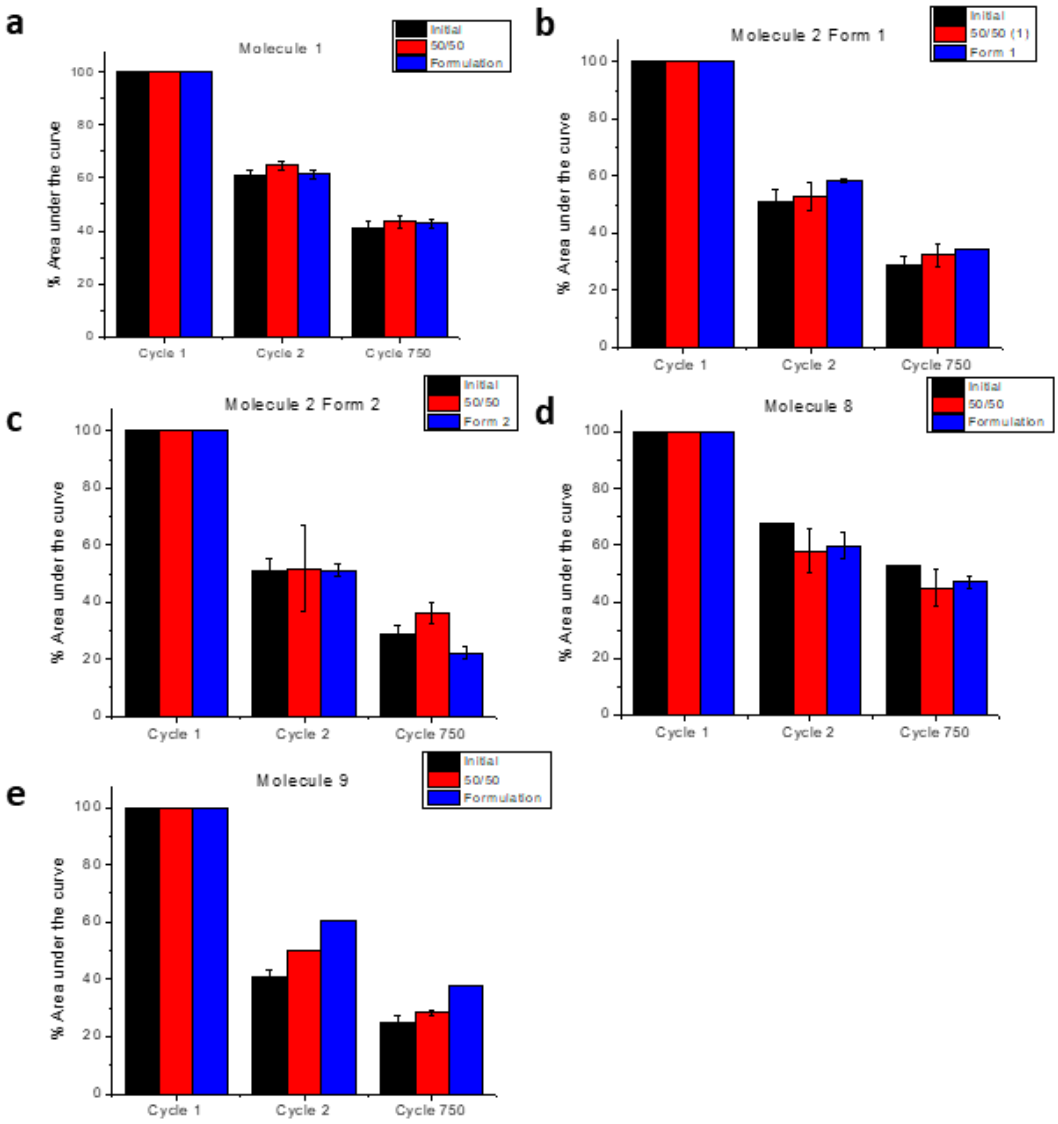

Figure 5.52: The hysteresis in percent area of molecule 1, 2, 8, and 9 in the TFF processing buffers. Panel a represents molecule 1. Panel b represents molecule 2 (Form 1). Panel c represents molecule 2 (Form 2). Panel d represents molecule 8. Panel e represents molecule 9. TFF processing buffers used are initial (black), 50/50 (red), and formulation (blue) at cycle 1, cycle 2 and cycle 750. Data shown is an average of n=2 measurements with error bars representing the data range.

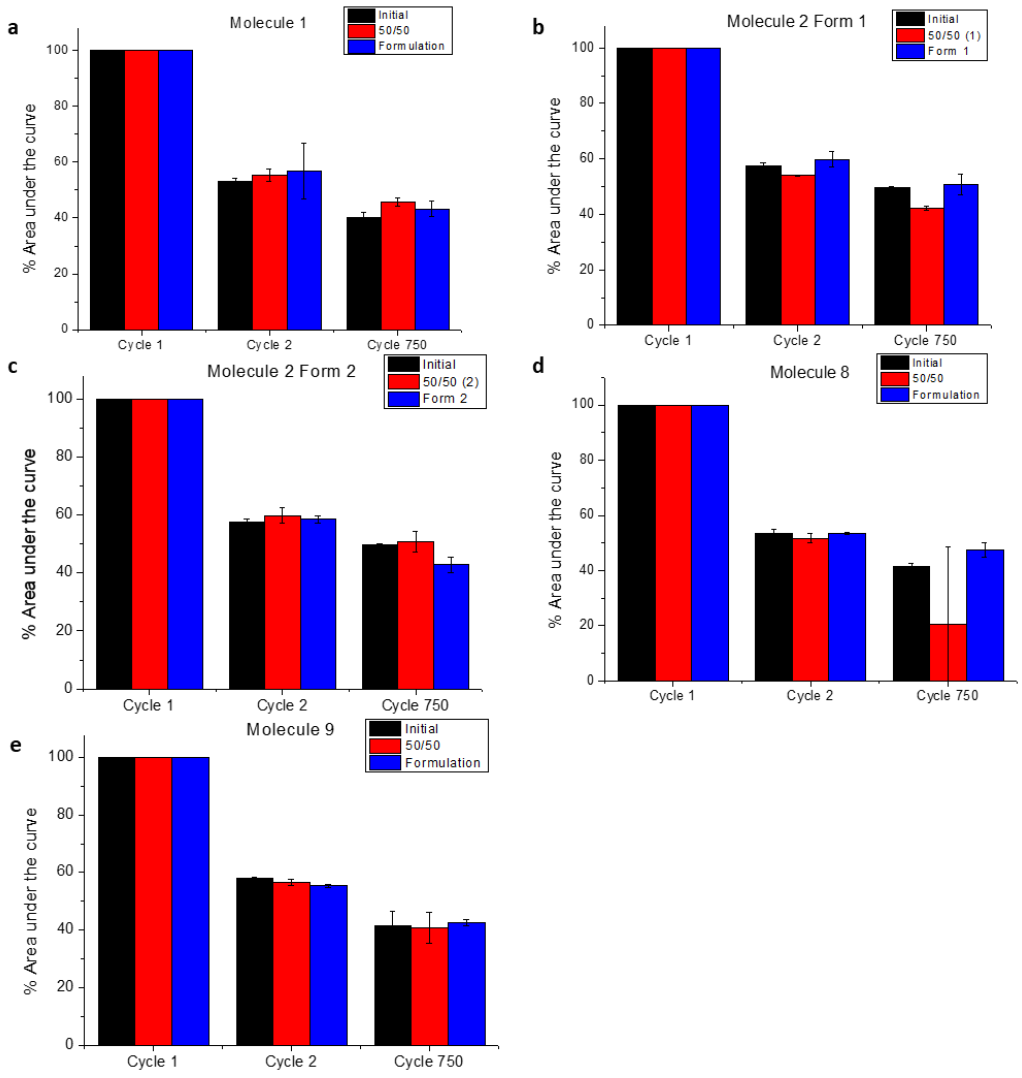

Figure 5.53: The hysteresis in percent area of molecule 1, 2, 8, and 9 in the TFF processing buffers with 0.01% PS80.

Panel a represents molecule 1. Panel b represents molecule 2 (Form 1). Panel c represents molecule 2 (Form 2). Panel d represents molecule 8. Panel e represents molecule 9.TFF processing buffers used are initial (black), 50/50 (red), and formulation (blue) at cycle 1, cycle 2 and cycle 750. Data shown is an average of n=2 measurements with error bars representing the data range.

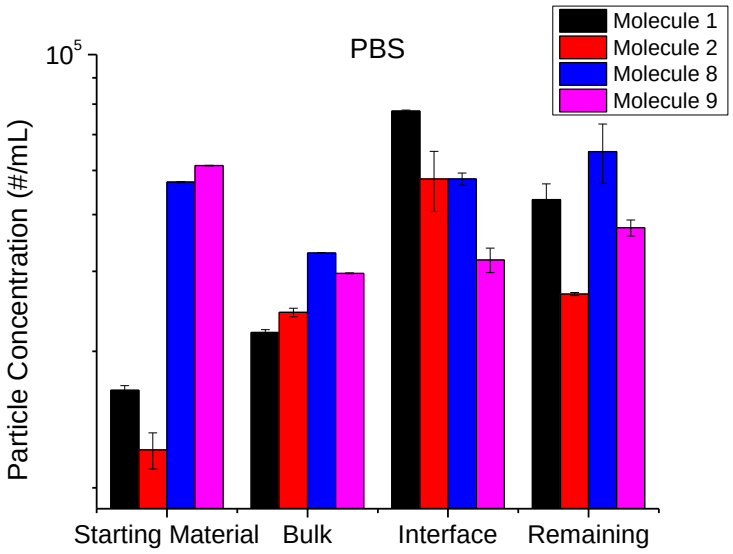

Figure 5.54: Subvisible particle concentration (as measured by MFI) of solutions of Ab molecules 1 (black), molecule 2 (red), molecule 8 (blue), and molecule 9 (pink) in PBS buffer after 750 cycles of compression and expansion using the Langmuir trough.

Data shown is an average of n=2 measurements with error bars representing the data range.

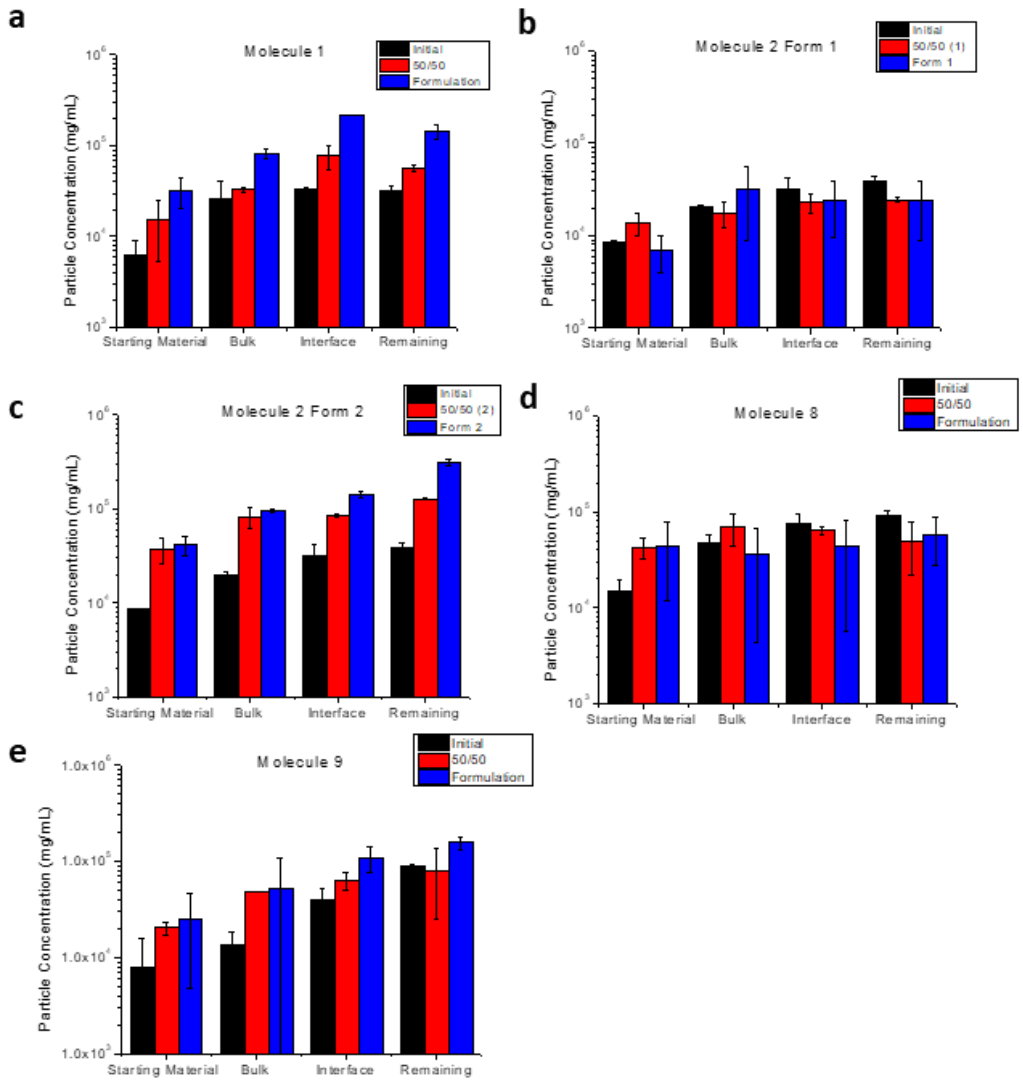

Figure 5.55: Subvisible particle concentration (as measured by MFI) of solutions of Ab molecules 1, 2, 8, and 9 in TFF processing buffers after 750 cycles of compression and expansion using Langmuir trough.

Panel a represents molecule 1. Panel b represents molecule 2 (Form 1). Panel c represents molecule 2 (Form 2). Panel d represents molecule 9. Panel e represents molecule 9. TFF processing buffers used are initial (black), 50/50 (red), and formulation (blue). Data shown is an average of n=2 measurements with error bars representing the data range.

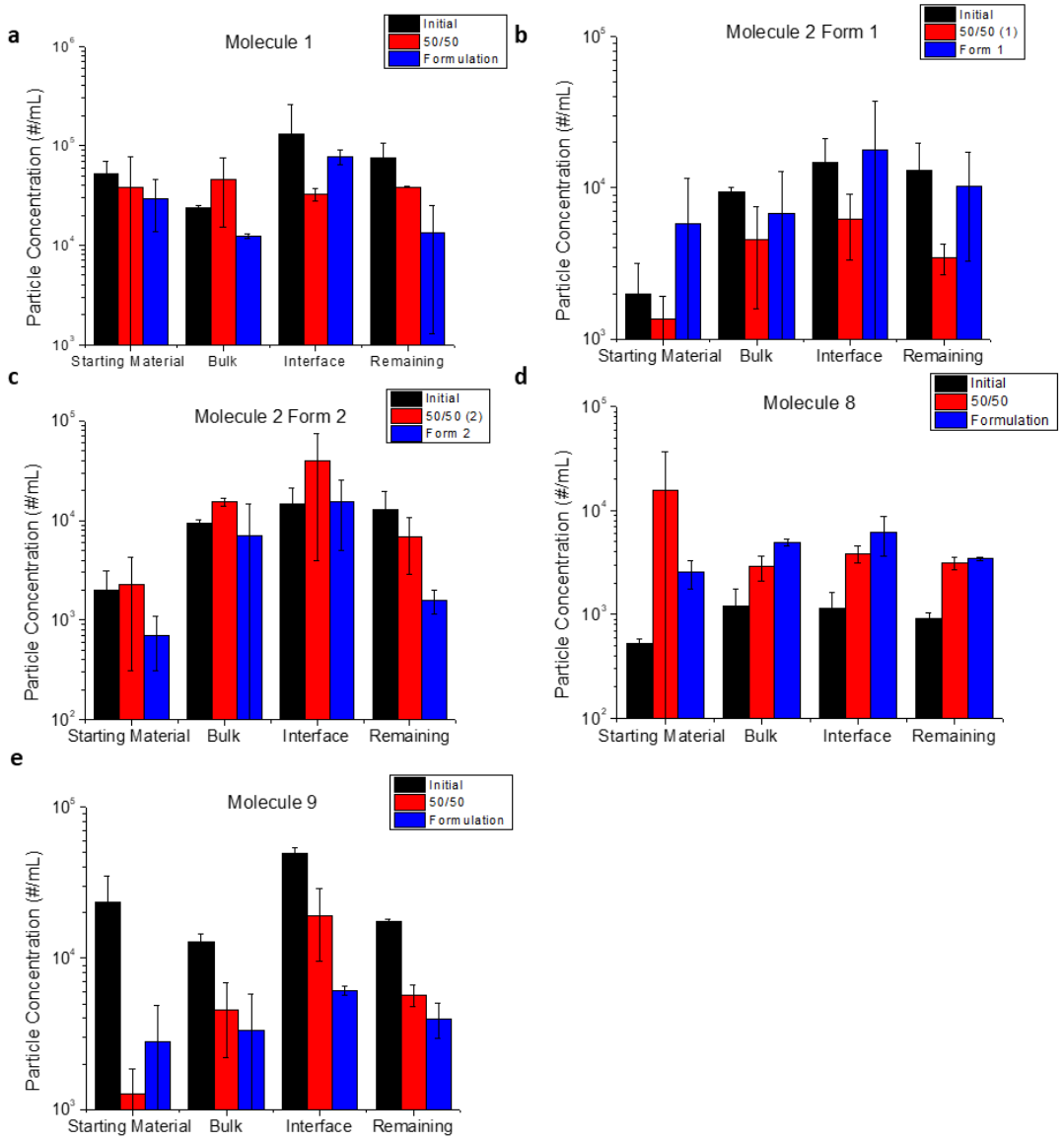

Figure 5.56: Subvisible particle concentration (as measured by MFI) of Ab molecules 1, 2, 8, and 9 in TFF processing buffers with 0.01% PS80 after 750 cycles of compression and expansion using Langmuir trough.

Panel a represents molecule 1. Panel b represents molecule 2 (Form 1). Panel c represents molecule 2 (Form 2). Panel d represents molecule 9. Panel e represents molecule 9. TFF processing buffers used are initial (black), 50/50 (red), and formulation (blue). Data shown is an average of n=2 measurements with error bars representing the data range.

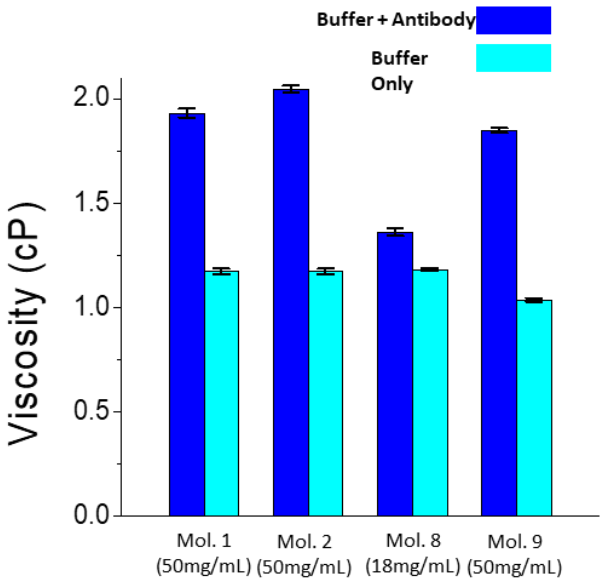

Supplementary Figure 5.1: Viscosity values of Ab molecules 1, 2, 8, and 9 in their stock solution (blue) and values of buffers alone (teal).

Error bars represent standard deviation for n=3 replicates.

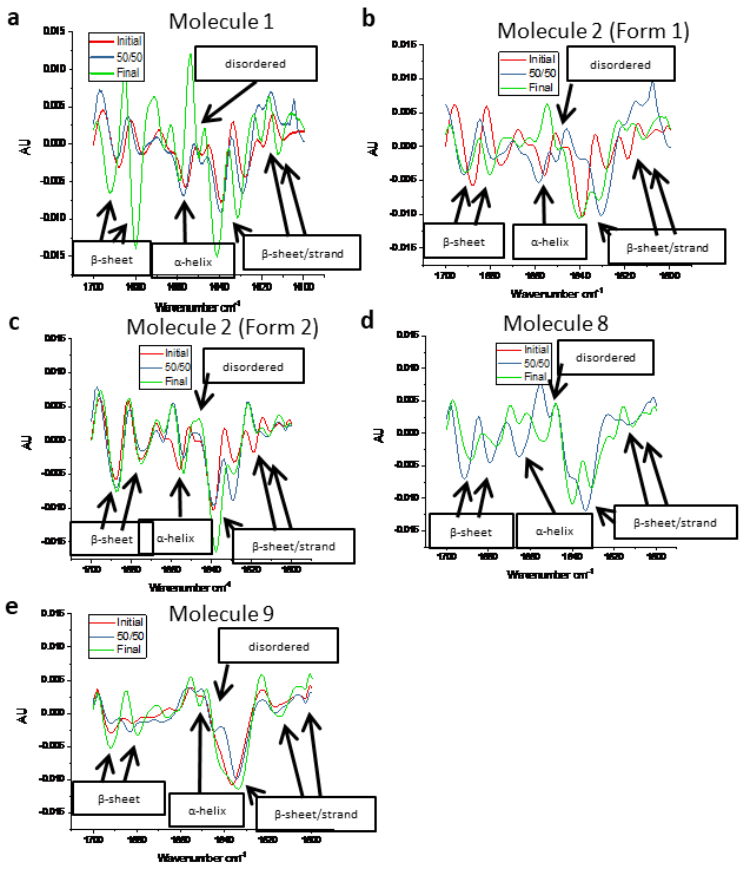

Supplementary Figure 5.2: Representative deconvoluted second derivative FTIR spectrum of molecules 1, 2, 8, and 9 in TFF processing buffers.

Panel a represent molecule 1. Panel b represent molecule 2 (Form 1). Panel c represent molecule 2 (Form 2). Panel d represent molecule 8. Panel e represent molecule 9. Molecules in their TFF processing buffers are initial (red), 50/50 (blue), and formulation (green) are shown.

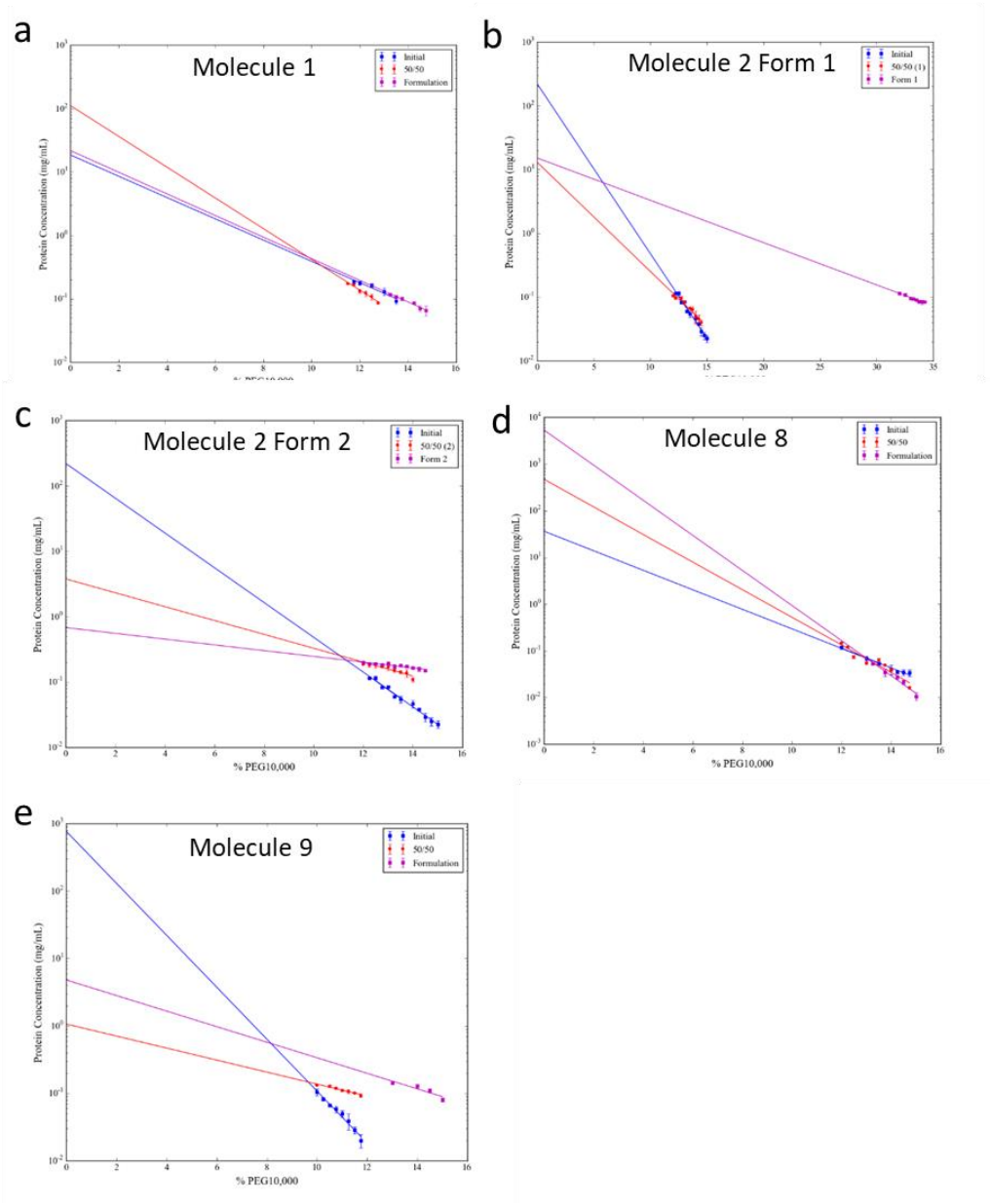

Supplementary Figure 5.3: PEG solubility assay on a logarithmic scale for extrapolation of linear fit to determine the relative apparent solubility with 0% PEG.

Panel a represents molecule 1. Panel b represents molecule 2 (Form 1) in the TFF processing buffers. Panel c represents molecule 2 (Form 2). Panel d represents molecule. Panel e represents molecule. TFF processing buffers are initial (blue), 50/50 (red), and formulation (pink). Error bars represent standard deviation for n=3 replicates.

5.4 Reference

1. 2003. Protein Concentration and Diafiltration by Tangential Flow Filtration. Millipore Technical Brief.

2. Kurnik RT, Yu AW, Blank GS, Burton AR, Smith D, Athalye AM, Reis Rv 1995. Buffer exchange using size exclusion chromatography, countercurrent dialysis, and tangential flow filtration: Models, development, and industrial application. Biotechnology and Bioengineering 45(2):149-157.

3. Harris RJ, Shire SJ, Winter C 2004. Commercial Manufacturing Scale Formulation and Analytical Characterization of Therapeutic Recombinant Antibodies. Drug Development Research 61(3):137-154.

4. Ingham KC, Busby TF, Sahlestrom Y, Castino F. 1980. Seperation of macromolecules by ultrafiltration:Influence of Protein adsorption, protein-protein interactions, and concentration polarization Ultrafiltration Membranes and Applications, ed.: Springer, Boston, MA. p 141-158.

5. Meireles M, Aimar P, Sanchez V 1991. Effects of protein fouling on the apparent pore size distribution of sieving membranes. Journal of Membrane Science 56:13-28.

6. Gibson TJ, McCarty K, McFadyen IJ, Cash E, Dalmonte P, Hinds KD, Dinerman AA, Alvarez JC, Volkin DB 2011. Application of a high-throughput screening procedure with PEG-induced precipitation to compare relative protein solubility during formulation development with IgG1 monoclonal antibodies. Journal of Pharmaceutical Sciences 100(3):1009-1021.

7. Toprani VM, Joshi SB, Kueltzo LA, Schwartz RM, Middaugh CR, Volkin DB 2016. A Micro-Polyethylene Glycol Precipitation Assay as a Relative Solubility Screening Tool for Monoclonal Antibody Design and Formulation Development. Journal of Pharmaceutical Sciences 105(8):2319-2327.

8. Wuchner K, Buchler J, Spycher R, Dalmonte P, Volkin DB 2010. Development of a Microflow Digital Imaging Assay to Characterize Protein Particulates During Storage of a High Concentration IgG1 Monoclonal Antibody Formulation. Journal of Pharmaceutical Sciences 99(8):3343–3361.

6. Summary, Conclusions and Future Work

6.1. Overview

6.2. Chapter summaries and future work

6.2.1. Chapter 2

In this work, a previously described GroEL-BLI–based method[1] was further optimized and automated (using an Octet system, 96-well plate format) to bind and detect partially structurally altered intermediates (preaggregates) formed in stressed solutions of several different therapeutic Ab candidates including IgG1, IgG4, and bispecific antibodies. TEM images of stressed Ab samples bound to the GroEL showed the formation of Ab preaggregate GroEL complexes. The utility of this approach for use in protein formulation development was explored with various mAbs (IgG1 and IgG4) exposed to various stress conditions as well as by using a relatively less stable Bis-3. For the latter, significant binding amplitudes were observed with the GroEL-BLI biosensor at room temperature at significantly lower protein concentrations (i.e., unstressed conditions), compared to the other mAbs, indicating its relatively enhanced hydrophobic nature, and by correlation, aggregation propensity. When Bis-3 was incubated at 50°C, increases in GroEL-BLI binding amplitude were observed before any increases were seen for irreversible aggregate/particle formation as measured by SEC and MFI. When examining the more stable mAb-D (IgG4), upon exposure to different stresses including elevated temperatures, acidic pH, and addition of Gdn-HCl, the GroEL-BLI biosensor could detect preaggregate formation before, or in some cases concomitantly with, irreversible aggregate formation as measured by SEC and MFI. Thus, in this case, the GroEL-BLI biosensor can supplement information gained from more traditional aggregation detection methods to

better detect preaggregate species that may be involved in the formation of longer term deleterious protein aggregates.

The GroEL biosensor technology provides protein-specific information about the presence of potentially aggregation-prone species. In some instances, this technology reports the formation of preaggregate transient species (GroEL binders) before larger scale aggregation is even detected by other analytical tools. The specificity of this GroEL-Ab interaction can be confirmed by ATP-induced reversal of Ab binding, and the GroEL-Ab complexes can be easily visualized by TEM analysis. This method can rapidly assess solution stability and preaggregate formation within the relatively short time window of minutes. This rapid detection of preaggregate species using an automated platform can be particularly useful for protein formulation development. This early BLI detection method can be used to identify stabilizing conditions and excipients that diminish preaggregate formation which may correlate with aggregation profiles during long-term stability studies.

6.2.2. Chapter 3

The ability to directly compare data gathered for mAb-D in different solutions (containing either commonly used pharmaceutical excipients or control additives known to destabilize proteins) allowed us to evaluate correlations between HX-MS data and other mAb-D stability data sets (e.g., conformational stability using DSC and accelerated stability studies monitoring protein aggregation by SEC and MFI using both temperature and agitation as stresses). The effect of additives on the relative local flexibility of specific C_H2 peptide segments within mAb-D correlated well with conformational stability and aggregation propensity under accelerated stability conditions involving heat stress, confirming the C_H2 aggregation hotspot, identified in

previous work with IgG1 mAbs,[2] with this IgG4 mAb. There were, however, no convincing correlations between HX-MS data and stirring stress for additive effects on the stability of mAb-D. These results indicate that potentially useful correlations between HX-MS data (using minimal material and a streamlined data analysis approach focusing on key peptide segments) with accelerated and real-time stability data to identify stabilizing additives as part of formulation development will be dependent on a particular mAbs degradation pathway(s) and the type of stresses used for the additive screening studies. To this end, using a variety of different mAbs, additional correlations of HX readouts in various formulations with more comprehensive accelerated and real-time stability data sets will need to be generated as part of future work.

6.2.3. Chapter 4

We have presented here a case study in low-viscosity formulation development of ultra-high concentration monoclonal antibodies that were previously formulated for maximized storage stability but possessed problematically high-solution viscosities. By evaluating a relatively large and diverse list of pharmaceutical excipients and additives, we were able to cover many of the classes of compounds that have previously been reported to possess viscosity-reducing effects. Optimized formulations for mAb A (10 mM histidine, 75 mM NaCl, 50 mM arginine, 5% sucrose, 0.02% polysorbate 20) and mAb C (10 mM histidine, 75 mM NaCl, 50 mM lysine, 5% sucrose, 0.02% polysorbate 20) were identified based on these screening studies. The best-performing excipients identified in this study to reduce viscosity are consistent with previously published results and models with other mAbs where charge interactions are involved in the PPI mechanism. Some compounds (like polar solvents), however, did not perform as well with mAb A and mAb C as they did in previous studies with other mAbs, reflecting the empirical nature of formulation development with the goal of obtaining low-viscosity, high protein

concentration mAb preparations for parenteral injection. Although some viscosity-reducing excipients affected the inherent conformational stability of mAb A (but not mAb C), as determined by a lower thermal onset temperatures as observed by DSC, the addition of these compounds did not affect the storage stability of either mAb (as measured by aggregation propensity) at storage temperatures well below the T_{onset} values. In addition, the solution osmolality, although somewhat hypertonic, was in the range used previously for parenteral drug products. In the presently described experiments, a systematic approach to developing maximally concentrated target formulations with acceptable viscosities and stabilities that can be delivered via self-administration by auto-injectors or patch pumps was demonstrated.

Due to the physicochemical differences inherent to individual monoclonal antibodies, high concentration formulation development studies to optimize protein stability and solution viscosity require either a detailed, but time-consuming and technically challenging mechanistic studies[3,4] or a more rapid but empirical approach of excipient screening (or a combination of both approaches). The generalized formulation development approach and workflow outlined in this work should be applicable to the rapid, empirical approach to the high concentration formulation development of many mAbs, especially those of the IgG1 and IgG4 subclasses. In addition, once promising additives are identified, more mechanistic studies of structure–activity relationships between the mAb and the excipients can be pursued. Thus, it is our hope that this case study provides a formulation platform approach that others can use in the future to rapidly identify optimized, ultra-high concentration mAb formulations that balance excipient effects on protein conformational stability, aggregation propensity, solution viscosity, and solution osmolality.

6.2.4. Chapter 5

Molecules 1 and 2 were demonstrated by BMS as being more stable during the large scale TFF processing compared to molecules 8 and 9, which were shown to have problems with aggregation and particle formation. The first step in probing the cause of this was to duplicate these results using a small scale TFF setup in our laboratory. When performing the small scale TFF, similar trend was observed in terms of Molecules 1 and 2 showing "good behavior" and Molecules 8 and 9 showing "bad behavior", however, these effects were less apparent at small scale. Molecule 2 showed the best correlation to having "good behavior" and molecule 8 showed the best correlation to having "bad behavior". Based on these results, it is feasible to establish a scale down model in the laboratory of the TFF process at large scale which will allow for greater flexibility in the future for trouble shooting and analysis of TFF processing conditions and their effects on Ab stability. Being able to perform such process development experiments at a small scale will allow for better TFF processing conditions to be developed with less material and time than if such work was performed at a large scale.

Next, biophysical properties such as structural integrity and conformational stability were examined for each of four Ab molecules in PBS buffer and in their respective TFF processing buffers (initial, 50/50 and formulation; see Table 2). Overall, a trend was observed in that each "good" molecule (i.e., more stable during TFF) had higher melting onset values as seen by several techniques. Several of these techniques showed molecule 8 to be the least stable indicated by the lower T_{onset} values. However in some cases, molecules 1, 8 and 9 appeared to have comparable thermal stability profiles and thus inherent conformational stability of the four Ab molecules does not consistently explain or predict the instability behavior during TFF processing.

Out of all four molecules, molecule 8 ("bad") showed the most negative k_{D2} value indicting the most likely to self-associate but was overall still low. The PEG solubility assay did not show a

good correlation with the "good vs bad behavior". In PBS molecule 1 showed the highest midpoint solubility and molecule 8 with the lowest, but molecule 9 showed higher solubility than 2. In the TFF processing buffers, molecule 2 had a very high midpoint solubility in the formulation 1 buffer but the all other molecules and buffers were comparable. Therefore, the reversible self-association properties do not consistently explain or predict the instability behavior of the TFF process

The four Abs' aggregation propensity was then examined by agitation stress using stirring and shaking in PBS buffer and in their respective TFF processing buffers with and without 0.01% PS80 present. In PBS, molecule 2 was the most stable and showed little visible aggregation after 7 hrs of stirring and no aggregation during shaking stress up to 3 days. Molecule 8 showed the most visible aggregation during shaking and molecule 9 was observed to form the most during stirring stress. When the molecules were examined in the TFF processing buffers, molecule 8 showed the highest amount of visible aggregation during the shaking stress and molecule 9 showed the highest amount during the stirring stress. Molecule 2 showed the least amount of visible aggregation with both stirring and shaking. When 0.01% PS80 was added to the buffers, no visible aggregation was seen during stirring and shaking in all the molecules with the exception of molecule 9 post-stirring. However, the amount of aggregation was decreased compared to the amount seen in samples without PS80 present. Overall, molecule 2 was the most stable and molecule 8 and 9 were the least depending on the agitation type. Molecule 1 was less stable than molecule 2 but was not the most unstable in any case. Therefore, shaking and stirring studies do not consistently explain or predict the instability behavior of the TFF process but gave a trend that overall the "good" molecules show less aggregation and the "bad" molecules can show moderate to large aggregation.

Analysis by Langmuir trough was used to examine the molecules tendency to go to the air-water interface and the likeliness to have inter-molecular interactions. Overall, molecule 8 showed the highest propensity to go to the interface and molecule 2 showed the lowest amount. When PS80 was added to the solutions, this interaction was blocked and the molecules showed lower tendencies to aggregate. In PBS, molecule 2 was the least likely to go to the air-water interface and molecule 8 was the most likely. Molecules 1 and 9 were comparable, although molecule 1 stayed at the interface more readily than molecule 9. Therefore, Langmuir trough was the best tool to explain and predict the instability behavior of the TFF process but still did not completely correlate.

Future work will be performed using the Langmuir trough to better understand and correlate the interfacial properties of each Ab to the results seen in the TFF process. This work includes using different concentrations of each Ab to see if predicting the likelihood of problems during the TFF can be seen with lower amounts of material. Different speeds and number of cycles during the compression and expansion will also be examined to correlate to the agitation seen by the TFF. This additional work will allow for a better understanding of the predictive ability of the Langmuir trough technique in terms of identifying an Ab molecule's TFF behavior (at both laboratory and large-scale processing) using minimal amount of protein.

6.3. References

1. Naik S, Kumru O, Cullom M, Telikepalli S, Lindboe E, Roop T, Joshi S, Amin D, Gao P, Middaugh C, Volkin D, Fisher M 2014. Probing structurally altered and aggregated states of therapeutically relevant proteins using GroEL coupled to Bio-Layer Interferometry. Protein Science 23(10):1461-1478.

2. Manikwar P, Majumdar R, Hickey JM, Thakkar SV, Samra HS, Sathish HA, Bishop SM, Middaugh CR, Weis DD 2013. Correlating excipient effects on conformational and storage stability of an IgG1 monoclonal antibody with local dynamics as measured by

hydrogen/deuterium-exchange mass spectrometry. Journal of Pharmaceutical Sciences 102(7):2136–2151.

3. Arora J, Hickey JM, Majumdar R, Esfandiary R, Bishop SM, Samra HS, Middaugh CR, Weis DD, Volkin DB 2015. Hydrogen exchange mass spectrometry reveals protein interfaces and distant dynamic coupling effects during the reversible self-association of an IgG1 monoclonal antibody. mAbs 7(3):525-539.

4. Arora J, Hu Y, Esfandiary R, Sathish HA, Bishop SM, Joshi SB, Middaugh CR, Volkin DB, Weis DD 2016. Charge-mediated Fab-Fc interactions in an IgG1 antibody induce reversible self-association, cluster formation, and elevated viscosity. mAbs 8(8):1561-1574.